

N73-12676

R-733

SPACE SHUTTLE AVIONICS  
A REDUNDANT IMU ON-BOARD CHECKOUT  
AND REDUNDANCY MANAGEMENT SYSTEM

(INTERIM REPORT)

**CASE FILE  
COPY**

**CHARLES STARK DRAPER  
LABORATORY**

**MASSACHUSETTS INSTITUTE OF TECHNOLOGY**

CAMBRIDGE, MASSACHUSETTS, 02139

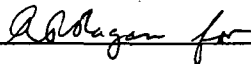
R-733

SPACE SHUTTLE AVIONICS  
A REDUNDANT IMU ON-BOARD CHECKOUT  
AND REDUNDANCY MANAGEMENT SYSTEM  
(INTERIM REPORT)

Charles Stark Draper Laboratory  
Massachusetts Institute of Technology  
Cambridge, Massachusetts  
02139

Approved:  Date: 9-26-72

N. E. SEARS, ASSOCIATE DIRECTOR  
CHARLES STARK DRAPER LABORATORY

Approved:  Date: 26 Sept 72

D. G. HOAG, ASSOCIATE DIRECTOR  
CHARLES STARK DRAPER LABORATORY

Approved:  Date: 26 Sept 72

R. R. RAGAN, DEPUTY DIRECTOR  
CHARLES STARK DRAPER LABORATORY

## ACKNOWLEDGMENT

This report was prepared under DSR Project 55-46700, sponsored by the Marshall Spaceflight Center of the National Aeronautics and Space Administration through Contract NAS 8-27624.

This report is the work of the following authors:

Richard A. McKern  
David G. Brown  
David W. Dove  
Jerold P. Gilmore  
Martin E. Landey  
Howard Musoff  
Joseph St. Amand  
Kenneth T. Vincent, Jr.

Further acknowledgment is made of the contribution and support of Mr. Harrold Brown and Mr. Billie Doran of NASA/MSEC. The authors wish to thank Robert Weatherbee, Bernadette Erikson, Lynne Sherman, Ellen Hurley, Bill Eng, and David Farrar of the MIT/CSDL Technical Publications Group.

The publication of this report does not constitute approval by the National Aeronautics and Space Administration of the findings or the conclusions contained herein. It is published only for the exchange and stimulation of ideas.

R-733

SPACE SHUTTLE AVIONICS  
A REDUNDANT IMU ON-BOARD CHECKOUT  
AND REDUNDANCY MANAGEMENT SYSTEM  
(INTERIM REPORT)

ABSTRACT

The results of the twelve month study for the NASA/Marshall Space Flight Center by the Charles Stark Draper Laboratory Division of MIT are reported.

This work develops a failure detection and isolation philosophy applicable to multiple "off-the-shelf" gimballed IMUs. The equations developed are implemented and evaluated with actual shuttle trajectory simulations. The results of these simulations are presented for both powered and unpowered flight phases and at operational levels of four, three, and two IMUs. A multiple system checkout philosophy is developed and simulation results presented. The final task develops a laboratory test plan and defines the hardware and software requirements to implement an actual multiple system and evaluate the interim study results for space shuttle application.

September 1972

## TABLE OF CONTENTS

1.0	INTRODUCTION	1
1.1	TASK I REQUIREMENTS	2
1.1.1	FDI Theory (Powered and Unpowered Flight Phases)	2
1.1.1.1	Hard Failure Philosophy	2
1.1.1.2	Soft Failure FDI Implemented for 4, 3, 2 IMU Operation	3
1.1.2	Prelaunch and Checkout Ties to FDI	3
1.1.3	Off the Shelf Performance for Shuttle Application	4
1.2	TASK II REQUIREMENTS	4
1.3	FUTURE WORK EFFORT	4
1.3.1	Task III Work Effort	5
1.3.2	Task IV Work Effort	5
2.0	FAILURE DETECTION AND ISOLATION PHILOSOPHY	7
2.1	CURRENT APPLICATIONS OF FDI	7
2.2	SHUTTLE FDI REQUIREMENTS	8
2.3	IMU RELIABILITY VS. REDUNDANCY REQUIREMENTS	9
3.0	FAILURE DETECTION AND ISOLATION EQUATION IMPLEMENTATION	17
3.1	HARD FAILURE DETECTION AND ISOLATION	17
3.2	SOFT FAILURE DETECTION AND ISOLATION EQUATION DEVELOPMENT	18
3.2.1	Velocity FDI Equations	18
3.2.2	Attitude FDI Equations	21
3.2.3	Two IMU FDI Equations	24
3.3	ISOLATION THEORY	31
3.4	SUMMARY	32
4.0	FAILURE DETECTION AND ISOLATION SIMULATION DESCRIPTION	37
4.1	SHUTTLE TRAJECTORY DESCRIPTION AND MISSION REQUIREMENTS	37
4.2	REDUNDANT INERTIAL SUBSYSTEM SIMULATION METHOD	44
4.3	FAILURE DETECTION AND ISOLATION IMPLEMENTATION	49
4.3.1	Velocity FDI Verfiication Program (Powered Flight)	49
4.3.2	Gyro Drift FDI Verification Program (Unpowered Flight)	53
5.0	FAILURE DETECTION AND ISOLATION SIMULATION RESULTS	55
5.1	NOMINAL BOOST VELOCITY FDI TEST RESULTS	55
5.2	BOOSTER ABORT FDI TEST RESULTS	58
5.3	ORBITER ENTRY VELOCITY FDI TEST RESULTS	64
5.4	ORBITAL FLIGHT GYROSCOPE FDI TEST RESULTS	64

5.5	TWO IMU FDI SIMULATION RESULTS	76
5.5.1	Nominal Boost	76
5.5.2	Booster Abort	77
5.5.3	Orbiter Entry	77
5.5.4	Unpowered Flight	82
6.0	SYSTEM CHECKOUT PHILOSOPHY AND PRELAUNCH VERIFICATION	85
6.1	CHECKOUT PHILOSOPHY	85
6.2	VERIFICATION TESTS	87
6.2.1	Testing Against Limits	87
6.2.2	Testing by Performance Comparison	89
6.3	TWO PROPOSED CHECKOUT PROCEDURES	89
6.3.1	Required Assumptions	89
6.3.2	Six Position Verification Test	90
6.3.3	Verification Test Using Powered Flight FDI	94
6.4	CONCLUSIONS	98
7.0	MULTIPLE IMU SYSTEM MODEL AND SIMULATIONS OF PRELAUNCH CHECKOUT PROCEDURES	101
7.1	SINGLE IMU MODEL	101
7.2	MULTIPLE IMU MODEL	103
7.3	SIMULATION RESULTS	103
7.3.1	Six Position Test	103
7.3.2	Three Position Test Using FDI as Monitor	
7.4	SUMMARY	104
8.0	LABORATORY TEST PLAN	107
8.1	INTRODUCTION	107
8.2	TEST PLAN PHASES	107
8.2.1	IMU Calibration	
8.2.1.1	Instrument Parameter Verification	109
8.2.1.2	Gimbal Chain Calibration	115
8.2.1.3	Gimbal Flip Region Evaluation	118
8.2.2	Gyro Compassing Multiple Systems	
8.2.2.1	System Testing	120
8.2.2.1.1	Single IMU G/C Verification	120
8.2.2.1.2	Multiple IMU G/C Verification	122
8.2.2.2	Basic Ground Alignment Program	122
8.2.3	Prelaunch Verification of Multiple Systems	128
8.2.4	Land Navigation Performance Verification	128

8.2.4.1	System Testing	129
8.2.4.2	Land Navigation Program	129
8.2.5	Failure Detection and Isolation Testing	133
8.2.6	Attitude Loop Demonstration	134
9.0	LABORATORY TESTING HARDWARE AND SOFTWARE REQUIREMENTS	135
9.1	HARDWARE REQUIREMENTS	135
9.1.1	Delta Velocity Pulses	135
9.1.2	Gimbal Angle Outputs	135
9.1.3	System Input Discretes	136
9.1.3.1	Gyro Torquing Discretes	136
9.1.3.2	Analog Torquing and Other Discrete Commands	136
9.1.4	System Output Discretes	137
9.1.5	Avionics Interface	137
9.1.6	General	137
9.2	SOFTWARE-EXECUTIVE CONTROL	137
9.3	COMPUTATIONAL REQUIREMENTS	140
9.3.1	4 $\pi$ - CP2 Computer	140
9.3.2	Preliminary Estimates for Input/Output Operations	141
9.3.3	Preliminary Estimates of Computational Requirements	141
10.0	PRESENT WORK EFFORT SUMMARY	143



## LIST OF FIGURES

1-1	Proposed Test Configuration	6
2-1	MTBF Required For 0.99 Mission Success Probability	10
2-2	Probability of Mission Success Vs. FDI Effectiveness, 5 IMUs	12
2-3	Probability of Mission Success Vs. FDI Effectiveness, 4 IMUs	13
2-4	Probability of Mission Success Vs. FDI Effectiveness, 3 IMUs	14
2-5	Probability of Mission Success Vs. FDI Effectiveness, 2 IMUs	15
2-6	Probability of Mission Success Vs. FDI Effectiveness, 1 IMUs	16
3-1	Logic Flow Chart of Velocity FDI Technique	22
3-2	Attitude Soft Failure Detection and Isolation Logic	25
3-3a	Two IMU Failure Detection and Isolation, Velocity Logic	27
3-3b	Two IMU Failure Detection and Isolation, Attitude Logic	28
3-4	Four IMU Voting - First Failure Isolation Equations	33
3-5	Three IMU Voting, First Failure Isolation Equations	34
4-1	Nominal Boost Mission Detection Thresholds	40
4-2	Booster Entry Mission Thresholds	41
4-3	Orbiter Entry Mission Detection Thresholds	43
4-4	Gimbaled IMU Model Flow Chart	45
4-5	Multiple IMU Simulation Flow Chart	46
4-6	Single IMU Flow Diagram	48
4-7	Velocity FDI Verification Program Flow Diagram	50
4-8	Gyroscope FDI in Cruise Flight	54
5-1	Nominal Boost Mission Simulation Results (1 Fail)	56
5-2	Nominal Boost Mission Simulation Results (2 Fail)	57
5-3	Nominal Boost Mission Simulation Results (3 Fail)	59
5-4	Nominal Boost Mission Simulation Results (3 Fail)	60
5-5	BoosterEntry Mission Simulation Results (1 Fail)	61
5-6	BoosterEntry Mission Simulation Results (2 Fail)	61
5-7	BoosterEntry Mission Simulation Results (2 Fail)	62
5-8	BoosterEntry Mission Simulation Results (3 Fail)	62
5-9	BoosterEntry Mission Simulation Results (3 Fail)	63
5-10	BoosterEntry Mission Simulation Results (3 Fail)	63
5-11	Orbiter Entry Mission Simulation Results (1 Fail)	65
5-12	Orbiter Entry Mission Simulation Results (2 Fail)	66
5-13	Orbiter Entry Mission Simulation Results (2 Fail)	67
5-14	Orbiter Entry Mission Simulation Results (3 Fail)	68
5-15	Orbiter Entry Mission Simulation Results (3 Fail)	69
5-16	Unpowered Flight Simulation Results (1 Fail)	70
5-17	Unpowered Flight Simulation Results (2 Fail)	71
5-18	Unpowered Flight Simulation Results (2 Fail)	72



5-19	Unpowered Flight Simulation Results (3 Fail)	73
5-20	Unpowered Flight Simulation Results (3 Fail)	74
5-21	Unpowered Flight Simulation Results (3 Fail)	75
5-22	Two IMU FDI Simulation, Nominal Boost	78
5-23	Two IMU FDI Simulation, Nominal Boost	78
5-24	Two IMU FDI Simulation, Booster Entry	79
5-25	Two IMU FDI Simulation, Booster Entry	79
5-26	Two IMU FDI Simulation, Orbiter Entry	80
5-27	Two IMU FDI Simulation, Orbiter Entry	81
5-28	Two IMU FDI Simulation, Unpowered Flight	83
5-29	Two IMU FDI Simulation, Unpowered Flight	83
6-1	Flow Chart of The Six Position Verification Test	95
6-2	Flow Chart of Multiple IMU Verification Test Using Redundant Data and Powered Flight FDI	99
7-1	$V_{ER}$ of East Axis for Drift About North Axis	105
8-1	HP2116 Display (Gyrocompass)	121
8-2	HP2116 Display (Land Navigation)	130
8-3	HP2116 Display (Debug)	131
A-1	Accelerometer to Reference Triad Misalignment	149
A-2	Gyroscope to Reference Triad Misalignment	149
A-3	Inertial Platform Mechanical Schematic	151

## 1.0 INTRODUCTION

This is an interim report on the Space Shuttle Avionics Study, NASA/MSFC Contract NAS8-27624. This contract was awarded to the Draper Laboratory of M.I.T. on July 7, 1971. As set forth in the statement of work, the study objective was summarized in the following sentences:

"To define an onboard checkout, failure detection, isolation and redundancy management scheme for a redundant IMU system that meets a fail operational/fail operation/fail safe (FO/FO/FS) criterion. In addition an experimental program that will implement the onboard checkout, failure detection, isolation and redundancy management scheme will be defined."

The approach taken to study the failure detection and isolation (FDI) accuracy requirements was to use actual shuttle mission trajectory simulations with defined terminal accuracy requirements. Acceptable threshold requirements for evaluation of FDI implementations were then defined by showing the accuracy requirements of individual system coefficients in each trajectory phase and observing error propagation characteristics in position and velocity. By use of actual trajectory phases and required IMU characteristics to meet terminal accuracy requirements, threshold requirements for the multiple system FDI were obtained. This formed the basis of all FDI evaluations.

The requirement of a failure operational/failure operational/failure safe capability (FO/FO/FS) defines a system of at least four complementary IMUs where failure detection and isolation must be reliably accomplished, within mission accuracy thresholds, with any pair of operational systems. Notice, five IMUs are required for FO/FO/FS if two IMU skewed FDI capability is not assumed. Only this depth of gimballed system FDI will permit a final true fail safe capability. It should be noted that the current shuttle concept is FO/FS implying at least a three IMU system definition. The FDI technique presented is directly applicable to this definition. Reliability considerations for the shuttle missions are presented in Chapter 2, where the probability of mission success with various redundancy levels are described. The influence of single IMU reliability (MTBF) and FDI effectiveness on these calculations is shown.

Another primary study area will define, in both hardware and software terms, the requirements to implement a laboratory test plan at NASA/MSFC designed to prove the concepts developed in this program.

It should be noted that this study assumes "off-the-shelf" IMU technology and does not attempt to use the unique features of any IMU manufacturer in implementing the redundancy performance isolation logic. Simultaneous gimbal readouts and reference triad incremental velocity information is assumed to be available from each operational IMU. Thus, the FDI methods presented here are compatible with all developed aircraft inertial systems.

## 1.1 TASK I REQUIREMENTS

### 1.1.1 FDI Theory (Powered And Unpowered Flight Phases)

It should be observed that the operational IMU systems under consideration in this paper have good quality, finely quantized velocity loops in common. In contrast, the present gimbal angle readout chains involve a low quality single speed synchro as a primary sensor. In addition, they have poor gimbal orthogonality and synchro null repeatability and use a four-gimbal mechanization with only a three-gimbal readout capability. Thus, emphasis in this study is concentrated upon failure detection and isolation methods using velocity as the primary source of decision information. In unpowered flight phases, of course, attitude chain information is all that is available for monitoring the IMU gyroscopes to insure performance levels commensurate with later mission phase performance requirements.

In outlining the requirements for the redundant gimballed inertial measurement unit FDI problem, consideration of all shuttle mission phases, including both powered and unpowered flight, is required. In powered flight phases, an FDI technique is employed utilizing only incremental inertial velocity information on an axis by axis basis. During unpowered flight, only gimbal generated attitude information is available for FDI evaluation.

#### 1.1.1.1 Hard Failure Philosophy

In addition to supplementary IMU status information from electronic hard failure detection available for the computer, an additional hard failure logic level is implemented in software to insure data reasonability. Gimbal angle readouts and incremental velocity information are verified for reasonability with respect to maximum expected levels prior to any attitude control or navigation updates. Both of these hard failure detection implementations serve as additional detection and isolation information to permit better management and thus provide more reliability in the (soft) performance failure detection and isolation processing.

#### 1.1.1.2 Soft Failure FDI Implemented For 4, 3, 2 IMU Operation

The powered flight phases use individual IMU systems operating with stable member reference axes and gimbal axes approximately colinear. This configuration is used for both first and second failure detection and isolation capabilities.

After second failure isolation is accomplished, in a four IMU system, detection of a third failure is possible. In order to properly isolate this failure, however, one of the two remaining IMUs must be torqued out of the colinear configuration into a skewed instrument axes orientation. In this manner, enough redundant information is generated on an instrument axis basis to enable achievement of an acceptable isolation confidence level. The fail safe criterion set forth earlier is met only when instrument failure isolation is possible in a two IMU configuration.

The colinear alignment at launch of the multiple IMUs permits each system to have its stable member independently aligned in the earth reference frame. Aircraft navigators have been well developed in this area and do an excellent job. It would be possible to torque all stable members into a defined skew orientation frame before launch after prelaunch alignment or to perform initial alignment directly to skewed orientations. It is felt this would unnecessarily degrade the inherent IMU accuracy due to torquing uncertainties. It would complicate and degrade the sensitivity of the resultant FDI and the associated velocity information used for navigation. To purposely degrade the available colinear FDI to a skew orientation FDI before it is absolutely required would increase the overall IMU accuracy requirements. This could show up as a decrease of the resulting FDI reliability or would increase overall IMU performance requirements to meet the same mission threshold requirement. One further objection to having all platforms initially colinear is that the slewing process will introduce errors through the dynamic error terms (i.e., centripetal acceleration, OA coupling, etc.) of the instrument models. A study of these rotational terms at angular velocities achievable in the KT-70 indicates that such errors are negligible, and need not even be compensated.

In the unpowered orbital mission phases similar logic is used for colinear and two-IMU skew orientations using information on rates derived from the individual gyroscope axes. Accelerometer performance is, of course, monitored directly in orbital mission phases.

#### 1.1.2 Prelaunch And Checkout Ties To FDI

Investigations are made in this study in how best to use the multiple system information as an indication of individual IMU parameter verification within expected levels of

performance. This is done in the prelaunch verification by investigating the direct use of the colinear FDI implementation for individual system integrity testing. Another critical prelaunch verification before initializing the powered flight FDI at launch concerns a coarse verification within two milliradians of the initial earth referenced stable member position between individual IMUs using the gimbal readout chains. This is required to insure close stable member alignment on an axis by axis basis prior to initialization of the powered flight FDI method.

### 1.1.3 Off The Shelf Performance For Shuttle Application

It has been the intent in this work to establish a method of FDI which is compatible with the off-the-shelf IMU, which can be lab demonstrated and which satisfies a baseline of accuracy requirements derived for the shuttle mission. It is shown the present off-the-shelf attitude chain accuracy is marginal to attain the in-flight alignment accuracy requirement prior to the normal reentry mission phase. Thus, it is of prime importance for shuttle application to update the attitude chain hardware and develop and demonstrate applicable attitude chain calibration techniques. This is, however, not believed to be required directly for the FDI problem solution.

## 1.2 TASK II REQUIREMENTS

The test plan for demonstration of a multiple IMU system at NASA/MSFC is defined directly for three production Kearfott KT-70 IMUs and their supporting electronics, mated to an IBM 4 $\pi$ -CP2 computer. The computerized test facility available at NASA/MSFC, known as SSCMS (Strapdown System Control and Monitor Station)<sup>1</sup>, will be used in monitoring system performance. This facility was designed and constructed by the Hamilton Standard System Center.

The test plan presented includes single IMU calibration and gimbal flip evaluations as well as multiple IMU gyrocompassing, land navigation and powered as well as unpowered flight FDI demonstrations.

## 1.3 FUTURE WORK EFFORT

An extension to this work was approved on 3 August, 1972. The extension of work will be to provide both hardware interfaces and software coding in implementing the laboratory demonstration of the multiple IMU system.

### 1.3.1 Task III Work Effort

The hardware definition is determined principally by given laboratory facilities and available operating equipment. Figure 1.1, Proposed Test Configuration, shows the system as presently defined.

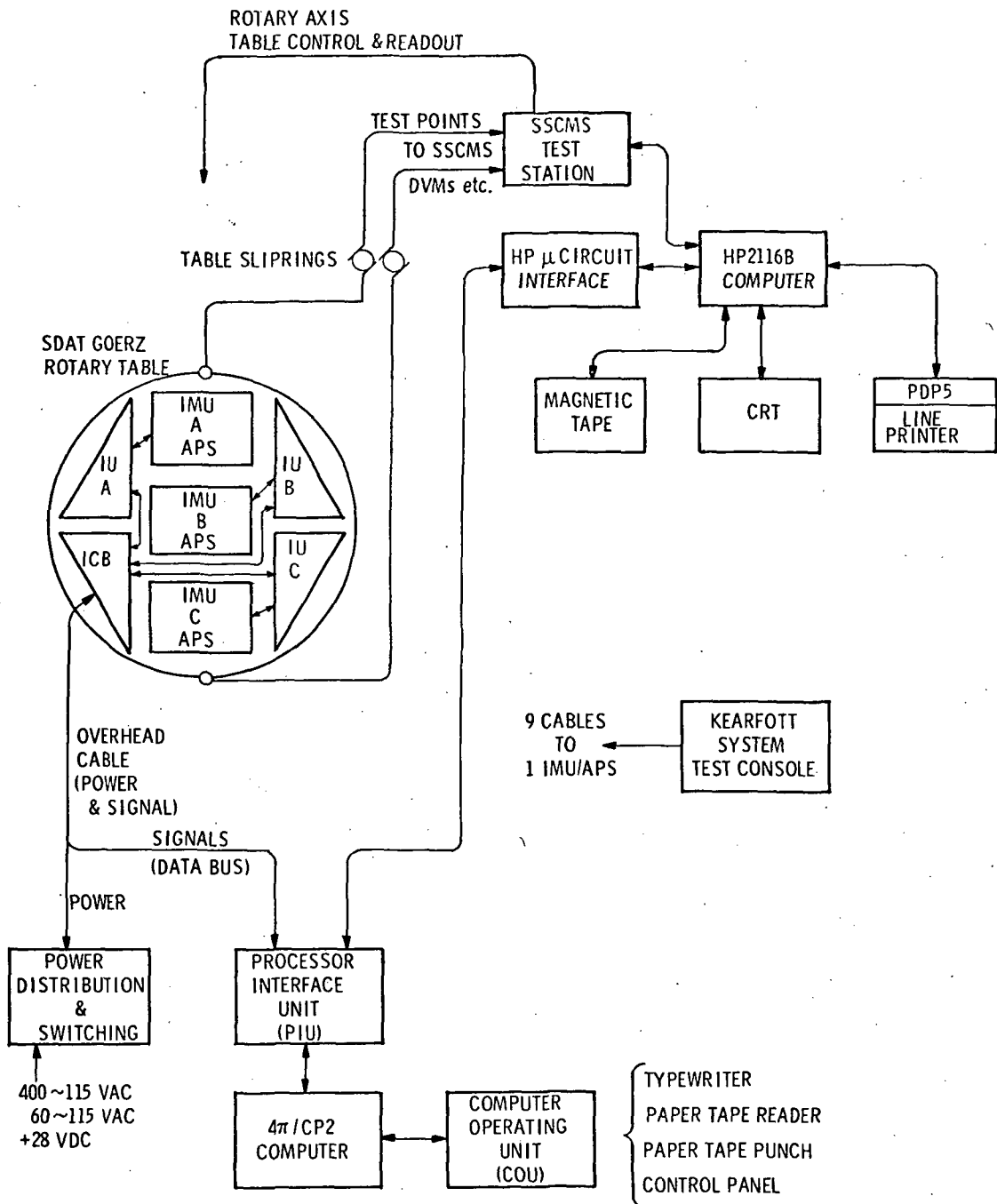
The system is based on three KT-70 IMUs with their adapter power supplies. These are mounted on a Goerz test table, together with three identical interface units (IU/SIUs) and an interconnect box for power and signal distribution. Overhead cables will be used for system power and data bus signals. Table slip rings will be used for analog signals to be recorded or displayed, such as system voltages and table angle information.

The data bus terminates at a rack mounted processor interface unit (PIU), the system's interface with the 4 $\pi$ -CP2 computer. Further, this PIU provides the digital link between the 4 $\pi$ -CP2 and the test station computer (HP 2116B).

### 1.3.2 Task IV Work Effort

Task IV comprises definition, design, coding and checkout of the operational software for the laboratory demonstration system. In addition, certain other software must be written: executive routines for the 4 $\pi$ -CP2, I/O routines and software interfacing with the HP2116B.

The system demonstration software will be organized in such a way as to contain a self-sufficient, independent software package for each major phase of the laboratory demonstration. This software will be assembled on a 360/75 using the IBM cross assembler. Initial testing will be performed on the 360/75 with a 4 $\pi$ -CP2 simulator. The majority of the software verification will be performed on the actual 4 $\pi$ -CP2 hardware using a single KT-70 IMU and the hardware interface developed under Task III. The laboratory demonstration system software will be modeled as close to possible shuttle system software requirements as possible.



- IU - CONTAINS IU, SIU, POWER SUPPLIES, SYNCHRO/DIGITAL CONVERTERS, TEST POINTS
- ICB - INTERCONNECT BOX  $\rightarrow$  DISTRIBUTION OF POWER & SIGNALS ON THE TABLE
- IMU/APS - ADAPTER POWER SUPPLY MOUNTED OVER IMU

Fig. 1:1 Proposed Test Configuration.



## 2.0 FAILURE DETECTION AND ISOLATION PHILOSOPHY

### 2.1 CURRENT APPLICATIONS OF FDI

Former space flight equipment, both manned and unmanned, has attempted to meet the stringent reliability requirements by use of a simplistic or primary/backup philosophy which utilized either ground or crew capability to judge the value of the outputs from each system and switch to such alternate systems, methods or plans as were available or could be contrived. The basic mission rule was to degrade mission goals with apparent equipment problems or to abort with a major equipment malfunction. Apollo provided several demonstrations of the effect of this philosophy on mission performance.

Similarly, airline use of inertial navigation equipment, even with dual or triple redundancy, relies almost entirely on the crew to provide FDI by monitoring and comparing the indications from the inertial navigators and from externally available sources of position and velocity data.

The basic philosophy of the Space Shuttle system of reusable launch and delivery vehicles is not compatible with either of the earlier approaches. Each mission phase is now required to have a fail operational capability. The rapid decision requirements of the critical shuttle mission phases require an advanced approach to FDI.

One method under active development utilizes an integral system of failure detection. In this method the output data from the Navigation and Control system is compared with precomputed mission reasonability limits. Reliability is provided by automatic transfer to a non-failed redundant system whenever the comparison exceeds preset values. Unfortunately, a performance degradation which could be critical for space shuttle mission safety will not be detected by simple reasonability limit comparisons.

A second stage in the development of FDI technology is exemplified in the SIRU system.<sup>2</sup> This system is a redundant strapdown mechanization utilizing gyroscopes and accelerometers mounted on six functional axes arranged in a dodecahedron array. The advantage of this arrangement for FDI results from the generation of a self contained FDI algorithm based on the output measurements of the individual instrument loops. This FDI algorithm automatically screens data to mission thresholds at the system update rate. The generation of an instrument operational status matrix then permits continuous data processing to a computational triad as transformed by a least squares solution. The FDI portion of the SIRU system has

been demonstrated in the laboratory environment to be capable of detecting and self-isolating performance degradations of less than  $0.375^{\circ}/\text{hr}$  (25  $\mu\text{eru}$ ) of gyro drift and  $0.1 \text{ cm}/\text{sec}^2$  of accelerometer bias. This FDI performance is achieved utilizing only 4% of the available computer time and 1600 words of memory on a DDP-516 computer. The corresponding algorithm update rate is twenty per second, which has been shown as satisfactory for the present dynamic models representative of the shuttle missions.<sup>3</sup> The redundant configuration of the SIRU system is capable of self contained failure detection and isolation of up to two each of the six gyroscopes and accelerometers and failure detection of a third instrument of each type. This FDI performance closely matches the needs of the space shuttle system.

## 2.2 SHUTTLE FDI REQUIREMENTS

Failure detection and isolation techniques employing redundant gimbal technology present a uniquely different problem when implemented at a level commensurate with Space Shuttle performance requirements. Basically, the gimbaled system output data consists of gimbal angle attitude and incremental inertial velocity information. Insight into the solution of the redundant gimbaled technology FDI problem may be gained by a close examination of the redundant strapdown system. In the SIRU system, gyroscope error drifts as well as accelerometer bias and scale factor errors are detected separately by independent gyroscope and accelerometer loop FDI implementations. In contrast, gimbal system gyroscope error drifts are reflected as changes in both the attitude and velocity output while accelerometer error sources appear directly in the velocity output only.

One other major difference between the redundant strapdown and redundant gimbaled problem involves the prelaunch and in-flight alignment sequence. In the fixed instrument geometry strapdown implementation, the FDI method is completely independent of either prelaunch or in-flight alignment requirements. In contrast, the redundant gimbaled system problem requires each IMU to be aligned independently. This independent gyrocompassing in pre-flight is the most accurate method available (without the direct use of optics) for aligning the stable member reference axes with respect to a known geographic coordinate frame. The gyrocompassing reference axis alignment can be further verified by comparing the azimuth attitude among inertial units using the available gimbal readout capability. Because of the large sensitivity of the inertial velocity information to the launch alignment accuracy, the FDI method employed is strongly influenced by initial alignment errors. This work assumes that the maximum error in azimuth between inertial system reference axes at launch is limited to the gimbal readout capability of the inertial measurement unit employed.

In addition to performance failure mechanization, hard failure detection methods are implemented for reasonability of incremental inertial velocity and attitude information. All failure FDI processing is time synchronized with the attitude control and navigation update rate requirements such that all data is screened and evaluated prior to processing.

### 2.3 IMU RELIABILITY VS. REDUNDANCY REQUIREMENTS

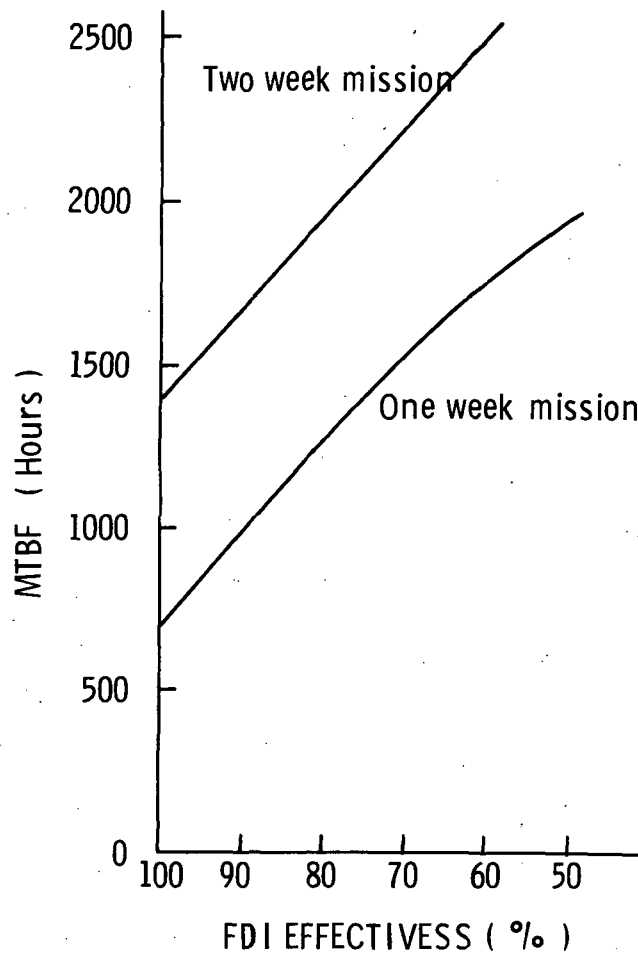
The actual implementation of all of these redundancy levels requires increasingly better IMU system performance parameters as the available redundant information decreases. For example, the required IMU performance necessary to operate with a two IMU skewed redundancy configuration is more severe than if four or three IMU redundancy were available and either configuration has more severe requirements than if a single IMU were specified to operate in a specific mission without redundancy. Indeed, this reasoning implies that the strictly "off-the-shelf" IMU technology may be more economically applied at the four or three IMU level (where performance requirements approach those required by a single IMU) than at the two IMU level where considerable performance improvements in present technology may be warranted. This type of tradeoff is, of course, limited by basic simplex IMU reliability since at some point further redundancy levels cannot improve overall system reliability.

Survival probabilities, that is, the probabilities of at least one IMU surviving, have been calculated and plotted for multiple IMU-systems used in one and two week shuttle missions. Imperfect FDI is assumed, with reliability of the FDI ranging from 50 to 100%.<sup>4</sup> Individual IMUs are assumed to have identical mean time between failure (MTBF) values. For this study, individual IMU MTBF varies over the range 0 to 2,500 hours. Initial configurations are 5,4,3,2 and single IMUs operating continuously in a parallel configuration.

FDI effectiveness of  $x\%$  is taken to mean that, if there is a failure, the probability that it is correctly found (detected and isolated) is given by  $(x/100)$ . Undetected and false detected failures imply mission failure.

Figure 2.1 presents the individual IMU MTBF in order to attain a mission success probability of 0.99 with a system consisting initially of three IMUs. It can be seen that, as FDI effectiveness decreases, the MTBF required for the individual IMU increases for both the 1 and 2 week mission. It should be emphasized when discussing MTBF values that the IMU MTBF is dictated by IMU performance screening to the required shuttle mission accuracy and is more than a hard failure history of the

Figure 2.1 - MTBF required for 0.99 Mission Success  
Probability for 3 IMU System, vs. FDI  
Effectiveness



component parts. Typical MTBF values assumed for the "off-the-shelf" systems being considered in this study, i.e. KT-70 and Carousel, are in the range of 1500 hours. In this case, a 0.99 probability of mission success may be attained with FDI effectiveness ratings of 98% and 70% for the two week and one week missions respectively. From this data, it should be observed that the probability of success margin for a given IMU MTBF is directly dependent upon the FDI effectiveness.

Figures 2.2 - 2.6 illustrate the probability of mission success vs. FDI effectiveness given the individual IMU MTBF values for systems consisting initially of 5, 4, 3, 2, and single IMUs, respectively. Several interesting observations can be made from these graphs. First, as the number of IMUs in a system increases, the probability of mission success for given individual IMU MTBF values generally increases. These increases can be seen to be largest in areas of high FDI effectiveness while even small decreases are seen with high MTBFs in areas of low FDI effectiveness. This phenomenon is due to the fact that an FDI algorithm with a low effectiveness level such as 50% will exhibit more false and missed failures in a system of N IMUs than in a system of N-1 IMUs. Thus, for a system of five IMUs with MTBF of 1000 hours, an FDI algorithm that is 50% effective yields a 2 week mission success probability of 0.88 while a system of four IMUs yields a mission success probability of 0.89.

Finally, it can be seen that for a 2 week mission, a system of three IMUs with an individual IMU MTBF value of 1000 hours will not yield a 0.99 probability of success even at a 100% FDI effectiveness. A system of four IMUs, on the other hand, as well as five IMUs, does meet this 0.99 success probability with MTBF values of 1000 hours. If a system of three IMUs is employed in the space shuttle, a minimum individual IMU MTBF of 1410 hours must be specified in order to attain a mission success probability of 0.99 for two week mission times.

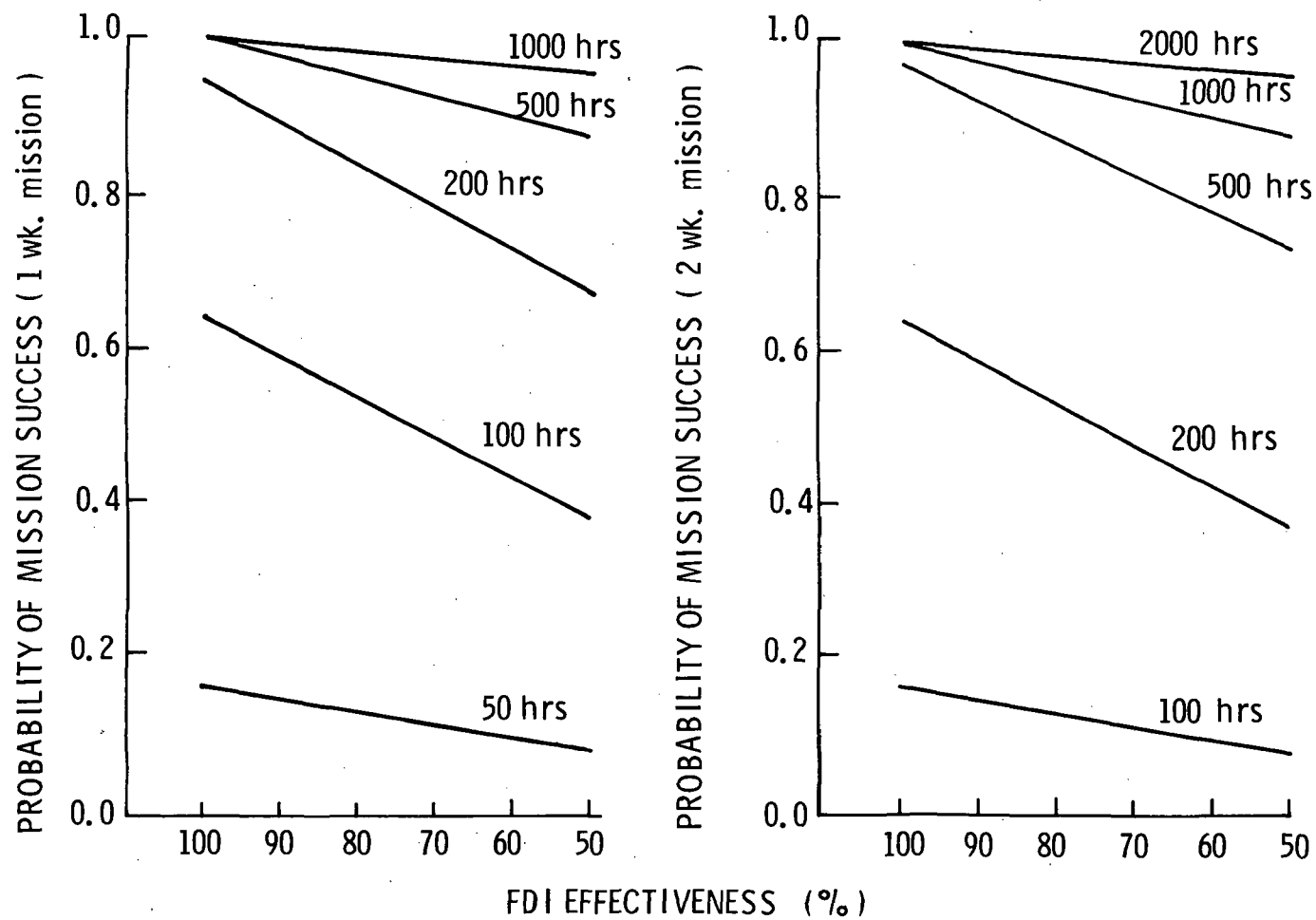


Figure 2.2 - Probability of Mission Success vs. FDI Effectiveness for a system of 5 IMUs Given Individual IMU MTBF

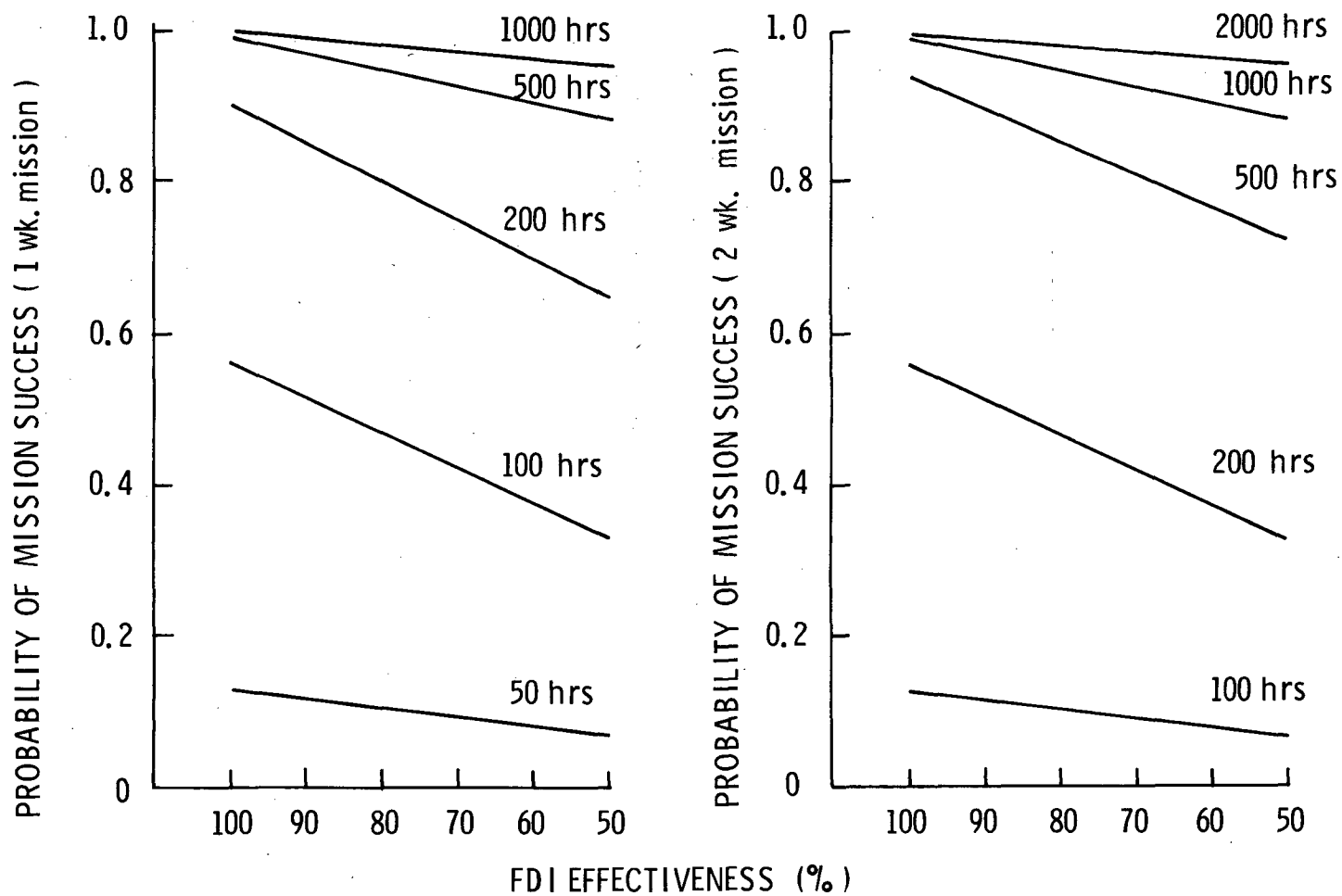
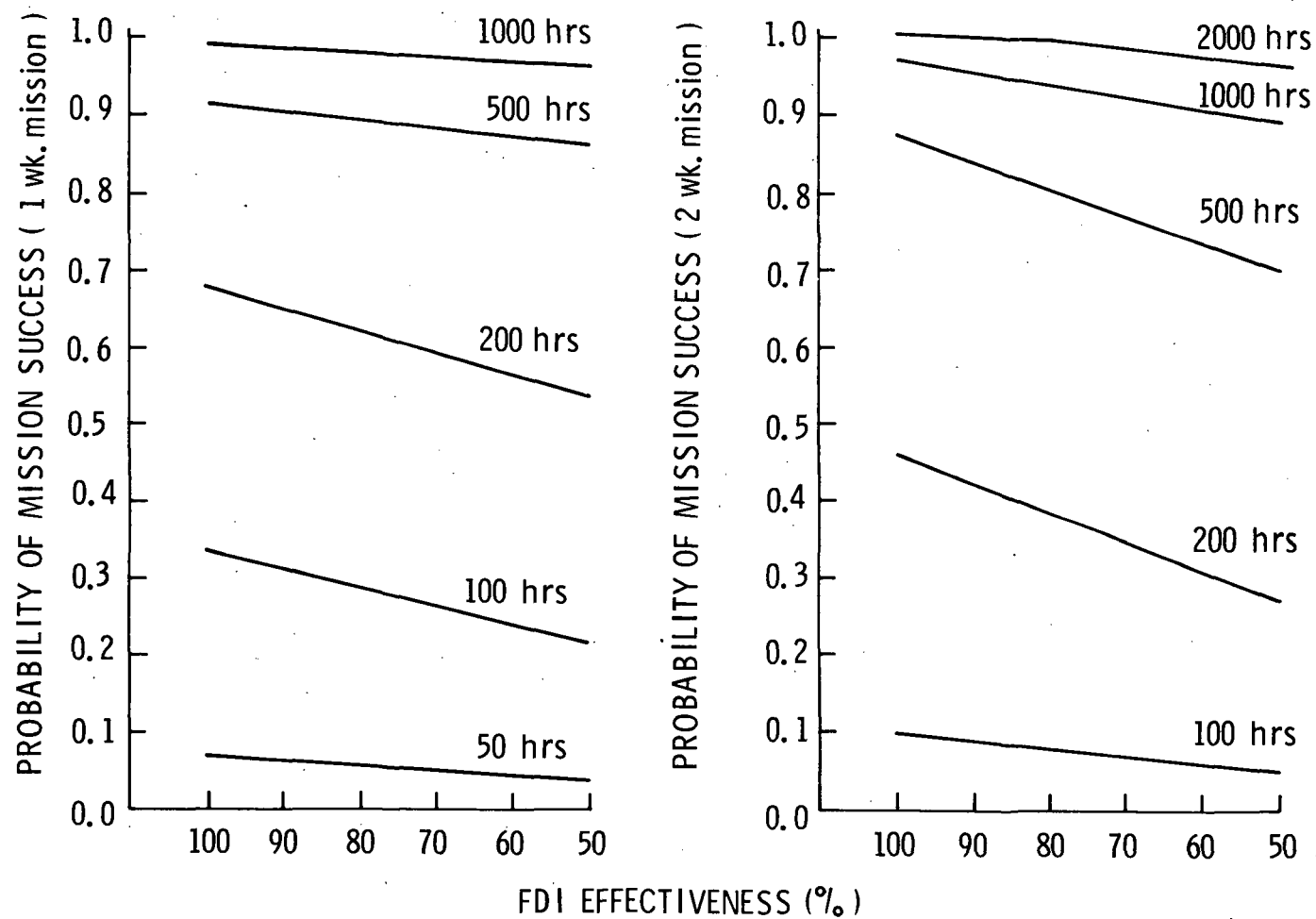


Figure 2.3 - Probability of Mission Success vs. FDI Effectiveness for a System of 4 IMUs Given Individual IMU MTBF



Figure 2.4- Probability of Mission Success vs. FDI Effectiveness for a System of 3 IMUs Given Individual IMU MTBF



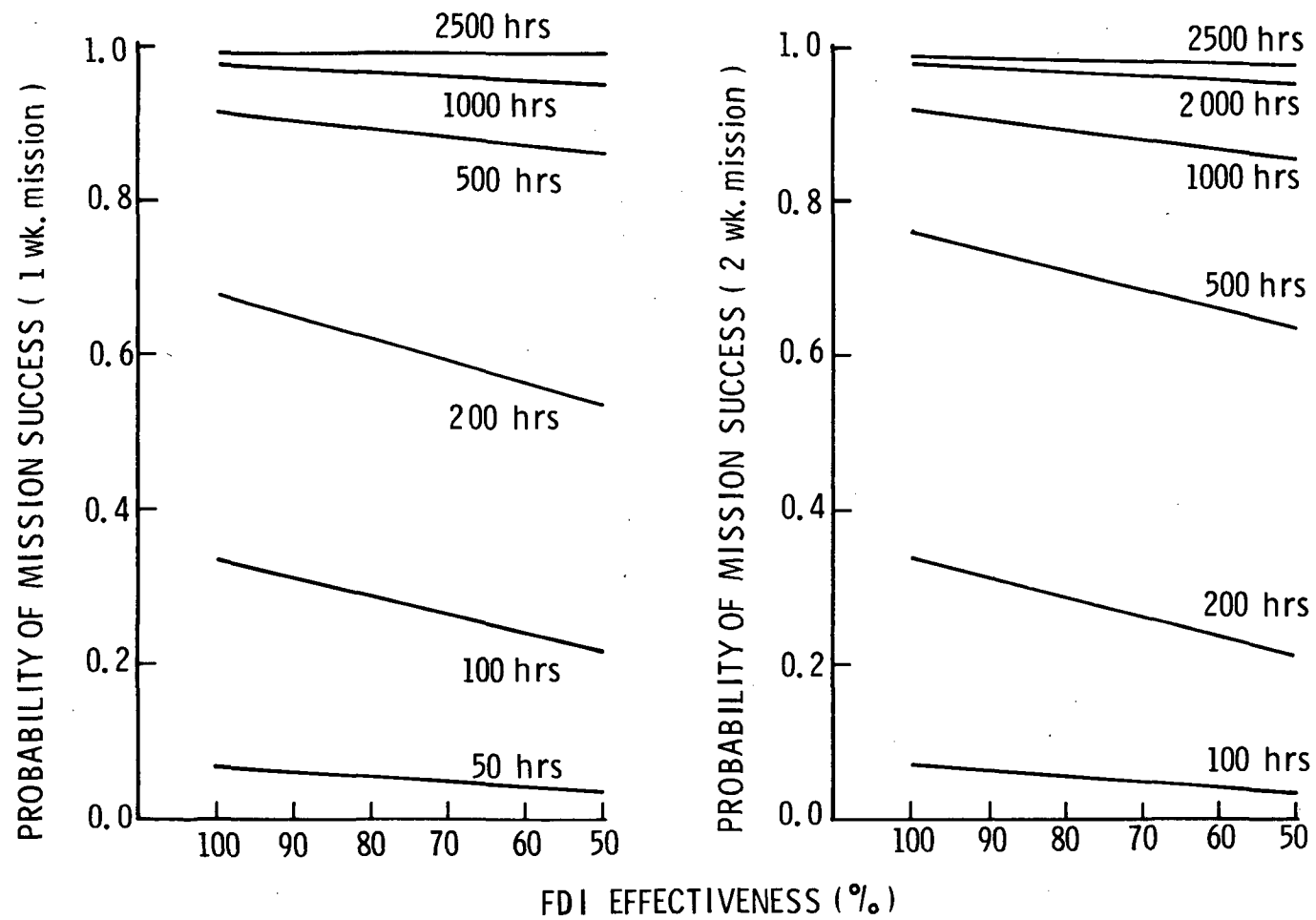


Figure 2.5 - Probability of Mission Success vs. FDI Effectiveness for a System of 2 IMUs Given Individual IMU MTBF

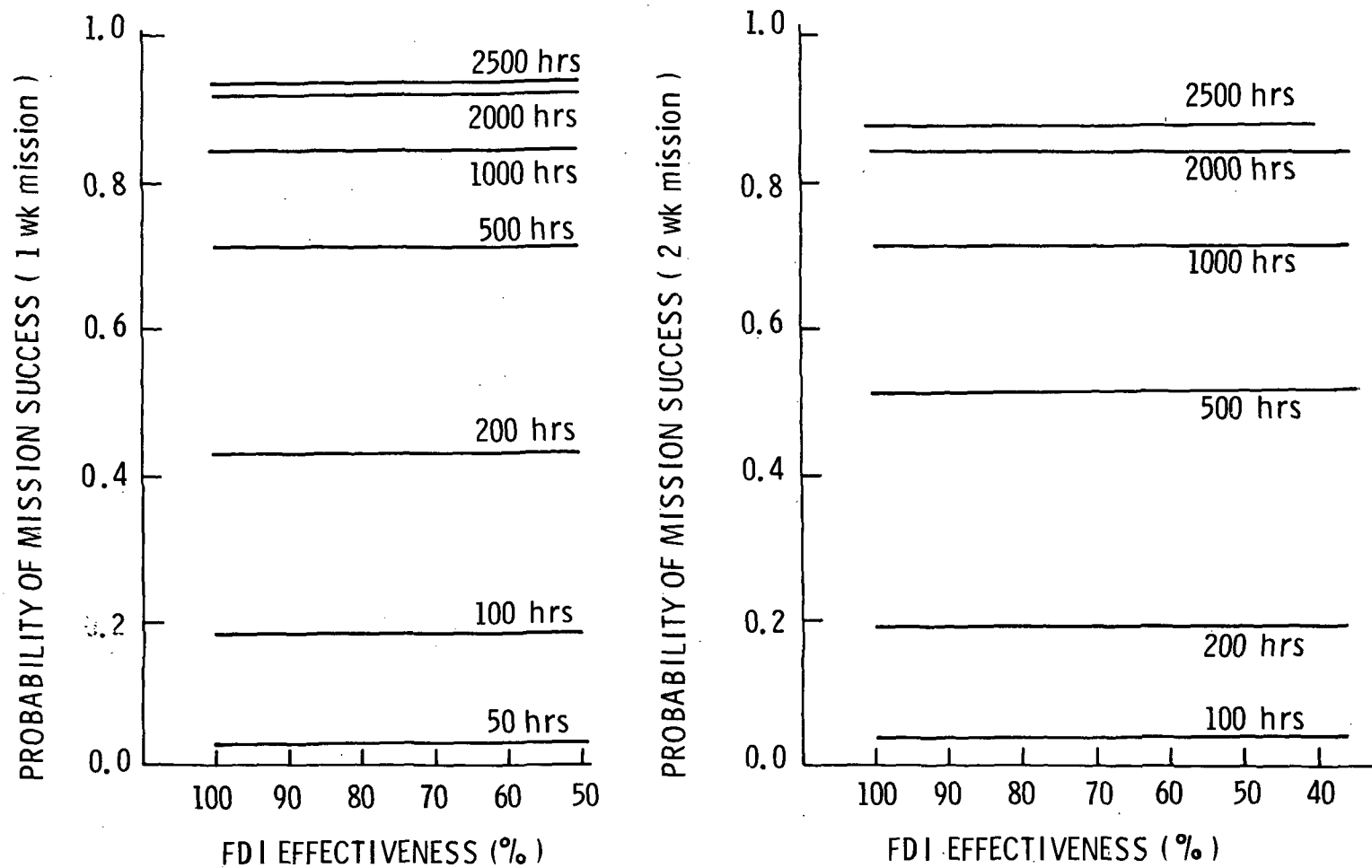


Figure 2.6 - Probability of Mission Success vs. FDI Effectiveness for a System of 1 IMU Given Individual IMU MTBF

### 3.0 FAILURE DETECTION AND ISOLATION EQUATION IMPLEMENTATION

#### 3.1 HARD FAILURE DETECTION AND ISOLATION

Historically, failure detection and isolation of faulty inertial measurement units has been accomplished on an instrument output level. Basically, the individual instrument output is checked for reasonableness within some predetermined output level limits. A study of all ground test failures experienced in the Apollo Primary G&N Inertial Measurement Unit has shown that electronic failure detection capability of this type would have isolated less than 30% of the total failures of a level presenting problems in the shuttle mission. The largest number of these undetected failures lie in the area of degraded instrument performance at a level unacceptable for shuttle requirements.<sup>5</sup>

It is clearly evident that a method must be developed to detect and isolate these performance failures. However, it is equally important that a hard fail, electronic monitor FDI method be implemented in the shuttle mission so as to detect and isolate any unreasonable  $\Delta\theta$  or  $\Delta V$  information prior to processing.

As stated before, implementation of the hard failure electronic monitor is done on a reasonability level. For example, the maximum slew rate expected during a normal boost phase in the shuttle mission is  $10^\circ/\text{sec}$ . If  $\Delta\theta$  indicated a rate higher than this, the IMU in question would be failed due to unreasonable data output.

$$\Delta\theta/\Delta t > R + \epsilon_A R \Rightarrow \text{HARD ATTITUDE FAIL} \quad (3-1)$$

Equation (3-1) represents the hard failure reasonability condition where  $R$  is the maximum expected mission angular rate, and  $\epsilon_A$  is a percentage tolerance limit for attitude maneuver.

A hard fail velocity scheme may be developed in much the same manner, i.e.,

$$\Delta V/\Delta t > f + \epsilon_V f \Rightarrow \text{HARD VELOCITY FAIL} \quad (3-2)$$

where  $f$  represents the maximum specific force expected on the shuttle mission and  $\epsilon_V$  represents a percentage tolerance level.

The choice of  $\epsilon_A$  and  $\epsilon_V$ , the percentage tolerance levels for attitude and velocity hard failure detection, must be tempered by inherent IMU noise characteristics

such a quantization. For example, at maximum specific force inputs, an uncertainty in accelerometer bias of 5 standard deviations should not signal a hard failure.

For the test laboratory demonstration proposed in Task II of this study, a maximum specific force of 1g is seen by the instrument package. Thus, a hard fail detect criterion may be presented as

$$(\Delta V_x^2 + \Delta V_y^2 + \Delta V_z^2)^{1/2} / \Delta t - 1 g > \epsilon_v \quad (3-3)$$

where  $\Delta V_x$ ,  $\Delta V_y$ , and  $\Delta V_z$  represent incremental accelerometer outputs on the x, y, and z stable member axes.

The hard fail electronic monitors of critical signal levels presently used for detection and isolation are employed by the failure management logic to permit an additional decision level to exist, but are not used as a substitute for any performance failure detection and isolation level.

In addition to supplementary IMU status information from electronic hard failure detection, a hard failure logic level in the computer is implemented to insure data validity. Gimbal angle readout and incremental velocity information must be verified for reasonability with respect to maximum expected levels prior to any attitude control or navigation updates. Both of these hard failure detection implementations serve as additional detection and isolation information to permit better management and thus provide more reliability in the parallel performance failure detection and isolation software processing.

### 3.2 SOFT FAILURE DETECTION AND ISOLATION EQUATION DEVELOPMENT

#### 3.2.1 Velocity FDI Equations

The velocity failure detection and isolation equations developed here are consistent with realizable redundancy management techniques.<sup>6</sup> To begin with, assume that available information consists of a velocity vector in stable member coordinates from each operational IMU. An average velocity vector may then be formed as:

$$\underline{V}_{AVE} = \sum_{i=1}^N \underline{V}_i / N \quad (3-4)$$

This average velocity vector is used as an estimate of the true velocity state of the vehicle. Thus, it will be used as the navigation velocity by the on-board computer

for steering updates. Therefore, it will be necessary for all failure detection and isolation logic to occur prior to acceptance of the average velocity vector as an acceptable multiple system solution.

In order to detect the presence of a failure, a velocity error of each IMU is established with respect to the average velocity vector.

$$\underline{V}_{E_i} = \underline{V}_{AVE} - \underline{V}_i \quad (3-5)$$

This velocity error vector is an indication of the performance of one IMU with respect to all operational IMUs.

A problem is immediately realized here in that the allowable performance (velocity) error will be a function of both mission phase and time into the mission. In order to desensitize the error velocity vector to these two variables, equation (3-5) is normalized with respect to the total average velocity.

$$\underline{V}_{ER_i} = \frac{\underline{V}_{E_i}}{|\underline{V}_{AVE}|} \quad (3-6)$$

This term, identified as the error ratio, is not directly mission or mission time dependent. Equation (3-6) may be written in index notation as:

$$V_{ER_{ij}} = \frac{V_{E_{ij}}}{|V_{AVE}|} \quad (3-7)$$

where i indicates the IMU, and j the stable member axis.

A total squared error may now be defined for each stable member axis as:

$$V_{ET_j}^2 = \sum_{i=1}^N V_{ER_{ij}}^2 \quad (3-8)$$

Detection of a failure occurs when this total squared error exceeds a constant known as the detection constant.

$$V_{ET_j}^2 > K_{D_j} \Rightarrow \text{DETECTION} \quad (3-9)$$

It must be recalled now that the error velocity vector was defined for each IMU as:

$$\underline{V}_{E_i} = \underline{V}_{AVE} - \underline{V}_i \quad (3-10)$$

Substituting equation (3-4) into equation (3-10) gives:

$$\underline{V}_{E_i} = \sum_{k=1}^N \frac{\underline{V}_k}{N} - \underline{V}_i \quad (3-11)$$

or for a system of four IMUs:

$$\underline{V}_{E_i} = \frac{\underline{V}_1 + \underline{V}_2 + \underline{V}_3 + \underline{V}_4}{4} - \underline{V}_i \quad (3-12)$$

It can be seen immediately from equation (3-12) that a bias is introduced into the calculation of the error velocity for each IMU due to the definition of the average velocity vector, e.g. for  $i=1$

$$\underline{V}_{E_1} = \frac{\underline{V}_2 + \underline{V}_3 + \underline{V}_4}{4} - \frac{3}{4} \underline{V}_1 \quad (3-13a)$$

The true definition of  $\underline{V}_{E_1}$  without bias in the measurement, is:

$$\underline{V}'_{E_1} = \frac{\underline{V}_2 + \underline{V}_3 + \underline{V}_4}{3} - \underline{V}_1 \quad (3-13b)$$

The relationship between  $\underline{V}_{E_1}$  and  $\underline{V}'_{E_1}$  can be expressed as:

$$\underline{V}_{E_1} = \frac{4}{3} \underline{V}'_{E_1} \quad (3-13c)$$

Thus, the bias is seen to be  $4/3$  for a system consisting of four IMUs. More generally, the bias may be expressed as  $(N/N-1)$  for a system of  $N$  operational IMUs. In this manner, equation (3-9) must be modified to compensate for this inherent bias.

$$V_{ET_j}^2 > \left( \frac{N-1}{N} \right) K_{D_j} \quad (3-14)$$

Equation (3-14) represents the true detection condition for a system of  $N$  operational IMUs.

Isolation of a detected failure is accomplished by measuring the error of each IMU on an axis by axis basis with respect to the total squared error derived in equation (3-8).

$$\frac{V_{ER_{ij}}^2}{V_{ET_j}^2} > K_I \Rightarrow \text{ISOLATION} \quad (3-15)$$

If a major part of the total squared error can be attributed to any one IMU, then a failure has been isolated. The choice of an isolation constant to implement this



logic decision must be based on several factors including the number of IMUs in the system and the acceptable signal to noise ratio.

A logic flow chart of the velocity soft failure detection and isolation method is shown in Figure 3.1.

### 3.2.2 Attitude FDI Equations

The attitude failure detection and isolation equations developed here are expressly tailored to a four-gimbal IMU, such as the KT-70. However, implementation of the technique to more conventional three-gimbal IMUs presents no problem. To begin with, it is assumed that the only information available from each of the IMUs is the gimbal angles. Using these gimbal angles, a quaternion may be developed which represents a rotation from the navigation base to the stable member platform.

$$Q_{B_i}^{SM} = Q_{0_i} Q_{1_i} Q_{2_i} Q_{3_i} \quad (3-16)$$

where  $Q_{0_i}$ ,  $Q_{1_i}$ ,  $Q_{2_i}$ ,  $Q_{3_i}$  are quaternion representations of the four gimbal angles for the  $i^{th}$  IMU. It is assumed here no fixed attitude misalignment transformations are used to maintain the calibration of each IMU.<sup>7</sup> This is critical in the two IMU problems presented in section 3.2.3.

Since the quaternion developed in equation (3-16) may be represented as:

$$Q_{B_i}^{SM} = \cos\left(\frac{\theta_i}{2}\right) + i_x \sin\left(\frac{\theta_{x_i}}{2}\right) + i_y \sin\left(\frac{\theta_{y_i}}{2}\right) + i_z \sin\left(\frac{\theta_{z_i}}{2}\right) \quad (3-17)$$

a rotation vector may be defined as:

$$R_{B_i}^{SM} = i_x \theta_{x_i} + i_y \theta_{y_i} + i_z \theta_{z_i} \quad (3-18)$$

It must be noted here that the rotation vector,  $R_{B_i}^{SM}$  is essentially a set of Euler angle rotations and, as such, will be represented as a vector for convenience sake only.

An average rotation vector may then be defined as:

$$R_{AVE} = \sum_{i=1}^N \frac{R_{B_i}^{SM}}{N} \quad (3-19)$$

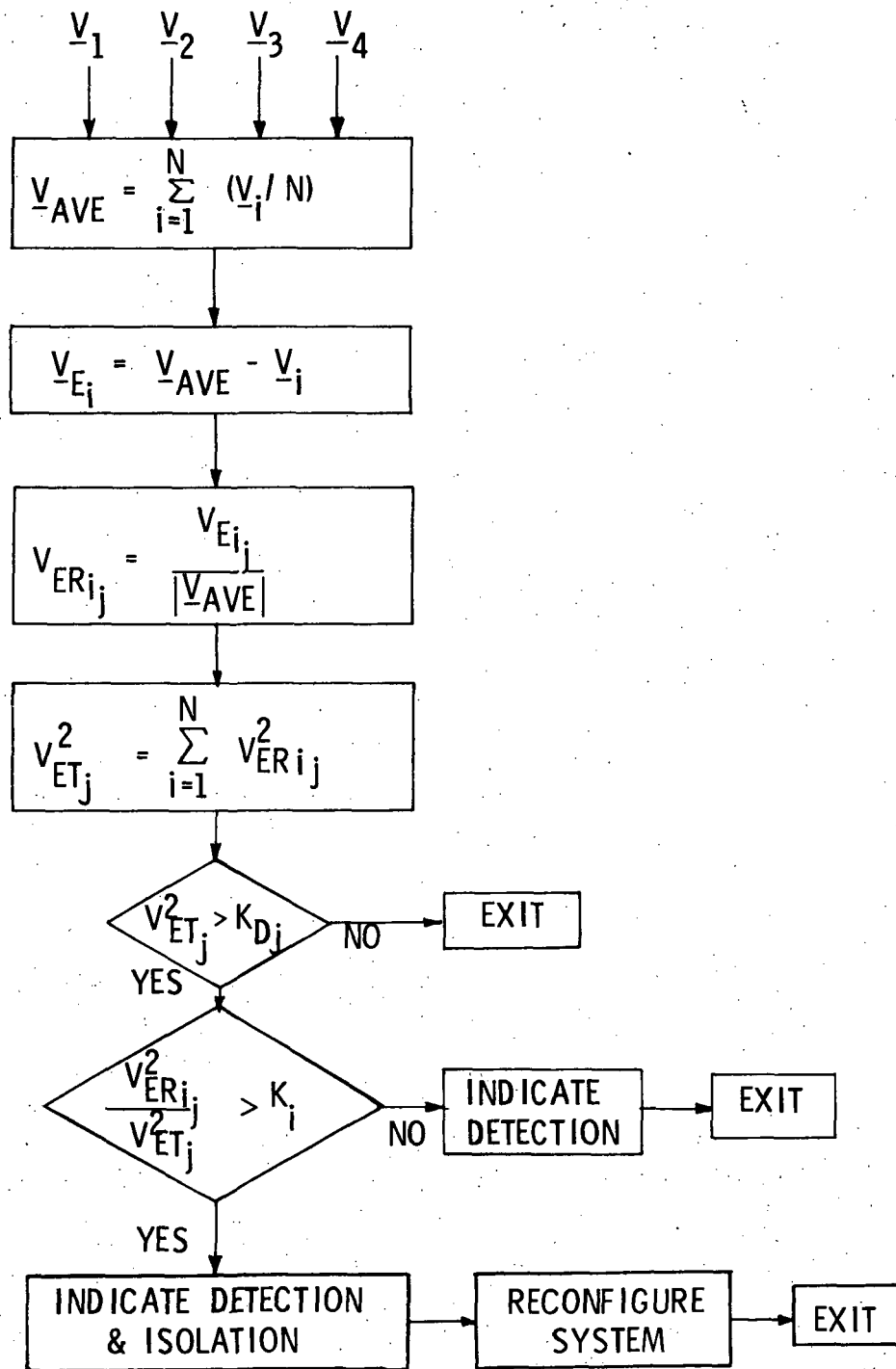


Figure 3.1 - Logic Flow Chart of Velocity FDI Technique (Powered Flight)

In order to perform vector functions,  $\underline{R}_{AVE}$  must be transformed into quaternion form, i.e.

$$Q_{AVE} = \cos\left(\frac{\theta_{AVE}}{2}\right) + i_x \sin\left(\frac{\theta_{xAVE}}{2}\right) + i_y \sin\left(\frac{\theta_{yAVE}}{2}\right) + i_z \sin\left(\frac{\theta_{zAVE}}{2}\right) \quad (3-20)$$

An error quaternion may now be developed as:

$$Q_{E_i} = Q_{AVE}^* Q_i \quad (3-21)$$

where

$$Q_{AVE}^* = \cos\left(\frac{\theta_{AVE}}{2}\right) - i_x \sin\left(\frac{\theta_{xAVE}}{2}\right) - i_y \sin\left(\frac{\theta_{yAVE}}{2}\right) - i_z \sin\left(\frac{\theta_{zAVE}}{2}\right) \quad (3-22)$$

It is once more convenient to return to rotation vector form for the detection and isolation process. Therefore, let

$$\underline{R}_{E_i} = i_x \theta_{x_{E_i}} + i_y \theta_{y_{E_i}} + i_z \theta_{z_{E_i}} \quad (3-23)$$

from equation (3-21).

The error rotation vector information is stored in the computer so that time histories of the vector may be established. In this manner, a drift vector may be defined as

$$\underline{DRIFT}_i = (\underline{R}_{E_i} - \underline{R}_{ELAST_i}) / \Delta t \quad (3-24)$$

where  $i$  indicates the IMU and  $\Delta t$  the time step between measurement of  $\underline{R}_{E_i}$  and  $\underline{R}_{ELAST_i}$

By defining the attitude error in terms of a drift rate rather than a whole angle, problems involving absolute attitude accuracy are relieved. This is especially important in an IMU with inherently poor gimbal readout chains.

A total squared error may now be derived from equation (3-24) as

$$DRIFT_T^2_j = \sum_{i=1}^N DRIFT_{i_j}^2 \quad (3-25)$$

where  $j$  represents the stable member axes and  $i$  the IMU.

Detection of a failure is accomplished by comparing the total squared error developed in equation (3-25) to a predefined detection constant based on maximum performance deviations allowable in the system.

$$DRIFT_T^2_j > K_{D_j} \quad (3-26)$$

As with the velocity failure detection method presented earlier, a bias is introduced in the total squared error shown in equation (3-25) due to the definition of the average rotation vector. Thus, equation (3-26) must be implemented as

$$\text{DRIFT}_{T_j}^2 > \left( \frac{N-1}{N} \right) K_{D_j} \Rightarrow \text{DETECTION} \quad (3-27)$$

Isolation of a detected failure is accomplished, as with the velocity FDI technique, by measuring the error of each IMU, on an axis by axis basis, with respect to the total squared error.

$$\frac{\text{DRIFT}_{i_j}^2}{\text{DRIFT}_{T_j}^2} > K_I \Rightarrow \text{ISOLATION} \quad (3-28)$$

Like the velocity FDI scheme, the choice of an isolation constant is based on the number of operational IMUs in the system and the acceptable signal to noise ratio. Theory behind the choice of a proper isolation constant is presented later.

A logic flow chart of the attitude failure detection and isolation scheme is shown in Figure 3.2. Notice, the logic of both methods implemented when error detection without the subsequent isolation occurs is to recycle and reverify the detection condition. This is the circumstance when simultaneous large errors occur on the same IMU axis. It is exactly this circumstance for which a higher level of redundancy management must be implemented using the performance failure, hard failure, other possible subsystem information and experience on the implemented systems to form an operating method acknowledging two simultaneous IMU axis errors.

### 3.2.3 Two IMU FDI Equations

Failure detection and isolation in a system consisting of two colinear gimbale IMUs such as the KT-70 presents a unique problem not encountered in a system of three or four colinear IMUs. This problem exists because, while detection of soft failures is possible by means already presented herein, isolation of the detected failure cannot be accomplished. The problem is circumvented by taking the approach outlined earlier, i.e., skew one IMU with respect to the other by an optimum Euler angle rotation. In this manner, although only two gimbale systems are employed, enough redundant data is available to properly isolate any detected failure.

To begin with, assume that available information consists of a velocity vector from each operational IMU (two in number) in its respective stable member platform coordinates. Since the two IMUs are skewed with respect to each other by a known

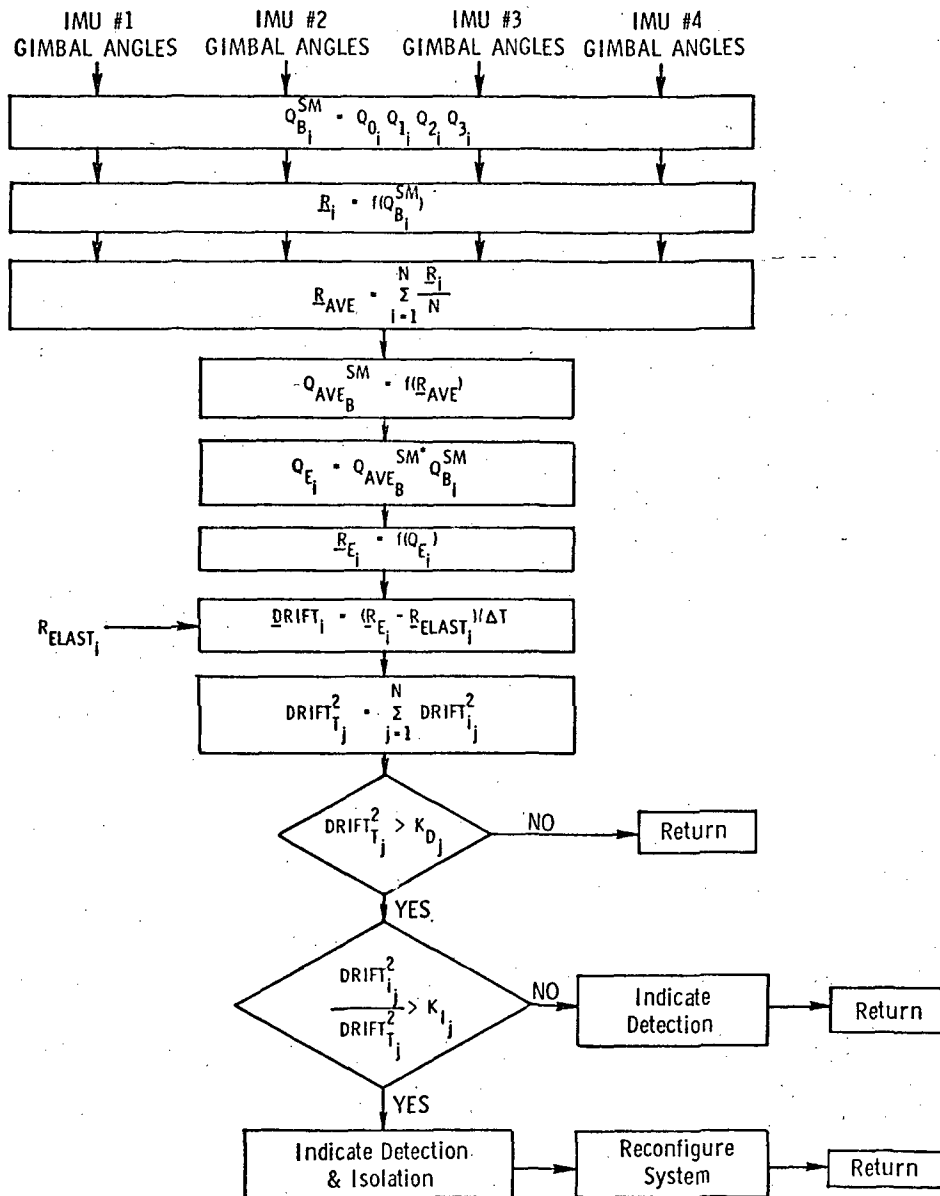


Figure 3.2 - Attitude Soft Failure Detection and Isolation Logic (Unpowered Flight)

rotation vector the relationship between the two velocity vectors may be represented ideally as:

$$\underline{V}_1 = q_0 \underline{V}_2 q_0^* \quad (3-29)$$

where  $\underline{V}_1$  is the velocity vector from IMU<sub>1</sub>,  $\underline{V}_2$  is the velocity vector from IMU<sub>2</sub>, and  $q_0$  is a quaternion representation of the Euler angle transformation from IMU<sub>2</sub> stable member coordinates to IMU<sub>1</sub> stable member coordinates.

Given this velocity information, detection of an accelerometer failure may be accomplished by utilizing the magnitude difference of the two vectors, i.e.,

$$V_E^2 = \left( \left| \underline{V}_1 \right| - \left| \underline{V}_2 \right| \right)^2 \quad (3-30)$$

where  $V_E^2$  is a scalar representative of the total velocity error magnitude. To avoid any direct dependence upon the mission being flown, it is convenient to normalize  $V_E^2$  by the total squared average velocity, i.e.  $\underline{V}_1 \underline{V}_2$ . Detection of a failure in the velocity chain is then accomplished by comparing the normalized squared error velocity to a pre-determined detection constant.

$$\frac{V_E^2}{\left| \underline{V}_1 \right| \left| \underline{V}_2 \right|} > K_{DV} \Rightarrow \text{DETECTION} \quad (3-31)$$

If this scalar exceeds the detection constant, then an attempt to isolate the faulty IMU is made. If not, attitude failure detection and isolation logic is entered to check the status of all gyroscopes. The flow of this logic can be seen in Figures 3.3a and 3.3b.

To isolate a detected accelerometer failure, two velocity error vectors are formed.

$$\underline{VE}_1 = \underline{V}_1 - q_0 \underline{V}_2 q_0^* \quad (3-32a)$$

$$\underline{VE}_2 = \underline{V}_2 - q_0^* \underline{V}_1 q_0 \quad (3-32b)$$

In equation (3-32a),  $\underline{V}_2$  is computationally transformed into a coordinate system colinear with that of IMU<sub>1</sub>. In this manner,  $\underline{VE}_1$  is a vector representative of the velocity error in IMU<sub>1</sub>. Similarly,  $\underline{VE}_2$  is a vector representative of the velocity error in IMU<sub>2</sub>. If an accelerometer failure has occurred, then a major portion of the magnitude of either  $\underline{VE}_1$  or  $\underline{VE}_2$  will lie along a single stable member axis. For example, if an accelerometer failure has occurred on the Y-axis of IMU<sub>1</sub>, then a large part of the magnitude of  $\underline{VE}_1$  will lie along the Y-axis. In a similar manner, while this same failure would cause a theoretically identical error in magnitude

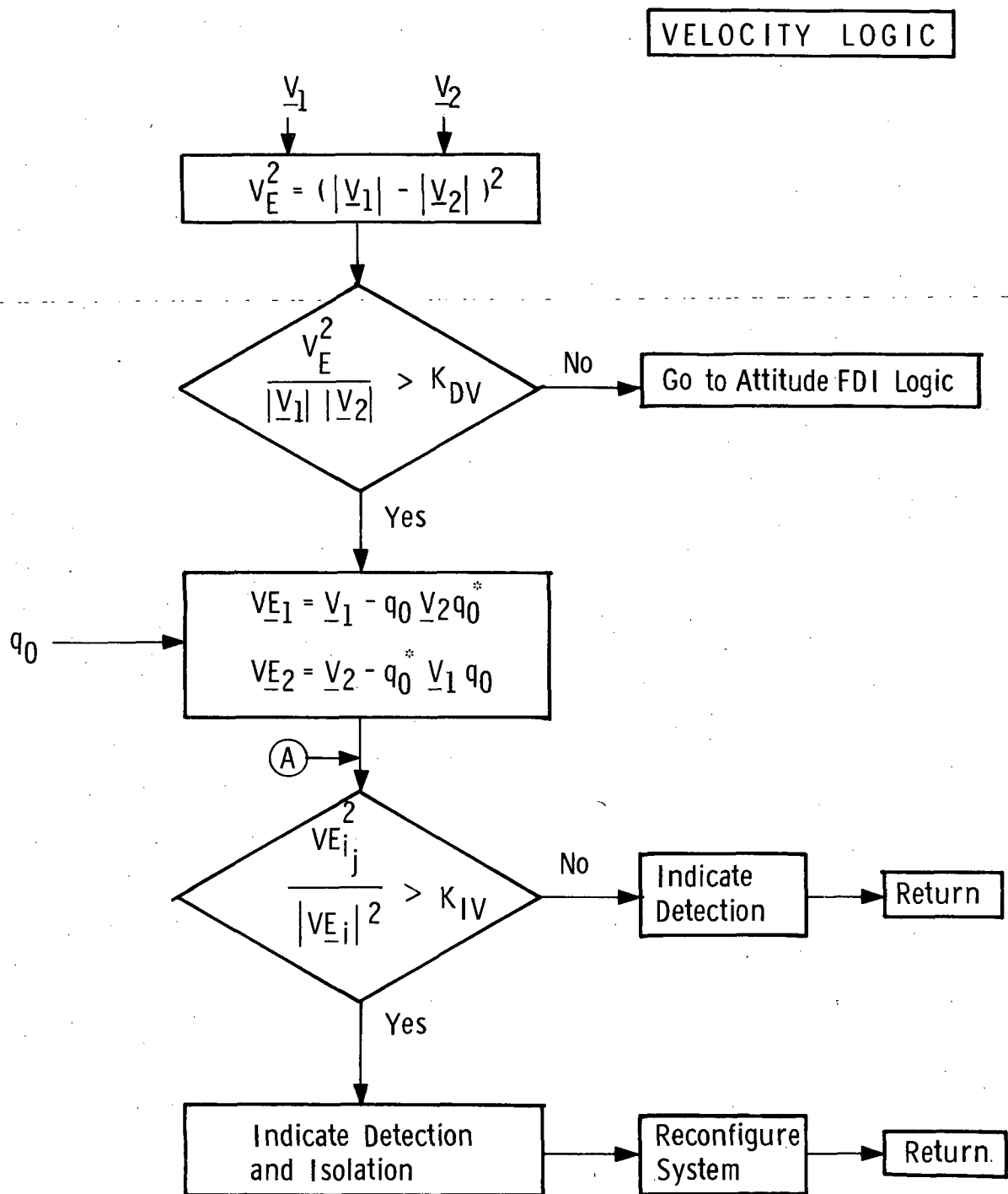


Figure 3.3a - Two IMU Failure Detection and Isolation, Velocity Logic (Powered Flight)



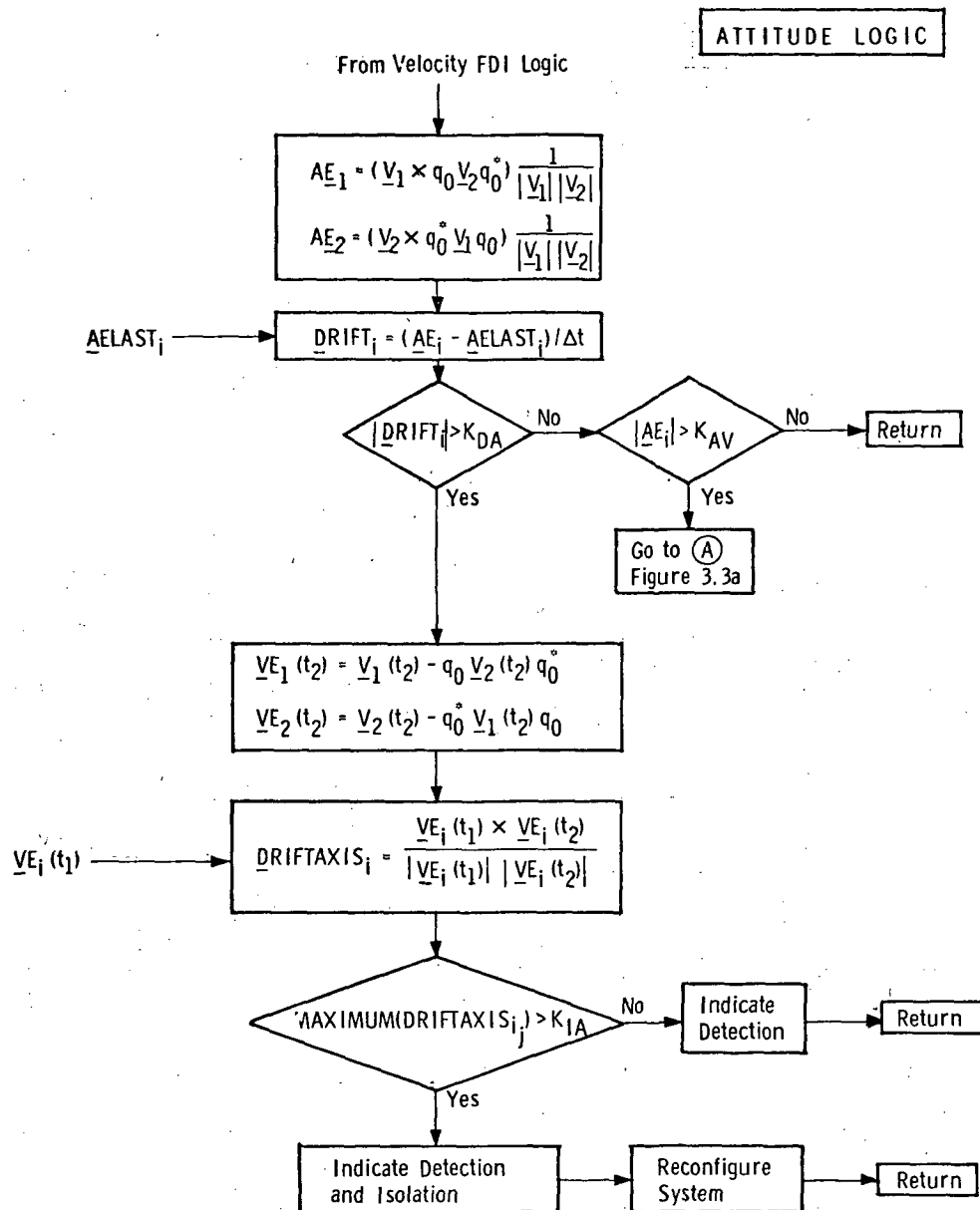


Figure 3-3b. Two IMU Failure Detection and Isolation, Attitude Logic (Powered Flight)

of  $\underline{VE}_2$  however, no major portion of this error would lie along any one stable member axis in IMU<sub>2</sub>. This is because the two IMUs are skewed with respect to each other and therefore have no two axes colinear.

To increase the sensitivity of the velocity error vector, a squared error ratio is formed as:

$$\frac{VE_{ij}^2}{|\underline{VE}_i|^2} > K_{IV} \quad (3-33)$$

where  $K_{IV}$  represents an isolation constant. Choice of the proper isolation constant must be made with respect to actual system signal to noise considerations.

Detection of a gyroscope failure in powered flight is accomplished in a manner similar to that of the accelerometer failure just described. To begin with, a dimensionless attitude error unit vector is derived for each IMU.

$$\underline{AE}_1 = \left( \underline{V}_1 \times q_o \underline{V}_2 q_o^* \right) \frac{1}{|\underline{V}_1| |\underline{V}_2|} \quad (3-34a)$$

$$\underline{AE}_2 = \left( \underline{V}_2 \times q_o^* \underline{V}_1 q_o \right) \frac{1}{|\underline{V}_1| |\underline{V}_2|} \quad (3-34b)$$

In this manner,  $\underline{AE}_1$  is representative of an error rotation in IMU<sub>1</sub> stable member coordinates and  $\underline{AE}_2$  is representative of an error rotation in IMU<sub>2</sub> stable member coordinates.

Detection of a gyro failure is accomplished by employing the attitude errors derived in equations (3-34a) and (3-34b). A drift vector is defined for each IMU as:

$$\underline{DRIFT}_i = (\underline{AE}_i - \underline{AE}_{LAST_i}) / \Delta t \quad (3-35)$$

In this manner, detection can be based on an acceptable level of drift rather than whole error angles.

$$\underline{DRIFT}_{ij} > K_{DA} \rightarrow \text{DETECTION} \quad (3-36)$$

Isolation of a detected gyroscope failure is done so as to locate the direction of the maximum drift vector. A velocity error vector is formed for each IMU in its

respective stable member reference frames after gyro torquing is completed.

$$\left. \begin{aligned} \underline{VE}_1(t_1) &= \underline{V}_1(t_1) - q_0 \underline{V}_2(t_1) q_0^* \\ \underline{VE}_2(t_1) &= \underline{V}_2(t_1) - q_0^* \underline{V}_1(t_1) q_0 \end{aligned} \right\} \quad \begin{aligned} (3-37a) \\ (3-37b) \end{aligned}$$

These velocity error vectors are formed after skewing is completed so as to eliminate any gyro torquing scale factor errors which may be inherent in the system. This is important since typical gyro torquing scale factor errors are specified to be quite large for the Kearfott KT-70 IMU.

At the time an unacceptable drift is detected (equation (3-36)), another velocity error vector is formed for each IMU in its respective stable member reference frame.

$$\left. \begin{aligned} \underline{VE}_1(t_2) &= \underline{V}_1(t_2) - q_0 \underline{V}_2(t_2) q_0^* \\ \underline{VE}_2(t_2) &= \underline{V}_2(t_2) - q_0^* \underline{V}_1(t_2) q_0 \end{aligned} \right\} \quad \begin{aligned} (3-38a) \\ (3-38b) \end{aligned}$$

The stable member axis exhibiting the maximum gyro drift over the time interval  $(t_2 - t_1)$  may now be found by crossing the two velocity error vectors as

$$DRIFTAXIS_1 = \left| \frac{\underline{VE}_1(t_1) \times \underline{VE}_1(t_2)}{|\underline{VE}_1(t_1)| |\underline{VE}_1(t_2)|} \right| \quad (3-39a)$$

$$DRIFTAXIS_2 = \left| \frac{\underline{VE}_2(t_1) \times \underline{VE}_2(t_2)}{|\underline{VE}_2(t_1)| |\underline{VE}_2(t_2)|} \right| \quad (3-39b)$$

The theory behind use of equation (3-39a) and (3-39b) is that maximum velocity deviations over the time interval  $(t_2 - t_1)$  will lie in a plane perpendicular to the maximum gyro drift. The cross product of these two velocity error vectors will, therefore, identify the axis of drift over the time interval  $(t_2 - t_1)$ . The maximum component of the vectors  $DRIFTAXIS_1$  and  $DRIFTAXIS_2$  isolates the faulty gyroscope and thus the faulty IMU.

$$MAXIMUM (DRIFTAXIS_{ij}) > K_{IA} \Rightarrow ISOLATION \quad (3-40)$$

It must be noted here that the isolation technique presented above is valid only when a drift detection has been positively identified. Probability limits as to the decision of a failure are inherent in the isolation constant. As with all previous

choices of the isolation constant, signal to noise consideration must be taken into account.

One further failure detection condition must be introduced into the two IMU FDI problem to check the IMU attitude error. If a large attitude error is present, the velocity FDI technique will not detect it because no great difference in magnitudes will exist. Further, the attitude FDI technique will not detect it because no drift is occurring. However, the presence of the large IMU attitude error is capable of failing mission performance criteria and therefore must be considered.

In order to detect an unacceptable IMU attitude error the whole-angle offset between the two velocity vectors is defined as

$$\text{PHI} = \left| \frac{\underline{V1} \times \underline{V2}}{|\underline{V1}| |\underline{V2}|} \right| \quad (3-41)$$

If PHI exceeds a whole angle detection constant  $K_{AV}$ , an unacceptable IMU attitude error has been detected, i.e.

$$\text{PHI} > K_{DV} \rightarrow \text{DETECTION} \quad (3-42)$$

Isolation of a detected failure is done in a manner exactly as all other velocity failures (equation (3-36)). It should be noticed here that a preferred order of detection is presented as:

1. velocity magnitude error,
2. drift errors, and
3. whole angle errors between velocity vectors.

This preferred order has been established so as to minimize isolation problems. For example, certain accelerometer performance errors could cause a drift failure detection condition. Isolation of this failure would be difficult by anything other than the velocity vector comparison outlined in equations (3-33) to (3-36). First priority should always be a magnitude check, then drift, and finally whole angle offset for IMU attitude errors.

### 3.3 ISOLATION THEORY

Choice of a proper isolation constant, as stated earlier, involves the consideration of two major items, i.e. signal to noise ratio and the number of operational IMUs

in the system. Signal to noise ratio, in this context, represents the ratio of the error signal from a single IMU to be isolated to the magnitude of the normally expected uncompensated parameter uncertainties from all other operational IMUs in the system. Figures 3.4 and 3.5 illustrate the relationship between all possible isolation constants and error signal to noise ratios for redundant systems employing four and three operational IMUs respectively. It can be seen that the choice of a proper isolation constant is well bounded by the probability of missing true failures and the probability of isolating false failures. Further, an area controlled by instrument noise is evident at low error signal to noise ratios. This phenomenon arises due to improper choice of a detection constant. For example, if a detection constant is chosen so as to recognize a small error level, the error signal to noise ratio will also be small since the errors detected will be of the same order of magnitude as the uncompensated parameter uncertainties. Detection at a low error signal to noise ratio, therefore, implies that an isolation decision must be made in a region controlled by instrument noise. In order to avoid this problem, the detection constant must be chosen at a level high enough to permit proper isolation decision capabilities.

If both the detection and isolation constants are chosen properly, under the design considerations illustrated in Figures 3.4 and 3.5 no single failure detection or isolation problems will arise. If a specific isolation decision cannot be made, however, multiple simultaneous failures have occurred. If simultaneous failures are indicated in an FDI implementation with known high reliability then the identification of simultaneous failures itself is useful knowledge for implementation with other status information for redundancy management.

### 3.4 SUMMARY

The FDI method presented here has several advantages over other failure detection and isolation methods. To begin with, during time critical mission phases, the technique utilizes only velocity vectors from the IMUs. Thus, the hardware change tradeoffs in off-the-shelf four-gimbal inertial measurement units are based upon factors other than the redundancy management implementation such as the capability of inflight alignment.

Secondly, the technique does not break down under most multiple simultaneous performance failure conditions. Since all detection and isolation is done on an axis by axis basis, simultaneous failures on different inertial axes cause no problems in the FDI process. If multiple simultaneous failures occur even on the same inertial axis, FDI techniques will not break down provided the velocity error propagations

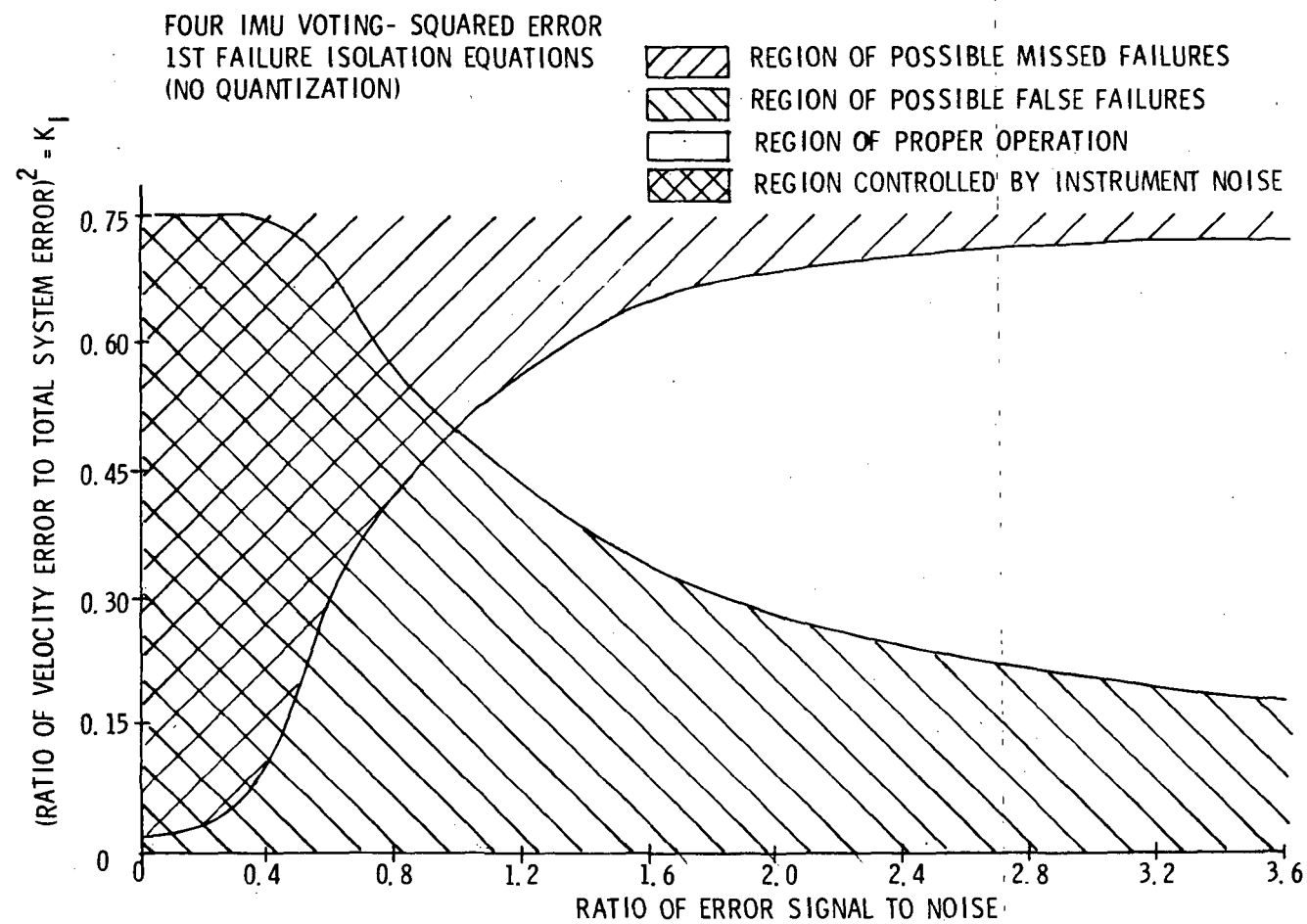


Figure 3.4

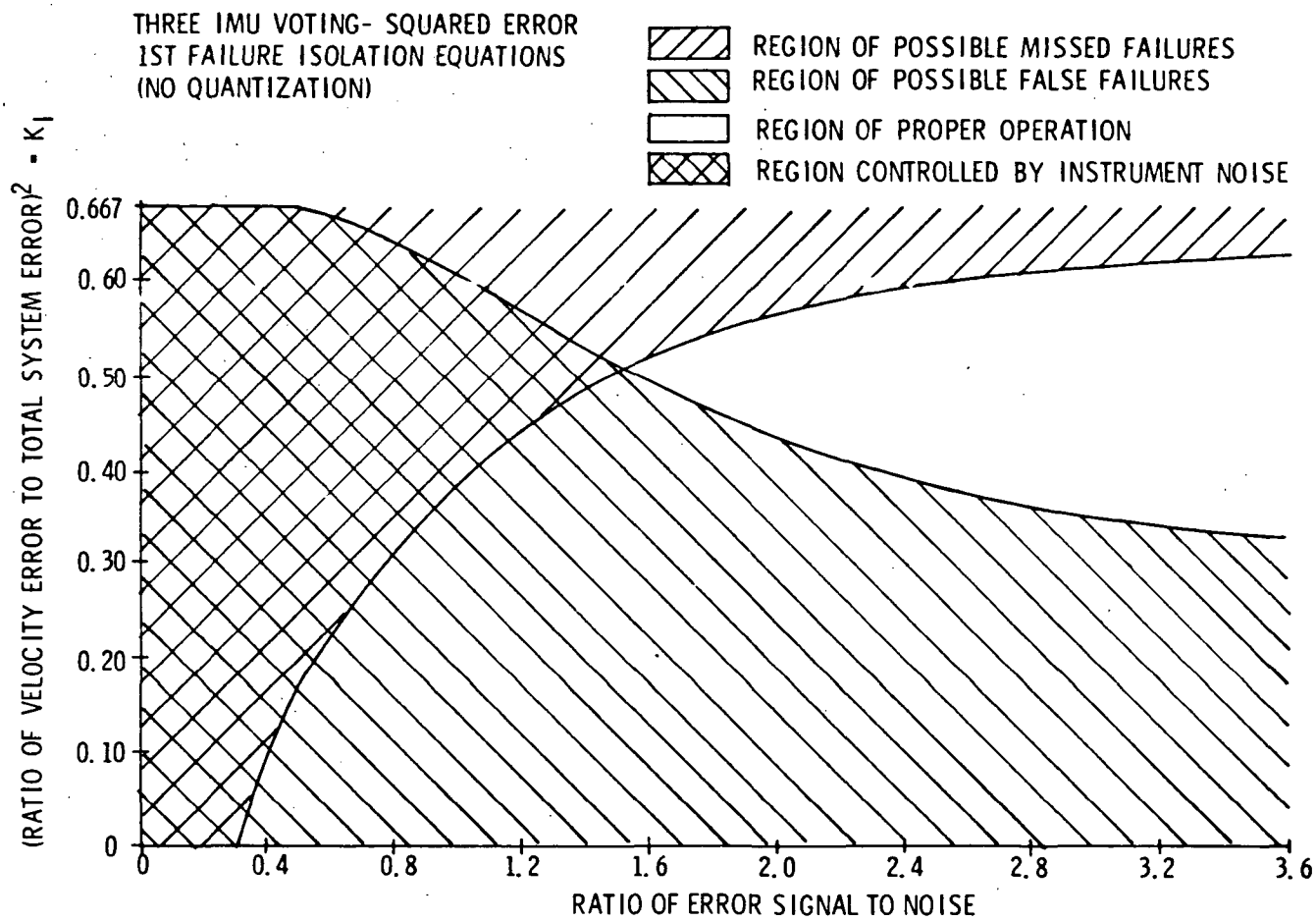


Figure 3.5

are significantly different. Thus, only those performance errors that occur on the same inertial axis with similar velocity error propagation characteristics will not be isolated. Detection of this multiple failure situation will, however, be accomplished. If this detection is coupled with other hard failure or external information, a redundancy management method can be implemented.



**Page intentionally left blank**

#### 4.0 FAILURE DETECTION AND ISOLATION SIMULATION DESCRIPTION

##### 4.1 SHUTTLE TRAJECTORY DESCRIPTION AND MISSION REQUIREMENTS

The evaluation of a performance failure detection and isolation method, suitable for the shuttle mission, requires a variety of mission phases. The critical phases with respect to an FDI study are the boost, cruise and entry phases. The trajectories chosen for the FDI evaluation, then, are

- 1) Boost Trajectory
- 2) Booster Entry Trajectory
- 3) Orbiter Entry Trajectory
- 4) Cruise

The nominal boost trajectory, in the simulations to follow, has a duration of 1302 seconds prior to orbital insertion, with a launch at Kennedy Space Center. The booster profile consists of a 12-second vertical rise followed by a constant pitch rate maneuver. The vehicle then flies an approximate zero angle of attack with booster acceleration limited to 2.5g until staging occurs at 225 seconds. The orbiter stage acceleration is limited to 3g with engine shutdown occurring at 424 seconds. The final duration of the boost phase consists of unpowered flight with no vehicle rates. The only vehicle acceleration realized in this period is due to the presence of atmospheric drag.

To establish acceptable threshold levels for the FDI problem, some criteria must be derived so as to distinguish unacceptable performance from acceptable performance. This task is a difficult one for the nominal boost trajectory since there is no defined "footprint" for the vehicle. The maximum allowable errors acceptable for IMU performance in a nominal ascent trajectory must be a function of whether these errors place the safety of the crew in jeopardy. The safe-orbit determination is, therefore, the only valid criterion for establishing absolute red-line IMU performance parameters. Whether these parameters are in terms of actual instrument performance levels, e.g.,  $0.9^{\circ}/\text{hr}$  bias on the east gyro, or system performance levels, e.g., velocity error of 50 ft/sec, is of minor concern since either may be employed as an acceptable measure of safety. The study of four redundant gimbal IMUs, however, requires the use of system performance parameters as the criterion since the on-board computational facility will have estimated state vectors (one from each IMU) available for use by the failure detection and isolation equations. Differences in position, velocity, or attitude among four IMU estimated states are thus the only measurements that may be taken. A problem

is immediately realized here in that FDI techniques must operate on four estimated states in an attempt to meet a criterion based on the true state of the vehicle, namely a safe orbit. The establishment of required individual IMU red-line performance parameters, therefore, should involve a closed-loop simulation where all IMU errors are fed back into the guidance equations of the vehicle so as to control the true state.

Simulations of this type predict minimum instrument error sources that are capable of failing the safe-orbit criterion.<sup>8</sup> These results are presented in Table 4.1. Note that the gyro bias drift rate specifies two values, i.e.  $-0.9^{\circ}/\text{hr}$  and  $-2.0^{\circ}/\text{hr}$ . The  $-0.9^{\circ}/\text{hr}$  represents the maximum allowable drift if this gyro is used for gyrocompassing during pre-launch. The  $-2.0^{\circ}/\text{hr}$  represents the maximum allowable drift if the gyro is specified only on the basis of the time dependent drift error from the time of launch to orbiter engine shutdown, assuming an external method of controlling the azimuth error.

Table 4.1  
Red-Line Instrument Errors  
(Nominal Ascent Trajectories)

	<u>Error Source</u>	<u>Magnitude</u>
Cross Range	Gyro Bias Drift	$-0.9^{\circ}/\text{hr}$ ( $-2.0^{\circ}/\text{hr}$ )
Cross Range	Gyro A Sensitive Drift About The Spin Axis	$-2.25^{\circ}/\text{hr/g}$
Cross Range	Accelerometer Bias	$5.10 \text{ cm/sec}^2$
Down Range	Accelerometer Bias	$\pm 3.26 \text{ cm/sec}^2$
Altitude	Accelerometer SF Error	$-6750 \text{ ppm}$
Down Range	Accelerometer SF Error	$-2010 \text{ ppm}$

It should be remembered that the values given in Table 4.1 represent the minimum allowable individual instrument error uncertainties for a single IMU to fail the safe-orbit criterion for a nominal ascent trajectory. For the case of four IMUs, however, navigation is executed on the basis of the average of the individual outputs. Determination of the maximum threshold level tolerable (red-line limit) must then be accomplished by observing what system errors are realized in the estimated state when the minimum allowable uncompensated instrument error sources presented in Table 4.1 are employed in a closed-loop IMU simulation. The results of these simulations may be presented in a manner consistent with that proposed in the FDI method defined previously, i.e. a time profile of  $V \text{ error}/V \text{ total}$  where  $V \text{ error}$  is

coordinatized in the launch stable member frame. In addition to a red-line performance criterion, an IMU performance criterion is established in much the same way. However, instead of red-line values being used in the simulations, individual  $3\text{-}\sigma$  IMU parameter values are used to predict estimated state errors. A root sum square (RSS) is then taken of all of the contributions in order to describe a "worst case"  $3\text{-}\sigma$  IMU performance. Figure 4-1 identifies the resultant normalized thresholds that were used in the simulation for the nominal boost trajectory. It should be noted that pre-launch azimuth gimbal monitoring among IMUs was used to limit pre-launch azimuth error to 2 mrad. A shift in the performance failure threshold is evident at 225 seconds. This shift is a result of several factors. First, instrument error sensitivities are unusually high near the region of maximum dynamic pressure. These error sensitivities are found to decrease after staging. Secondly, the red-line thresholds as well as the  $3\text{-}\sigma$  IMU thresholds shown are straight-line approximations of the actual thresholds derived. The actual  $3\text{-}\sigma$  curves are also shown.

After orbiter engine shutdown, only attitude FDI methods are employed. Identification of red-line parameters for the attitude FDI evaluation is based upon the required gyroscope performance levels specified for the entry mission phase.

The booster entry trajectory<sup>9</sup> subjects the vehicle, and thus the IMU(s), to a more severe dynamic environment and performance requirement than the nominal ascent trajectory. The duration of the booster entry trajectory is 600 seconds. The vehicles separate at 215 seconds. An apogee of 53.7 miles is reached 50 seconds after separation. The vehicle then undergoes a transition maneuver after which it turns around and proceeds back to the launch site. Maximum acceleration during the entire flight is limited to 4.0g. For simulation purposes, all performance evaluation is terminated at an altitude of 50,000 feet.

Evaluations similar to those for the nominal boost trajectory were accomplished for the booster entry trajectory to determine red-line and  $3\text{-}\sigma$  IMU performance specifications. However, the red-line criterion chosen for this trajectory is a 5-nautical-mile-radius circle at 50,000-foot altitude. Maximum allowable IMU error sources which meet this criterion were derived and are shown in Table 4.2. The resultant normalized redline and  $3\sigma$  thresholds are shown in Figure 4-2.

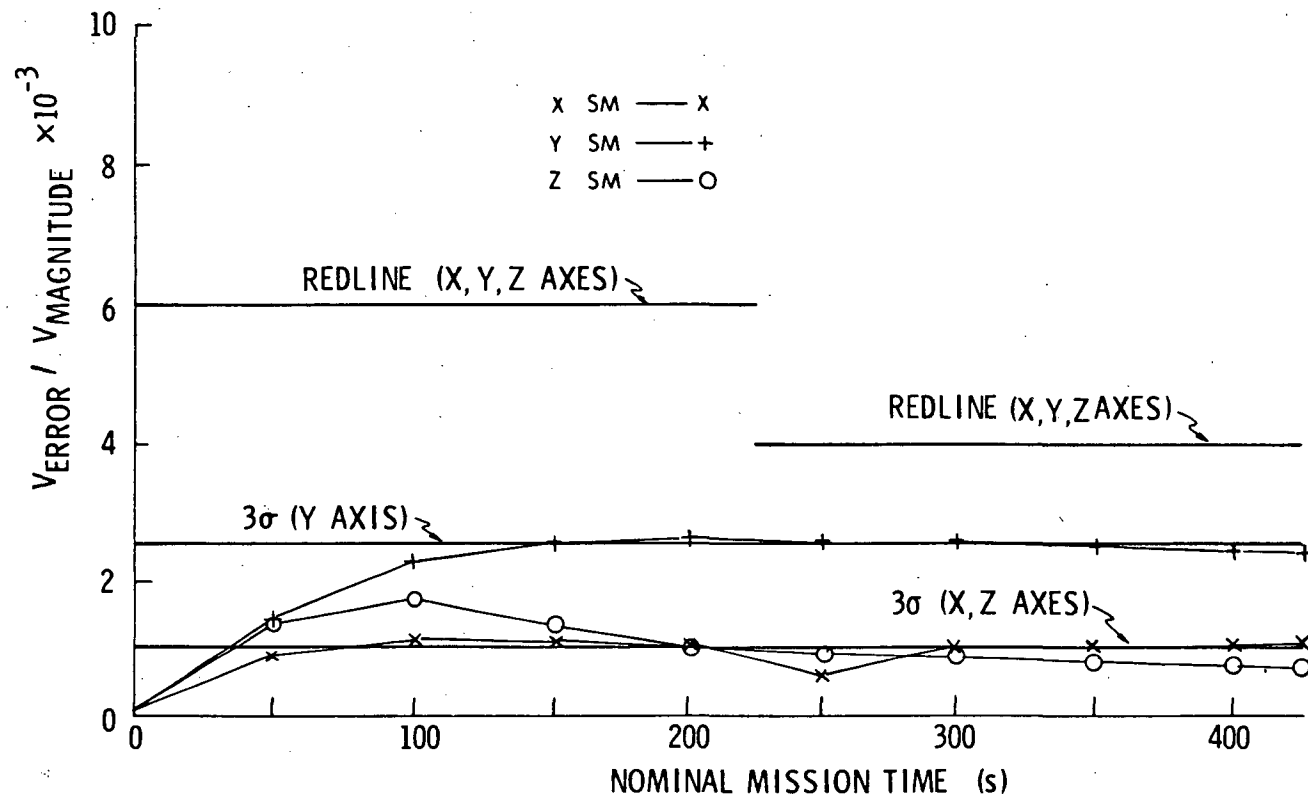


Figure 4.1  
Nominal Boost Mission Detection Thresholds.  
(Prelaunch Azimuth Error 2.0 mrad Max.)

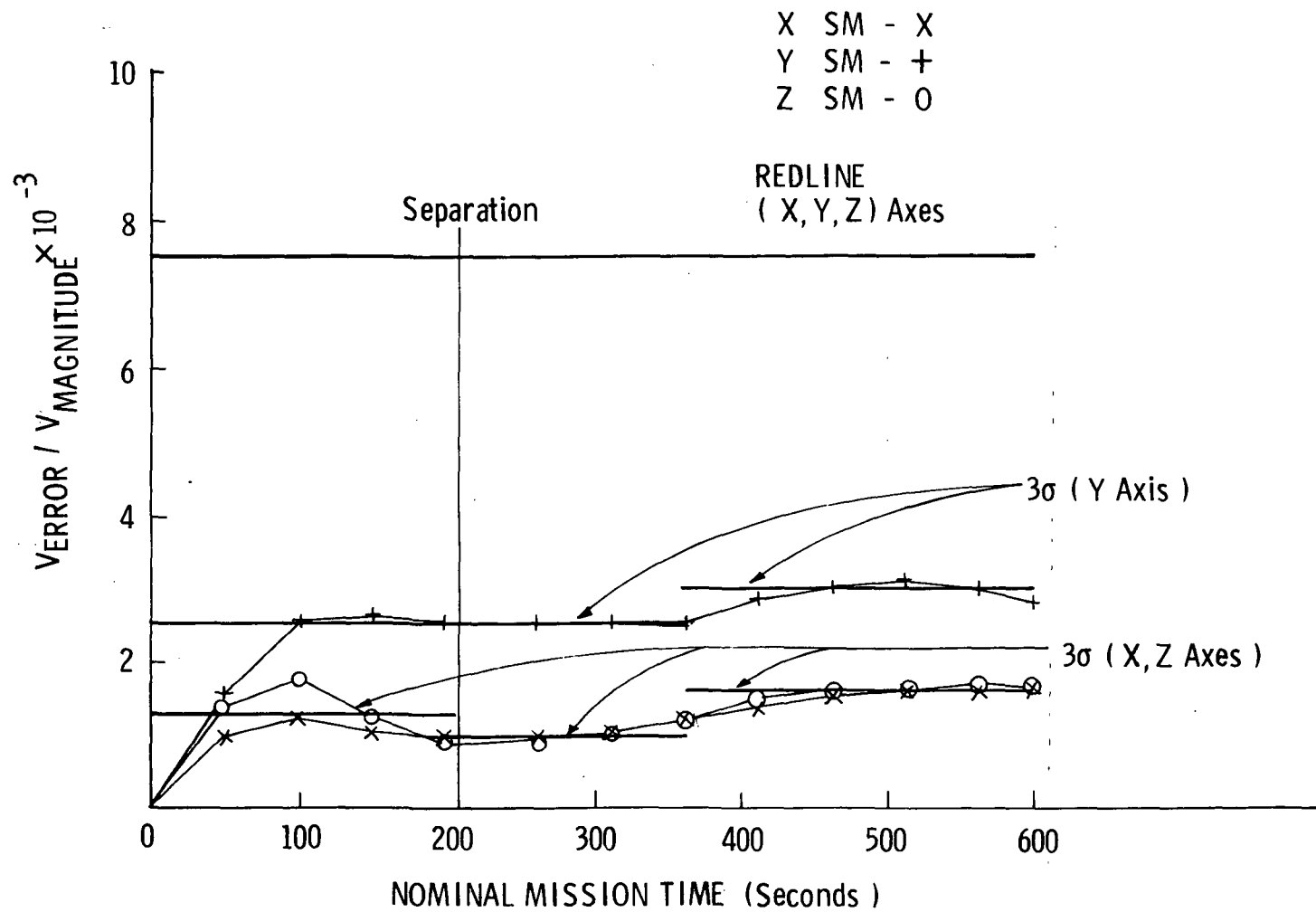


Figure 4.2. Booster Entry Mission Thresholds. (Prelaunch Azimuth Error 2 mrad max.)

Table 4.2  
Red-line Instrument Errors  
(Booster Entry)

Cross Range	Accelerometer Bias	$\pm 2.15 \text{ cm/sec}^2$
Down Range	Accelerometer Bias	$\pm 2.86 \text{ cm/sec}^2$
Down Range	Accelerometer SF Error	$\pm 5200 \text{ ppm}$
Cross Range	Gyro Bias Drift	$0.1^\circ/\text{hr}$ ( $4.3^\circ/\text{hr}$ )
Cross Range	Gyro A Sensitive Drift About the Spin Axis	$8.4^\circ/\text{hr/g}$

The orbiter entry trajectory provides the longest time duration and the most difficult performance requirements of all mission phases. The orbiter vehicle is initially assumed to be in an equatorial orbit with a deorbit burn maneuver occurring 15 minutes prior to entry interface. Further, the vehicle is assumed to have performed an inflight alignment just prior to the deorbit burn. The orbiter entry employs a thermal protection system guidance law<sup>10</sup> which navigates the vehicle along a minimum g-loading path. Its configuration consists of a high cross-range capability which is utilized 260 seconds after entry interface to perform an attitude maneuver which places the vehicle into a 550 nmi cross-range trajectory. A vehicle transition maneuver occurs at 90,000-feet altitude.

Development of red-line and 3- $\sigma$  performance specifications for the orbiter entry trajectory follow the same logic as presented for the nominal boost and booster entry trajectory. These performance specifications are shown in Figure 4-3.

The criterion chosen for the orbiter entry trajectory is a 12-nautical-mile-radius circle at 100,000 feet altitude. Maximum allowable IMU error sources that meet this criterion are shown in Table 4.3.

Table 4.3  
Red-line Instrument Errors  
(Orbiter Entry)

Altitude	Accelerometer Bias	$\pm 1.77 \text{ cm/sec}^2$
Cross Range	Accelerometer Bias	$\pm 2.34 \text{ cm/sec}^2$
Down Range	Accelerometer Bias	$\pm 4.00 \text{ cm/sec}^2$
Altitude	Accelerometer SF Error	9300 ppm
Altitude	Gyro Bias Drift	$1.98^\circ/\text{hr}$

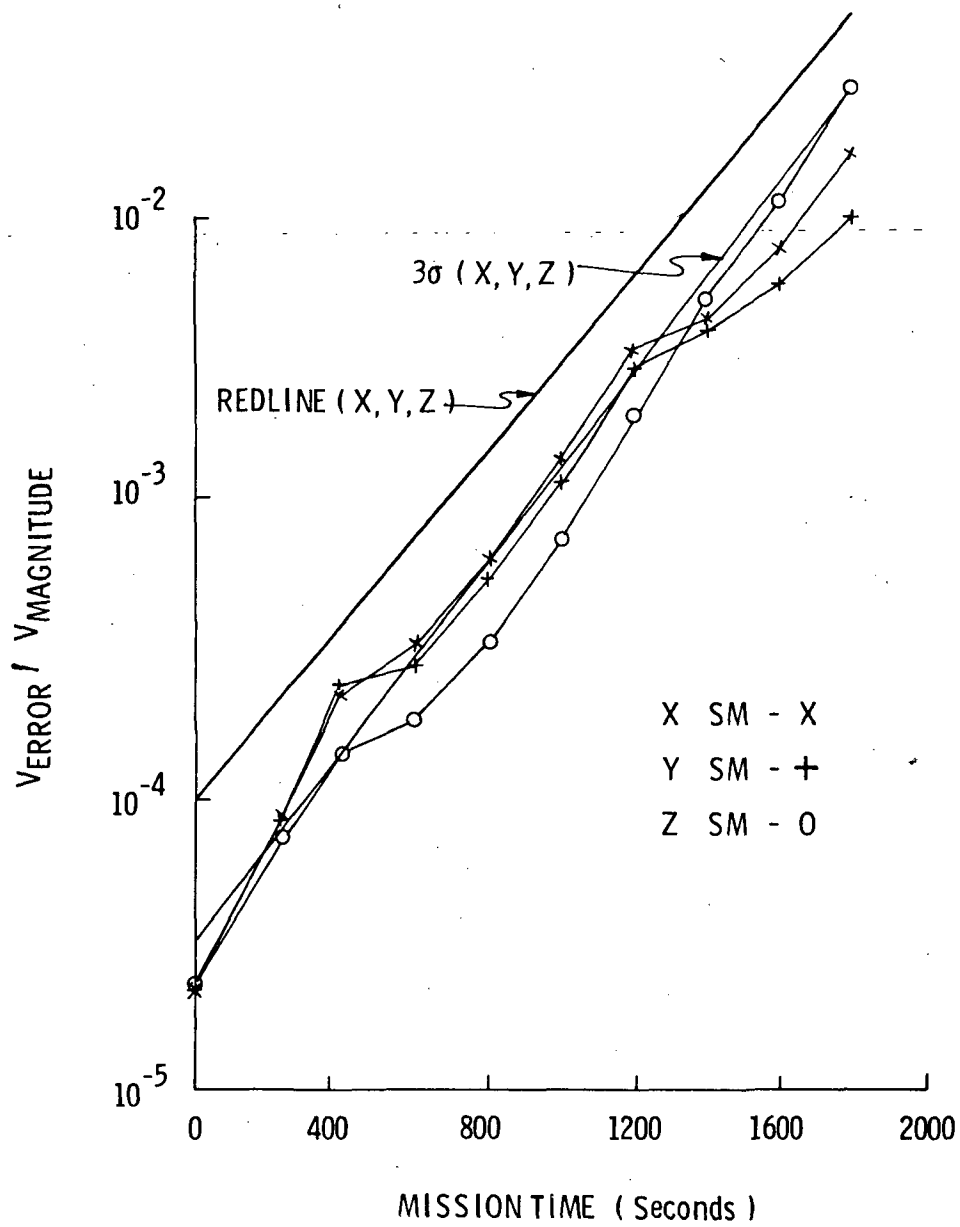


Figure 4.3  
Orbiter Entry Mission Detection Thresholds.



Cross Range	Gyro Bias Drift	3.27°/hr
Down Range	Gyro Bias Drift	0.75°/hr
Cross Range	Gyro A Sensitive	
	Drift About the Spin Axis	2.45°/hr/g
Down Range	Gyro A Sensitive	
	Drift About the Spin Axis	13.50°/hr/g
	In-flight Alignment	±5 mrad

## 4.2 REDUNDANT INERTIAL SUBSYSTEM SIMULATION METHOD

Three basic software subroutines have been developed for the evaluation of the FDI methods with shuttle mission requirement. A detailed single four-gimbaled IMU model representing existing "off-the-shelf" performance characteristics was created. A block diagram of the model is shown in Figure 4-4. The essential features can be described as follows:

1. A perfect state vector of the vehicle with respect to a reference frame is derived from the given trajectory inputs.
2. The computational state vector of the vehicle with respect to a reference frame is derived using the gyroscope and accelerometer models.
3. The actual gimbal readout chain is modeled to generate realistic attitude information.
4. An evaluation process is implemented to demonstrate the performance of the actual IMU mechanized.

This IMU model is used to generate a series of data files, each of which represents a single IMUs data output to be utilized in the final multiple IMU simulation. Figure 4-5 shows the features of the multiple IMU simulation method. It can be seen that each IMUs data output is employed with the FDI equation set which is being evaluated. In this manner, simulations may be made utilizing any number of IMU models, each with different performance characteristics.

### 4.2.1 Description of a Single IMU Simulation

The IMU model that is simulated is described in Appendix A. The IMU model error sources discussed below may optionally be specified by data cards, but normally are determined by a random number generator with normal distribution, zero mean,

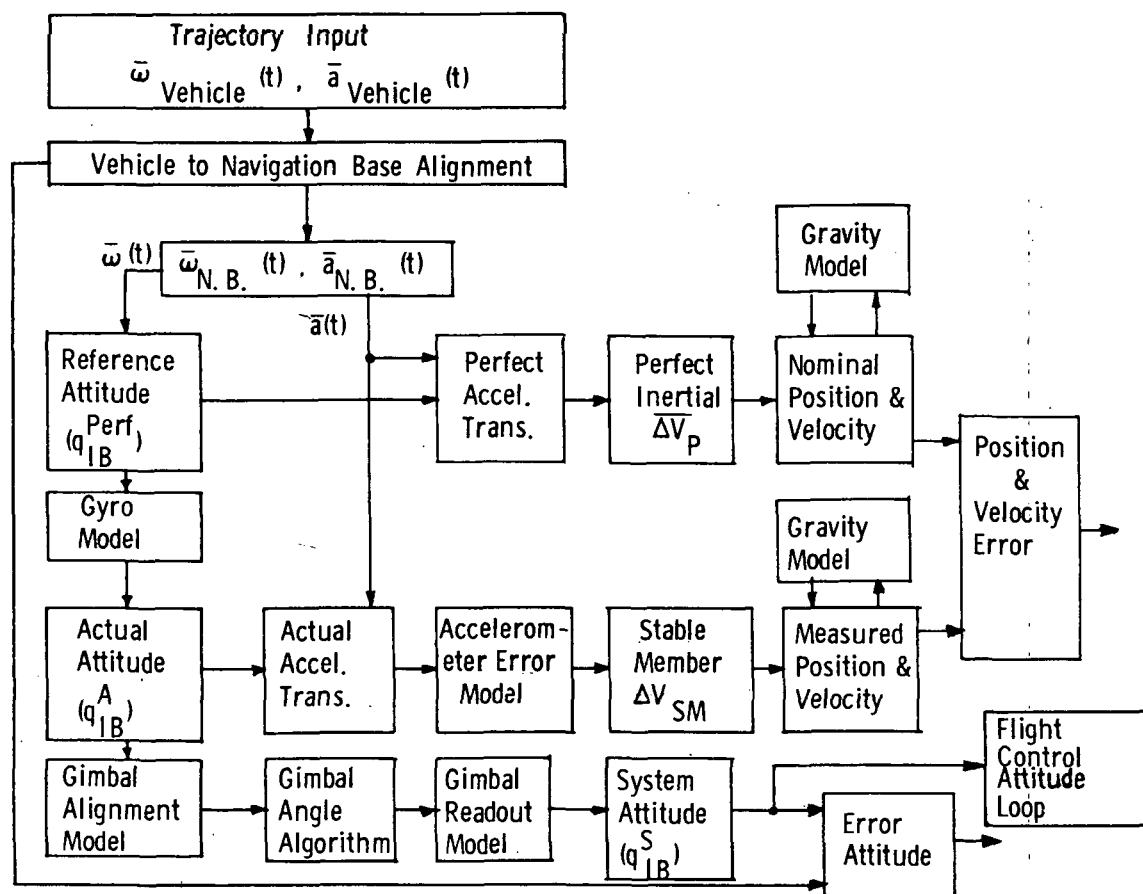


Figure 4.4  
Gimbaled IMU Model Flow Chart.

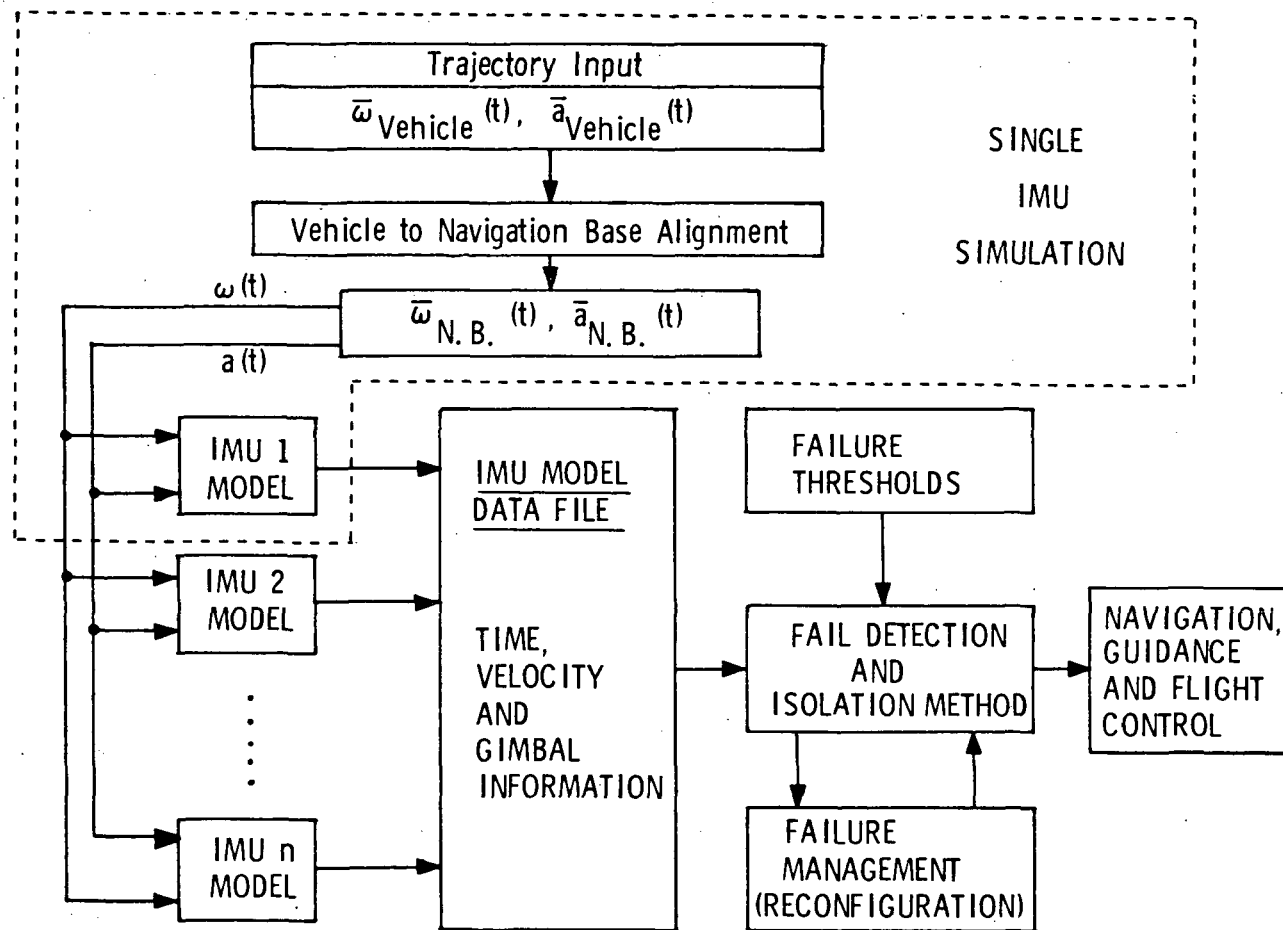


Figure 4.5  
Multiple IMU Simulation Flow Chart.

and variance equal to the values listed in Appendix A. Once determined, each error source is carried through the mission at this single value. Instrument errors included in this simulation are bias drift and acceleration sensitive drift for the gyros, and bias and scale factor errors for the accelerometers. Misalignment terms are also modeled and simulated.

The initial platform misalignment represents pre-launch gyro compassing error or inflight alignment error.

The leveling error is proportional to down range and cross range accelerometer biases. The azimuth error is dominated by the effective east gyro drift. It has been found that the ability to do the prelaunch gyrocompassing directly affects the sensitivity of the FDI method. If the standard KT-70 IMU subsystem is assumed, a gimbal chain calibration will allow knowledge of the azimuth readout axis of each IMU to within two milliradians. The simulation program then limits the azimuth error sources in each IMU to two milliradians.

In the inflight alignment case, the alignment errors and the time from alignment are inputted. The initial error is then the sum of the alignment error and the gyroscope bias drift multiplied by the time from alignment.

For simplicity, the accelerometer triad misalignment is specified by three angles. One angle specifies the nonperpendicularity of the two level accelerometers relative to each other. The other two angles indicate the nonperpendicularity of the radial accelerometer relative to the level plane.

Gimbal-non-orthogonalities and the redundant gimbal bias are specified by five separate quaternions. The gimbal readout model allows quantization error, constant readout bias, and a sinusoidal readout error which varies as a function of gimbal angle.

Referring to Figures 4-6a and 4-6b, the IMU simulator program will now be defined. This program simulates the four gimbal KT-70 and a dedicated navigation computer. The output is a file of IMU measurements and navigation quantities.

The values of the IMU model error sources are determined at the beginning of each run. In the cases of the "perfect" IMU these values are introduced by data cards specifying all zeros. The "red line" IMUs are generated by selectively introducing the required error values.

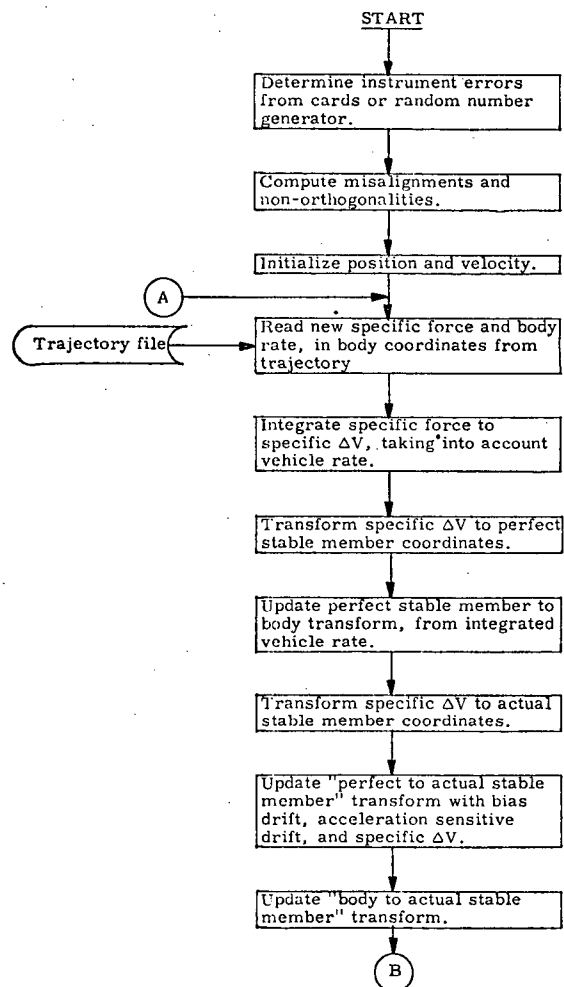


Figure 4-6a Single IMU Flow Diagram

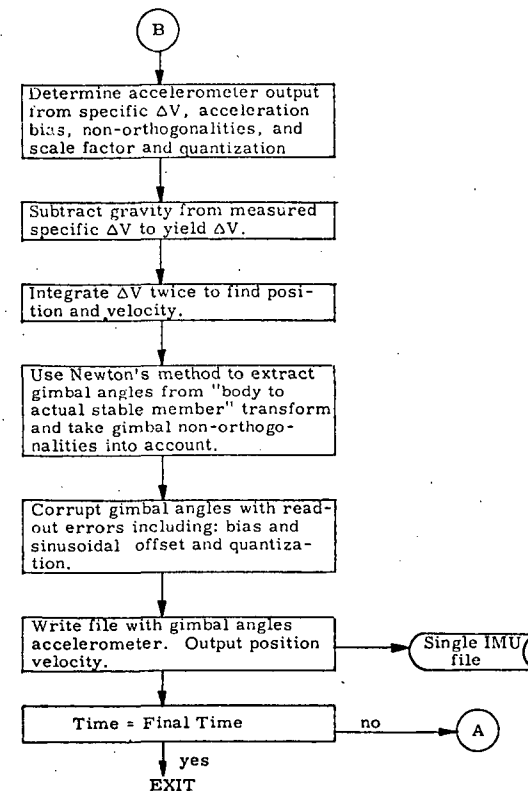


Figure 4-6b Single IMU Flow Diagram

The simulation loop reads a mission phase trajectory file. These files contain specific force in body coordinates, body rate in body coordinates and time. The average specific delta velocity in body coordinates due to the rotation of the vehicle is computed. This is then transformed into "perfect" stable member inertial coordinates. The transformation from body to perfect stable member is updated as a function of body rate. The specific  $\Delta V$  is then transformed into actual stable member coordinates by the quaternion representing gyroscope errors. This error quaternion is then updated as a function of gyroscope bias, and acceleration sensitive drift. The accelerometer outputs are the specific  $\Delta V$  degraded by accelerometer bias, non-orthogonalities, scale factor errors and quantization. Position and velocity are then updated by the accelerometer outputs after gravity computer processing.

Gimbal angles are extracted from the body to actual stable member quaternion using Newton's method of iteration. This process automatically considers fixed gimbal non-orthogonalities. The gimbal readout model then degrades these angles considering readout bias and sinusoidal offset error models and the quantization error of the readout device. The simulation program writes an output file of gimbal angles, accelerometer outputs, position, velocity and time.

These procedures are performed periodically, and synchronized with the trajectory file, until the mission is completed.

#### 4.3 FAILURE DETECTION AND ISOLATION IMPLEMENTATION

The four IMU failure detection and isolation encompasses two methods corresponding to powered and unpowered flight. The two programs used to implement and verify these methods will be described below. These programs have been run with boost, entry and coasting flight trajectories, with one, two and three IMU failures. The result of these simulations will be discussed in the next section. Both of these analysis programs require five IMU files. One file represents the perfect IMU. The other four represent the four operational IMUs. There may be one, two or at most three separate red line IMUs, while the remaining IMUs represent normal "one sigma" performance models.

##### 4.3.1 Velocity FDI Verification Program (Powered Flight)

The following is a description of the velocity FDI Verification Program, to be used in conjunction with Figures 4-7a to 4-7c. The program reads detection and isolation threshold constants which depend on mission phase and were established as shown

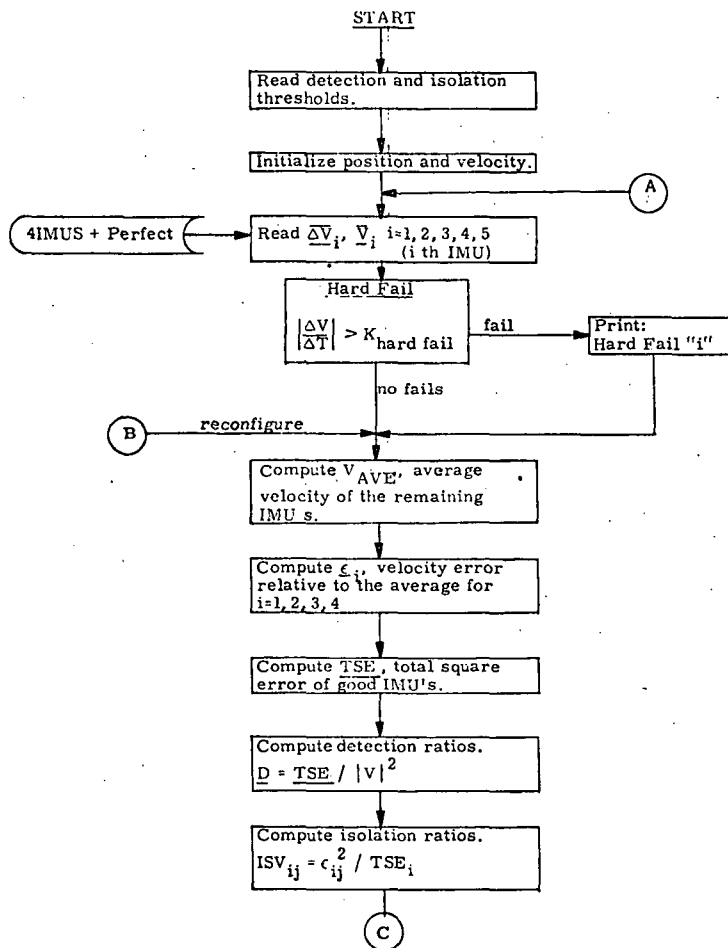


Figure 4-7a Velocity FDI Verification Program Flow Diagram

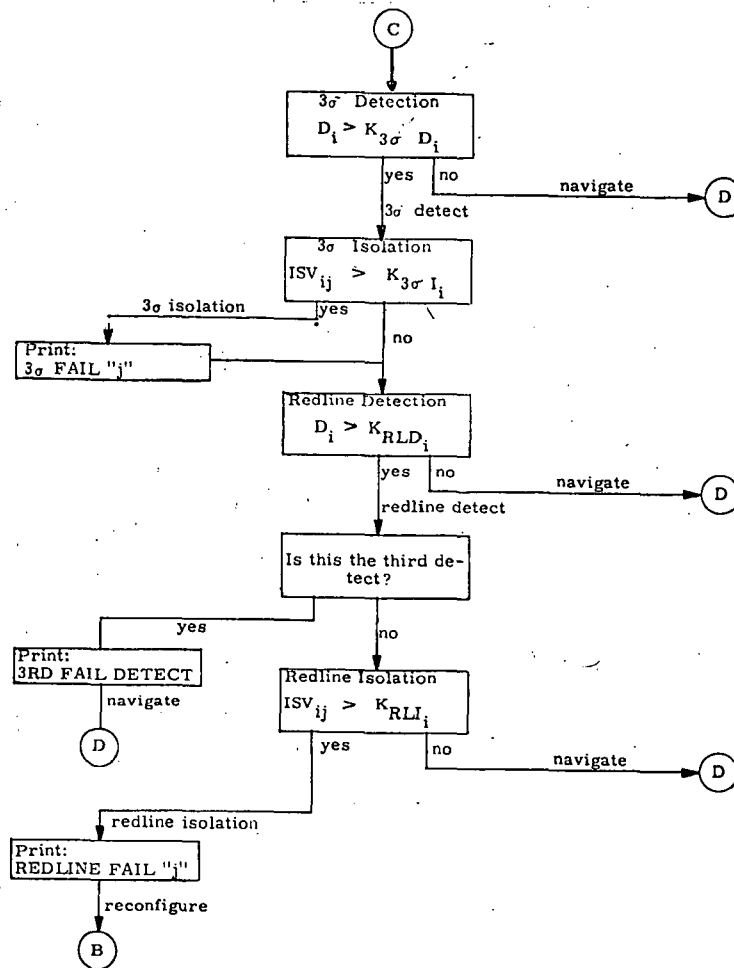


Figure 4-7b Velocity FDI Verification Program Flow Diagram

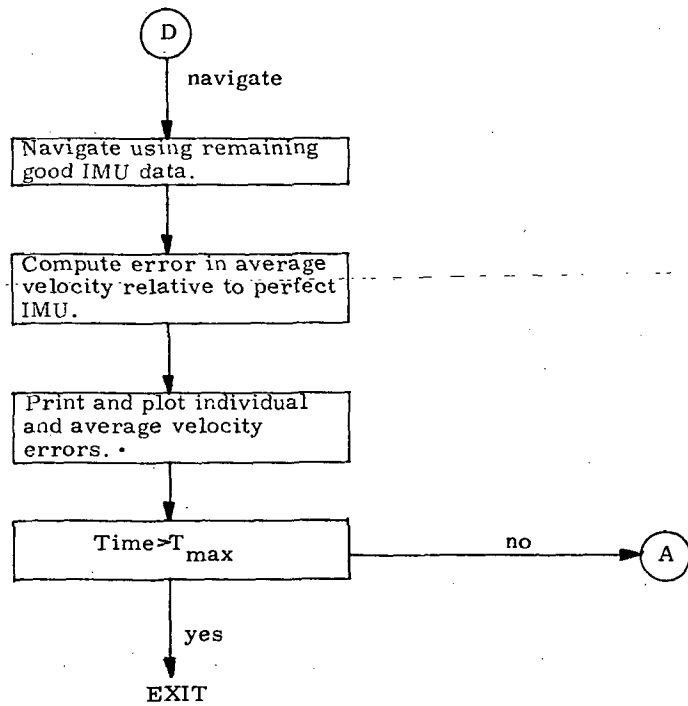


Figure 4-7c Velocity FDI Verification Program Flow Diagram



in 4-6a. The position and velocity are also initialized with respect to each separate mission.

Velocity and  $\Delta V$  for the four operational and the perfect IMUs are read from the data file. The perfect IMU data is used only for performance verification and display and does not enter into FDI computations.

At each time step, a reasonability test on  $\Delta V$  is made to isolate hard failures.

The first step in the FDI computation is to determine the average velocity of the remainder of the "good" IMUs, i.e. those IMUs not failed by reasonability criteria. An estimate of the individual IMU velocity errors is computed relative to this average velocity. TSE (Total Squared Error) is a vector whose components are the total of the squares of the estimated velocity errors for the remaining IMUs. The detection ratio vector is TSE normalized by the square of the magnitude of the average velocity. The isolation ratios form an array with an element for each axis and each IMU. It is computed by dividing the square of the estimated velocity error component by the corresponding component of TSE.

"Three Sigma" detection provides a warning and a necessary condition for further detection and isolation analysis in this FDI technique. The detection ratio vector is compared with the "Three Sigma" detection constants. Without detection at this level, the system will proceed with normal navigation. When a "Three Sigma" detection occurs, an attempt at isolation is performed. The isolation ratios for each of the remaining IMUs corresponding to the axis in which an error is detected are compared with the "Three Sigma" isolation threshold. Note that the detection process has performed one level of isolation, that is, it has isolated an error to a particular axis. Red line detection and isolation tests are performed independently of "Three Sigma" isolation. This is important insofar as third failure detection is concerned. The red line detection and isolation procedure is the same as the "Three Sigma" detection and isolation except that different thresholds are used, and the third detection is recognized.

If a red line error is detected and isolated, the system is reconfigured by removing the failed IMU. After reconfiguration the entire FDI is reiterated on the remaining IMUs in an attempt to screen additional simultaneous failures prior to proceeding with navigation. The navigation routine computes position and velocity updates based on the average delta velocity of the remaining IMUs. The result is compared with the perfect IMU and is printed and plotted as a figure of merit of the FDI scheme.

#### 4.3.2 Gyro Drift FDI Verification Program (Unpowered Flight)

The following description of the gyro drift verification program for cruise flight is to be used in conjunction with Figures 4-8a and 4-8b. The Detection and Isolation thresholds and gyro sampling are inputted using data cards.

The gimbal angles for the perfect and the four operational IMUs are read from their respective files.

A quaternion of rotation is computed for each IMU with these gimbal angles. This represents the transformation from a common body (nav base) frame to the stable member inertial frame. An average quaternion is derived from the individual quaternions of all operational IMUs. The product of these individual quaternions with the conjugate of the average quaternion yields an estimate of the error quaternion relative to the stable member reference frame. Error angles about each IMU axis are extracted from these error quaternions. Every  $\Delta T$  seconds an estimate of the square of the drift rate is obtained from present and past error angles. The detection parameter (TSE, total squared error) is the sum of the squares of the individual axis drifts. An isolation ratio is computed from the square of the individual drift error normalized by the corresponding component of TSE.

An error is detected when a component of TSE is greater than a maximum allowable drift squared. Isolation occurs when an error has been detected, and when a particular instrument axis contributes a significant portion of the total squared error. This is controlled by the isolation threshold. This system, mechanized for four IMUs, allows isolation of two failures and the detection of a third failure. After each isolation the system is reconfigured by removing the failed IMU and by reiteration of the FDI logic. The average attitude is compared with the perfect attitude at every time step. This figure of merit, along with the detection ratios and error angles, is both printed and plotted for evaluation.

Simulations are shown in the next chapter for the colinear IMU configuration, powered and unpowered flight phases. Simulations were also developed for the theory of implementation at the two IMU level from equations developed in Chapter 3. The simulation development follows the two IMU equation format directly and will not be represented in this chapter.

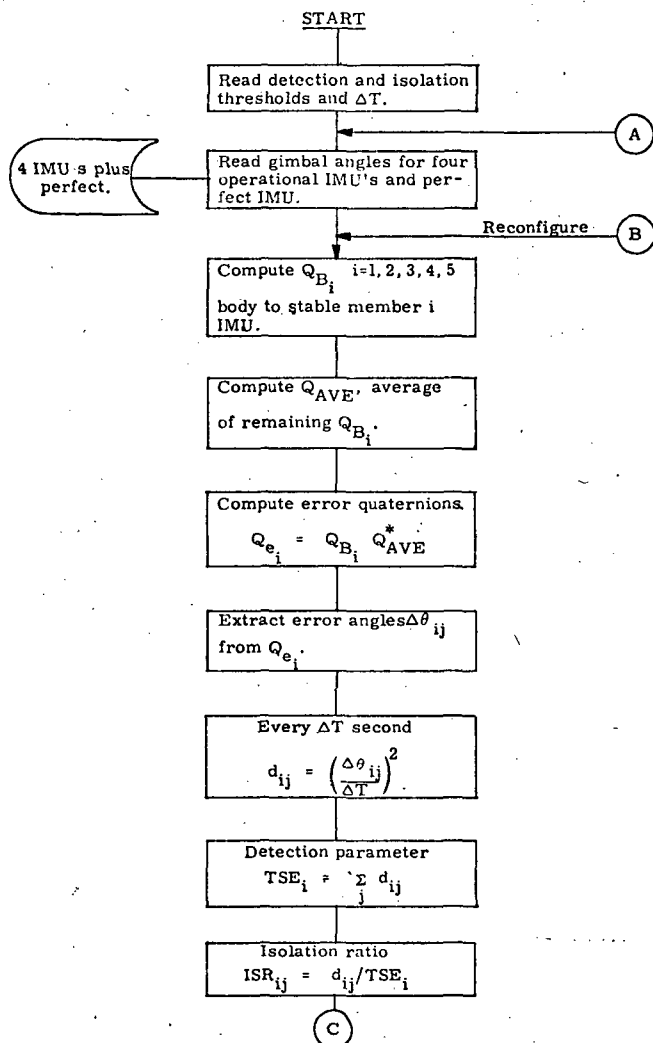


Figure 4-8a Gyroscopic FDI in Cruise Flight

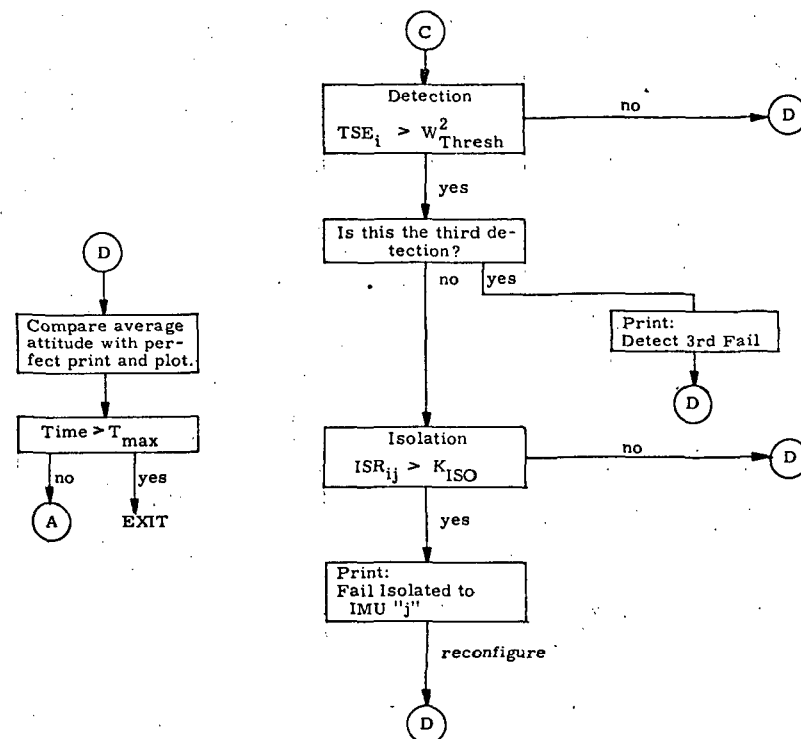


Figure 4-8b Gyroscopic FDI in Cruise Flight

## 5.0 FAILURE DETECTION AND ISOLATION SIMULATION RESULTS

A digital simulation of the multiple IMU system (Figure 4-5) has been prepared for use in evaluating the FDI techniques developed in this study. The full model is based upon four independent single KT-70 models.

In the simulations presented, a series of statistically generated standard  $1\sigma$  IMU error parameters is used to represent a normal system. Other IMU models, which include known performance degradation, are then utilized with the standard IMUs to form the multiple IMU set for FDI evaluation. The FDI logic is tested by evaluating its performance in locating the given degradation. The following sections are organized to present the colinear axis simulations for each mission phase in Sections 5.1 through 5.4. Section 5.5 then presents all the skewed axis simulation results.

### 5.1 NOMINAL BOOST VELOCITY FDI TEST RESULTS

An example of a simulation of this type is shown in Figure 5-1. In addition to three normal IMUs, a degraded IMU containing an error in the altitude channel accelerometer of 6750 ppm in scale factor is utilized for FDI evaluation. This system of four IMUs is evaluated using the powered flight segment of the nominal boost trajectory. The bottom picture of Figure 5-1 shows the time profile of the altitude channel detection ratio. It is seen that the red-line detection threshold established for this mission is violated at 36 seconds into the flight. The top of Figure 5-1 shows the altitude velocity error of the degraded IMU as well as the average navigation velocity error as a function of mission time. The velocity error of the degraded IMU increases until the detection, isolation and automatic reconfiguration is accomplished at 36 seconds. The reconfiguration of the system can be observed by the change in slope of the navigation error. Note that a  $3\sigma$  IMU performance detection and isolation of the degraded IMU occurred at 6 seconds, but no reconfiguration was done since mission safety was not in question.

An example of a dual failure simulation along a single axis for the nominal boost mission is shown in Figure 5-2. This system of four IMUs consists of two normal and two degraded IMUs at the time of launch. The IMU degradation models are both in the altitude axis accelerometers and are specified in the figure. The detection and isolation of IMU #1 and reconfiguration occur, as before, at 36 seconds. The detection, and isolation of IMU #2 and reconfiguration occur at 225 seconds. Notice that with dual simultaneous failures occurring on a single axis, the failure detection and isolation implementation was effective. This is possible since the velocity error propagation characteristics of both failures are significantly different. In general,

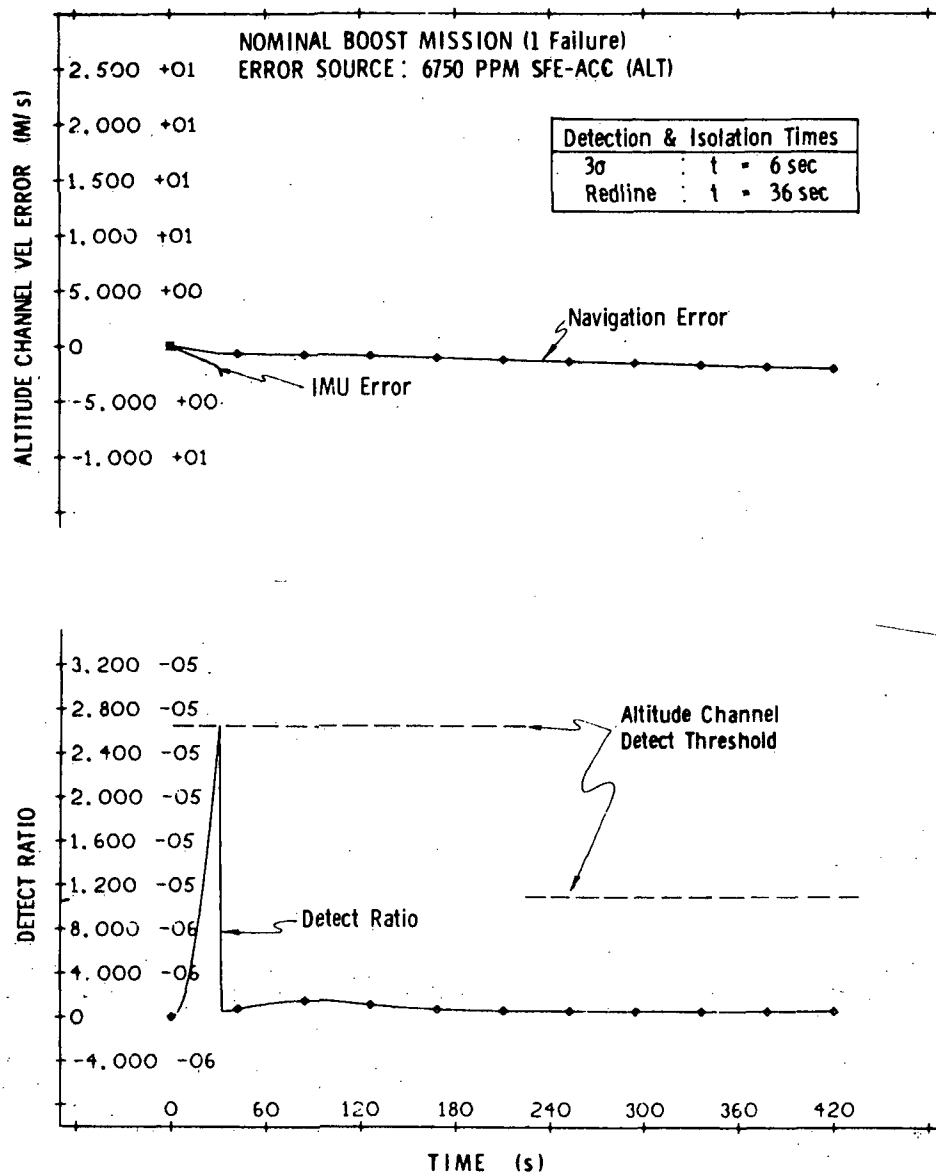


Figure 5.1  
Nominal Boost Mission Simulation Results.

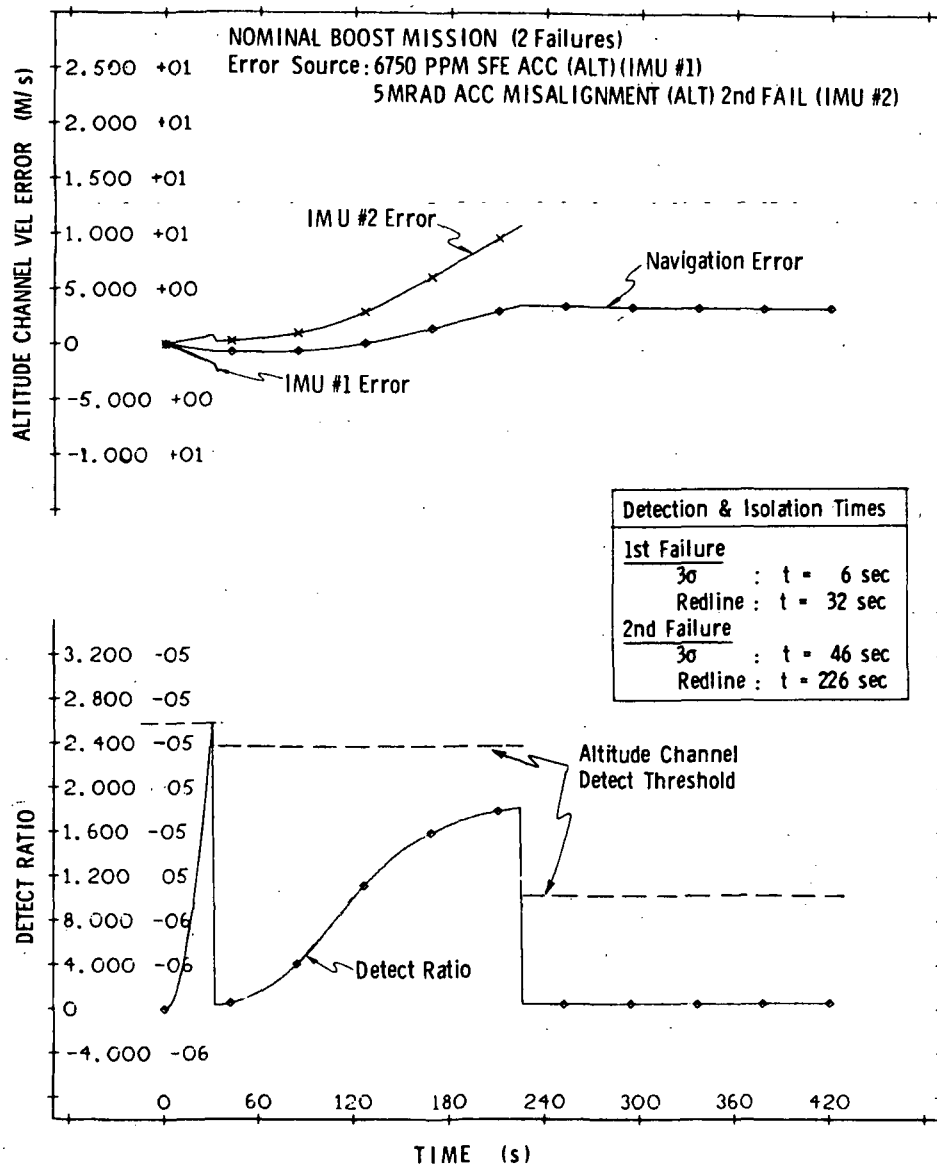


Figure 5.2  
 Nominal Boost Mission Simulation Results

dual simultaneous failures can be detected and isolated as a pair if their individual error propagations do not have similar simultaneous magnitudes.

In general, dual simultaneous failures not associated with the same axis are identifiable with the use of this FDI scheme. Simultaneous failures along the same axis can not be individually isolated, however, unless the error propagations are significantly different. If appropriate failure detection and isolation constants are defined dual simultaneous failures can be detected and isolated as a pair if their individual error propagations do not have similar simultaneous magnitudes.

An example of third failure detection during nominal boost is shown in figures 5-3 and 5-4. These represent the down range and altitude channels respectively. The third error source of  $3330\mu\text{g}$  accelerometer bias has been included in addition to those described in figure 5-2. The effect of scale factor error and accelerometer bias are felt early in the flight and hence are detected and isolated at 30 seconds and 34 seconds after liftoff. Note that the addition of an error source has not appreciably affected the detection and isolation times associated with IMU #1. Figure 5-4 shows the third detection. It has occurred at 226 seconds which coincides with separation at which time the redline threshold velocity is reduced.

## 5.2 BOOSTER ENTRY FDI TEST RESULTS

Figures 5-5 through 5-10 represent the results of one fail, two fails and a third detect for the booster entry trajectory. The first fail case, figure 5-5, is caused by a bias of  $2.86 \text{ cm/sec}^2$  in the down range accelerometer. The failed IMU is isolated after 45 seconds into the flight. The two failure situation is shown in figures 5-6 and 5-7. Figure 5-6 depicts the isolation of IMU #1 at 75 seconds. The error source is a constant  $2.15 \text{ cm/sec}^2$  accelerometer bias along the cross range axis. The second failure, 5200 ppm scale factor error on the down range accelerometer, is shown in figure 5-7. One can see the effect of scale factor error on the navigation error as a representation of the thrust profile. Also note that the squared criteria detect ratio has magnified this effect in order to insure positive detection. Detection and isolation for this case was accomplished at 381 seconds.

The three failure situation for booster entry is shown in figures 5-8 to 5-10. Figures 5-8 and 5-10 are the down range components for IMU #1 and IMU #3 and thus the plot of detect ratios are identical. It is seen that IMU #1, with  $2.86 \text{ cm/sec}^2$  down range accelerometer bias, is isolated after 45 seconds. After 75 seconds the  $2.15 \text{ cm/sec}^2$  A-bias along cross range has been detected and isolated, as seen in figure 5-9. The third failure, down range accelerometer scale factor error, is detected

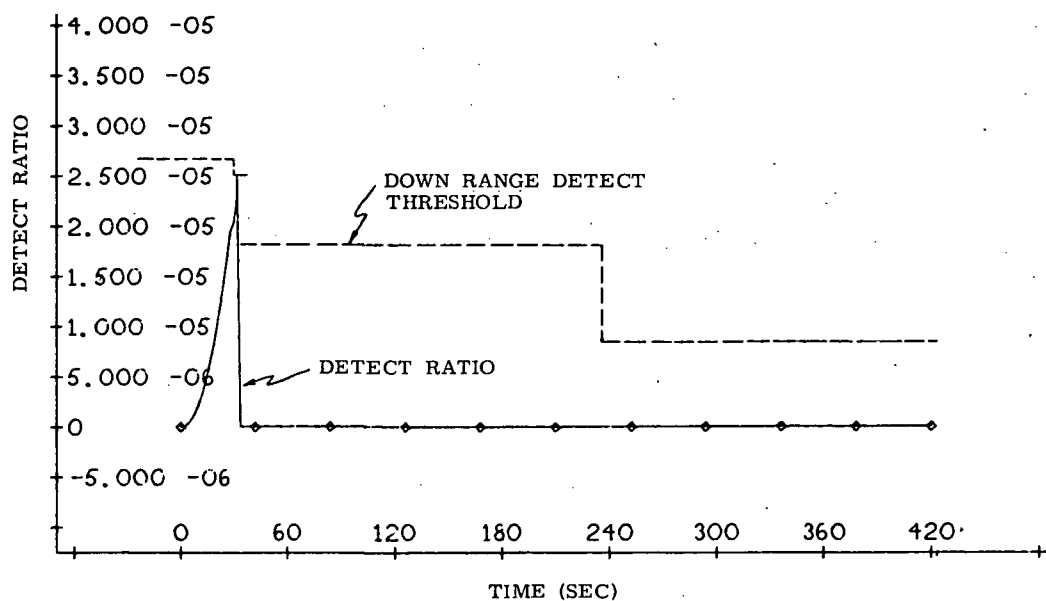
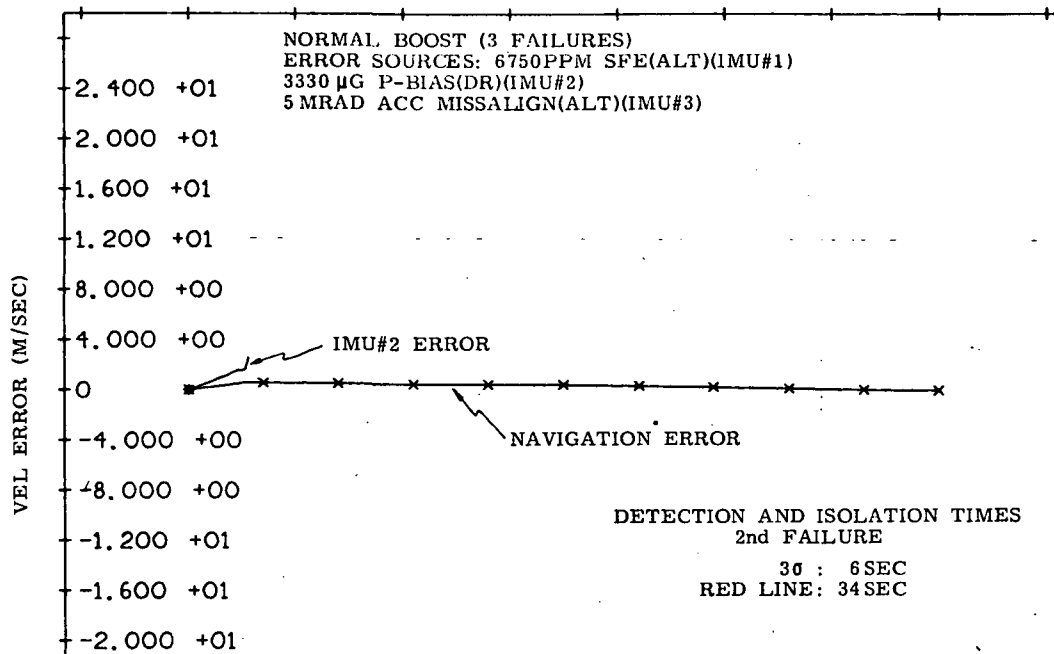


Figure 5.3

NOMINAL BOOST MISSION SIMULATION RESULTS



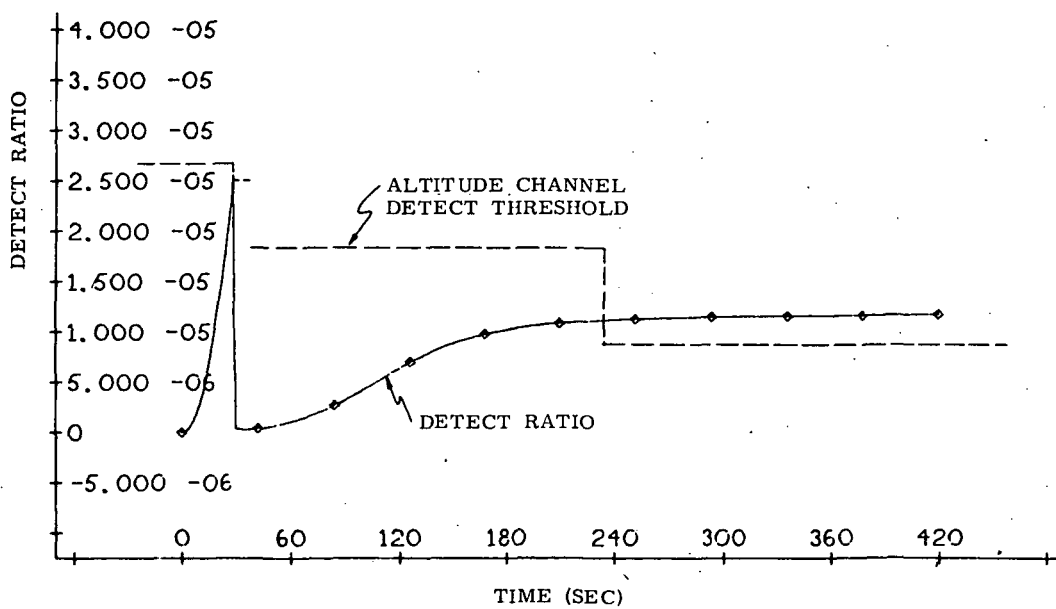
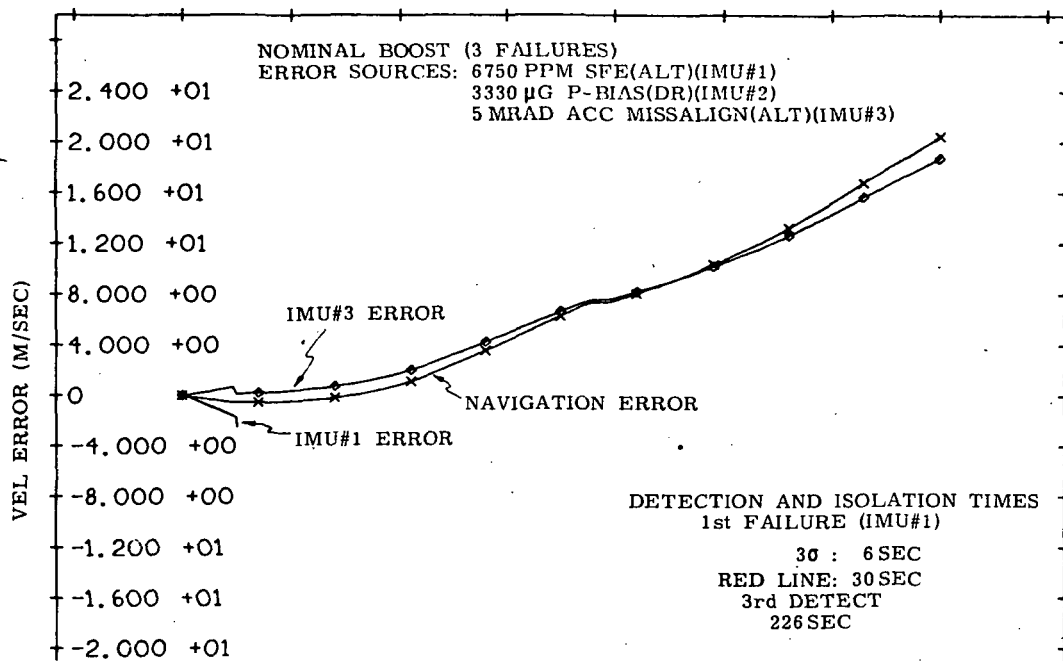
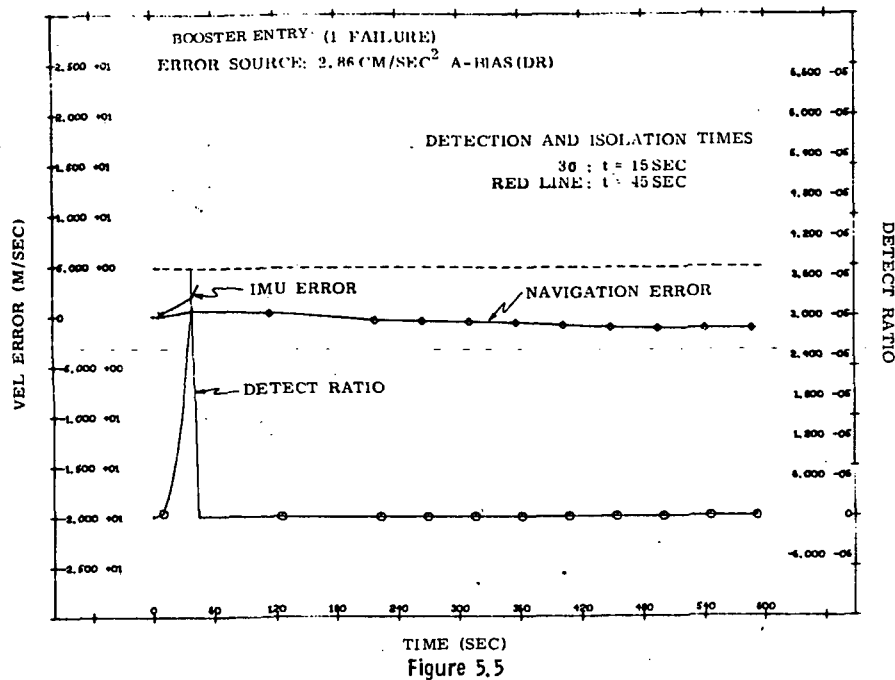
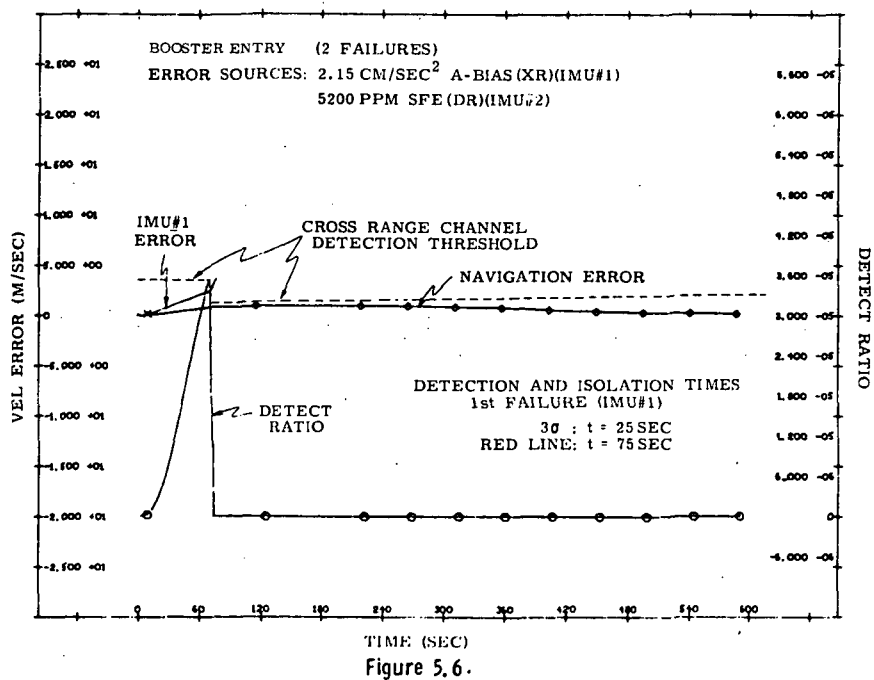


Figure 5.4

NOMINAL BOOST MISSION SIMULATION RESULTS



### BOOSTER ENTRY MISSION SIMULATION RESULTS



### BOOSTER ENTRY MISSION SIMULATION RESULTS

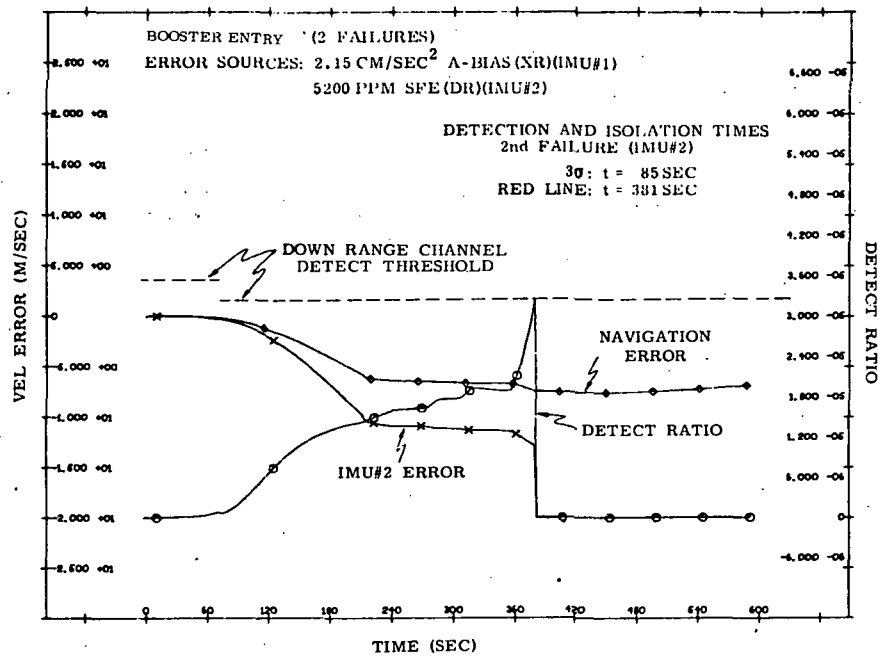


Figure 5.7

### BOOSTER ENTRY MISSION SIMULATION RESULTS

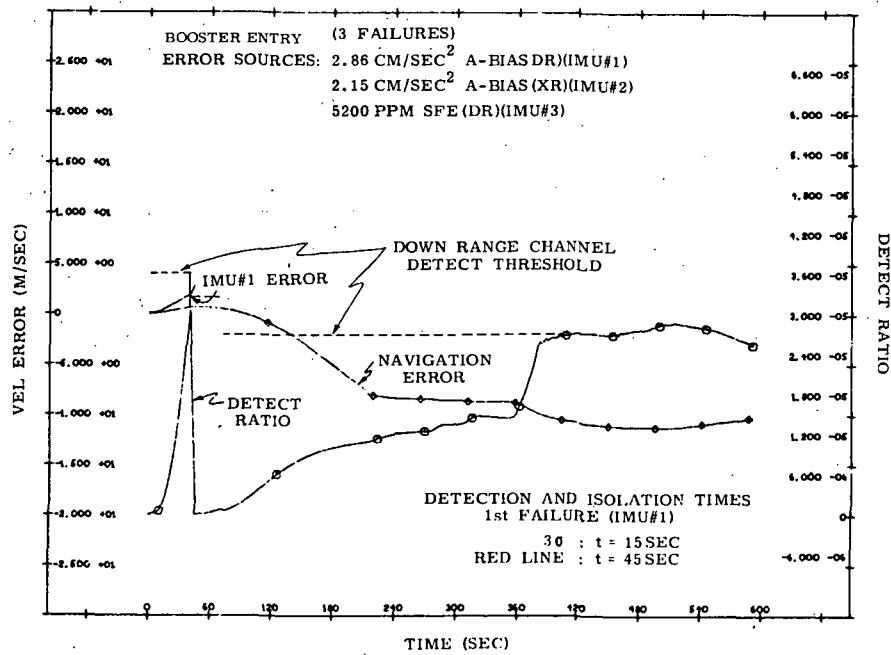


Figure 5.8

### BOOSTER ENTRY MISSION SIMULATION RESULTS

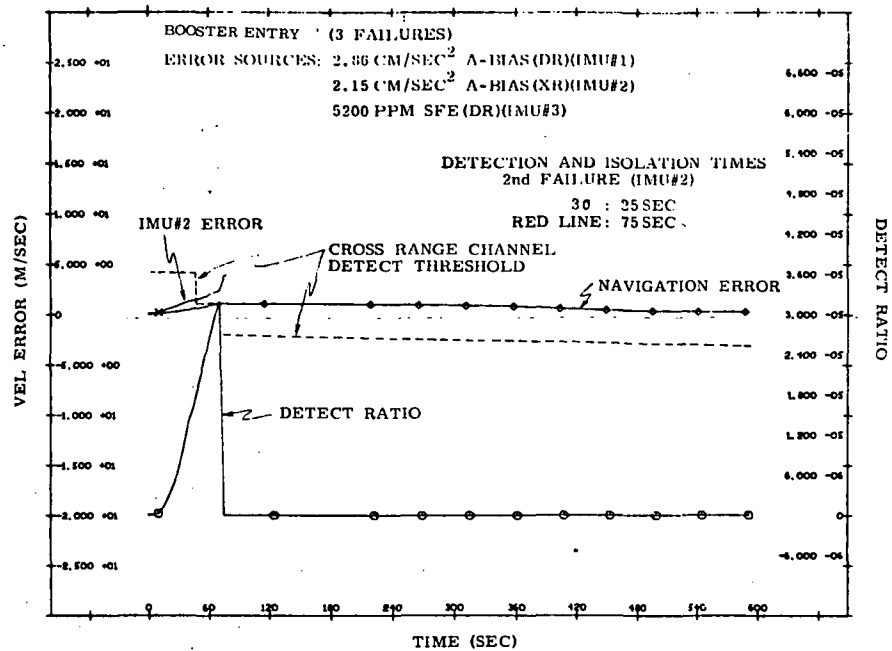


Figure 5.9

### BOOSTER ENTRY MISSION SIMULATION RESULTS

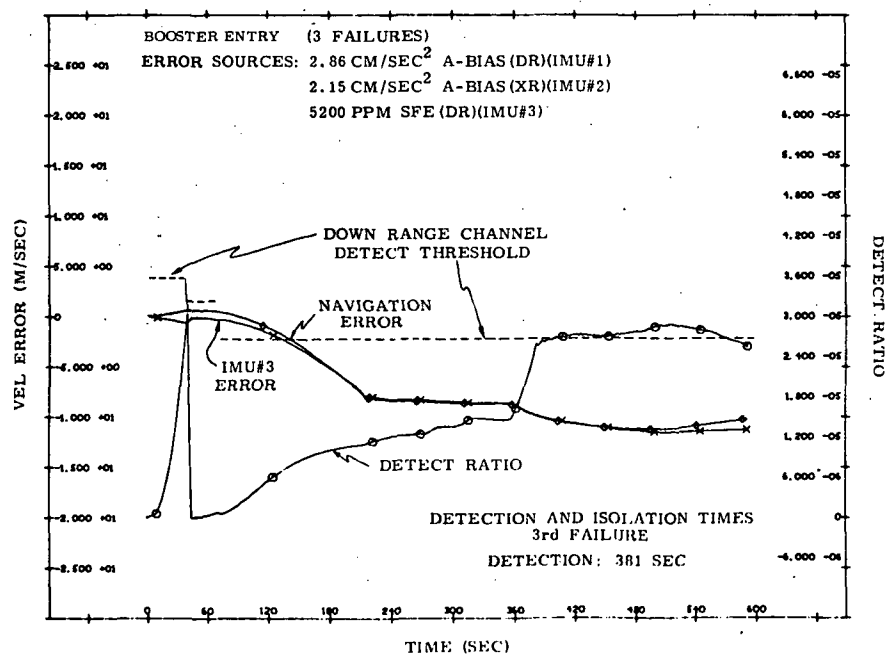


Figure 5.10

### BOOSTER ENTRY MISSION SIMULATION RESULTS

after 381 seconds. Review of figures 5-8 through 5-10 again demonstrates that detection and isolation times are independent of the number of error sources.

### 5.3 ORBITER ENTRY VELOCITY FDI TEST RESULTS

The two levels of error isolation and third detect for the orbiter entry trajectory are demonstrated in figures 5-11 through 5-15. The redline threshold for this trajectory is unique in that it is represented by an exponential in time, rather than a piecewise constant. A first failure of .75 deg/hour (50 meru) bias drift on the z-gyro is shown in figure 5-11. Detection and isolation time is 5502 seconds into the flight or 1088 seconds after FDI initialization. The FDI is started at 4414 seconds into the flight for all orbiter entry simulations.

The two failure case (figures 5-12 and 5-13) is the same as the first case, with the addition on a 5m radian inflight alignment error for all axes of IMU #2. It can be seen from figure 5-12 that 12 more seconds ( $t=5514$ ) are required to isolate the .75 deg/hr bias drift in IMU #1. The inflight alignment error is isolated at 5902 seconds into the flight or 1488 seconds from FDI initialization. This is shown in figure 5-13.

The third detect is demonstrated by augmenting the system with an IMU containing an accelerometer whose bias is  $2400\mu g$ . Figure 5-14 shows the first fail (accelerometer bias) at 4430 seconds and third detect at 4831 seconds. The second failure (inflight alignment error) is detected and isolated at 4682 seconds seen in figure 5-15.

Notice that the orbiter cases have not shown the perfect consistency in detection and isolation times that were evident in the nominal boost and booster abort trajectories, and that they are by far the most sensitive test of the FDI implementation.

### 5.4 ORBITAL FLIGHT GYROSCOPE FDI TEST RESULTS

Figures 5-16 through 5-21 summarize the simulation results for the gyroscope drift failure detection and isolation.

The trajectory for these simulations is a 100 nm equatorial orbit. The x-axis of the IMU is out of plane, directed north. There is a constant vehicle rate about the x-axis equal to the orbital rate (i.e. the vehicle is in a local vertical mode). The failure drift threshold is set at .75deg/hours (50 meru). This value represents the reentry requirement of gyroscope bias uncertainty. All drift errors put in the

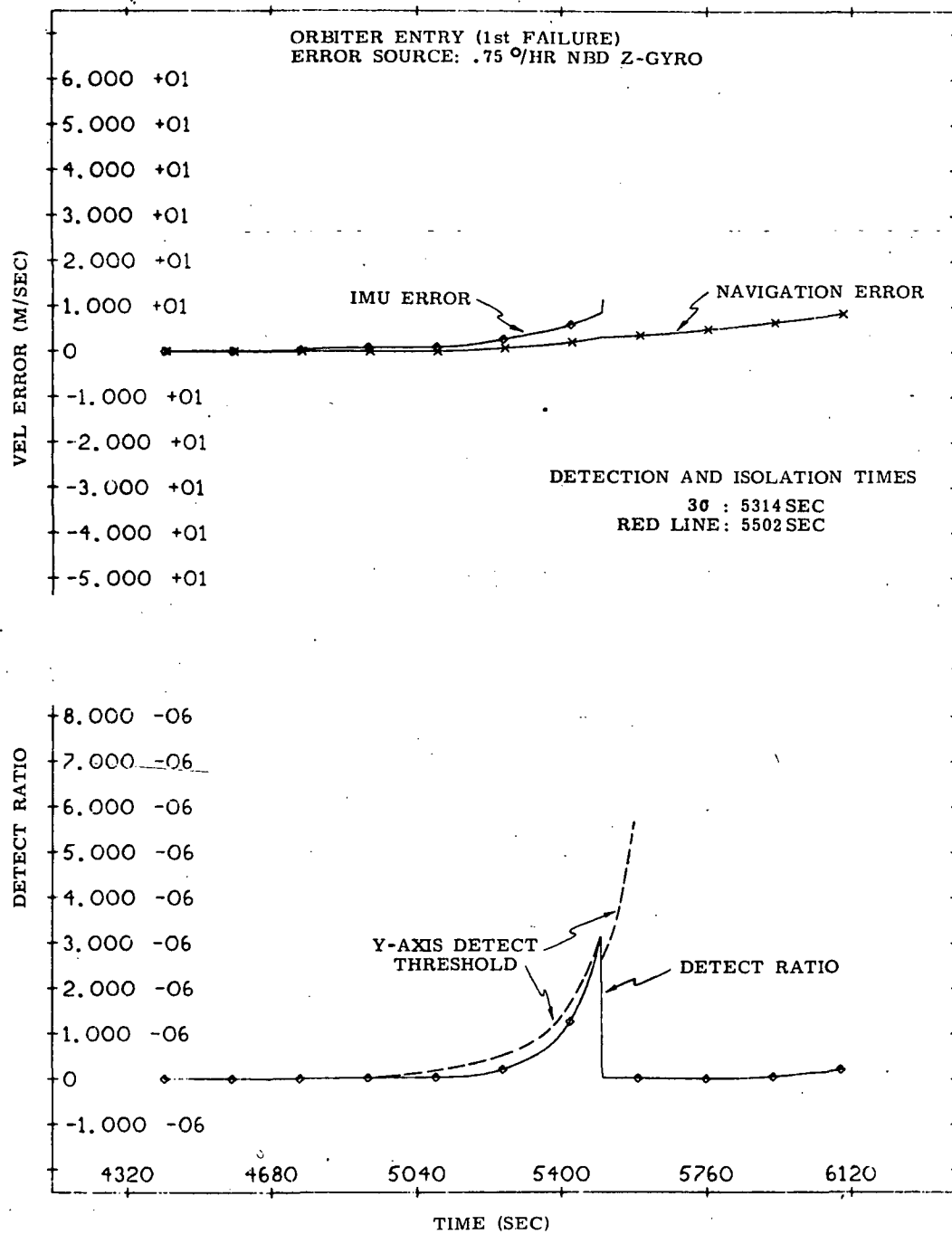


Figure 5.11

# ORBITER ENTRY MISSION SIMULATION RESULTS

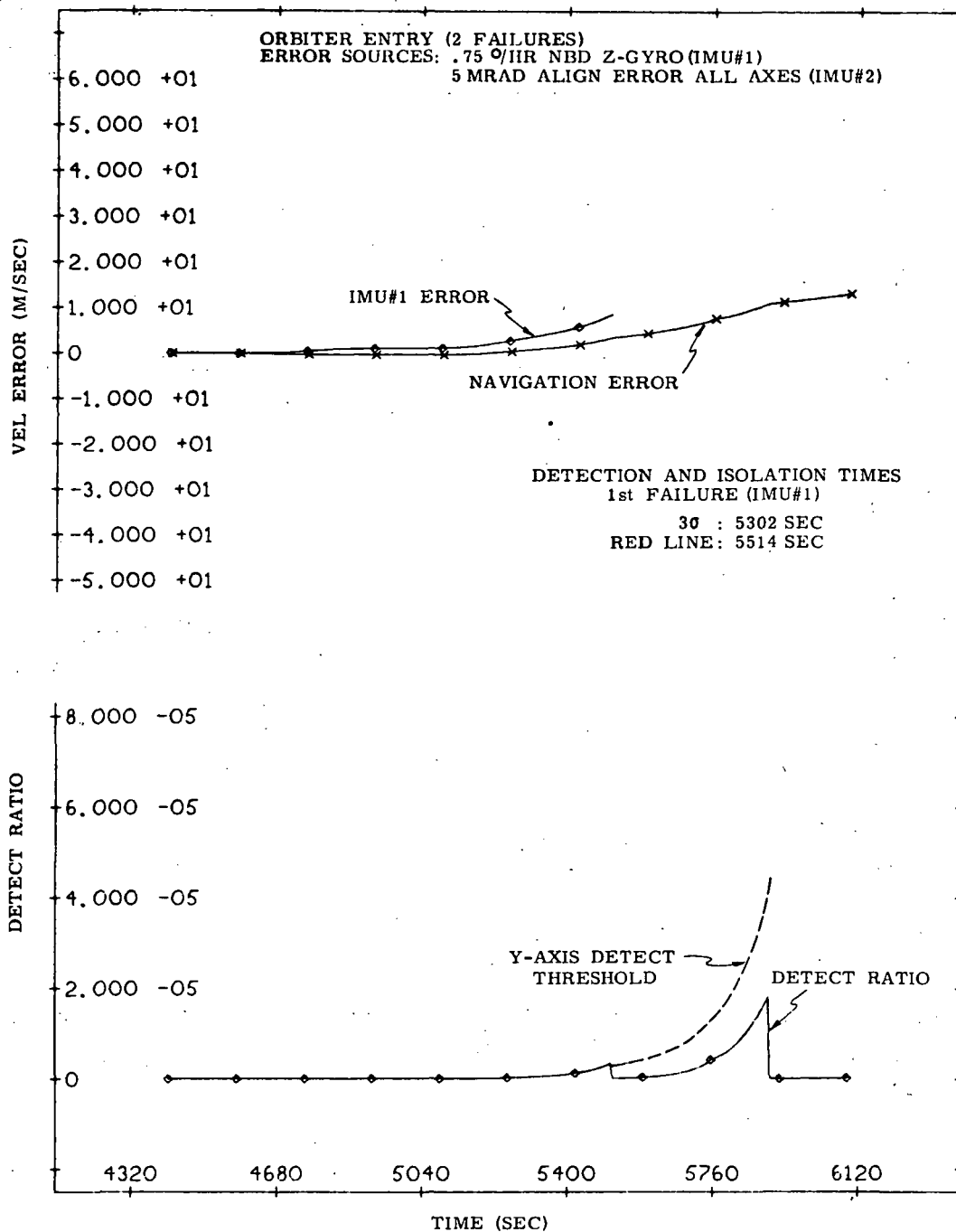


Figure 5.12

ORBITER ENTRY MISSION SIMULATION RESULTS

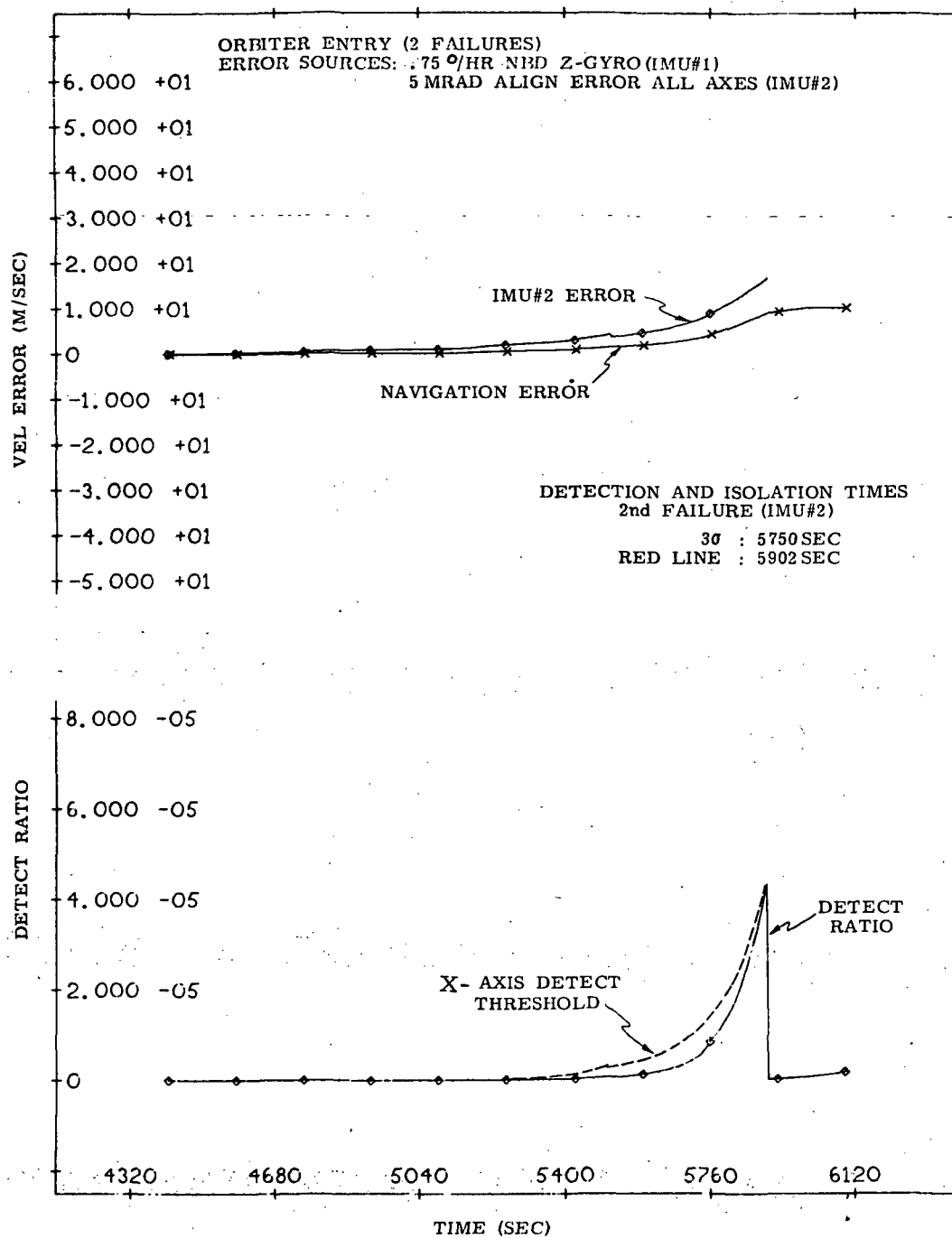


Figure 5.13

# ORBITER ENTRY MISSION SIMULATION RESULTS



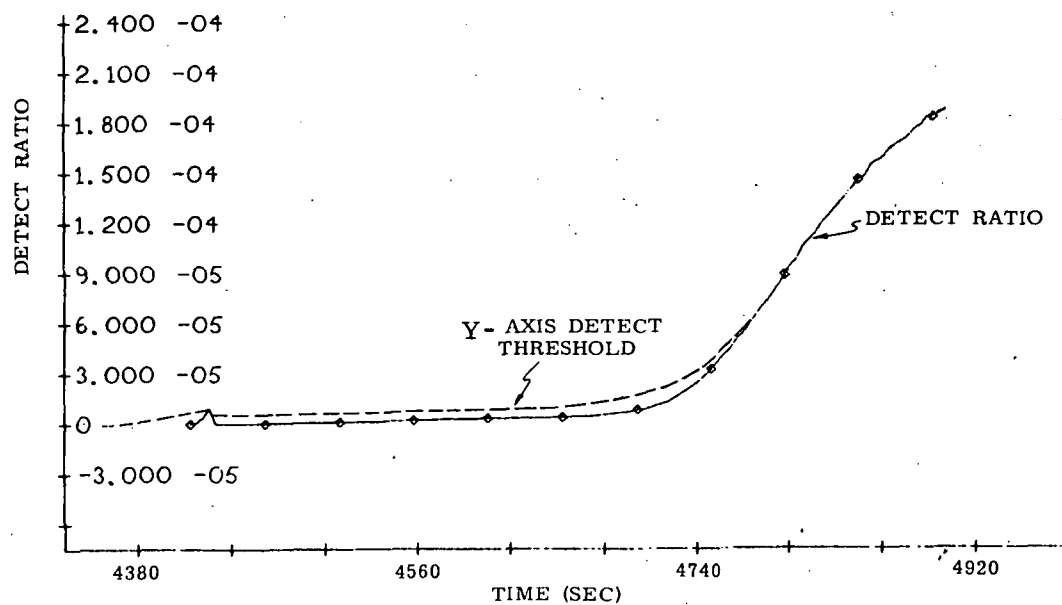
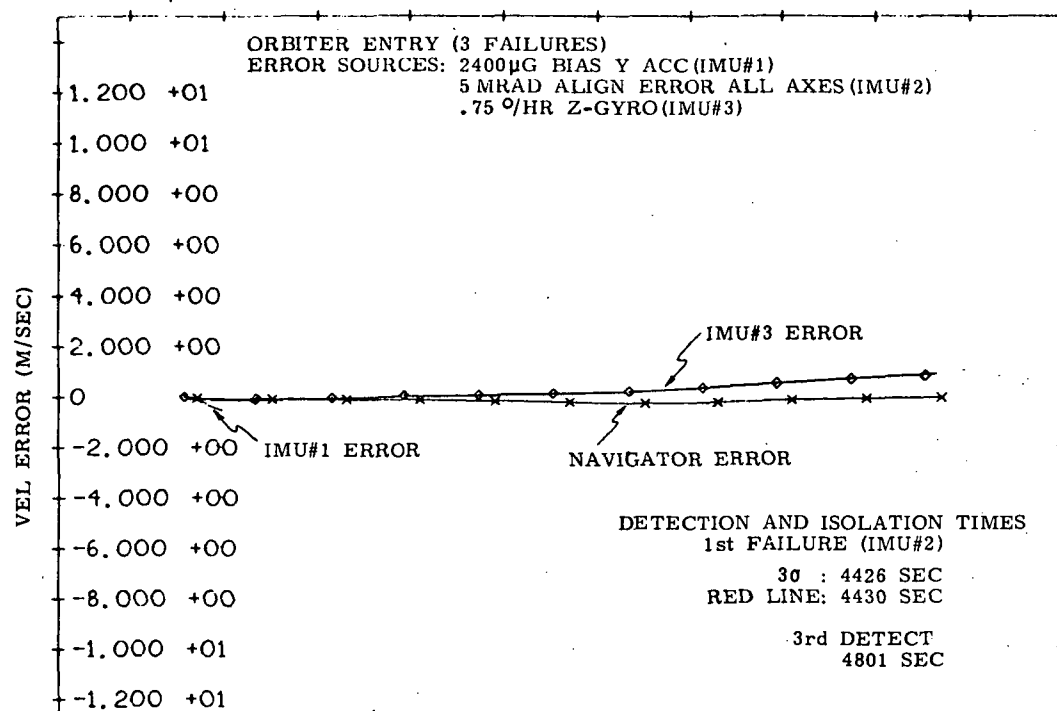


Figure 5.14  
 ORBITER ENTRY MISSION SIMULATION RESULTS

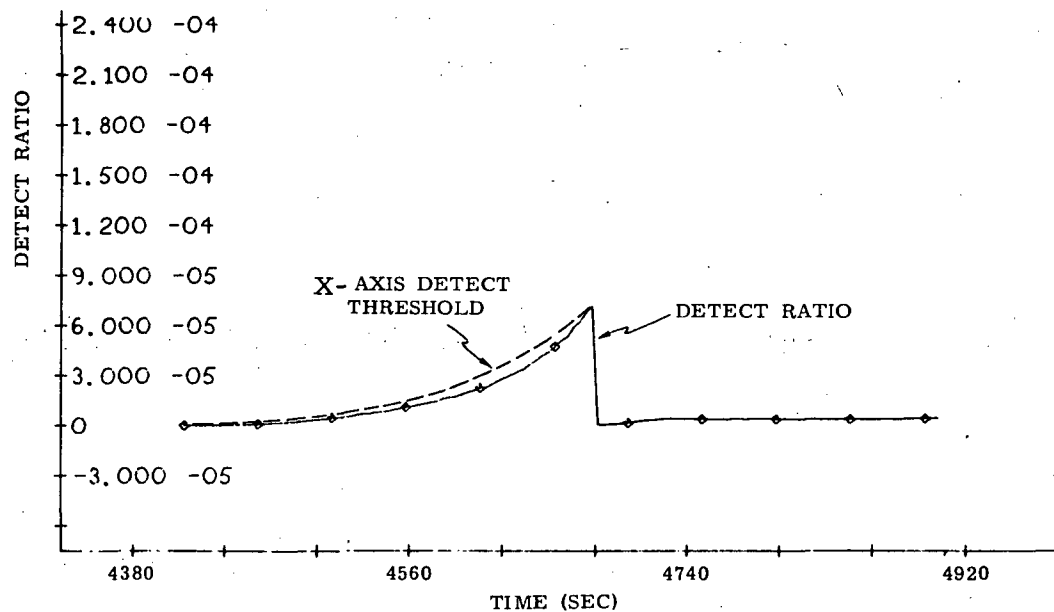
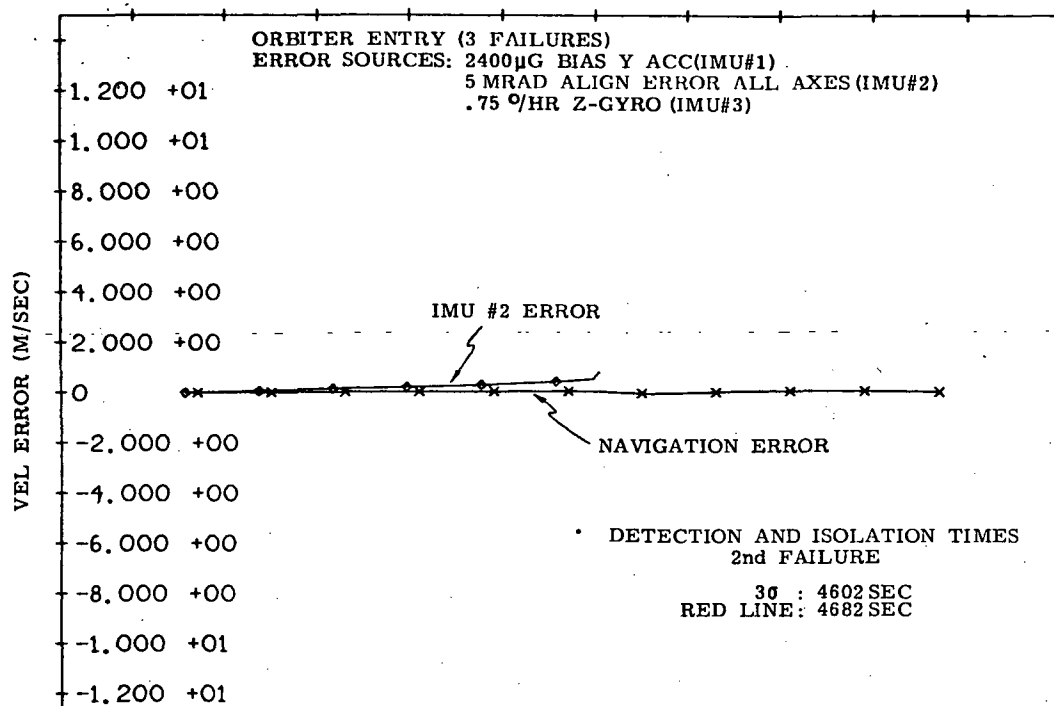


Figure 5.15

ORBITER ENTRY MISSION SIMULATION RESULTS

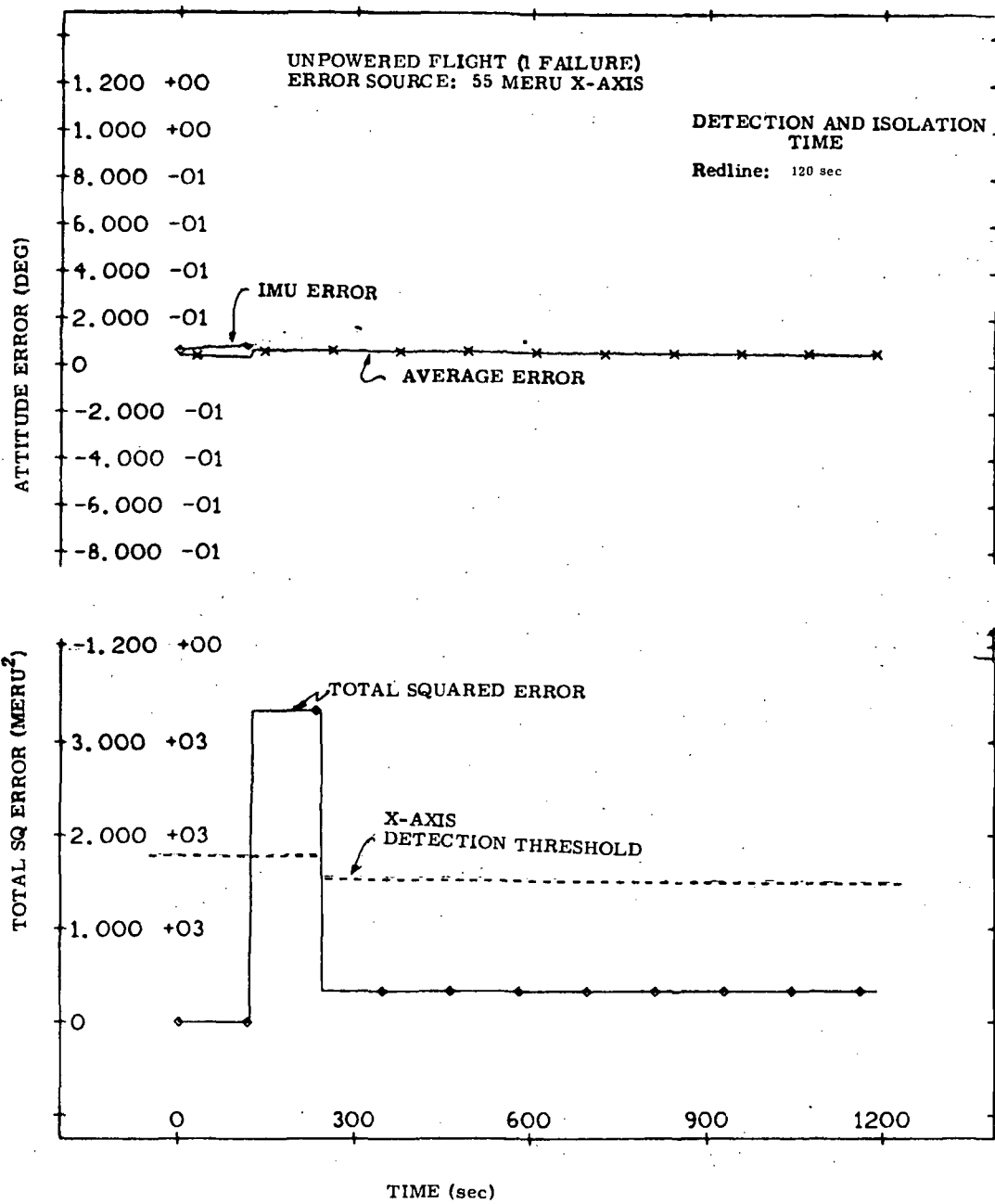
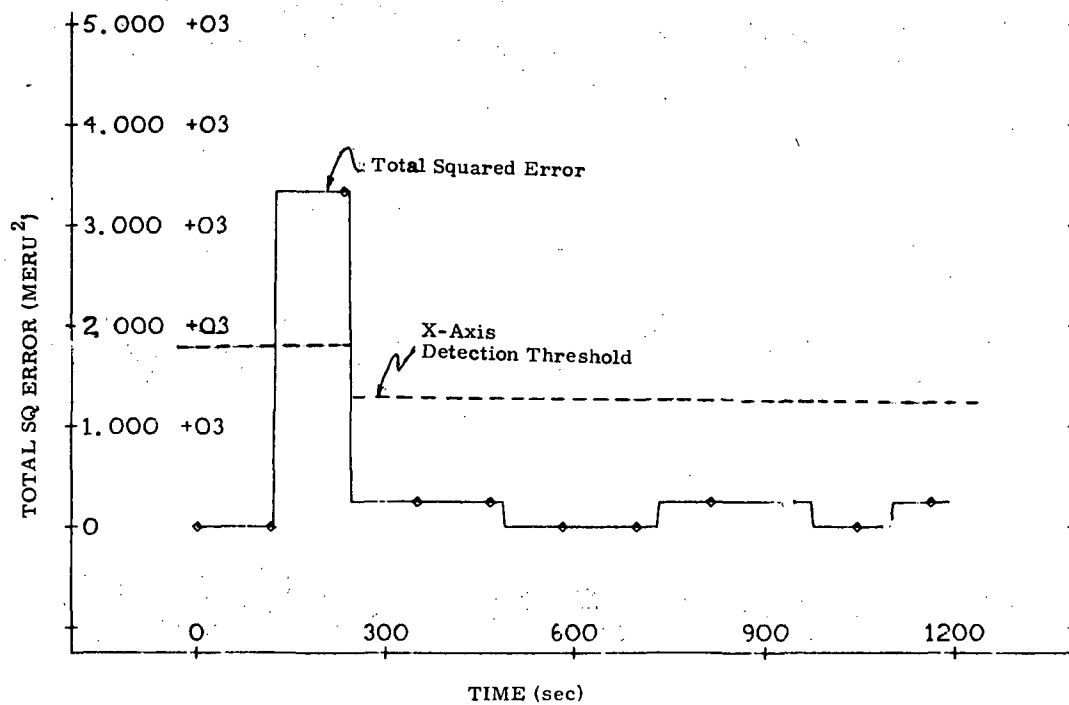
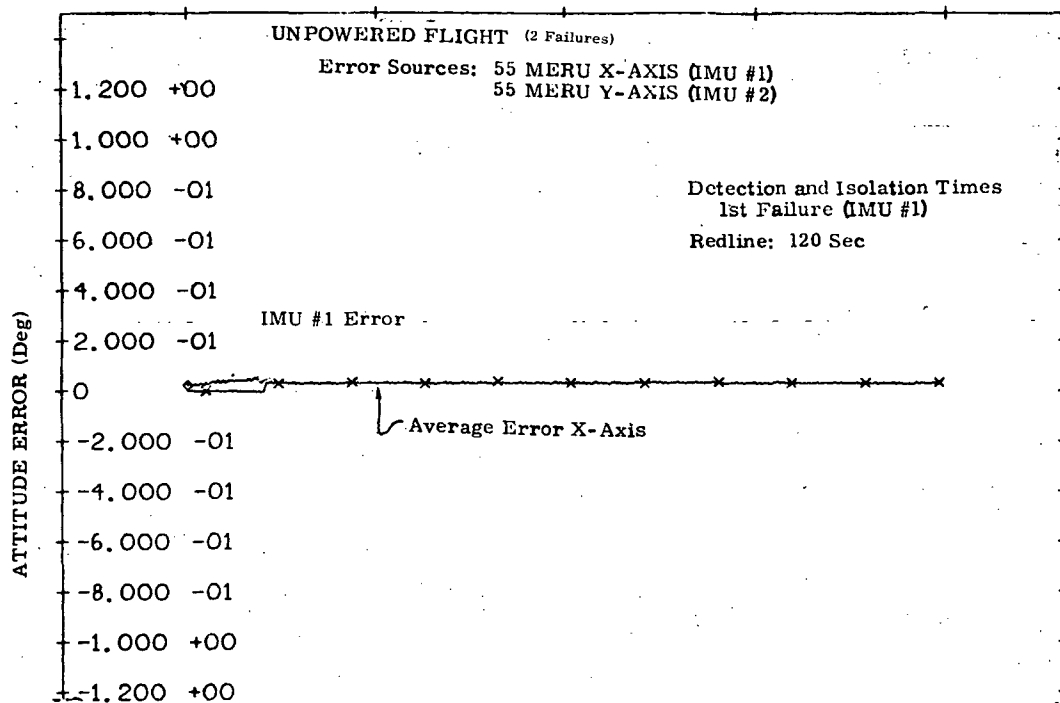


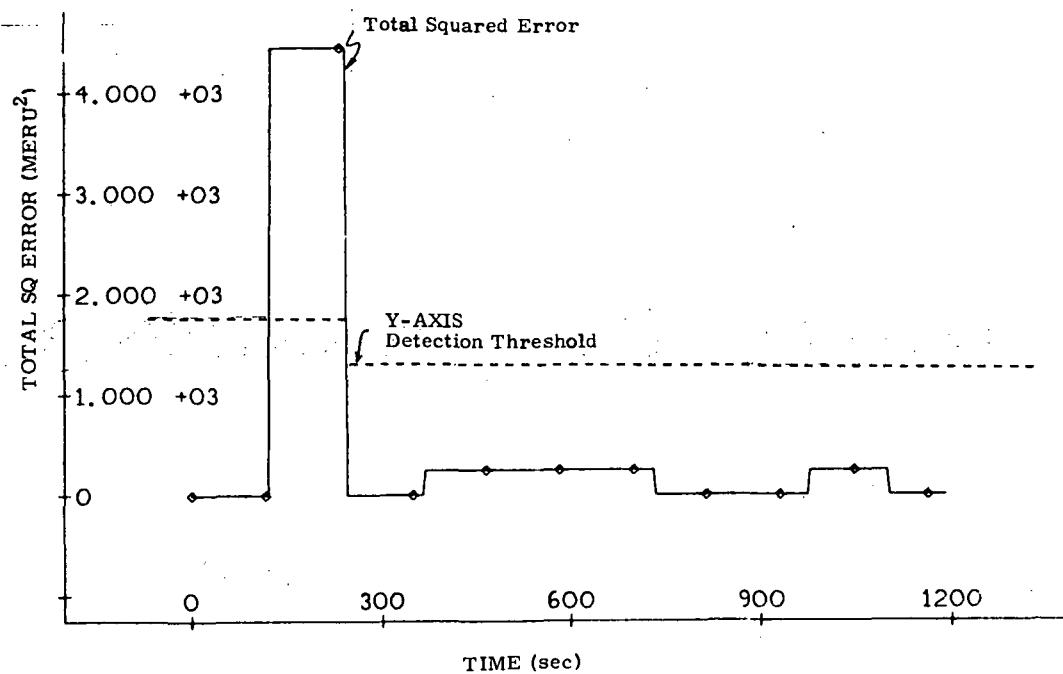
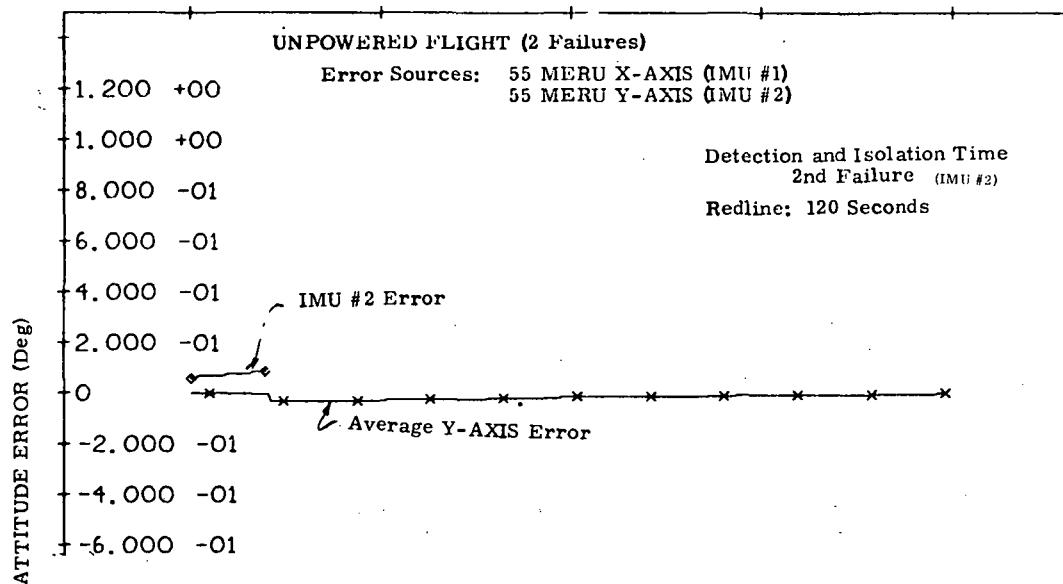
Fig 5-16

# UNPOWERED FLIGHT SIMULATION RESULTS



# UNPOWERED FLIGHT SIMULATION RESULTS

Fig 5-17



### UNPOWERED FLIGHT SIMULATION RESULTS

Fig 5-18

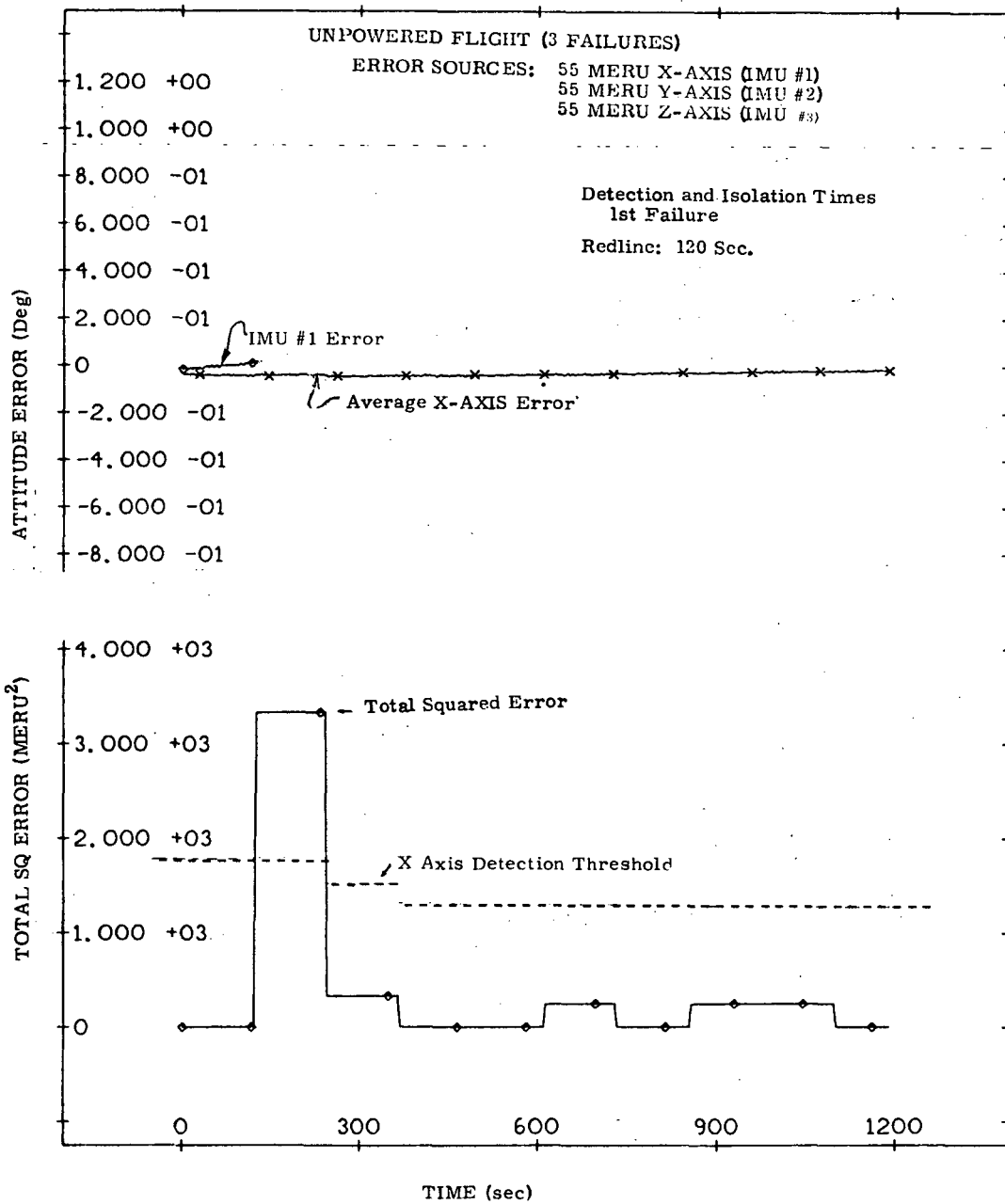
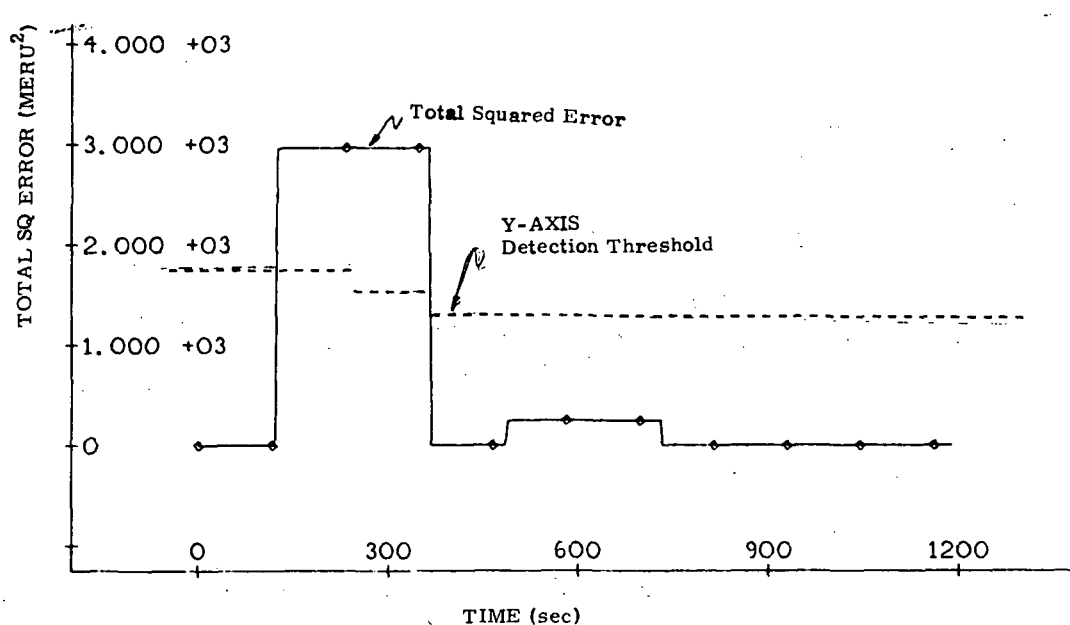
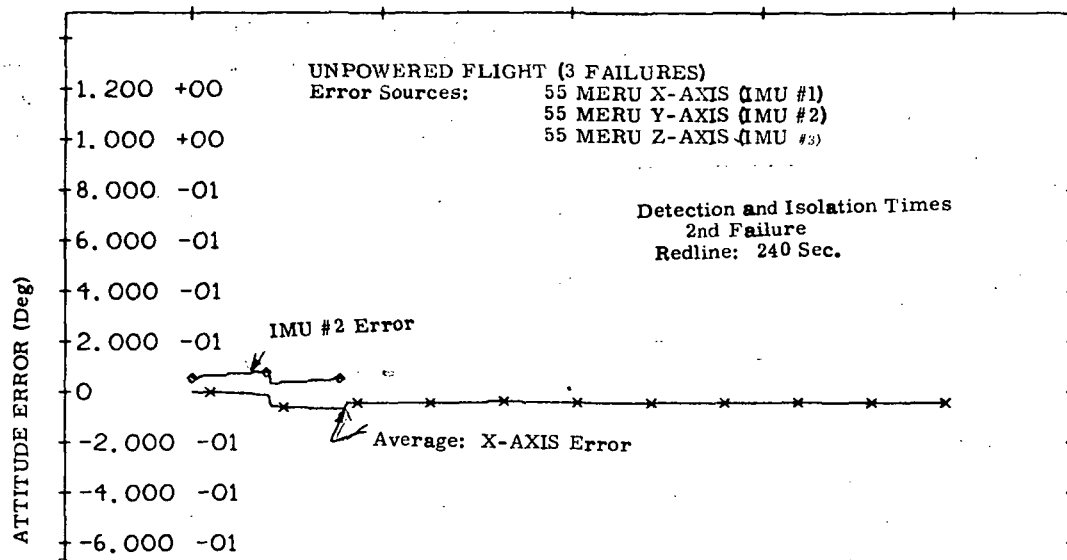


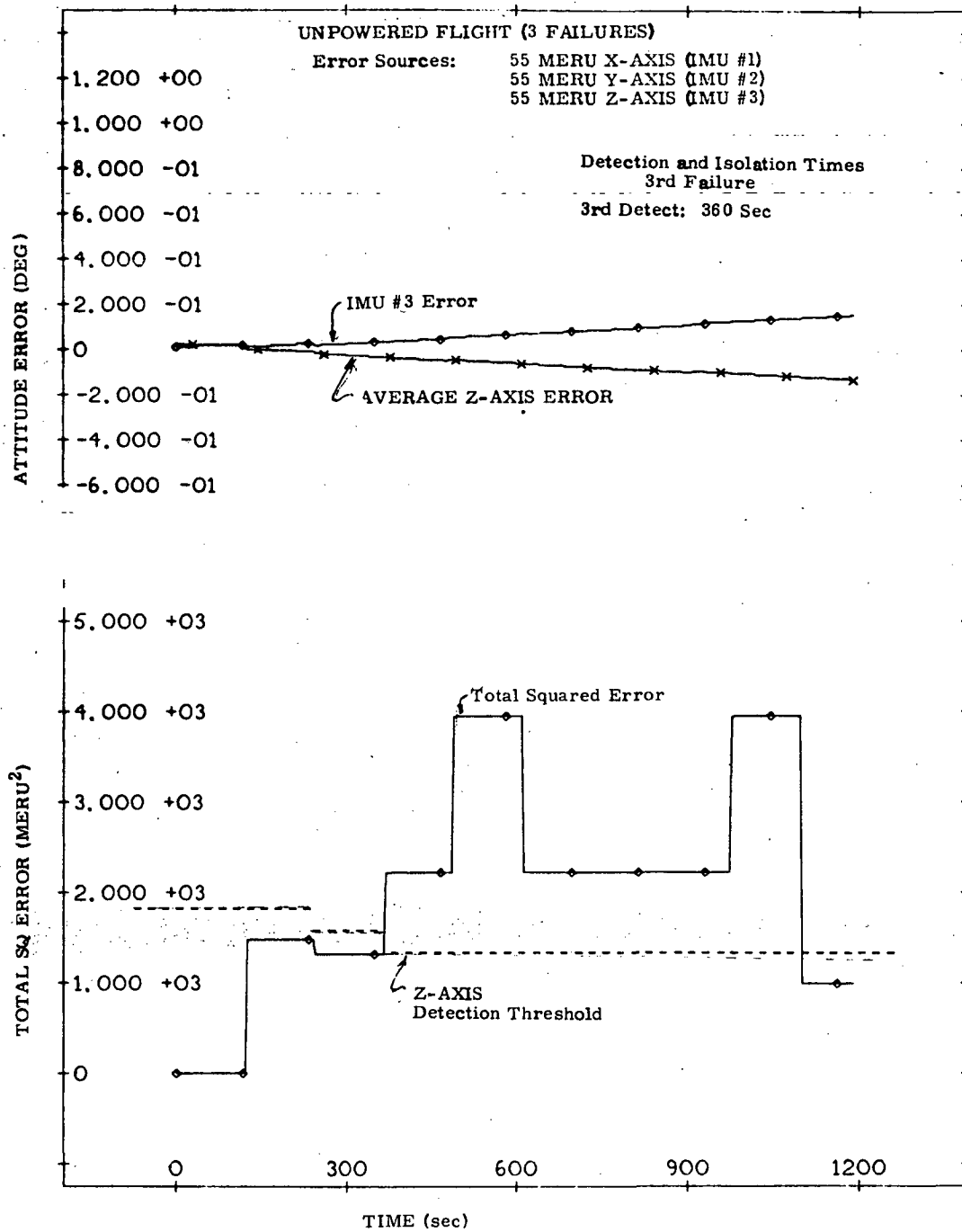
Fig 5-19

# UNPOWERED FLIGHT SIMULATION RESULTS



# UNPOWERED FLIGHT SIMULATION RESULTS

Fig 5-20



### UNPOWERED FLIGHT SIMULATION RESULTS

Fig 5-21



simulations are 10% above this required threshold. The gimbal angle quantization level is assumed to be 40 arcseconds, and the  $\Delta T$  used in estimating angular rate is set at 120 seconds. That is, all detection and isolation variables are computed every 120 seconds and remain constant over the succeeding 120 seconds. Thus the total squared error (TSE) in all the graphs appears as quantized steps.

The first failure case is represented in figure 5-16. As mentioned previously, the input drift is .825deg/hour (55 meru) on the x-axis. A single time step was required to detect and isolate this failure.

Figures 5-17 and 5-18 show the results of two failures. These failures are 55 meru on the x-axis of IMU #1 and 55 meru on the y-axis of IMU #2. Both failures are detected and isolated in one time step.

The third detection capability is shown in figures 5-19 to 5-21. The third error is 55 meru on the z-axis of IMU #3. The first failure (fig. 5-19) is detected and isolated in one time step. It can be seen from figure 5-20 that the detection threshold is satisfied in one time step for the second failure, but two steps are required to provide isolation. The third failure is detected (fig. 5-21) after 3 time steps. It should be noted all cruise flight simulations were also exercised at drift levels slightly below the .75°/hr critical threshold and no detection or isolation was found.

## 5.5 TWO IMU FDI SIMULATION RESULTS

The simulation results in the next four parts demonstrate FDI capability when only two IMUs are remaining and detection and isolation are at the instrument level. In these four cases, one of the IMUs has been skewed by 60 degrees about an axis which is diagonal to the instrument triad axes.

The first three cases represent powered flight FDI in nominal boost, booster abort and orbiter entry. Each case demonstrates one of the three possible powered flight detection criteria (i.e. velocity magnitude error, platform angular error, and platform drift error).

The final case represents unpowered flight, drift error detection and isolation.

### 5.5.1 Nominal Boost

The nominal boost simulation is an extension of the test shown in figures 5-3 and 5-4. The error sources are 6750 ppm SFE in the altitude accelerometer

of IMU#1,  $3330\mu g$  bias in the down range accelerometer of IMU#2, and 5 mrad accelerometer misalignment in IMU#3. In addition to these errors, an analog torquing scale factor of -1000 ppm was assumed to be introduced while slewing the IMU to its skewed orientation. Figures 5-22 and 5-23 show the altitude navigation velocity error and the detect ratio. Slewing starts after the second failure is isolated at time=34 seconds as shown in figure 5-3 and is completed at 104 seconds. Detection and isolation is accomplished at  $t=226$  when the red line threshold is reduced. The effect of reconfiguration is displayed in the navigation velocity error.

This same simulation was performed with an assumed +1000 ppm analog torquing scale factor error. This torquing error reinforces the accelerometer misalignment so that third failure detection and isolation is accomplished earlier ( $t=192$  seconds).

#### 5.5.2 Booster Entry

The booster entry simulation is a continuation of the three failure simulation shown in figures 5-9 and 5-10. The error sources are  $2.86\text{cm/sec}^2$  down range accelerometer bias in IMU#1,  $2.15\text{cm/sec}^2$  cross range accelerometer bias in IMU#2, and 5200 ppm down range accelerometer scale factor error in IMU#3. The analog torquing scale factor error is again set at +1000 ppm.

Figures 5-24 and 5-25 show the down range navigation velocity error and the velocity magnitude detect ratio. Slewing starts after isolation of the second failure ( $t=60$  seconds) and is completed at  $t=130$  seconds. The third failure is isolated to IMU#3 at  $t=363$  seconds. Removal of IMU#3 can be seen in the navigation velocity error.

#### 5.5.3 Orbiter Entry

The orbiter entry simulation extends the results shown in figures 5-14 and 5-15. The error sources are  $2400\mu g$  accelerometer bias on the y-axis of IMU#1, 5mrad inflight alignment error on all axes in IMU#2, and .75degree/hour NBD in the z-axis gyro of IMU#3.

Figures 5-26a,b,c show the navigation error of the average IMU velocity with respect to the perfect IMU velocity for all three axes and figure 5-27 is the two IMU attitude drift detect ratio. After IMU#1 and IMU#2 have been removed from the system, the major sources of error are the  $.75^\circ/\text{hr}$  NBD on the

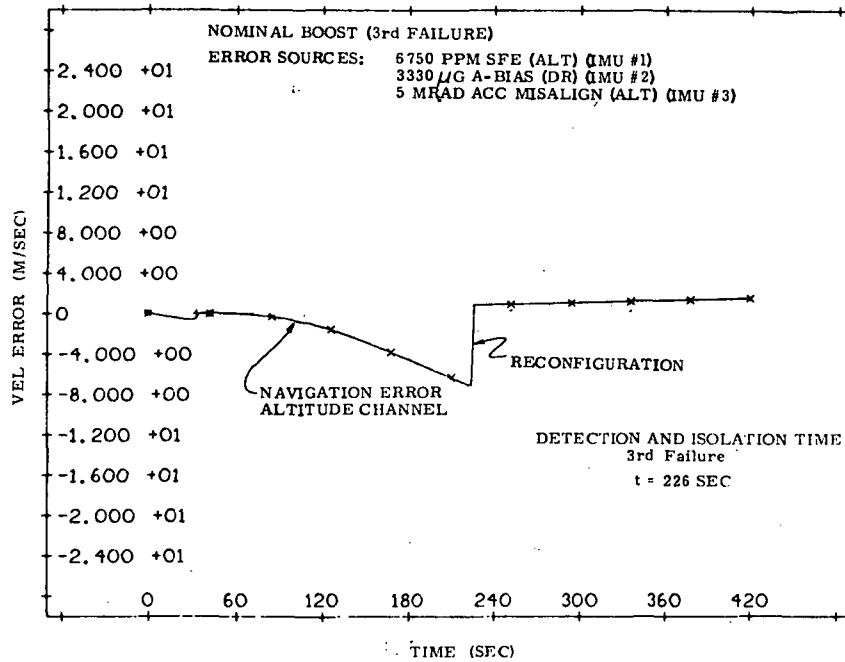
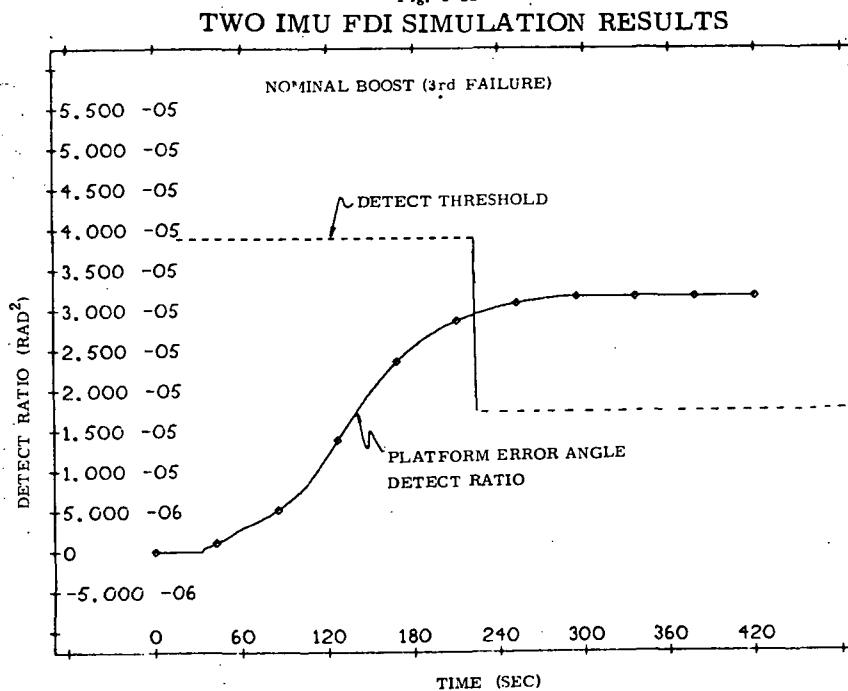


Fig. 5-22



TWO IMU FDI SIMULATION RESULTS

Fig. 5-23

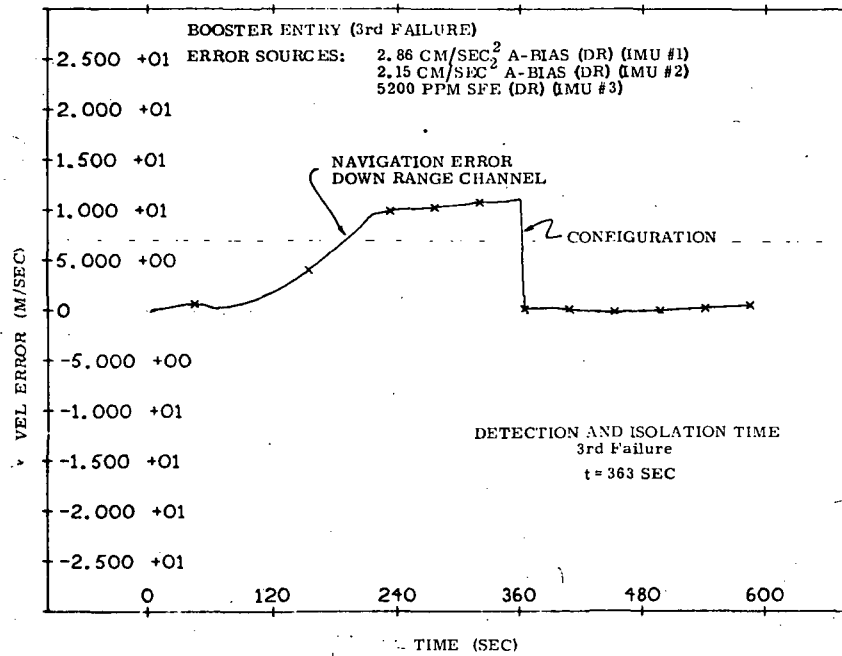


Fig. 5-24

### TWO IMU FDI SIMULATION RESULTS

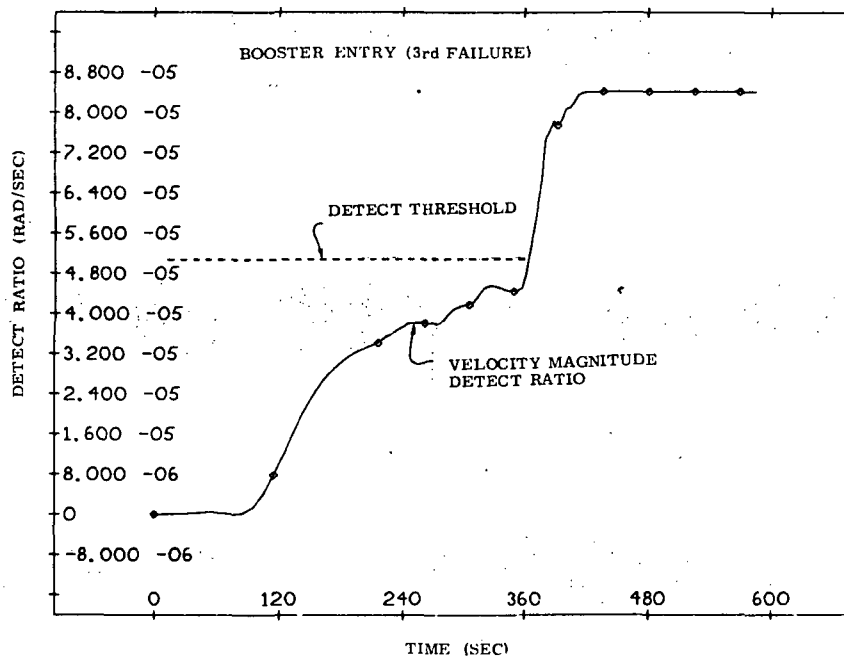


Fig. 5-25

### TWO IMU FDI SIMULATION RESULTS

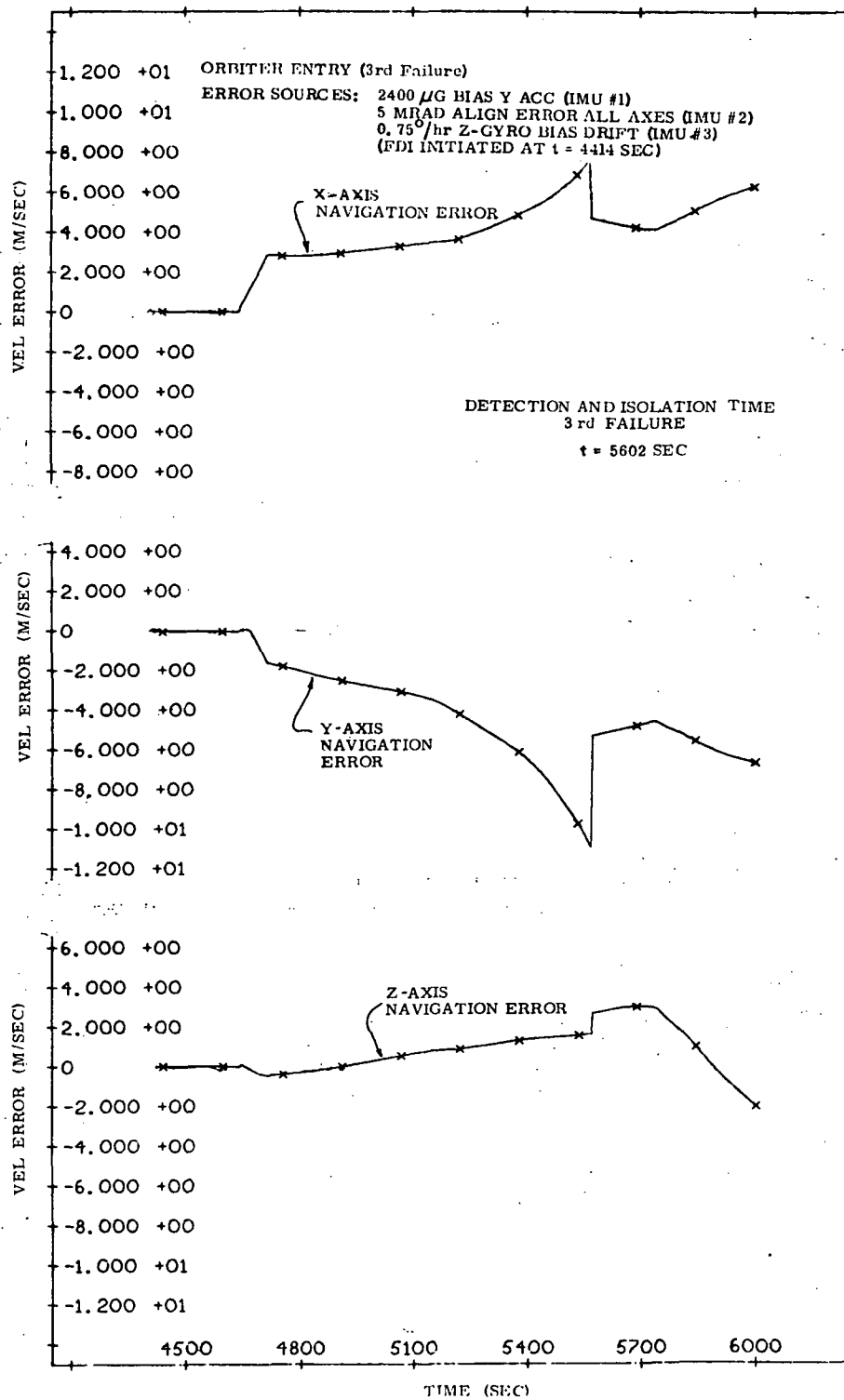


Fig. 5-26

## TWO IMU FDI SIMULATION RESULTS

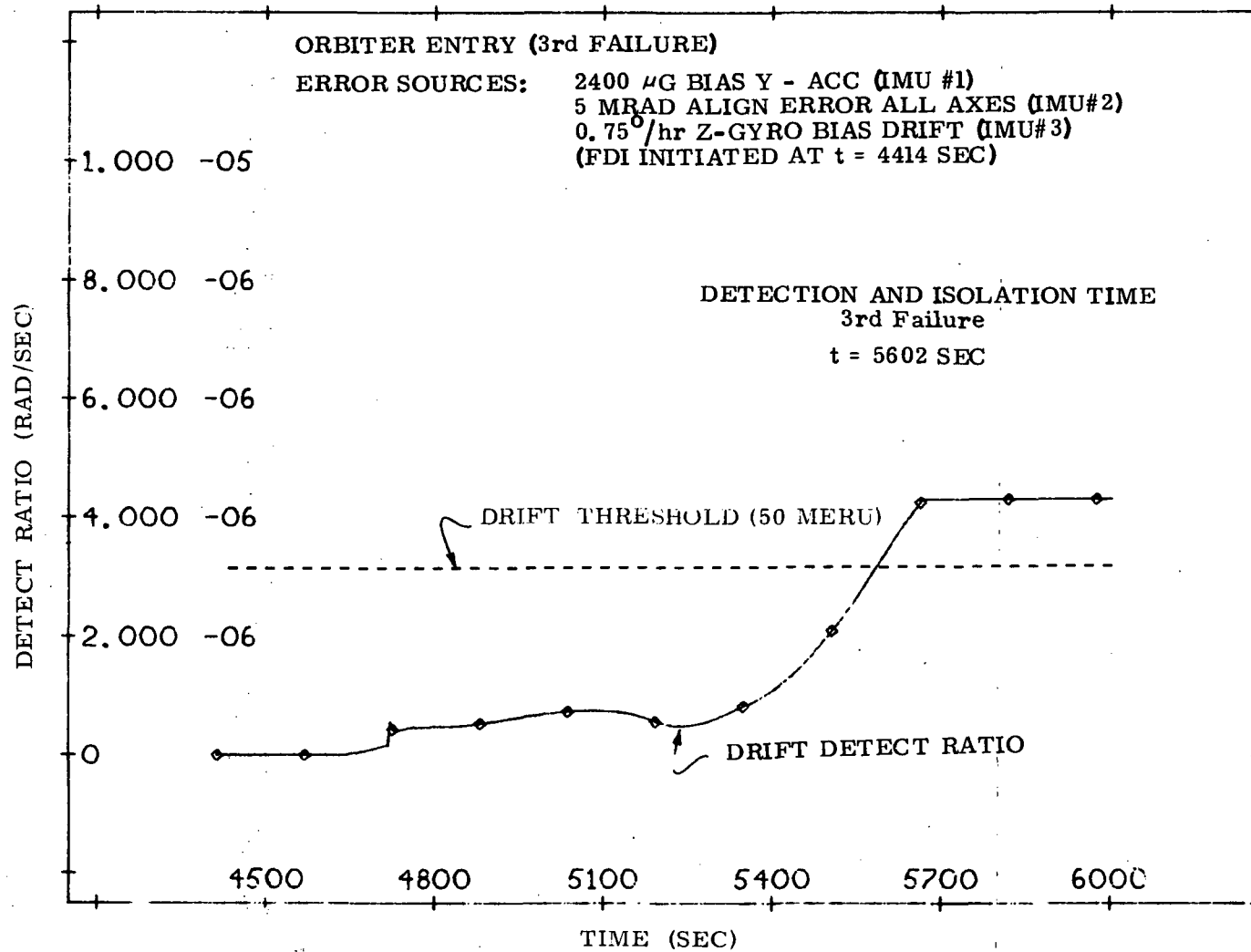


Fig. 5-27

TWO IMU FDI SIMULATION RESULTS

z-axis of IMU#3 and the assumed 1000 ppm analog torquing scale factor error. Slewing was initiated after the second failure was isolated at t=4682 sec. The bias drift error is detected and isolated at 5602 seconds. It can be seen that the drift error has the least effect on the Z velocity. The effect of the analog torquing scale factor error can be seen in all velocity error profiles at 4600 seconds. This effect is not negligible.

#### 5.5.4 Unpowered Flight

The unpowered flight demonstration of two IMU FDI is mechanized by simulating two IMUs in a skewed configuration. IMU#1 is a simulated 1 $\sigma$  instrument. IMU#2 contains a 55 meru bias drift on the y-axis. The FDI algorithm estimates drift by differencing angular error estimates at two times, 300 seconds apart. As can be seen from figures 5-28 and 5-29 only one sample period is required to correctly detect and isolate the failed IMU.

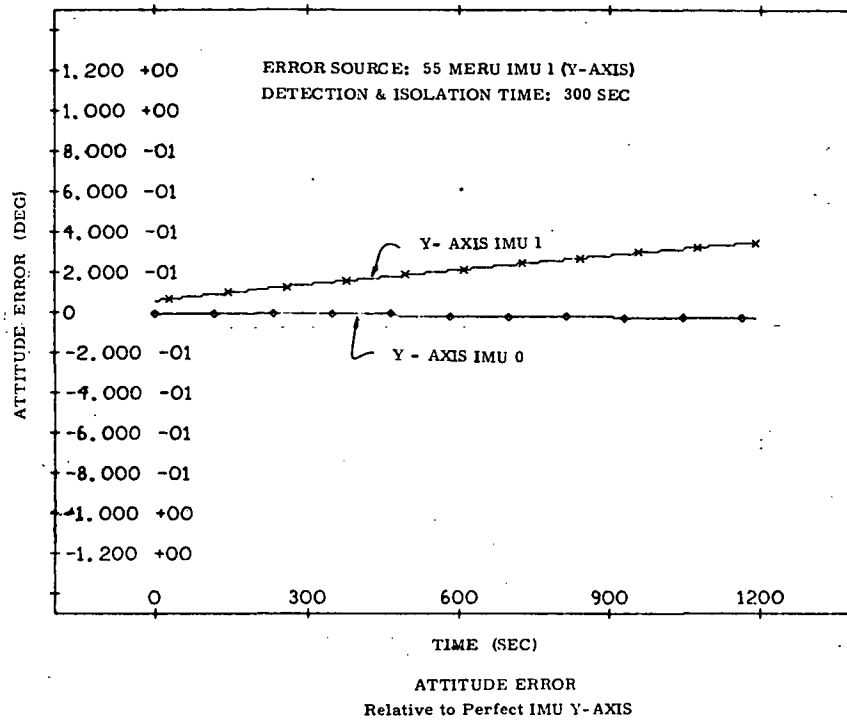


Fig. 5-28

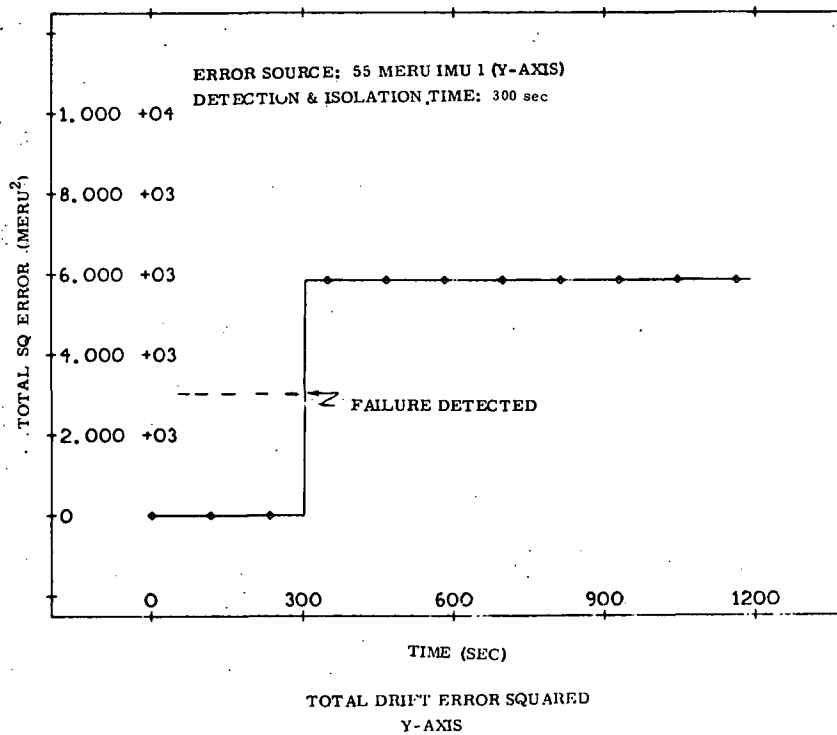


Fig. 5-29



**Page intentionally left blank**

## 6.0 SYSTEM CHECKOUT PHILOSOPHY AND PRELAUNCH VERIFICATION

Multiple IMU inertial system checkout methods differ markedly from those of conventional, single IMU systems. They enjoy a significant advantage in that internally redundant data can be used for self checking to reasonability limits. Further, in implementations which do not include external optical data for absolute external alignment, the component IMUs can be initialized independently and verified with respect to each other.

In view of the unique characteristics of a multiple system, an appropriate checkout philosophy and technique must be developed. The goals of the checkout remain identical with those of earlier inertial systems: completeness and precision with a minimum test time. To these must be added the requirement that the test sequences be completely on-board and self-contained. Presumably, the inherent features of the multiple system would be exploited during checkout. The discussion which follows assumes a baseline system consisting of four four-gimbaled IMUs with parallel triads mounted on a single navigation base. This discussion also applies directly to the three IMU implementation. An onboard computer monitors and controls all IMUs. It will be assumed that no optical alignment aids are available, either as a sextant mounted on the navigation base or an optical path to mirrors mounted on the stable members.

This chapter comprises a brief discussion of the checkout philosophy proposed and describes two possible verification tests. A multiple position test enabling solution for accelerometer error parameters and a reasonability comparison of gyro drift measurements with reasonability estimates drawn from previous calibration loads is recommended for implementation.

### 6.1 CHECKOUT PHILOSOPHY

Interest here is directed toward a system verification test to be performed during the countdown prior to launch. It should be emphasized that shuttle vehicle operational requirements demand a countdown which is short compared to the multiple day Apollo checkout. In turn, this necessitates shorter individual tests, and, further, that individual subsystem tests become almost entirely autonomous.

In short, the shuttle vehicle requirements envisioned dictate a prelaunch test and alignment program employing no external or carry-on GSE, no optics, and, if possible, no human interpretation or intervention. One additional goal is to perform the prelaunch verification and alignment sequence in less than four hours.

The foregoing requirements will dictate the form of the prelaunch checkout. Its underlying philosophy, however, follows from the goal of the test. This goal, simply stated, is to determine that the projected performance and reliability of this system is sufficient to allow committing the vehicle to the mission.

It must be assumed, at this point, that a considerable body of knowledge about the characteristics of the flight hardware is available. Given this information, tests of reliability can be devised. The Apollo IMU provides a clear example of testing techniques devised from comprehensive knowledge of the flight hardware. The acceleration sensitive drift term due to specific force along the gyro's IA was normally stable to within  $0.075^{\circ}/\text{hr/g}$  (5 meru/g). A shift of  $0.375^{\circ}/\text{hr/g}$  (25 meru) proved to be a reliable indication of impending wheel bearing failure.<sup>11</sup> Experience proved that a gyro exceeding the "Delta 25 criterion" would operate with acceptable performance for at least an additional 200 wheel hours, long enough to carry the IMU through an Apollo flight even if the shift was found during prelaunch checkout. It is only from experience with a given instrument in a system that such criteria may be devised.

The prelaunch checkout test will not serve as a system calibration procedure. It will seek only to compare present performance (as defined by lumped error parameters) with previous calibration history, and to answer the following questions.

Are measured shifts within acceptable limits? Is the present reliability projected for the system sufficient for the mission? In summary, are any soft failures present? The test must also answer the more mechanical question: have any hard failures occurred either intermittently or continuously?

Since no external references are provided, the only judgements which may be made compare the output of one instrument or IMU with another, or with an average of all the IMUs. In practical terms, this means that four values of drift about a gimbal axis will be measured, each of which can be compared with the rest. No absolute gyro drift term is extracted from these data.

The philosophy of the prelaunch checkout test may then be summarized. An autonomous test is to be defined which will estimate lump drift parameters and measure relative drifts. These errors will be compared with the system's calibration history, on one hand, and with predetermined thresholds, on the other. The end results of the test will be a projection of system reliability with a consequential go/no go decision. Possible remedial actions will be re-compensation and a full retest, or a call for external judgements.

## 6.2 VERIFICATION TESTS

The purpose of the verification test is to project inertial system reliability, and determine whether it meets mission requirements. This decision can be based only on measurements of system performance as close to actual flight as possible.

Two broad classes of verification test can be described. One seeks to measure inertial component parameters, and use them for comparison with established limits. These tests resemble the classical procedures closely, and need not utilize redundant properties of the system. A second class of tests measures IMU output and compares it with output of other IMUs. Comparison might be made, for instance, through use of the multiple IMU FDI. These tests rely on the redundant quality of available data.

### 6.2.1 Testing Against Limits

The limits against which current performance are checked can be a combination of the mission red lines (derived in Chapter 4), or current single IMU performance can be judged directly against the other IMUs in the multiple system.

Mission red lines have been treated extensively in Chapters 4 and 5. The red lines for each mission phase (tables 3.1 to 3.3) may be distilled down to the following limits (table 6.1), merely by taking the most stringent requirement on each term. Notice that all thresholds used must be redetermined considering the single gravity prelaunch environment. Limits on some axes are not, in the previous chapters, as stringent as on others. However, testing all axes to the most demanding requirement is sufficient and is simpler than testing against a large set of individually established thresholds. (Red lines of parameters not included in table 6-1 exceed estimated  $30\sigma$  performance.)

Table 6.1 Established Mission Red Line Performance

<u>Term</u>	<u>Uncompensated Errors</u>
Accelerometer Bias	$\pm 1.77 \text{ cm/s}^2$
Accelerometer Scale Factor Error	+2010 to -6750 ppm
Gyro Non-G-Sensitive Drift	$-0.10^\circ/\text{hr}$ (7 meru)
Cross Range Gyro Spin Axis G-Sensitive Drift	$2.25^\circ/\text{hr/g}$ (150 meru/g)

The foregoing values must be compared critically with attainable system performance and must also be updated when additional mission phases or vehicle models are implemented. Kearfott has tabulated expected performance of its instruments (see Appendix A). Parameters directly comparable with those in Table 6.1 are:

Table 6.2. Estimated System Performance Uncertainties

<u>Term</u>	<u>Kearfott 3<math>\sigma</math> Estimate</u>
Accelerometer Bias	$\pm 0.30 \text{ cm/s}^2$
Accelerometer Scale Factor Error	$\pm 900 \text{ ppm}$
Gyro Non-G-Sensitive Drift	$\pm 0.03^\circ/\text{hr}$ (2 meru)
Gyro Spin Axis G-Sensitive Drift	$\pm 0.15^\circ/\text{hr}$ (10 meru)

Clearly, system performance meeting the uncertainties of Table 6.2 will easily meet the red line values. That is, nominal system performance is significantly better than mission requirements. Hence, it is suggested that a test to  $3\sigma$  parameters is sufficient for checkout purposes. These limits give added confidence that all systems are operating in their normally expected performance range. Mission red lines will presently be discarded for the prelaunch verification.

The remaining suggested limit is a comparison of each IMU's output against a similar value predicted using the measurements of all others, its own expected measurement. For this comparison, an estimate of performance is drawn for each group of IMUs. Comparison of the excluded IMU with the group is then made. It must be understood that the values derived represent only short term variations of actual measurements, and should not be associated directly with IMU performance as represented by a data history. Thus, consider four measurements,  $W_i$ ,  $i=1, 2, 3, 4$  along or about each axis. Permit  $W_i$  to be either specific force (along X, Y, Z) or a gimbal axis drift rate (about roll, pitch, yaw). Then the expected value of  $W_j$ ,  $\langle W_j \rangle$  is

$$\langle W_j \rangle = \frac{\sum_{i \neq j} (W_i)}{3} \quad (6-1)$$

then

$$\Delta W_{ij} = |\langle W_j \rangle - W_i|, i \neq j$$

$$\sigma = \left[ \frac{1}{2} \sum_{i \neq j} (\Delta W_{ij})^2 \right]^{\frac{1}{2}} \quad (6-2)$$

$$\epsilon_{ij} = 3\sigma_j - \Delta W_{ij}, i \neq j \quad (6-3)$$

notice that, if any  $\epsilon_{ij}$  is negative, a violation has occurred. A review of solutions for all four IMUs will serve to identify a failed system along with an indication of the quality of all systems.

In prelaunch tests where instrument parameters can be isolated, comparison with prescribed limits will yield a decision. For those procedures where specific terms cannot be accessed, comparison with other IMUs must be used.

### 6.2.2 Testing By Performance Comparison

In multiple IMU systems, the redundant information may be utilized in evaluating performance of individual IMUs. Procedures which do not yield estimates of error parameters can, therefore, be employed.

It is suggested that the powered flight FDI is an effective tool for screening IMUs. With the system in a single gravity field, variations in measured  $\Delta V$  can only be due to instrument errors. The FDI logic, by its nature, should not be effected by vehicle sway (as all IMUs will yield the same error specific force due to sway). The implementation of FDI derived in Chapter 3 is designed to be mission and time independent. In conjunction with thresholds chosen to reflect prelaunch test procedures and desired resolution, faulty IMUs can be isolated without requiring solution for individual terms. More details concerning use of this mechanization will be shown in the next section.

## 6.3 TWO PROPOSED CHECKOUT PROCEDURES

Two significantly different prelaunch checkout procedures will now be developed. The first is a fairly conventional six-position test, with the IMU sequenced so that data is accumulated with each of the stable member axes up and down. The second method aligns all of the IMUs. Then, they are released (inertial mode), subject to the earth's rotation and gravity. The powered flight FDI is then used to screen accelerometer and gyro failures. With this test employed in three positions, all significant g-sensitive drifts can be examined.

### 6.3.1 Required Assumptions

Several assumptions are made. Of primary importance, a model of the system will be available such that there is a reference value with which to compare each

IMUs output. Typically, this model includes equations for gyros and accelerometers such as;

$$W_{out} = W_{in} + W_{bias} + W_{g \text{ sensitive biases}} + \dots$$

$$a_{out} = (a_{in} + a_{bias} + \dots) (1 + K_{SE}) K_S$$

In these equations, the terms are taken to be physically measurable drifts which can be compensated in the onboard computer. The model is limited to those terms assessable by the verification test chosen. A full model of the KT-70 IMU, and a multiple system made up of KT-70 IMUs, appears in Appendix A.

A second assumption is that an accurate calibration of all modelled parameters is available so that loaded compensation values are nearly correct. In effect, then, this checkout is designed to demonstrate that system performance (as it may be compared against a model) is not sufficiently degraded to jeopardize mission success.

Finally, a full set of parameter variances is assumed to be given, representing KT-70 performance limits. Error parameter values determined by the onboard computer's checkout program are compared with these values, and appropriate operational or non-operational decisions are made along with possible problem diagnosis.

### 6.3.2 Six Position Verification Test

The classical form of the prelaunch checkout of gimbal systems by calibration is a multiple position test. Measurements of gravity and platform drift in each position are used to calculate instrument parameters. The derived parameter values may then be compared with loaded error terms for the go/no-go decision.

It is proposed that the instrument parameters found in such a test naturally invite comparison with pre-established limits in order to determine the system's flightworthiness.

The proposed multiple IMU implementation includes full flight computer control of stable member positioning, allowing autonomous, multiple position testing. Interest is centered on a six position test in which each stable member axis is initially positioned up and down. In each position, the platform is then released with earth rate compensation. Accelerometer data is taken for two minutes, permitting nearly exact solution (hence, excellent compensation) for scale factor and bias error of

each accelerometer sensitive axis. Gimbal angles are read at time zero, and again approximately at thirty minutes, in three of the positions.\* Then, gimbal resolved measurements of gyro drifts plus earth rate components may be compared among the four initially aligned IMUs. (It will be noted that even with an error drift of twenty percent of earth rate about one gyro axis, the resulting gimbal angle difference at the test's end will be a "small angle". Therefore, direct comparison without concern for commutativity errors will be possible.)

Including the time required to slew and level the platform for each position, this test will consume three hours. Initial alignment for launch would still be required. The full test, then, could be completed and allow initial alignment within four hours of initiation.

The resolution afforded by this test is assessed as follows: the data collected in each position must pass a reasonability test. All measured magnitudes of the g vector must agree within a value derived from a specified tolerance on each axis. (It is noted that the magnitude is independent of gyro errors.) The accelerometer SF and bias values are derived from input axis up and down counts.\*\* The dominant uncertainty is inexact knowledge of gravity due to instrument misalignment, platform drift over the test interval and leveling errors.

Steady state leveling errors ( $\phi$ ) are a function of bias and alignment uncertainties of the horizontal accelerometers and to some extent drift uncertainties of the horizontal gyros. The sense of  $\phi$  will change between the up and down positions for each axis.

Platform drift, due to uncompensated gyro drifts, will yield an average offset over the measurement time of:

$$\rho = \frac{1}{2} \omega t$$

The polarity of the offset remains the same in both up and down positions. Further,

---

\* Gyro drift measurements require large time intervals for sufficient resolution depending upon available A/D resolution and signal/noise resolution of gimbal information. Therefore, the proposed test limits drift measurements to the three positions which excite the g-sensitive drifts most significant to the mission: X-up, Y-up or down, Z-up.

\*\* Positions are found by leveling the two "horizontal accelerometers".



the overall mechanical misalignment,  $\psi$ , will also retain its sense. Therefore, these two errors may be lumped together by:

$$\theta = \psi + p$$

With these definitions, the up and down measurements of the  $j$ th accelerometer may be written:

$$\begin{aligned} A_{out_j}^{up} &= \left[ g (\cos\phi \cos\theta - \sin\phi \sin\theta) + A_{Bj} \right] / K_S (1 + K_{SEj}) \\ A_{out_j}^{dn} &= \left[ g (\cos\phi \cos\theta + \sin\phi \sin\theta) + A_{Bj} \right] / K_S (1 + K_{SEj}) \end{aligned} \quad (6-4)$$

$A_{Bj}$  is the unknown bias of the  $j$ th accelerometer, and  $K_{SEj}$  is its unknown scale factor error.  $K_S$  is the nominal accelerometer scale factor.

These two equations (6-4) may then be solved to obtain:

$$K_{SEj} = \frac{2g \cos\phi \cos\theta}{K_S (A_{out_j}^{up} - A_{out_j}^{dn})} - 1 \quad (6-5a)$$

where

$$\frac{\delta K_{SEj}}{\delta \phi} = - \frac{2g \cos\theta}{K_S (A_{out_j}^{up} - A_{out_j}^{dn})} \sin\phi \quad (6-5b)$$

$$\frac{\delta K_{SEj}}{\delta \theta} = - \frac{2g \cos\phi}{K_S (A_{out_j}^{up} - A_{out_j}^{dn})} \sin\theta \quad (6-5c)$$

and

$$A_{Bj} = \frac{K_S (A_{out_j}^{up} + A_{out_j}^{dn}) - 2g \sin\phi \sin\theta}{2} \quad (6-6a)$$

where

$$\frac{\delta A_{Bj}}{\delta \phi} = -g \sin\theta \cos\phi \quad (6-6b)$$

$$\frac{\delta A_{Bj}}{\delta \theta} = -g \sin\phi \cos\theta \quad (6-6c)$$

It can be seen (equations (6-5b and 6-5c)) that the solution for scale factor error is nearly insensitive to misalignments. For small angles, with  $A_{out_j}^{up} \sim -A_{out_j}^{dn}$ ,

$$\Delta K_{SEj} = \frac{\delta K_{SEj}}{\delta \phi} \Delta \phi \sim \phi^2 \quad (6-7)$$

This shows a leveling error of 1 milliradian, equivalent to  $1 \text{ cm/s}^2$  of non-compensatable bias in a horizontal accelerometer, will introduce a 1 ppm error in the calculated  $K_{SEj}$ . With the same small angle assumptions, equations 6-6a and 6-6b yield

$$\Delta A_{Bj} = \frac{\delta A_{Bj}}{\delta \phi} \Delta \phi = -g \theta \phi$$

Thus, the bias sensitivity to a leveling error of 1 milliradian together with a platform drift of  $0.1^\circ/\text{hr}$  (7 meru) over the two minute measurement time will introduce an error of  $0.001 \text{ cm/s}^2$  in the bias determination.

Theoretical resolution of the gyro test is given by the incremental angle uncertainty divided by the measurement interval. The worst case present system angle uncertainty is the sum of the gimbal angle uncertainty (2 min) and A/D quantization (1.3 min). Thus, the  $1\sigma$  resolution becomes:

$$W_{\text{res}} = \frac{\text{uncertainty}}{\text{time interval}} = \frac{3.3 \text{ min}}{33 \text{ min}} = 0.1 \frac{\text{min}}{\text{min}} = 0.1^\circ/\text{hr. (7 meru)}$$

The resolution is seen to be inversely proportional to test time. The one sigma resolution cited above is comparable to expected system performance, and is within mission tolerances.

If the A/D conversion is found to have good signal/noise characteristics, the measurement of platform drift can be mechanized to eliminate A/D quantization. Separate counts are made of elapsed angle (in bits) and time (in system clock pulses). The time count initiated with the first pulse following the zeroeth bit (which is not counted). The time count ends simultaneously with the last bit. Then the resolution is given directly by the linearity of the A/D converter.

Resolution of lump drift parameters is seen to be sufficient in this test. However, it must be borne in mind that no external reference value is available for this parameter. Only relative drift of the IMUs can be compared. For this comparison, the logic shown in equations 6-1 to 6-3 is employed. A  $3\sigma$  estimate of each IMU's drift is formed using the measured drift of the other platforms. Then, the measured drift of each is compared with its estimate.

With sufficient resolution believed available, gyroscopes meeting the criterion shown in equation 6.3 are considered flightworthy.

A summary of the six position test procedure outlined would be that the resolution available is sufficient to show that each IMU meets mission requirements at launch. Within stated uncertainties, accelerometer bias and SFE parameters may be compensated exactly. Gyro lump parameters can be resolved to within expected system performance levels. The time required for this test procedure is presently estimated to be 2.5 hours. This is a conservative estimate and depends directly on system characteristics. Including initial alignment, the full prelaunch sequence will consume less than four hours.

A flowchart of the six position test appears as figure 6-1. It should be understood that all operations must be carried out for each on line IMU.

### 6.3.3 Verification Test Using Powered Flight FDI

The second class of tests described above compares the outputs of the IMUs in order to establish expected reliability on the basis of relative performance. A three position test which makes this comparison by using the powered flight FDI developed in Chapter 3 is described here.

Each IMU has been calibrated in the recent past. Error parameters reflecting this calibration are loaded. All platforms are aligned initially, and are released (either in the inertial mode or earth rate compensated) at  $t=0$ . Monitoring of accelerometers and gyroscopes is accomplished by examination of velocity error ratios (equation 3-6). This test is performed in three positions, chosen to excite all g-sensitive gyro biases. Positions are determined by leveling the two horizontal accelerometer input axes.

As a first step, the magnitude of the gravity vector measurement of each IMU is compared with the known value. Any IMU whose measurement does not agree within acceptable limits is flagged as having an accelerometer failure.

It is obvious that bias and scale factor errors are not separable. The output of each measurement axis (scaled in pulses/sec) is given by

$$A_{outij} = \frac{(-g_j + A_{Bij})}{K_S (1 + K_{SEij})} \quad (6-10)$$

where  $i$  (the IMU number) = 1, 2, 3, 4;  $j$  = X, Y, Z.  $A_B$  is the bias,  $K_S$  the nominal scale factor, and  $K_{SE}$  the scale factor error. With each axis up only, and using each for leveling in the other two positions, separation is impossible.

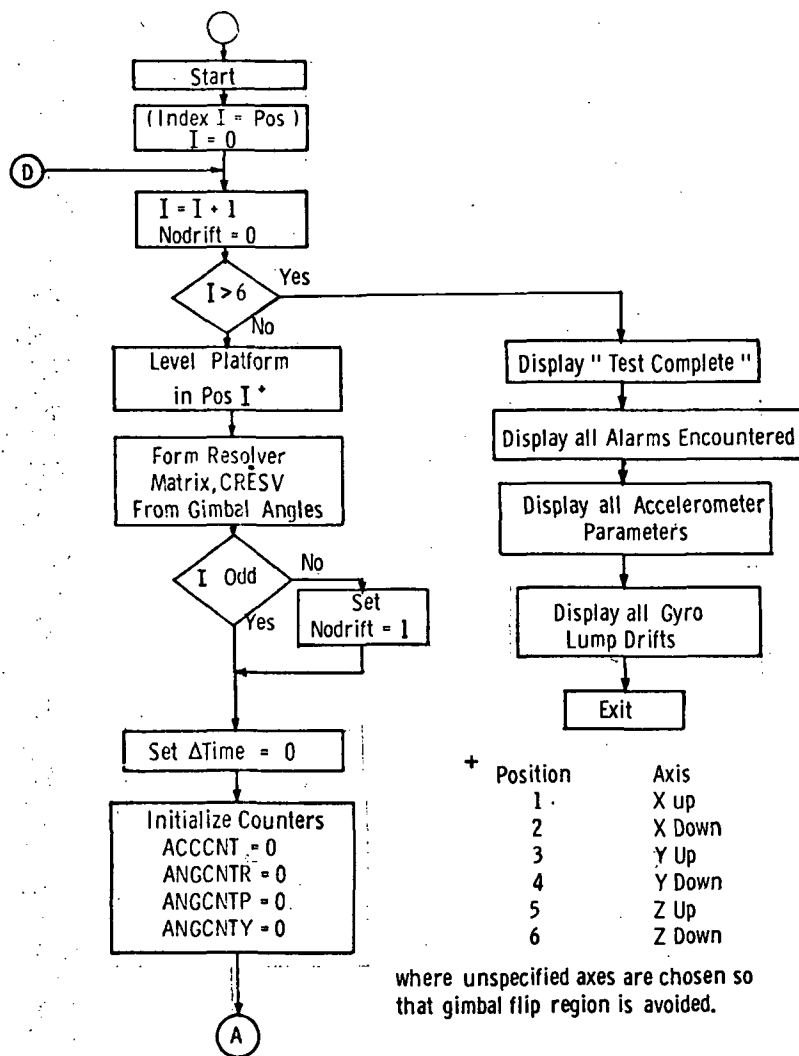


Figure 6-1a

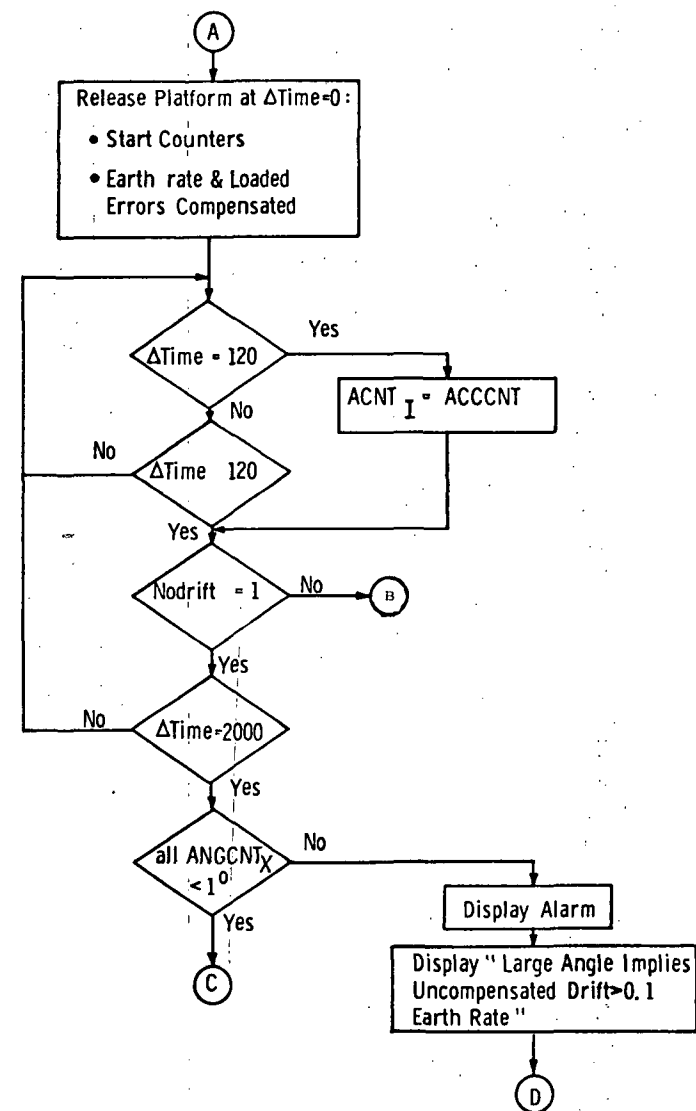


Figure 6-1b

Flow Chart of the Six Position Verification Test

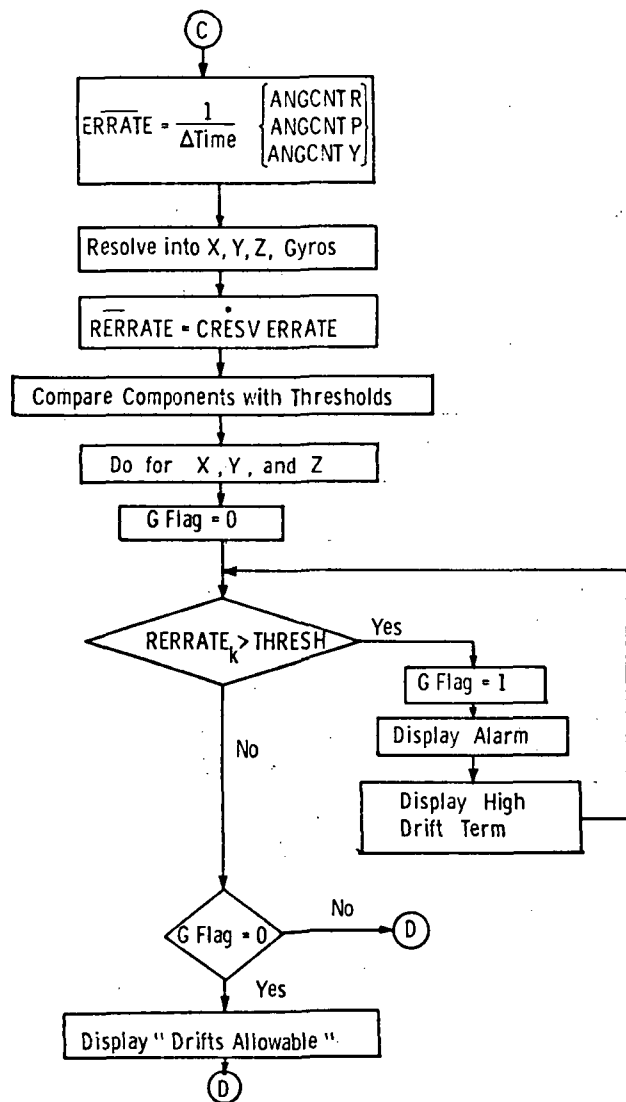


Figure 6-1c

Flow Chart of the Six Position Verification Test

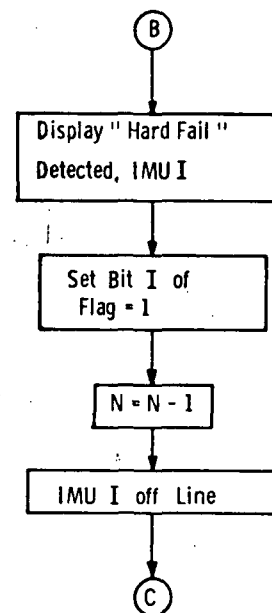


Figure 6-1d

However, in this proposed test redundant measurements of gravity and earth rate are available. These are incorporated into the powered flight FDI. A first cut at detection, for the prelaunch verification test, examines the time history of the velocity error ratio (Equation 3-6).

$$V_{erij} = \frac{V_{eij}}{|\underline{V}_{ave}|}$$

where  $i = \text{IMU } 1, 2, 3 \text{ or } 4$ ,  $j = X, Y, Z$ .  $\underline{V}_{ave}$  is the average inertial velocity calculated from the outputs of all the online IMUs. Given that the only system errors are miscompensated accelerometer biases, then it is easily established that

$$V_{erij} \propto A_{bij} \quad (6-11)$$

and is time independent. Clearly, then, detection and isolation depend simply on magnitude of the term and the thresholds used. Similarly, if only miscompensated SFE parameters are postulated, a time independent ratio

$$V_{erij} \propto \left[ \frac{1}{1 + K_{SE_{ij}}} \right] \quad (6-12)$$

is found. Again, detection and isolation are dependent on the relationship between error and the thresholds chosen. Examination of Equations (6-11) and (6-12) shows that bias and scale factor errors may be separable, but only if  $V_{ERij}$  is constant and the test conditions are well known. In general, they remain inseparable.

Gyro drifts, on the other hand, will result in time varying velocity error ratios. If the history of these ratios shows variation, analysis proceeds through the FDI logic presented in Chapter 3, equations 3-4 through 3-15.

Consider an IMU with a drift rate of  $w$  about a horizontal axis, compared with perfect IMUs. Then (for  $w\Delta t$  a small angle),

$$V_{er} \propto w\Delta t \quad (6-13)$$

In theory, detection and isolation is seen to vary with the parameter error, thresholds chosen and time. Given sufficient time, a constant error will be found. The problem remaining is to study the trade-off between resolution required and time available, and choose thresholds in line with the results.

The character of the velocity error ratio has been suggested for three parameters. As shown in the next chapter, describing simulation results, observation of these characteristics is an effective diagnostic tool.

The proposed test may be summarized, then, as follows: Using powered flight FDI logic with thresholds chosen for prelaunch verification, gyro errors above required resolution can be detected and isolated. Accelerometer errors can be detected similarly with the addition of a check on the time history of the velocity error ratio: a constant, non-zero ratio implies an error which can be detected by comparing  $V_{ER_{ij}}$  with an additional threshold. A flowchart for this test procedure is shown in Figure 6-2.

#### 6.4 Conclusions

The overall conclusion drawn from this work is that each of the two suggested tests is employable for the prelaunch checkout of a multiple IMU system. Each has sufficient resolution. A final choice cannot be made without detailed tradeoff studies of the candidate system and the desired resolution vs. available time and computer requirements. Evaluation of simulations of the two suggested tests is presented in the next chapter. The multiple position test is considered the best candidate.

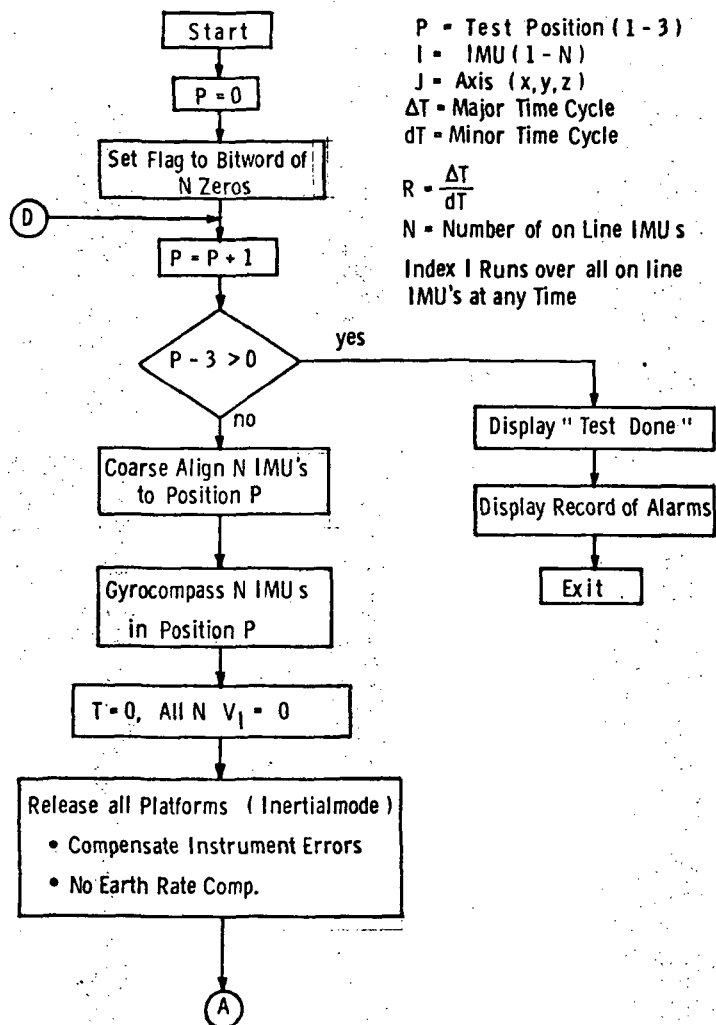


Figure 6-2a

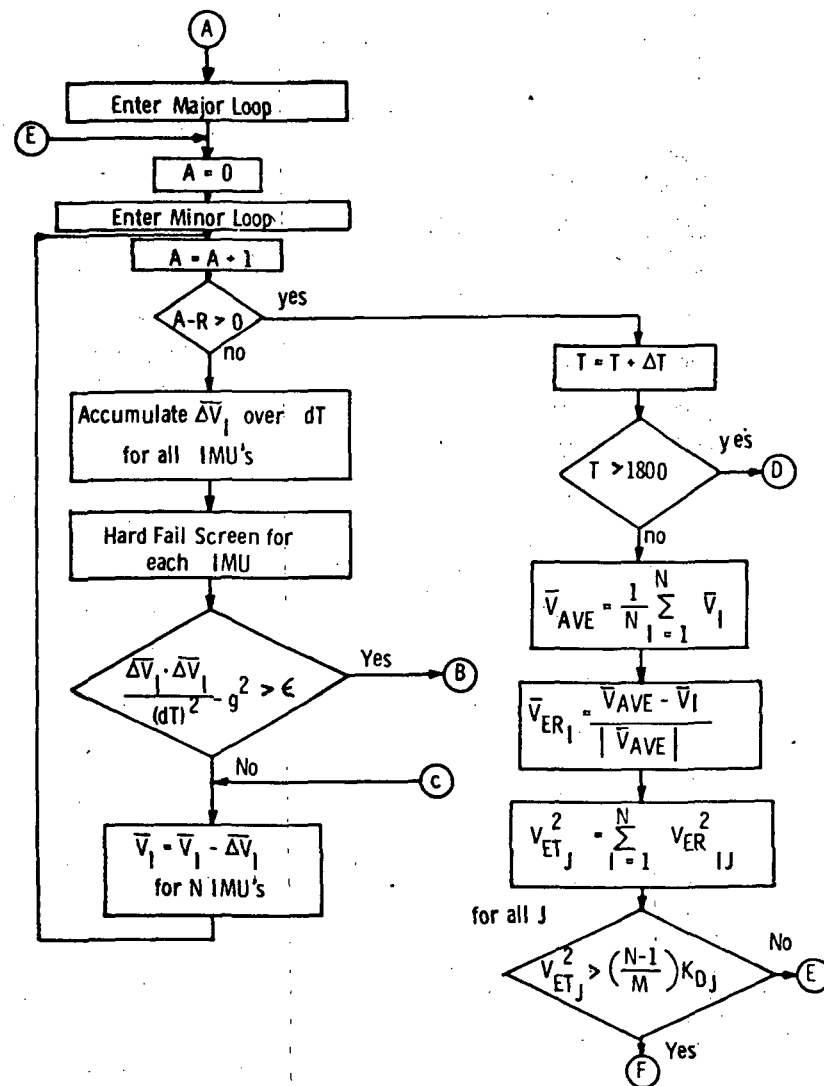


Figure 3-2b

Flow Chart of Multiple IMU Verification Test Using Redundant Data and Powered Flight FDI



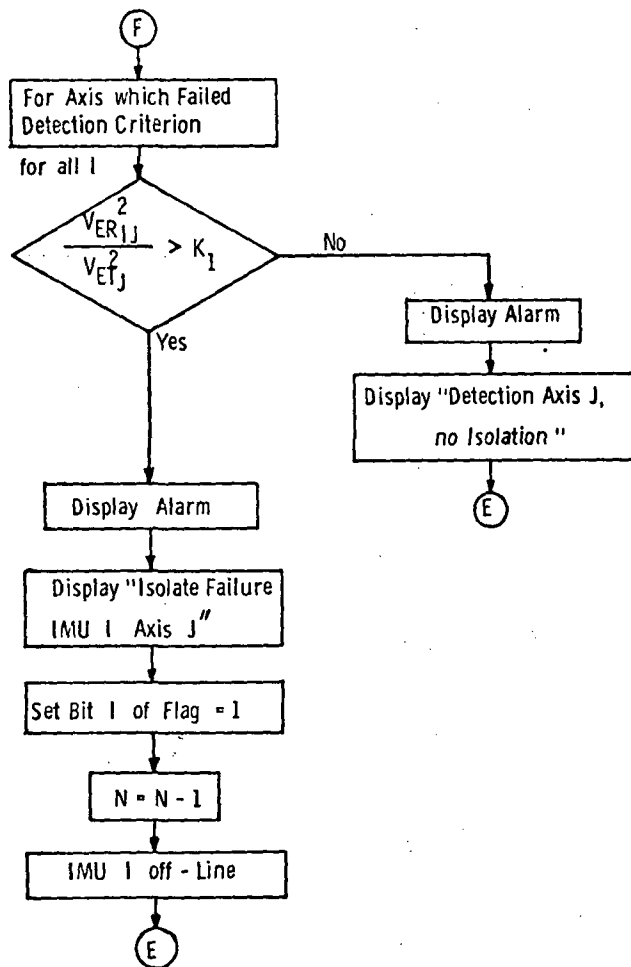


Figure 6-2c

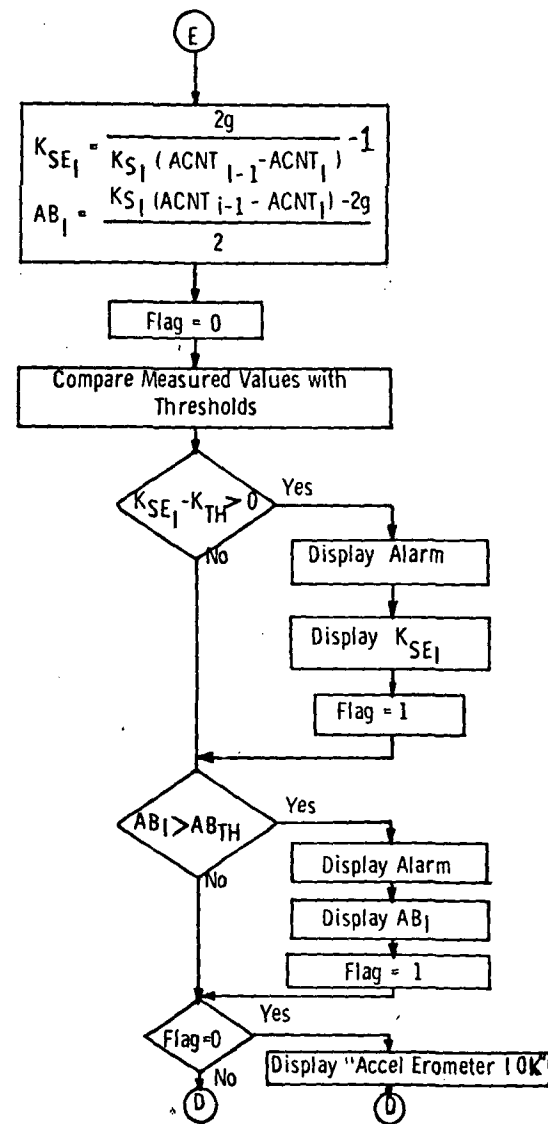


Figure 6-2d

Flow Chart of Multiple IMU Verification Test Using Redundant Data and Powered Flight FDI

## 7.0 MULTIPLE IMU SYSTEM MODEL AND SIMULATIONS OF PRELAUNCH CHECKOUT PROCEDURES

A digital model of the multiple IMU system has been coded, intended primarily for simulation and evaluation of the proposed prelaunch verification procedures. The model closely follows the single IMU model description which appears in Appendix A. Two versions of the prelaunch test were simulated. The results of these simulations are presented and discussed.

### 7.1 SINGLE IMU MODEL

A description of the KT-70 IMU appears as Appendix A of this report. Working from this description, a digital model of this IMU has been assembled. An extension of this work led logically to coding a model of the multiple IMU system.

The model of the single IMU centers on equations describing the output of the gyro and accelerometer "triads". Defining;

- $C_{JK}^*$  = The instantaneous laboratory to stable platform transformation.
- $G_{MIS}^*$  = The stable member reference triad to gyro input axes transformation.
- $C_{GSD}^*$  = A matrix including all g-sensitive uncertainty terms.
- $\underline{W}_{IEL}$  = The earth rate vectors in laboratory coordinates.
- $\underline{G}_L$  = The gravity vector in laboratory coordinates.
- $\underline{BD}$  = Non-g-sensitive uncertainty drift.

Then, with  $\underline{BD}$  and  $C_{GSD}^*$  representing the noncompensatable uncertainties of the drift (drift errors),

$$\underline{W}_{OUT} = G_{MIS}^* C_{JK}^* \underline{W}_{ICL} + \underline{BD} + C_{GSD}^* G_{MIS}^* C_{JK}^* \underline{G}_L \quad (7.1)$$

In a gimbale system, these rates will be counteracted by counter rotation of the gimbals. Taking  $C_{RESV}^*$  to be the instantaneous representation of the resolver chain, then the gimbal angles ( $\underline{G}_{ANG}$ ) will change according to:

$$\underline{G}_{ANG} = -C_{RESV}^* \underline{W}_{OUT} \quad (7.2)$$

Clearly,  $C_{JK}^*$  and  $C_{RESV}^*$  are functions of  $\underline{G}_{ANG}$ , and will vary with time.

Accelerometers are modeled using the following definitions:

$C_{JK}^*$  = The instantaneous laboratory to stable platform transformation.  
 $A_{MIS}^*$  = The stable platform reference frame to accelerometer input axes transformation.

$\underline{AB}$  = A vector of accelerometer bias uncertainties.

$A_{CRC}^*$  Represents the measurement and cross coupling errors in the accelerometers, given by

$$A_{CRC}^* = \begin{bmatrix} 1 & A_{CXY} & A_{CXZ} \\ A_{CYX} & 1 & A_{CZY} \\ A_{CZX} & A_{CZY} & 1 \end{bmatrix}$$

$A_{SFM}^*$  Represents scale factor error, given by

$$A_{SFM}^* = \frac{1}{SF} \begin{bmatrix} \frac{1}{1+K_{SEX}} & 0 & 0 \\ 0 & \frac{1}{1+K_{SEY}} & 0 \\ 0 & 0 & \frac{1}{1+K_{SEZ}} \end{bmatrix}$$

Then the output of the accelerometers, without CAPRI quantization, is (in units of  $\Delta V$  pulses):

$$\underline{\Delta V}(\Delta t) = A_{SFM}^* (\underline{AB} - A_{CRC}^* A_{MIS}^* C_{JK}^* \underline{G}_L) \frac{1}{\Delta t} \quad (7.3)$$

Modeling of readout chain errors follows the model presented in the Appendix. Similarly, intergimbal nonorthogonalities are included in the transformation  $C_{JK}^*$ .

This model is now programmed for evaluation using the digital computer.

## 7.2 MULTIPLE IMU MODEL

A digital model of a multiple IMU system has been coded. Simulation of the hardware is made simply by extending the dimensions of the equations 7.1 to 7.3 to include twelve functional axes (four IMUs). This model is illustrated by flow chart in Appendix B. The salient feature of the model is the representation of the gimbal angles by a differential equation driven by resolved gyro drift.

Both of the prelaunch verification tests described in the previous chapter are included in the programs which make up the simulation. Each has been exercised in simulations designed to determine whether theoretical resolution can be achieved.

### 7.3 SIMULATION RESULTS

Use has been made of the digital simulation of the multiple IMU system in a prelaunch environment in evaluating the two proposed verification tests. The first of these tests, in summary, is a six position test yielding exact accelerometer parameters and gimbal rate estimates for comparison among IMUs. The second test initially aligns all platforms and then monitors all instruments using powered flight FDI. This test is performed in three orientations so that all significant gyro g-sensitive drifts are excited. In each case, a stable base was assumed.

#### 7.3.1 Six Position Test

Examination of simulation results indicates that uncertainties in accelerometer parameters agree well with theoretical results. In runs for which the only errors assumed were accelerometer bias or scale factor errors, the solution was exact. Bias uncertainties were found to be linearly dependent upon misalignment and platform drift.

Resolution of gyro lump parameters, using this model of the KT-70 with gimbal nonorthogonalities, a full gimbal chain error model, but without noise in the A/D conversion, appeared to be limited to  $0.22^{\circ}/\text{hr}$  (15 meru) in the 30 minute/position testing period. The resolution is well within the mission redlines.

In these simulations, gyro drifts were calculated from gimbal rates. Each lump drift derived was also measured against the standard deviation of like axis drifts on other platforms. This method of comparison, excluding the term to be compared from the standard, was chosen to avoid degradation of all instrument uncertainty estimates by a single bad unit. It was verified that drifts on the order of three times the standard deviation of the three comparable terms could be isolated with high certainty. This indicates that the redundant quality of the data in a multiplicative system can be used in system checkout.

#### 7.3.2 Three Position Test Using FDI As Monitor

Extensive simulations with both deterministic and random errors used in the instrument models have verified the predictions that velocity error ratios are proportional to accelerometer bias errors and inversely proportional to one plus the scale factor error. Resolution of gyro errors, as anticipated, is time dependent.

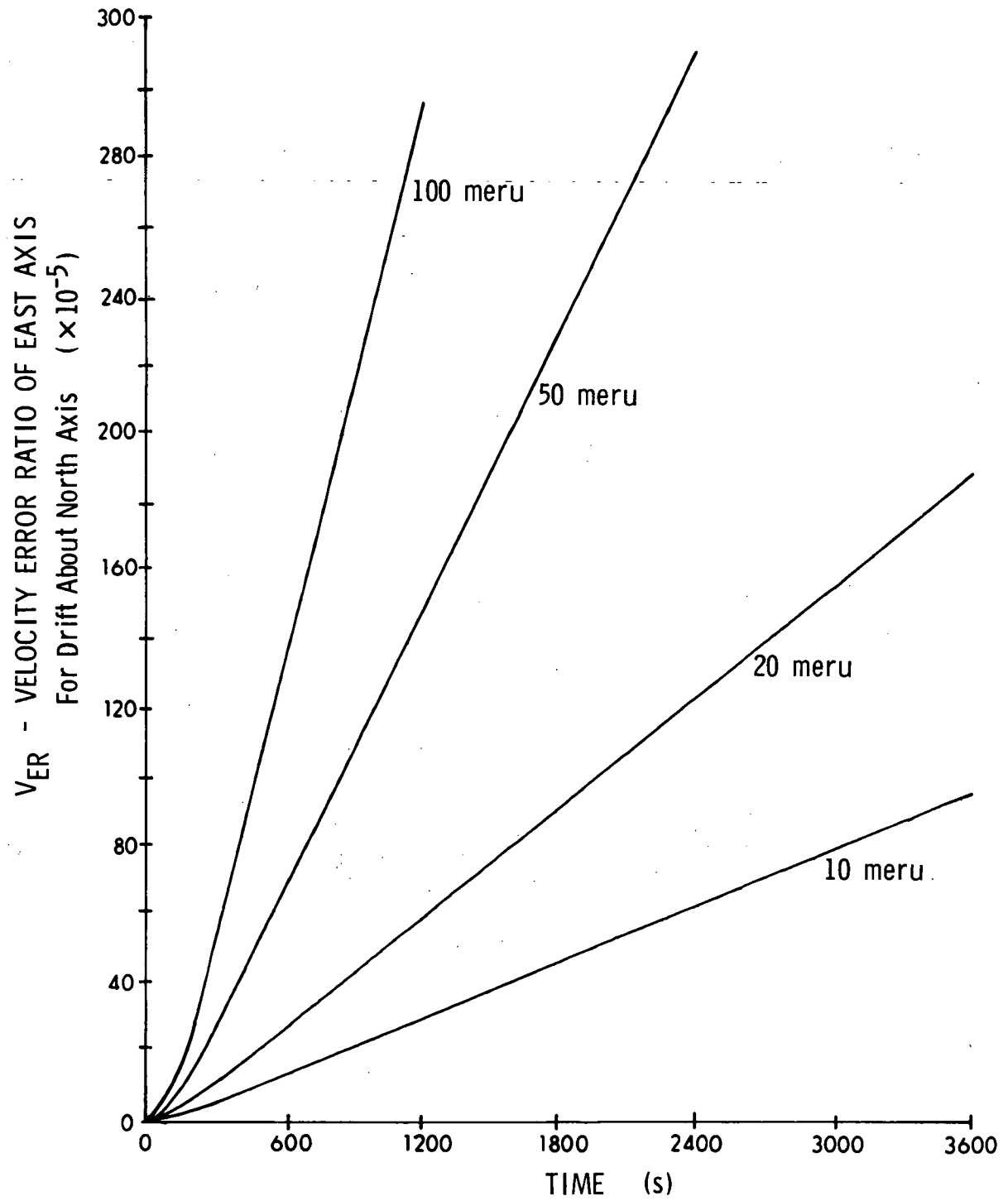
Figure 7.1 shows that the prelaunch checkout procedure simulation yields  $V_{ER}$  linear in time for various drift rates. Similar data has been found in simulations with combinations of drift terms about any two accelerometer axes simultaneously observing proper polarity. The simulations have also demonstrated that  $V_{ER}$  is linear with accelerometer bias and scale factor error.

Although a more complex decision algorithm will be required, it is believed that a three position test monitoring system performance through use of powered flight FDI will be a sufficient prelaunch checkout. The decision algorithm will have to consider time dependence and magnitude of the  $V_{ER_{ij}}$  term along each axis in each position, thirty six terms in all.

#### 7.4 SUMMARY

To the extent that a simulation can be trusted in modeling a real system the two suggested prelaunch checkout tests have been shown to serve as predicted. The six position test method appears to have advantages over FDI monitoring, and is therefore recommended for two reasons. One, the former test determines accelerometer errors with good resolution while FDI monitoring yields numerical values only with difficulty. Two, a highly complex decision algorithm will be required for the FDI test implementation.

Figure 7.1 -  $V_{ER}$  of East Axis for Drift About North Axis



**Page intentionally left blank**

## 8.0 LABORATORY TEST PLAN

### 8.1 INTRODUCTION

It should be recognized that the test plan to follow directly addresses the laboratory testing of three production KT-70 IMUs and their supporting electronics. This test plan will identify laboratory testing requirements which are of prime importance to be able to qualify an air navigation type ISS for the shuttle mission. The standard IMU configuration is known to contain marginal areas of performance with respect to the shuttle mission. The testing will be designed to include evaluation of these areas, unless prior work eliminates this need. This will include the IMU shock mounts, the gimbal chain calibration stability, temperature gradient effects due to stable member temperature control, attitude control during gimbal flip, as well as the multiple IMU system grounding problems. Many of these areas require evaluation to develop testing techniques as well as to determine available performance. One example of special interest is the development of a testing technique for gimbal chain calibration as well as determining if the calibration stability of the gimbal chain after resolver updating (expected total calibration stability is around one arc minute) is adequate for the shuttle.

### 8.2 TEST PLAN PHASES

#### 8.2.1 IMU Calibration

IMU parameter sensitivity to various shuttle flight trajectories have been previously identified in this study. This section is concerned with the baseline calibration of the parameters of the Inertial subsystem prior to the prelaunch testing phase. The laboratory test plan will include an instrument calibration test patterned directly from the present Kearfott multiple position IMU calibration set implemented in the A7 D/E program.<sup>12</sup> This test will verify short and long term stability of the IMU instrument set and provide information to insure the adequacy of the instrument model which forms the basis of the IMU calibration parameters. Based upon the history of the individual instrument parameters, special test sequences can be established to confirm the instrument models used in the present calibration plan.

Two other areas will be studied in the test plan. Both areas must be investigated carefully if "off the shelf" IMU technology is to be applied to the space shuttle.

The first study area concerns the attitude chain calibration. The existing four gimbal attitude chain contains single speed synchro readouts on three of the four gimbal



axis. The present accuracy is not sufficient to do the normal in-flight alignment. During alignment, the IMU is commanded via the computer to attain a known stable member inertial frame (derived from the common navigation base optics system) as a reference frame to perform the entry mission phase. Various accuracy predictions have been made of the ability to calibrate these synchro chains including A/D electronics, and to determine the gimbal orthogonality, gimbal zero reference stability and the fourth gimbal offset characteristics. The total gimbal chain calibration tolerance, as observed by the expected accuracy of the three Euler angles orienting the body with respect to the stable member reference frame, is expected to be about two milliradians about each axis after calibration. This uncertainty (if it is true) still represents a large error source in the normal entry trajectory phase. It is believed that overall gimbal calibration stability can be greatly improved by replacing the synchros with multispeed resolvers. This retrofit should be implemented and evaluated. The ability to calibrate an operational system is dependent upon the basic angle readout stability over 360 degrees, and bias (offset) sensitivity to air coolant temperature changes. The air coolant system temperature variation and active stable member temperature controller set up a conductive temperature gradient in the KT-70 system in which the angular encoders are mounted. The actual temperature sensitivity of the gimbal calibration should be established by the planned testing. Another shuttle gimbal chain calibration uncertainty results from the unknown stability of the laboratory gimbal calibration of the IMU across the boost flight environment. The present failure detection implementation in powered boost flight is not directly dependent on the gimbal chain but uses the stable member incremental velocity output for detection and isolation of accelerometer and gyroscope malfunctions in this flight phase. It is essential, however, that the established IMU calibration survive the boost profile within known small residual offsets to accomplish a calibrated in-orbit IMU alignment prior to entry. Of special interest in this testing phase is the evaluation of the IMU shock isolation mounts. The maximum offset with known g loading must be determined, to establish the adequacy of the attitude control loop during boost. The residual alignment offset is also required for the transfer of the prelaunch calibration information into the in-orbit alignment problem. Another possible candidate method, if necessary, would be the in-orbit IMU alignment verification. This is based upon the evaluation of gimbal angle data using a set of known gimbal orientations with the system inertially referenced over several orbital periods. This method of gimbaled IMU in-orbit calibration for accurate attitude determination has been shown to be quite sensitive by a Draper Laboratory study performed to investigate fine attitude determination capability of a gimbaled system for satellite application.<sup>13</sup>

#### 8.2.1.1. Instrument Parameter Verification

The three IMU instrument parameter verification programs are a minor modification of the single IMU calibration program developed by Sperry Rand for NASA/MSFC.<sup>14</sup> The modifications presently envisioned pertain to the I/O data handlers and the addition of a routine for printout of all calibration parameters determined. That is, the program will be made compatible with the MIT Processor Interface Unit hardware data formats. The program will also have the ability to compute, save and verify the following parameters for any one of the three IMUs. IMU selection can be either automatic or operator controlled.

DX, Y, Z	average gyro drift
MGX, Y, Z	gyro torquing scale factor
BLX, Y, Z	accelerometer low gain average bias
BHX, Y	accelerometer high gain average bias
KLX, Y, Z	accelerometer low gain average scale factor
KHX, Y	accelerometer high gain average scale factor

The verification is mechanized by measuring and filtering North and West velocities and the heading rate at thirteen automatically selected IMU positions.

A Kalman Filter incorporates measurements of North and West velocity and the heading rate in estimating the following seven errors.

VN - North Velocity error	$\omega_e$ - Earth Rate
VE - East Velocity error	$\omega_N$ - North Gyro Drift
$\phi_N$ - Platform tilt about North axis	$\omega_E$ - East Gyro Drift
$\psi$ - Heading error	$\omega_U$ - Azimuth Gyro Drift
$\phi_E$ - Platform tilt about East axis	

The filter operates at ten second intervals after the platform has been stabilized in one of thirteen positions. The filter is reinitialized for each position. The dynamic error model in this testing can be represented by the following equations:

$$\dot{VN} = -K_x VN + g\phi_E \quad (8-1)$$

$$\dot{VE} = -K_y VE - g\phi_N \quad (8-2)$$

$$\dot{\phi}_N = \frac{1 + K_{YA}}{R_{WEST}} VE - (\omega_e \sin \lambda) \phi_E \quad (8-3)$$

$$\psi = K_{54} VE + (\omega_e \cos \lambda) \phi_E + K_{47} \omega_U \quad (8-4)$$

$$E = \frac{1 + K_{XA}}{R_{NORTH}} VN + (\omega_e \sin \lambda) \phi_N - (\omega_e \cos \lambda) \psi \quad (8-5)$$

$$\dot{\omega}_E = 0 \quad (8-6)$$

$$\dot{\omega}_U = 0 \quad (8-7)$$

The solution of the above equations is approximated by the vector difference equations;

$$\underline{X}_n = \left[ F_n \right] \underline{X}_{n-1} \quad \text{where } n = 1, 2, \dots, 10 \text{ seconds} \quad (8-8)$$

The state transition matrix is then

$$\Phi(t + 10, t) = F_{10} F_9 \dots F_1 \quad (8-9)$$

The linearized relationship between observables and state variables are;

$$VN = VN_{meas} \quad (8-10)$$

$$VE = VE_{meas} \quad (8-11)$$

$$K_{54} VE + (\omega_e \cos \lambda) \phi_E + K_{47} \omega_U = \psi_{meas} \quad (8-12)$$

That is,

$$\underline{Y}_{meas} = H \underline{X} \quad (8-13)$$

where

$$H = \begin{bmatrix} 1 & 0 & 0 & 0 & 0 & 0 & 0 \\ 0 & 1 & 0 & 0 & 0 & 0 & 0 \\ 0 & K_{54} & 0 & 0 & \omega_e \cos \lambda & 0 & K_{47} \end{bmatrix}$$

Thus, at ten second intervals the following equations are evaluated.

$$\hat{\underline{X}}'_{n+10} = \Phi(t + 10, t) \hat{\underline{X}}_n \quad (8-14)$$

$$\hat{\underline{Y}} = H \hat{\underline{X}}'_t + 10 \quad (8-15)$$

$$\delta \underline{M} = \underline{Y} - \hat{\underline{Y}} \quad (8-16)$$

(Y are the measured velocities and heading rate)

$$P'_{t+10} = \Phi P_t \Phi^T \quad (8-17)$$

(P is state covariance matrix)

$$K_{t+10} = P'_{t+10} H^T [H P'_{t+10} H^T + R]^{-1} \quad (8-18)$$

(R is the measurement covariance matrix)

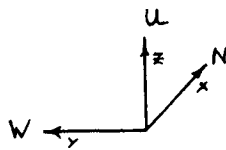
$$P_{T+10} = P'_{T+10} - K_{t+10} H P'_{T+10} \quad (8-19)$$

$$\hat{\underline{X}}_{t+10} = \hat{\underline{X}}'_{t+10} + K_{t+10} \delta \underline{M} \quad (8-20)$$

The estimated states are now used in the verification sequences described below to estimate gyro drift and gyro scale factor prior to measuring accelerometer bias and accelerometer scale factor.

#### Calibration Sequences and Positions

##### Position #1



Filter for at least 1800 seconds in position 1. Then store the following:

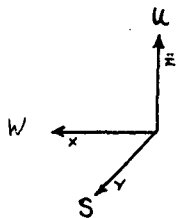
$$DELUA = \psi$$

$$DNA = \omega_N$$

$$DUA = \omega_U$$

$$DZRA = DZRA + DUA \text{ (calibrate Z gyro drift)}$$

##### Position #2



Filter for at least 500 seconds

$$DELUB = \psi$$

$$DNB = -\omega_N$$

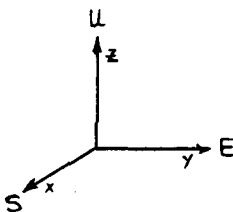
$$DX = DNA - \omega_e \cos \lambda (1 - \cos(DELUA))$$

$$DXRA = DXRA + DX \text{ (calibrate X gyro drift)}$$

$$DY = DNB - \omega_e \cos \lambda (1 - \cos(DELUB))$$

$$DYRA = DYRA + DY \text{ (calibrate Y gyro drift)}$$

##### Position #3

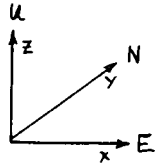


Filter for 500 seconds

$$DELUC = \psi$$

$$DNC = -\omega_N$$

Position #4



$$\text{DELUD} = \psi$$

$$\text{DND} = \omega_N$$

$$\text{DELU2} = \text{DELUB} - \frac{(\text{DNA} + \text{DNC})}{2\omega_e \cos \lambda}$$

$$\text{DELU4} = \text{DELUD} + \frac{(\text{DNA} + \text{DNC})}{2\omega_e \cos \lambda}$$

$$\text{KGY} = \frac{\text{DND} - \text{DNB}}{2\omega_e \cos \lambda} + 1/2 [(\cos (\text{DELU2}) + \cos (\text{DELU4}))^{-1}]$$

(relative change in Y-gyro scale factor)

$$\text{DY} = -1/2 [(\text{DNB} + \text{DND}) (1 + \Delta \text{KGY}) - (\cos (\text{DELU2}) - \cos (\text{DELU4})) \omega_e \cos \lambda]$$

$$\text{DELU1} = \frac{(1 + \Delta \text{KGY}) (\text{DELUA} - \text{DY})}{\omega_e \cos \lambda}$$

$$\text{DELU3} = \frac{(1 + \Delta \text{KGY}) (\text{DELUA} - \text{DY})}{\omega_e \cos \lambda}$$

$$\Delta \text{KGX} = \frac{\text{DNA} - \text{DNC}}{\omega_e \cos \lambda} + 1/2 [\cos (\text{DELU1}) + \cos (\text{DELU3})]^{-1}$$

(relative change in X-gyro scale factor)

$$\text{DX} = 1/2 [(\text{DNA} + \text{DNC}) (1 + \Delta \text{KGX}) - (\cos (\text{DELU3}) - \cos (\text{DELU1})) \omega_e \cos \lambda]$$

$$\text{MGX} = \text{KGX} + (1 + \Delta \text{KGX}) \text{ (calibrate X-gyro scale factor)}$$

$$\text{MGY} = \text{KGY} + (1 + \Delta \text{KGY}) \text{ (calibrate Y-gyro scale factor)}$$

$$\text{DXRA} = \text{DXRA} + \text{DX} \text{ (refine X-gyro drift calibration)}$$

$$\text{DYRA} = \text{DYRA} + \text{DY} \text{ (refine Y-gyro drift calibration)}$$

measure  $\Delta V_Z$  in up position at lowgain

$$\text{CAPZU} = \Delta V_Z$$

Position 4.1 Same as position 4, except Z gyro torqued with a square wave signal.

Filter for at least 500 seconds

$$\text{DELU9} = \psi$$

$$\text{K9SEQ} = \omega_U$$

$$\text{DZRA} = \text{DZRA} - (\text{K9SEQ} - 1) \omega_e \sin \lambda$$

(refine Z gyro drift)

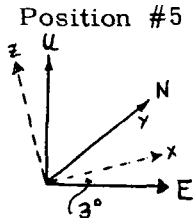
$$\text{KGZ} = \text{K9SEQ} - \text{KGZ}$$

(calibrate Z-gyro scale factor)

Return to Level position 4

measure  $\Delta V_X$ ,  $\Delta V_Y$  over 100 seconds at high gain.

$$\left. \begin{array}{l} \text{HXSQIO} = \Delta V_X \\ \text{HYSQIO} = \Delta V_Y \end{array} \right\} \text{High gain in level position}$$

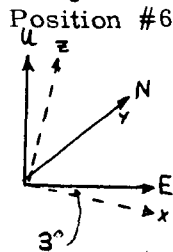


Measure  $\Delta V_X$  over 100 seconds at low, high, low gains.

X1SQ11 =  $\Delta V_X$  Low gain at 3° above horizontal

X2SQ11 =  $\Delta V_X$  High gain at 3° above horizontal

X3SQ11 =  $\Delta V_X$  Low gain at 3° above horizontal

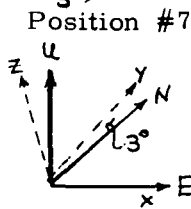


Measure  $\Delta V_X$  over 100 seconds at low, high, low gains.

X1SQ12 =  $\Delta V_X$  Low gain at 3° below horizontal

X2SQ12 =  $\Delta V_X$  High gain at 3° below horizontal

X3SQ12 =  $\Delta V_X$  Low gain at 3° below horizontal

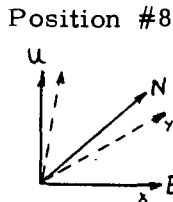


Measure  $\Delta V_Y$  over 100 seconds at low, high, low gains.

Y1SQ13 =  $\Delta V_Y$  Low gain at 3° above horizontal

Y2SQ13 =  $\Delta V_Y$  High gain at 3° above horizontal

Y3SQ13 =  $\Delta V_Y$  Low gain at 3° above horizontal

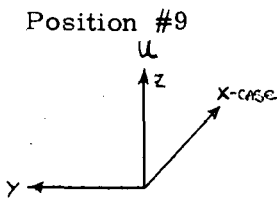


Measure  $\Delta V_Y$  over 100 seconds at low, high, low gains

Y1SQ14 =  $\Delta V_Y$  Low gain at 3° below horizontal

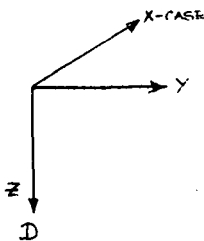
Y2SQ14 =  $\Delta V_Y$  High gain at 3° below horizontal

Y3SQ14 =  $\Delta V_Y$  Low gain at 3° below horizontal



This is an intermediate position in which no computations are made.

Position #9.1



Measure  $\Delta V_Z$  over 100 seconds in the down position using low gain.

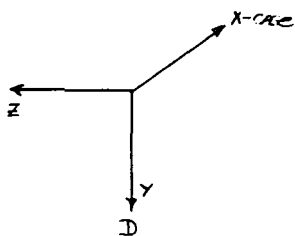
$$\text{CAPZD} = \Delta V_Z$$

$$\text{KLZ} = \frac{2g\Delta T}{\text{CAPZU} - \text{CAPZD}}$$

(calibrate average Z-accelerometer low gain scale factor

$$\text{BLZ} = \frac{\text{CAPZU} + \text{CAPZD}}{2\Delta T} \text{KLZ}$$

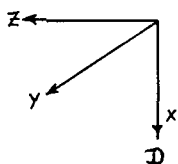
Position 10



Measure  $\Delta V_Y$  over 100 seconds in down position  
using Low gain

$$CAPYD = \Delta V_Y$$

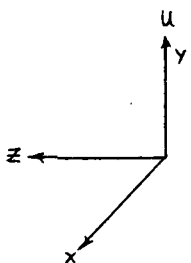
Position 11



Measure  $\Delta V_X$  over 100 seconds in the down position  
using Low gain.

$$CAPXD = \Delta V_X$$

Position 12



Measure  $\Delta V_Y$  over 100 sec in the up position using  
Low gain.

$$CAPYU = \Delta V_Y$$

$$KLY = \frac{2 g \Delta T}{CAPYU - CAPYD}$$

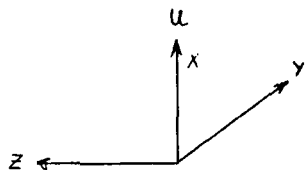
(calibrate Y-accelerometer low gain average scale  
factor)

$$KLY = -KLY \quad (\text{convert to east reference})$$

$$BLY = \frac{(CAPYU + CAPYD)}{2 \Delta T} KLY$$

(calibrate Y-accelerometer low gain average bias)

Position 13



Measure  $\Delta V_X$  over 100 seconds in the up position  
using Low gain

$$CAPXU = \Delta V_X$$

$$KLX = \frac{2 g \Delta T}{CAPXU - CAPXD}$$

(calibrate X-accelerometer low gain average scale factor)

$$BLX = \frac{CAPXU + CAPXD}{2 \Delta T}$$

(calibrate X-accelerometer low gain average bias)

$$KHX = \frac{(X1SQ11 + X3SQ11) - (X1SQ12 + X3SQ12)}{2 (X2SQ11 - X2SQ12)}$$

(calibrate X-accelerometer high gain average scale factor)

$$KHY = \frac{(Y1SQ14 + Y3SQ14) - (Y1SQ13 + Y3SQ13)}{2 (Y2SQ14 - Y2SQ13)}$$

(calibrate Y-accelerometer high gain average scale factor)

$$BHX = \left( \frac{KHX}{\Delta T} \right) (HXSQ12) + BHX$$

(calibrate X-accelerometer high gain bias)

$$BHY = \left( \frac{KHY}{\Delta T} \right) (HYSQ12) + BHY$$

(calibrate Y-accelerometer high gain bias)

With this last calculation, verification of this IMU is completed. The appropriate parameters are stored and displayed, and the procedure is repeated on the next IMU.

During the entire test plan execution it is assumed that all calibration parameter results will be documented for continuing stability evaluation and analysis.

#### 8.2.1.2 Gimbal Chain Calibration

An accurate attitude determination of the IMU stable member orientation with respect to a known body frame is of importance for rendezvous and entry performance as well as the verification of FDI initialization during prelaunch. The gimbal chain error sources consist of the synchro zero offset, readout errors over  $360^\circ$  at the A/D converter output, the gimbal offsets and non-orthogonality errors of all gimbal assemblies including the slaved fourth gimbal axis.



There is no proven method known to this author for calibrating the gimbal chains of the present air navigation subsystems at the ISS operating level. Historically, Apollo ISS was carefully calibrated and aligned to provide the capability of accurately pointing the stable member triad of accelerometers to perform the in-flight alignment of the subsystem stable member in a reference inertial frame established by the optical subsystem. The Apollo IMU calibration method is based upon establishing accelerometer axes in the local horizontal using a series of orientations of the gimbals when the ISS is mounted on a carefully calibrated positioning table. By zeroing the gimbal axes at a multispeed resolver null and establishing the local horizontal to attain specific accelerometer nulls using the fine positioning of a test table and compensating known instrument bias effects, it is possible to completely calibrate the stable member with respect to the ISS navigation base. The gimbal readouts are then calibrated by directly comparing the A/D output with a positioning table over  $360^{\circ}$  after the associated gyro loop is inertially stabilized.

The angular calibration implementation described for Apollo is not directly transferable to the present ISS candidates since no accurate gimbal zeroing loop is available with the present synchros. These systems do, however, have an accurate, finely quantized accelerometer loop implementation which might be directly applied to the angular calibration problem.

The calibration procedure for the gimbal readouts including the implemented A/D conversion electronics is relatively clear. It can be done by the ISS in the inertial mode (calibration axis perpendicular to earth rate) by compensating for earth rate and instrument uncertainties as well as possible, and then driving the gimbal axis in steps through  $360^{\circ}$  using a positioning table to reference the gimbal output readings. Another method would involve gyro torquing the calibration axis and simultaneously recording the gimbal output and the torquing history. This technique could be implemented entirely without the use of a positioning table and thus be available as a technique for pre-launch testing.

Another gimbal readout calibration method involves maintaining the stable member in the local vertical mode while using vertical earth rate compensation to maintain the remaining axis inertially stabilized. Each gimbal axis would be stabilized in the vertical position in turn and the  $360^{\circ}$  gimbal calibration would then be accomplished with either the vertical axis gyro torquing or the multiple table positioning methods.

Notice that thus far, only the gimbal axis calibration has been addressed, calibration of the fundamental error sources associated with gimbal non-orthogonalities and

the stability of the synchro's zero reference have not been considered. These error sources will certainly change between IMU assembly and ISS usage or whenever the ISS system is disassembled for instrument or electronic replacement. These errors may also be sensitive to temperature gradient changes from either the stable member controller or the outside environment. For example, in Apollo a single gimbal axis offset term would often change up to plus or minus two arc minutes due to reassembly of the gimbal axis hats. It should be noted that these error sources will remain to be analyzed after the multispeed resolver retrofit.

An efficient way to isolate these error sources in the ISS operating configuration is to lock the gimbals in accurately known positions and utilize the accelerometers to establish the stable member position with respect to various gimbal axes. The number of test positions required must be sufficient to isolate the known orientation error terms. These terms will include the four gimbal axis non-orthogonalities, the four gimbal offset errors, the accelerometer misalignments with respect to the reference stable member triad, the accelerometer bias, and the appropriate fixture misalignments. This technique is similar to the one successfully implemented in the Apollo ISS testing.

This testing method requires an external positional servo to electrically lock the gimbal orientations. This servo uses the amplified error voltage to derive an appropriate torque motor current for maintaining gimbal null. Testing is required in this area before the practicality of this approach is known.

Another possible gimbal calibration method is to record the accelerometer triad orientation in the known gravity field, with the gimbal axis readouts. This data would then be used to solve the gimbal chain calibration equations without a requirement for the electrical gimbal lock.

Data obtained during this testing phase must be documented. All error parameters must be evaluated for test stability and an investigation made to define the gimbal error compensation modeling requirements.

When a test procedure is defined and implemented it is anticipated that the acquired data will be outputted on the support typewriter.

In review, the calibration of the gimbal axis readout and electronics about the compass rose is straightforward. Three approaches are outlined. The approach presently favored is to fine position the stable member in the earth frame, and appropriately compensate the inertially stabilized system while simultaneously recording the torqued

gimbal axes A/D output with the instrument torquing history. The calibration of the gimbal non-orthogonality and axis offset errors is not so straightforward and will represent a problem, which must be solved even after the multispeed resolver retrofit. Calibration test techniques must be investigated further, the development of a calibration technique without direct dependence upon the gimbal locking positional servo loop is required.

#### 8.2.1.3 Gimbal Flip Region Evaluation

Another fundamental uncertainty in the use of a production type four-gimbaled system in the shuttle mission is the ability to operate normally in the region of gimbal flip. Throughout the multiple system simulations presented in this report it has been assumed that the ISS mounting is such that the normal outer roll axis is designated the orbiter pitch axis and the normal pitch axis becomes the orbiter yaw axis. This permits the defined azimuth axis to become the orbiter roll axis. The normal KT-70 gyrocompassing program may be used as the single two-degree of freedom accelerometer orientation is unaffected during prelaunch. This orientation is nominally free of "gimbal lock". Gimbal lock will occur only if the orbiter yaw angle becomes plus or minus ninety degrees with respect to the orbital plane. It is possible to keep the system from operating in the "gimbal lock" regions by using mission constraints but it should be determined if these constraints are even required. For example, is active management of attitude possible during gimbal flip? If not, simultaneous flip of all IMUs should be avoided, possibly by non colinear mounting of the IMUs. The problem of constraints is also of primary importance during two IMU operation where the orientations have been skewed to permit instrument axis voting.

The basic testing task, then, is to determine whether any performance degradation, temporary or permanent, can occur because of gimbal flip. During flip, it is desired to obtain a continuous attitude indication and a performance evaluation of the inertial components.

The gimbal flip region may be entered slowly or at a high angular velocity. The gimbal flip velocity will be a function of the conventional pitch angle  $\theta$  and the servo characteristics. Therefore, it is desirable to determine the gimbal angular velocity as a function of pitch angle and yaw gimbal rates.

The proposed basic test technique is as follows: The system is initialized in the inertial frame with roll axis-north, azimuth axis-down, and pitch axes-east, along table trunnion axis.

The azimuth gyro will now sense the major component of gimbal velocity. The 19.2 kc gyro preamp output of the azimuth gyro will be monitored during the test sequence using the automatic test point scanning capability of the SSCMS test facility. A near null signal during the maneuver would be an indication of flip integrity. Gyro data on the maximum pick-off output (i.e., at gyro stops) should be obtained from Kearfott prior to testing. Also monitored will be all the available gimbal A/D output data along with the slaved gimbal standoff angle.

The test is performed in the following manner: First, the system is stabilized in the inertial mode, preferably with earth rate and other drifts being compensated via the digital torquer. The test table would now be rotated about the trunnion axis (hence, changing the pitch angle proportionately) to a selected increment. Then, the table top would be rotated (simulating a yaw maneuver) to approximately  $90^{\circ}$  from its initial starting point.

The test sequence in Table 8.1 is suggested as a starting point. The azimuth gyro error signal should be monitored on a fast response analogue recorder and the gimbal readout used for deriving gimbal rates over the monitoring interval. The gimbal loop fault monitoring system might also indicate if the gimbals are lagging the gyro error signals.

Table 8-1

Test No.	<u>First</u>	<u>Second</u>
	T.A. Position from	Position R.A. + $90^{\circ}$
	Initial Point	Via the Following Slewrate
1	$-10^{\circ}$	$10^{\circ}/\text{sec.}$
2	$-30^{\circ}$	$10^{\circ}/\text{sec.}$
3	$-50^{\circ}$	$10^{\circ}/\text{sec.}$
4	$-70^{\circ}$	$2^{\circ}/\text{sec.}$
5	$-90^{\circ}$	$2^{\circ}/\text{sec.}$

The SSCMS will be used during this test sequence to provide a record of each test on magnetic tape for analysis. This tape will contain a simultaneous history of all four gimbal axis angles and rates, gyro error signals, and a record of table angles vs. time. This data may also be displayed at intervals on the HP2116B CRT.

### 8.2.2 Gyro Compassing Multiple Systems

The fundamental alignment program for the KT-70 system will be developed by Sperry Rand for NASA/MSFC.<sup>15</sup> A revision to this program will be required for

multiple system gyrocompassing to provide vertical gyro torquing logic to zero the azimuth error. In addition to the I/O modifications identified earlier for hardware data format compatibility, the Ground Alignment sequence will be capable of simultaneous and independent alignment of up to three KT-70s. It is planned that the short term bias data from each IMU be calculated and automatically used for instrument compensation. This bias data will also be collected and analyzed.

The automatic test station interface will be used in the gyrocompassing test phase for data acquisition and display. Data will be transferred from the 4 $\pi$ -CP2 to the test station using a fixed format. Among the test parameter transferred are attitude, attitude rate and attitude error. These parameters as well as other test variables will be saved on magnetic tape for later analysis. Using the HP2116B CRT, the real time display of these parameters will be available. Figure 8.1 represents a possible CRT gyrocompass display.

It may be required to convert the Sperry Code from floating point to fixed point arithmetic in order to reduce the real time load.

#### 8.2.2.1 System Testing

This testing phase will verify the complete software implementation and hardware performance attained by gyrocompassing multiple systems. Initially, verification will be made on each IMU individually. This will be a single IMU test series to verify the X and Y gyro drift estimates, and the response time of the vertical erection and azimuth loops. After this single IMU testing a series of tests will be conducted to verify each IMU system is truly independent. This is done by checking the individual gyrocompass settle out residuals and response time in a multiple system implementation. In addition known instrument miscompensation can be applied to check the individual IMU offsets using the gimbal attitude information.

##### 8.2.2.1.1 Single IMU G/C Verification

1. IMU instruments are to be recently calibrated<sup>6</sup>.
2. Put the IMU into normal G/C and allow the system to settle out.
3. Use the capability to torque the stable member from the inertial mode to attain a known angular offset in three dimensions. Reinitialize G/C mode and carefully use the SSCMS facility to acquire a record of the gimbal angles vs. time on magnetic tape. Plots of loop response and settleout offsets can then be generated. This testing should be done with both initial positive and negative offsets to verify software.

GYROCOMPASS			
	IMU 1	IMU 2	IMU 3
ATTITUDE			
PITCH	± XXXXX.XXXXX	± XXXXX.XXXXX	± XXXXX.XXXXX
ROLL	± XXXXX.XXXXX	± XXXXX.XXXXX	± XXXXX.XXXXX
AZIMUTH	± XXXXX.XXXXX	± XXXXX.XXXXX	± XXXXX.XXXXX
ATT. RATE			
PITCH	± XXXXX.XXXXX	± XXXXX.XXXXX	± XXXXX.XXXXX
ROLL	± XXXXX.XXXXX	± XXXXX.XXXXX	± XXXXX.XXXXX
AZIMUTH	± XXXXX.XXXXX	± XXXXX.XXXXX	± XXXXX.XXXXX
ATT. ERROR			
X TILT	± XXXXX.XXXXX	± XXXXX.XXXXX	± XXXXX.XXXXX
Y TILT	± XXXXX.XXXXX	± XXXXX.XXXXX	± XXXXX.XXXXX
AZIMUTH	± XXXXX.XXXXX	± XXXXX.XXXXX	± XXXXX.XXXXX
FAILSTAT	X	X	X
IMU STAT	± XXXXXX	± XXXXXX	± XXXXXX
DELTAV X	± XXXXXXXXXXXXX	± XXXXXXXXXXXXX	± XXXXXXXXXXXXX
DELTAV Y	± XXXXXXXXXXXXX	± XXXXXXXXXXXXX	± XXXXXXXXXXXXX
DELTAV Z	± XXXXXXXXXXXXX	± XXXXXXXXXXXXX	± XXXXXXXXXXXXX
TAB ANG	± XXX.XXXX		
TIME	± XXXXXXXX.XX		
VARIABLE FIELD			
1.	± XXXXXXXXXXXXX	± XXXXXXXXXXXXX	± XXXXXXXXXXXXX
2.	± XXXXXXXXXXXXX	± XXXXXXXXXXXXX	± XXXXXXXXXXXXX

Figure 8.1 - HP2116 Display (Gyrocompass)

4. Verify the X and Y short term drift compensation estimators by miscompensating the last instrument calibration value stored in the computer.

#### 8.2.2.1.2 Multiple IMU G/C Verification

1. Single IMU gyrocompass gimbal angle history should be available from prior testing.
2. Run the multiple IMU gyrocompass program and verify that the gimbal angle history is unaffected during multiple system operation. This should give an indication of the status of the multiple IMU grounding quality as well as verification of independent software.
3. Miscompensate the appropriate terms in a single IMU's instrument calibration stored in the computer and record on magnetic tape all gimbal angles as a function of time for later plotting and analysis.

#### 8.2.2.2 Basic Ground Alignment Program

The following is an explanation of the sequences and equations required to accomplish the ground alignment program.

##### Sequence 0

Condition for initiation: operator selection, ground align and system ready discretes are on.

Purpose: to slew the platform  $-90^0$  from its flight orientation

gyro torquing rate requirements:

$$\omega_y = \omega_e \cos \lambda - D_{YRA}$$

$$\omega_x = -D_{XRA}$$

##### Sequence 1

Condition for entry: 60 seconds to slewing have elapsed.

Purpose: to measure leveling errors. gyrotorquing rates requirements:

$$\omega_x = -D_{XRA}$$

$$\omega_y = \omega_e \cos \lambda - D_{YRA}$$

$$\omega_z = \omega_e \sin \lambda - D_{ZRA}$$

Measure velocity errors over 5 sec.

$$V_y = K_{HY} \sum_{\Delta t=0}^5 \Delta V_y - B_{HY} \text{ 5 sec}$$

$$V_x = K_{HX} \sum_{\Delta t=0}^5 \Delta V_x - B_{HX} \text{ 5 sec}$$

Compute level errors

$$\theta_{0X1} = \frac{V_y}{g \text{ 5 sec}}$$

$$\theta_{0Y1} = \frac{V_x}{g \text{ 5 sec}}$$

## Sequence 2

Condition for entry: 5 seconds have elapsed in sequence 1.

Purpose: torque out gross level errors, while still earth rate compensating.

$$\text{let } \Delta t_x = \frac{\theta_{0X1}}{\omega_{\max} - (-D_{XRA})}$$

$$\Delta t_y = \frac{\theta_{0Y1}}{\omega_{\max} - (\omega_e \cos \lambda - D_{YRA})}$$

Torque at maximum rate:

X gyro for  $\Delta t_x$  seconds

Y gyro for  $\Delta t_y$  seconds

Torque remaining gyros for  $\Delta t$  sec where applicable, using

$$\omega_x = -D_{XRA}$$

$$\omega_y = \omega_e \cos \lambda - D_{YRA}$$

$$\omega_z = \omega_e \sin \lambda - D_{ZRA}$$



### Sequence 3

Condition for entry:  $\Delta t$  seconds elapsed in sequence 2.

Purpose: refinement of level. Gyro torque during computations at rate given by equation (8-22) over 15 seconds compute:

$$A_x = \frac{1}{\Delta t} \frac{(\sum N^4)(\sum N v_{xN}) - \sum (N^2 v_{xN})(\sum N^3)}{(\sum N^2)(\sum N^4) - (\sum N^3)^2}$$

where  $\Delta t = 0.2$  sec and  $N = 1, 2, \dots, N_f$  with  $N_f \Delta t = 15$  sec

then let

$$\theta_{0X3} = \frac{A_y}{g}$$
$$\theta_{0Y3} = -\frac{A_x}{g}$$

Torque out these angles in the same way as Sequence 2 equations (8-25) and (8-26).

Reiterate Sequence 3 sixteen times, unless operator has indicated otherwise.

### Sequence 4

Condition for Entry: Sequence 3 has been iterated 16 times.

Purpose: measure azimuth error and to further refine level. Gyro torque during computations at rates given by equation (8-22). Over 80 seconds, evaluate equations (8-27) with  $N_f \Delta t = 80$  seconds then compute;

$$\theta_{0Y4} = -\frac{A_x}{g}$$
$$\theta_{0X4} = \frac{A_y}{g}$$
$$\psi_{E4} = \left(-\frac{2B_Y}{g} + (\omega_e \sin \lambda) \theta_{0Y4}\right) / \omega_e \cos \lambda$$

torque out  $\theta_{0Y4}$ ,  $\theta_{0X4}$  as in Sequence 2 equations (8-25) and (8-26).

### Sequence 5

Condition for Entry: angles have been torqued out.

Purpose: to torque out azimuth error

Periodically ( $\Delta t = 0.2$  sec) compute horizontal velocity

$$V_x = K_{LX} \Delta V_x - B_{LX} \Delta t - K_2 V_x$$

$$V_y = K_{LY} \Delta V_y - B_{LY} \Delta t - K_2 V_y$$

update gyro leveling rates and torque X, Y gyros at

$$\omega_x = -\frac{K_{1y} V_y}{R} - D_{XRA}$$

$$\omega_y = \omega_e \cos \lambda + K_{1x} \frac{V_x}{R} - D_{YRA}$$

Compute time to slew out azimuth error

$$t_s = \frac{\psi_{E4}}{\omega_{\max} - \omega_e \sin \lambda}$$

and perform azimuth slew for the period of time.

### Sequence 6

Condition for Entry: azimuth error has been slewed out.

Purpose: calibrate y-gyro drift.

Torque gyros during computation at rate given by equation (8-22)

over 200 seconds evaluate equations (8-27).

then compute tilt angles and drifts

$$\theta_{0x6} = \frac{A_y}{g}$$

$$\theta_{0y6} = -\frac{A_x}{g}$$

$$D_x = \frac{2B_y}{g}$$

$$D_y = -\frac{2B_x}{g}$$

estimate Y drift

$$D_{YR} - D_Y - (\omega_e \cos \lambda)(1 - \cos \psi_{E6}) + (\omega_e \sin \lambda)(\theta_{0x6} + \frac{D_x}{2} \frac{200}{2})$$

a failure will be indicated if

$$D_{YR} - D_{YRA} > 1 \text{ deg/hour}$$

Otherwise:

$$D_{YRA} = D_{YR}$$

#### Sequence 7

Condition for Entry: calibrated Y-gyro drift variation is acceptable.

Purpose: slew about azimuth to orientation shown below

Derive X, Y torquing rates as follows. Compute  $V_X$  and  $V_Y$  from equation (8-30) and compute rates as:

$$\omega_x = \omega_e \cos \lambda - \frac{K_{1Y} V_Y}{R} - D_{XRA}$$

$$\omega_y = \frac{K_{1Y} V_X}{R} - D_{YRA}$$

Compute time to slew

$$t_7 = \frac{90^\circ - \psi_{E6}}{\omega_{\max} - \omega_e \sin \lambda}$$

Slew about azimuth at max rate for  $t_7$  seconds

#### Sequence 8

Condition for Entry: Azimuth slew complete

Purpose: platform leveling and stabilization

Set  $\alpha = 0$  Compute gyro torquing rates

$$\omega_x = \omega_e \cos \lambda \cos \alpha - D_{XRA}$$

$$\omega_y = \omega_e \cos \lambda \sin \alpha - D_{YRA}$$

$$\omega_z = \omega_e \sin \lambda - D_{ZRA}$$

Repeat Sequence 3 five times.

### Sequence 9

Condition for Entry: sequence 3 has been iterated 5 times

Purpose: calibrate X gyro drift

Continue to torque using equation (8-37)

Evaluate, over 200 seconds, equations (8-27)

Compute tilt angles and drifts

$$\theta_{0x9} = \frac{A_y}{g}$$

$$\theta_{0y9} = -\frac{A_x}{g}$$

$$D_x = \frac{2B_y}{g}$$

$$D_y = -\frac{2B_x}{g}$$

Compute total X-gyro drift

$$D_{XR} = D_x - (\omega_e \cos \lambda)(1 - \cos \psi_{E9}) - \omega_e \sin \lambda (\theta_{0y9} + \frac{D_y 200}{2})$$

An error condition exists if

$$D_{XR} - D_{XRA} < 1 \text{ deg/hour}$$

Otherwise

$$D_{XRA} = D_{XR}$$

#### Sequence 10

Condition for Entry: X-gyro drift variation is acceptable

Purpose: platform errection and prepared for Navigation

Let

$$\theta_{0x10} = -\theta_{0x9} - D_x 200$$

$$\theta_{0y10} = -\theta_{0y9} - D_y 200$$

$$\alpha = \alpha + \psi_{E9}$$

Torque out these angles using the procedure of sequence 2 (equations (8-25) and (8-26)) using the following rate definitions

$$\omega_x = \omega_e \cos \lambda \cos \alpha - D_{XRA}$$

$$\omega_y = \omega_e \cos \lambda \sin \alpha - D_{YRA}$$

$$\omega_z = \omega_e \sin \lambda - D_{ZRA}$$

Continue to earth rate compensate until operator selects new mode.

#### 8.2.3 Prelaunch Verification of Multiple Systems

As discussed in Chapter 6 two methods are proposed to completely verify the performance within mission requirements of each IMU with respect to all operational IMUs. At least three cardinal positions are required to insure verification of all g sensitive as well as time dependent error sources. It is our present position that a six position test method be implemented for prelaunch verification. The six position test (flow gram in Chapter 6) is very closely associated with the IMU calibration both in data accumulation methods and in multiple positioning requirements.

The testing of this method will consist of a complete calibration to insure very small uncompensated errors. This is followed by an evaluation of the mechanization of the six position method by introducing known instrument miscompensations and checking the verification method threshold values versus time.

#### 8.2.4 Land Navigation Performance Verification

The land navigation program, developed by Sperry Rand, will operate from information provided by the velocity FDI. Each individual IMU output is compensated and data from all operational IMUs is averaged before utilization in the program.

The navigation program will integrate the delta velocity in an inertial coordinate system. Gyro torquing rates will be computed and mechanized to maintain all KT-70s in the inertial frame. It is presently assumed that vertical information will be clamped by the constant earth radius for laboratory fixed navigation. Periodically (every 2 seconds), latitude, longitude and heading will be computed for display and recording by the HP-2116b test station. A possible CRT display format for the land navigation phase is shown in Figure 8.2. This same data will be acquired on magnetic tape for subsequent analysis of navigation performance.

#### 8.2.4.1 System Testing

This testing program will be principally self evident and directly depend upon the reasonability of performance in the output position and velocity error profiles. If the land navigation program validity becomes subject to question it can easily be verified by introducing known instrument compensation errors and verifying the average velocity error effects in the land navigation performance against documented sensitivities.

#### 8.2.4.2 Land Navigation Program

Condition for entry: the operator selects land navigation mode while the system is in the gyro compass mode.

The three direction cosines are initialized as

$$C_{xx0} = \cos \lambda \cos \alpha$$

$$C_{xy0} = -\cos \lambda \sin \alpha$$

$$C_{xz0} = \sin \alpha$$

Where  $\alpha$  = the heading offset and  $\lambda$  = the local latitude. Every major cycle (.2 sec) the velocity FDI computes the average horizontal delta velocity:

$$\Delta V_x = \text{average of operational IMUs } (K_{LX} X_{CAPRI \text{ PULSES}} - B_{LX} 0.2)$$

$$\Delta V_y = \text{average of operational IMUs } (K_{LY} Y_{CAPRI \text{ PULSES}} - B_{LY} 0.2)$$

These are integrated as,

$$V_x(t) = V_x(t - 0.2) + \Delta V_x + 0.2 \{P_z + 2\omega_e C_{xz}\} V_y(t - 0.2) + 0.2 \{P_y + 2\omega_e C_{xy}\} V_z$$

NAVIGATION			
	IMU 1	IMU 2	IMU 3
ATTITUDE			
PITCH	± XXXXX.XXXXX	± XXXXX.XXXXX	± XXXXX.XXXXX
ROLL	± XXXXX.XXXXX	± XXXXX.XXXXX	± XXXXX.XXXXX
AZIMUTH	± XXXXX.XXXXX	± XXXXX.XXXXX	± XXXXX.XXXXX
ATT. RATE			
PITCH	± XXXXX.XXXXX	± XXXXX.XXXXX	± XXXXX.XXXXX
ROLL	± XXXXX.XXXXX	± XXXXX.XXXXX	± XXXXX.XXXXX
AZIMUTH	± XXXXX.XXXXX	± XXXXX.XXXXX	± XXXXX.XXXXX
LATITUDE	± XX.XXXXXXXXX		
LONGITUDE	± XXX.XXXXXXXXX		
ALTITUDE	± XXXXX.XXXXX		
NORTH VEL	± XXXXX.XXXXX		
EAST VEL	± XXXXX.XXXXX		
VERT VEL	± XXXXX.XXXXX		
FAIL STAT	X	X	X
IMU STAT	± XXXXXX	± XXXXXX	± XXXXXX
DELTAV X	± XXXXXXXXXXXXX	± XXXXXXXXXXXXX	± XXXXXXXXXXXXX
DELTAV Y	± XXXXXXXXXXXXX	± XXXXXXXXXXXXX	± XXXXXXXXXXXXX
DELTAV Z	± XXXXXXXXXXXXX	± XXXXXXXXXXXXX	± XXXXXXXXXXXXX
DETECT RATIO			
X	±.XXXXXXXXXX		
Y	±.XXXXXXXXXX		
Z	±.XXXXXXXXXX		
ISOLATION RATIO			
X	± X.XXXX	± X.XXXX	± X.XXXX
Y	± X.XXXX	± X.XXXX	± X.XXXX
Z	± X.XXXX	± X.XXXX	± X.XXXX
TAB ANG	± XXX.XXXX		
TIME	± XXXXXXXXXXX		
VARIABLE FIELD			
1.	± XXXXXXXXXXX	± XXXXXXXXXXX	± XXXXXXXXXXX
2.	± XXXXXXXXXXX	± XXXXXXXXXXX	± XXXXXXXXXXX

Figure 8.2 - HP2116 Display (Land Navigation)

# DEBUG

	IMU 1	IMU 2	IMU 3
GIMBAL ANGLE			
PITCH	XXXXXX	XXXXXX	XXXXXX
ROLL	XXXXXX	XXXXXX	XXXXXX
AZIMUTH	XXXXXX	XXXXXX	XXXXXX
DELTAV X ±	XXXXXX ±	XXXXXX ±	XXXXXX
DELTAV Y ±	XXXXXX ±	XXXXXX ±	XXXXXX
DELTAV Z ±	XXXXXX ±	XXXXXX ±	XXXXXX
GYPTO X ±	XXXX ±	XXXX ±	XXXX
GYPTO Y ±	XXXX ±	XXXX ±	XXXX
GYPTO Z ±	XXXX ±	XXXX ±	XXXX
DISCRETES	XXXXXX	XXXXXX	XXXXXX
SLEW	XXXXXX	XXXXXX	XXXXXX
TAB ANG ±	XXX.XXXX		
TIME	XXXXXXXXXXXX		

## VARIABLE FIELD

1.	±XXXXXXXXXXXX	±XXXXXXXXXXXX	±XXXXXXXXXXXX
2.	±XXXXXXXXXXXX	±XXXXXXXXXXXX	±XXXXXXXXXXXX

Figure 8.3 - HP2116 Display (Debug)



$$V_y(t) = V_y(t - 0.2) + \Delta V_y - 0.2 \{ P_z + 2\omega_e C_{xz} \} V_x(t) \\ + 0.2 \{ P_x + 2\omega_e C_{xx} \} V_z$$

Where  $V_Z$  (vertical velocity) is determined either from external information (e.g. altimeter) or a canned profile.

The velocities are then used to update the platform rates relative to the earth frame.

$$P_x = \frac{2\xi C_{xx} C_{xy} V_x + (1 - 2\xi C_{xx}^2) V_y}{R(1 - 2\xi) + h + 3R\xi C_{xz}^2}$$

$$P_y = \frac{2\xi C_{xx} C_{xy} V_y + (1 - 2\xi C_{xy}^2) V_x}{R(1 - 2\xi) + h + 3R\xi C_{xz}^2}$$

The altitude,  $h$ , is also derived from external information.

$$P_z = - \frac{C_{xx} P_x + C_{xy} P_y}{C_{xz} + 1}$$

The three direction cosines are updated.

$$C_{xx} = C_{xx} + 0.2(C_{xy} P_z - C_{xz} P_y)$$

$$C_{xy} = C_{xy} + 0.2(C_{xz} P_x - C_{xx} P_z)$$

$$C_{xz} = C_{xz} + 0.2(C_{xx} P_y - C_{xy} P_x)$$

Finally, the gyro torque rates for each major cycle are computed.

$$\omega_x = \omega_e C_{xx} + P_x - D_{XRA} + D_{\mu x}$$

$$\omega_y = \omega_e C_{xy} + P_y - D_{YRR} + D_{\mu y}$$

$$\omega_z = \omega_e C_{xz} + P_z - D_{ZRA} + D_{\mu z}$$

These are converted to period between pulses for the gypto output handler.

Every 10 major cycles (2 seconds) an output cycle will commence to compute the following navigation parameters:

IMU Heading:

$$\alpha = \tan^{-1} \left( -\frac{C_{xy}}{C_{xx}} \right)$$

$$\lambda = \tan^{-1} \left( \frac{C_{xz}}{C_{xy} \cos \alpha - C_{xy} \sin \alpha} \right)$$

North and East velocity:

$$V_E = -V_x \sin \alpha - V_y \cos \alpha$$

$$V_N = V_x \cos \alpha - V_y \sin \alpha$$

Longitude:

$$\phi = \phi + (2 \text{ seconds}) \frac{V_E \cos \alpha}{R C_{xx}}$$

Vehicle heading:

$$TH = \psi - \alpha$$

where  $\psi$  is the azimuth gimbal angle.

### 8.2.5 Failure Detection And Isolation Testing

In the laboratory (one g environment) the FDI implementation must be verified for hard and soft failure conditions at both the three IMU and two IMU operating levels while insuring smooth transition of velocity and attitude information during transfer between these operating levels.

The initial verification will insure that the hard failure reasonability levels have been successfully implemented to detect hard failure conditions prior to processing data from this error source. The soft fail implementation will use special red-line thresholds recognizing the laboratory environment. Verification of the computer software implementation for soft failure detection and isolation in powered flight will be verified with known instrument parameter miscompensations. The expected single IMU error propagation characteristics will be confirmed using the land navigator output recorded and displayed by the HP2116 facility. The system reconfiguration after failure isolation and the observed failure detection response time will also be recorded. The attitude FDI software implementation will be verified using gyro compensation errors designed to be demonstrated within reasonable time limits in the laboratory environment.

#### 8.2.6 Attitude Loop Demonstration

It is desirable to demonstrate the attitude loop in terms of absolute angle readout since the attitude FDI mechanization in unpowered flight uses rate information from each IMU and is not sensitive to the absolute attitude. A desirable feature of this attitude loop resolution demonstration would display and record attitude information from all individual systems as well as the total attitude loop information from the composite configuration.

For the NASA/MSFC test demonstration the vertical axis seems most appropriate. A testing and demonstration sequence for the vertical attitude indicators would consist of a plus and minus one degree vertical axis maneuver by the rotary table. A hard failure demonstration of the attitude FDI will be demonstrated by continuous torquing a single IMU axis.

The land navigation results can give an excellent demonstration of soft failure detection and IMU data reconfiguration in the velocity FDI implementation. To attain this demonstration for the attitude FDI implementation, a soft failure of the gyroscope is introduced by a miscompensation along the vertical axis in a single IMU. This IMU drift will be detected both as an attitude error indication of the single IMU and to a lesser degree in the composite system. An attitude display on the HP2116 CRT will then be used to demonstrate visually the FDI performance and the resulting system adaptation after error isolation.

The display quantities would be the individual and composite whole angle information and the error angle information of each IMU with respect to the composite angle (see Figure 8.2).

## 9.0 LABORATORY TESTING HARDWARE AND SOFTWARE REQUIREMENTS

### 9.1 HARDWARE REQUIREMENTS

It has been proposed that the demonstration test system of multiple four gimbaled IMUs be implemented at the Marshall Space Flight Center. Assigned to this study are three Kearfott AN/ASN-90 (KT-70) Inertial Measurement Systems, an IBM 4 $\pi$ /CP2 and the SSCMS test facility including the Goerz 500 test table. This demonstration requires the design and implementation of appropriate interfaces to allow computer control and monitoring of the three inertial measurement systems and test equipment for data acquisition, storage and display, table control and readout.

The AN/ASN-90 Inertial Measurement System consists of the KT-70 IMU, an Adapter Power Supply and a manual controller. In a multiple system laboratory test configuration it is desirable to have all moding under computer control.

An appropriate AN/ASN-90 interface must provide for the handling of the following signals.

#### 9.1.1 Delta Velocity Pulses

Plus and minus Delta Velocity ( $\Delta V$ ) output pulses from the IMU CAPRI electronics, for each of three accelerometer loops, can be best handled by an up/down counter of appropriate size. This counter would accumulate net pulses over an update interval. Since the CAPRI electronics are asynchronous in nature, provision must be made for bit storage during counter readout. Presently, it is planned to use three 16 bit (capacity of several seconds of data) up/down counters with single bit storage during readout as the accelerometer interface equipment.

#### 9.1.2 Gimbal Angle Outputs

Gimbal angle outputs are in the form of three (Roll, Pitch, Yaw) three wire single speed synchro signals. These synchros have uncalibrated peak errors on the order of 5-7 arc minutes.

Conversion of these synchro signals to digital binary form could be accomplished using a single multiplexed converter or three dedicated converters. It is thought that the advantage of simultaneous gimbal angle data will outweigh the cost of the extra converters. The multiplex converter necessarily

introduces data staleness. To this end three dedicated tracking synchro to digital converters will be used. These converters will have an accuracy of 14 binary bits (80 arc seconds) to provide sufficient accuracy to implement the IMU synchro calibration as discussed in chapter 8.

### 9.1.3 System Input Discretes

System input discretes are of two classes - gyro to torquing discretes (GYPTO commands), and other discretes (including analog torquing, accelerometer scale factor select, computer control, and moding discretes).

#### 9.1.3.1 Gyro Torquing Discretes

The gyros in the KT-70 IMU are torqued in a binary mode at a 200 pps rate. That is, the polarity of torquing signal must be supplied every 5 milliseconds. This required command rate can be reduced by using ternary commands and providing a ternary to binary converter in the interface. This would provide binary commands (plus alternating with minus) in the absence of computer intervention. The computer could provide a pulse pattern for torquing over a period of time to reduce the load even further. Four bits of torquing information and a torque sense (sign) bit for each of the three gyro loops would require 15 bits of command information and a maximum of one word transfer per 20ms. If no torque other than binary is required no command need be made. This command could be implemented in a single 16 bit computer output word.

The interface also requires an internal 5ms clock to operate the torquing interface.

#### 9.1.3.2 Analog Torquing and Other Discrete Commands

Provision must be made for the operation of analog slew and slew sense discretes for each of three axes (Xaxis, Yaxis, Azimuth) (6 lines). Several other input discretes must also be implemented. These include the accelerometer scale factor select discrete and mode selection discretes (Inertial, Normal, Ground Align). It is thought that these discretes could be implemented in a single 16 bit word. Discretes of this type are activated at a low rate and are not time critical.

#### 9.1.4. System Output Discretes

Several system output discretes must be input to the processor. These include IMS fail, system ready discretes and, possibly, some interface status and additional BITE information. Mode discretes are provided as an output from an AN/ASN-90 but, as manual moding is no longer provided, these are not implemented for the test system. Provision of a single 16 bit computer input word will be adequate for these signals. These output discretes also occur at a low rate and are not time critical.

#### 9.1.5. Avionics Interface

In the aircraft installation an AN/ASN-90, magnetic variation and heading information are provided to the IMS in certain modes. This interface requires a synchro input and several discretes. These functions will not be used in the laboratory test and no provision will be made for their implementation.

#### 9.1.6. General

It is thought that the multiple system interface would be provided as three identical interface units (IU), as described above. These units would be connected to the processor interface unit (PIU) by a multiplexing device using a serial bus. This processor interface unit would also contain provision for parallel transfer of information between the processor (IBM 4 $\pi$ /CP2) and the test station control computer (HP2116B). The processor interface unit would make use of the externally controlled input and output channels of the CP2 along with an external interrupt and several input and output discretes. The PIU would do most of the I/O housekeeping and work into the computer on a cycle stealing basis. The test station interface, similarly, is externally controlled and provides access to the rotary table controls and readouts, the magnetic tape unit, the CRT display and to a line printer.

### 9.2 SOFTWARE-EXECUTIVE CONTROL

In chapter 8 certain laboratory test software requirements have been discussed, including calibration, alignment, gyrocompass, velocity FDI, attitude FDI, and land navigation programs. In addition to these, a number of service programs are required to enable efficient performance of the laboratory test sequences. These service programs will be identified as the executive program.

Since the  $4\pi$ -CP2 is essentially dedicated to three KT-70s, it seems appropriate that the executive will be the synchronous, box car type. The gyro torquing and navigation requirements make a .02 second minor cycle and .2 second major cycle attractive. It has been estimated that most periodic calculations will fit into minor cycles, if these calculations are done in fixed point and not in simulated floating point. For maximum flexibility, however, floating point arithmetic will be used where feasible. Provisions will be made for four background major cycles on a time available basis. An example of a background major cycle is the update of a Kalman filter. The major/minor cycles will then be synchronized with the PIU by a .02 second real time interrupt supplied by the PIU. This same interrupt will signal when either the CAPRI, synchro data, or any other data is available from the PIU. Discrete bits will be used to identify this interrupt.

The coding for a complete multiple system test sequence will be capable of being stored entirely in memory at one time. The origin of the code will be magnetic tape, entered via the HP2116 and transferred to the  $4\pi$ /CP2 under PIU and executive control. Pertinent data will be sampled by the executive and transferred to the HP2116 for display and recording. The type and format of this data will be defined and will depend on the test sequence. Shown in Table 9-1 are some typical examples of data type and format.

A test subsequence will be defined by specifying, for the major cycle, what routines will be called in each minor cycle. Thus, for each subsequence there will exist a list of ten address constants. When a subsequence is in control, its address list will be stored in the executive's transfer vector. Transition between subsequences will be affected by replacing the executive transfer vector with a new address list. This can only occur at the end of a major cycle. Operator communication with the executive and control of the test sequences will be through the keyboard at a very low frequency. A test control program will exist as part of the executive. This program will decode keyboard messages, and format typewriter output. Keyboard messages will be simple commands. Examples of commands would be:

- a. Print Memory Location x
- b. Change Memory Location x to y
- c. Start Test Sequence x
- d. Stop Test
- e. Cause CP2 to Idle
- f. Change Instrument Compensation Values to Set x

TABLE 9-1

Data Name	Length	Scale	Subsequence	Exploitation
LAT,LON	DP	$\pm \pi$ Rad	Navigation	Latitude & Longitude
ALT	DP	(-1000,+38000)ft	Navigation	Altitude
VN,VE,VU	DP	$\pm 1000$ ft/sec	Navigation	North, East and Radial Velocity
$\Delta V_{ij}^*$	DP	$\pm 100$ ft/sec	Velocity FDI	Deviation from average velocity
DET <sub>j</sub>	DP	(0,10 <sup>-4</sup> )	Velocity FDI	Detection Ratio, Velocity
ISV <sub>i,j</sub>	DP	(0,1)	Velocity FDI	Isolation Ratio, Velocity
STATUS <sub>i</sub>	DP	0 or 1	Velocity & Attitude FDI	Failure Status
W <sub>i,j</sub>	DP	(0,200) meru	Attitude FDI	Estimate of error drift rate
TSE <sub>j</sub>	DP	(0,40000) meru <sup>2</sup>	Attitude FDI	Total squared error
ISR <sub>i,j</sub>	DP	(0,1)	Attitude FDI	Isolation Ratio, Attitude
OX <sub>i</sub>	SP	$\pm 2$ Rad	Alignment & gyro compass	X-tilt error
OY <sub>i</sub>	SP	$\pm 2$ Rad	Alignment & gyro compass	Y-tilt error
OZ <sub>i</sub>	SP	$\pm Y 1/2$ Rad	Alignment & gyro compass	Azimuth error
W <sub>i,j</sub>	SP	$\pm 70$ meru	All	Average drift
SF <sub>i,j</sub>	SP	.5 sec/pulse	All	Gyro torque scale factor
ABIASH <sub>i,j</sub>	SP	$\pm 2$ ft/sec <sup>2</sup>	All	Acc. bias high gain
ABIASL <sub>i,j</sub>	SP	$\pm 2$ ft/sec <sup>2</sup>	All	Acc. bias low gain
ASFH <sub>i,j</sub>	SP	.0004ft/sec <sup>2</sup> /pulse	All	Acc. SF high gain
ASFL <sub>i,j</sub>	SP	.04 ft/sec <sup>2</sup> /pulse	All	Acc. SF low gain
CAP <sub>i,j</sub>	SP	Integer	All	Sum of CAPRI pulses
O <sub>i,j</sub>	SP	$\pm \pi$ Rad	All	Gimbal angle

\* i=IMU1,2,3 \*j=X,Y,Z

The range or scale of the variables are subject to further definition.



Typewriter output will notify the operator of sequence transitions, error conditions, and changes in IMU moding.

COMPOOL (i.e. common data memory) is also considered part of the executive even though it does not contain instructions. This memory is accessible to all programs, including programs in different memory loads. In fact, its purpose is to provide a communication area for programs in different memory loads. The instrument calibration parameters are an example of the type of data stored in COMPOOL. Thus, the IMU calibration sequence communicates with the land navigation sequence via COMPOOL.

### 9.3 COMPUTATIONAL REQUIREMENTS

Computational requirements for the multiple IMU system are estimated in this section based upon three AN/ASN-90 IMUs working with a single 4 $\pi$ -CP2 computer.

#### 9.3.1 4 $\pi$ -CP2 Computer

The IBM 4 $\pi$ -CP2 is a general purpose digital computer. It has 16K words memory, each with 32 bits. Sixteen bit half words in memory are augmented with parity and storage protection bits. The CPU has thirteen parallel 16 bit registers for arithmetic work and three index registers. There are two independent, 16 parallel bit I/O channels.

Typical execution times for the CP-2 computer are given in Table 9-2.

Table 9-2 - Command Execution Times  
in the CP-2 Computer

Command	Time ( $\mu$ s)
Input/Output Word	4.17
Store Word	2.5
Double Store	5.0
Add , Load	3.75
Double Add	5.0
Multiply	18.0
Double Multiply	20.0

### 9.3.2 Preliminary Estimates for Input/Output Operations

#### 1. $\Delta V$ Readout

The accumulated  $\Delta V$  pulses are frozen on command, and the three registers are read (estimated requirement one update/sec). The required time is estimated at  $50 \mu s/s/IMU$ .

#### 2. Gimbal Angle Readout

The estimated requirement is an update every other second. The gimbal angle readout requirements are estimated at  $6 \mu s/s/IMU$ .

#### 3. GYPTO Decisions

GYPTO loops must be commanded at 200 updates/s. It is assumed the binary torquing logic is left in the interface, and the three loops in each IMU can be commanded by a single half word (16 bit) transfer. Then  $1 ms/s/IMU$  will be required. For 3 IMUs, therefore, gyro pulse torquing I/O will require 0.3% of the computer. If the binary torquing logic is not implemented in the interface, considerable I/O duty cycle time will result.

### 9.3.3 Preliminary Estimates of Computational Requirements

A rough estimate has been made in Table 9-3 to define the  $4\pi$ -CP2 requirements for the demonstration phase of this program. More specific estimates will be prepared when actual programs are available.

Table 9-3  
 $4\pi$ -CP2 Load Estimates - 3 IMUs

Program	Words	% real time
Gyro and Accl. Compensation	1200	7%
Interface Requirements	200	1%
Failure Detection ( $\Delta V$ )	500	2%
Failure Detection (Gimbal Angles)	1200	7%
Gyro Compass and Navigation	8000	75%-100%
Calibration	11000	40%

**Page intentionally left blank**

## 10.0 PRESENT WORK EFFORT SUMMARY

The results of this study are summarized below:

1. It is possible to establish reliable failure detection thresholds within normal variations of a nominal mission for either gimbaled or strapdown redundancy.
2. An FDI philosophy applicable to "off the shelf" IMU technology has been defined and simulated providing high reliability compatible with FO/FO/FS requirements in typical shuttle trajectories.
3. Fundamental design considerations concerning the error signal magnitude required with respect to the level of noise on normal redundant information are established. This permits a definition of the performance level that can be isolated in a particular FDI implementation with known good reliability.
4. A multiple system prelaunch checkout method has been defined compatible with the shuttle goals of minimum system verification time.
5. A system laboratory demonstration test plan is defined for hardware and software verification of this work.
6. A system hardware interface definition for multiple IMU laboratory demonstration is defined.

Further study is desirable in the following areas:

1. A "once-around-abort" mission should be evaluated for FDI requirements.
2. An analytical method to determine trajectory thresholds on the basis of terminal accuracy requirements only should be developed.
3. Integrated redundancy management should be investigated to provide additional G&N information, e.g. radio aids, for increased decision reliability.
4. Advanced statistical FDI techniques are presently available which enable a reliable decision capability in high noise fields. These techniques should be applied to this redundancy management problem.
5. The present FDI implementation should be expected to include a diagnostic capability in software for non-critical time period instrument level fault detection and isolation.
6. Continued evaluations to prove highly reliable FDI performance in the nominal entry mission are desirable.
7. Continued two IMU FDI evaluations are desirable to prove reliable performance.

In general, the FO/FO/FS capability using colinear stable member alignment requires five IMUs to implement. The final approach selected using four IMUs includes a skew stable member orientation at the two IMU level. This permits voting on an instrument axis level for implementation of the fail safe criteria.

A FO/FS capability is attainable with three IMUs either in a colinear or skewed stable member orientation. If a skewed orientation is utilized continuously from launch for three IMUs, several error sources not present in the colinear orientation become evident. First, independent gyrocompassing of each system will contain additional gyro torquing scale factor error sources. Another closely related error appears as a higher system noise level due to stable member orientation uncertainties. This attitude uncertainty, caused by gimbal axis errors as well as torquing errors, degrades the performance of the instrument orientation dependent FDI algorithm.

In addition, the software required for implementing an FDI algorithm capable of handling a three IMU skewed system is much more complicated than for the colinear system.

The inherent capability of a KT-70 IMU for FDI implementation using both colinear and skewed approaches will be carefully evaluated in both hardware and software during the laboratory demonstration program.

## BIBLIOGRAPHY

1. McNellis, J., Ruland, W., and Woods, D., "A Computerized Test Station for Strapdown Guidance Systems", AIAA Guidance, Control and Flight Mechanics Conference Paper #71-967, August, 1971, Hofstra University, Hempstead, NY.
2. Gilmore, J. and McKern, R., "A Redundant Strapdown Inertial Reference Unit (SIRU)", Journal of Spacecraft and Rockets, Vol. 9, No. 1, January, 1972, pp. 39-47.
3. McKern, R. and Musoff, H., "Performance Evaluation of Candidate Strapdown and Gimballed Systems Using Nominal and Abort Shuttle Trajectories", ION National Space Meeting, Huntsville, Alabama, 23-25 February, 1971.
4. Barry, T., "Trade-Offs of Redundancy vs MTBF", Memo #EG5-72-97, NASA/Manned Spacecraft Center, 7 August, 1972.
5. Edmonds, G.P., "Detection of IMU, PSA and PEA Failures by Existing Apollo Failure Detection Circuitry", MIT/DL, STG Memo #1675, Rev. 1, 13 October, 1971.
6. Dove, D. and McKern, R., "Redundancy Management of Multiple Inertial Systems for Space Shuttle", MIT/DL E-2652, April, 1972.
7. Brooks, Melvin, "Number of Gimbal Angle Readouts Required from Four Gimbal Platforms to Generate Accurate Vehicle Attitude Error Signals", NASA/Marshall Space Flight Center, S&E-ASTR-SG-15-72, 16 February, 1972.
8. Brand, T.J., and Higgins, J. P., "Allowable IMU Errors for a Safe Ascent to Orbit", MIT/DL, 23A STS Memo #36-70, 21 October, 1970.
9. Stokes, B.J., "General Dynamics Booster Reentry Trajectory for Configuration B-9U with Landing Site Acquisition", M-244-985, August, 1971.

10. Deyst, J. and Kriegsman, B. and Marcus, F., Entry-Trajectory Design to Minimize Thermal-Protection-System Weight, MIT/DL E-2614, November, 1971.
11. Miller, J. and Feldman, J., "Apollo Guidance, Navigation and Control System Gyro Reliability, MIT/DL E-2141, June, 1967.
12. Singer, Kearfott Division, "Inertial Measurement Unit Study for Space Shuttle Application", 10-1461, January, 1971.
13. Ogletree, G., Coccoli, J., McKern, R., Smith, M., White, R., "Interim Technical Report #2 Candidate Configuration Trade Study, Stellar-Inertial Measurement System (SIMS) for an Earth Observation Satellite (EOS)", MIT/DL E-2630, 31 January, 1972.
14. Sperry Rand Corporation, Space Support Division, "Land Version Calibration of Inertial Measurement Unit", 9 September, 1971.
15. Sperry Rand Corporation, Space Support Division, "Program Requirements Document for CP-2/IMS Inertial Ground Alignment and Pure Inertial Navigate Modes", SP-210-0591, 3 January, 1972.
16. Singer, Kearfott Division, "Performance Specification Inertial Measurement Unit and IMU Adjustable Mount", CP6KIA100C, Revision G, April, 1969.

## APPENDIX A

### A.1 REDUNDANT GIMBALED SYSTEM MODEL DEFINITION

This Appendix defines the actual AN/ASN-90 IMU and 4 $\pi$ /CP2 computer system (which is to be implemented at MSFC) in sufficient detail to evaluate gimbaled system failure detection and isolation methods. Both single and redundant IMU error models have been defined for simulations with shuttle vehicle trajectories. The IMU/system interface, which is left unchanged when employing an IMU in the multiple IMU system, is defined by a signal list. A tabulation of the critical design features required to permit failure detection and isolation in laboratory demonstrations, is also shown.

### A.2 IMU ERROR MODEL FOR GENERAL FOUR GIMBALED SYSTEM

This section of the Redundant System Model Definition describes a single IMU error model which is used as a building block in the digital simulation of the complete multiple IMU system. Areas of specific interest include:

1. Definition of the stable member reference triad and determination of the orientation of the accelerometer and gyroscope input axes with respect to this reference triad.
2. Definition of gimbal order.
3. Definition of gimbal non-orthogonalities.
4. Definition of gimbal angle readout chain errors.
5. Attitude transformations.

Not included in this model at this time are the servo characteristics:

#### A.2.1 Definition of a Reference Triad

Since the KT-70 IMU is mechanized for local vertical frame navigation, the stable member reference triad has been defined using the two horizontal accelerometer input axes.



In the space shuttle orbiter application, where inflight alignment of the IMU is required, it is desirable to define the stable member triad axes in a known orientation with respect to the inner gimbal axis. Thus, a known reference triad alignment can be obtained by the transfer of a known optical reference to the stable member axes by the use of the gimbal axis readout chain.

The reference triad shall be a right-handed stable member fixed triad which, through rotation of the gimbals commanded by the computer, can be placed in arbitrary orientations relative to the vehicle (or laboratory) frame.

To define the reference triad for the booster mission or for the purposes of the present feasibility demonstration, two axis horizontal accelerometer will be used to minimize earth frame alignment errors. The X and Y accelerometer input axes are leveled by nulling the accelerometer loop output with bias effects compensated.

The definition of the reference triad is illustrated in Figure 1 as:

$$\begin{aligned}\bar{X}_R &= \bar{X}_{AIA} \\ \bar{Y}_R &\perp \bar{X}_R \text{ in the } X_R Y_{AIA} \text{ plane} \\ \bar{Z}_R &= \bar{X}_R \times \bar{Y}_R\end{aligned}$$

Also shown in Figure 1 are three accelerometer alignment errors. The six gyroscope alignment errors, with respect to the defined triad, are shown in Figure 2.

#### A.2.1.1 Instrument Input Axes to Reference Triad Transformations

The transformations from the accelerometer and gyroscope axes to the reference triad do not represent true rotations. Instead, they reflect the instrument axes into that triad. The matrices representing these transformations (see Figures 1 and 2), are given below.

$$\begin{bmatrix} X_{AIA} \\ Y_{AIA} \\ Z_{AIA} \end{bmatrix} = C_R^A \begin{bmatrix} X_R \\ Y_R \\ Z_R \end{bmatrix}$$

$$\begin{bmatrix} X_{GIA} \\ Y_{GIA} \\ Z_{GIA} \end{bmatrix} = C_R^G \begin{bmatrix} X_R \\ Y_R \\ Z_R \end{bmatrix}$$

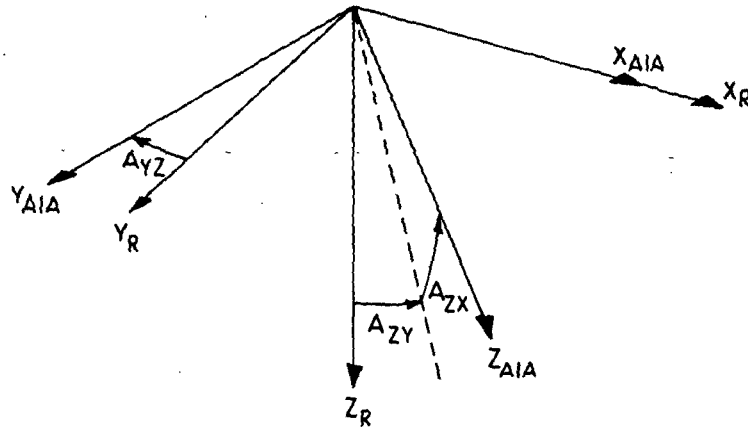


Fig. A-1 Accelerometer to Reference Triad Misalignment

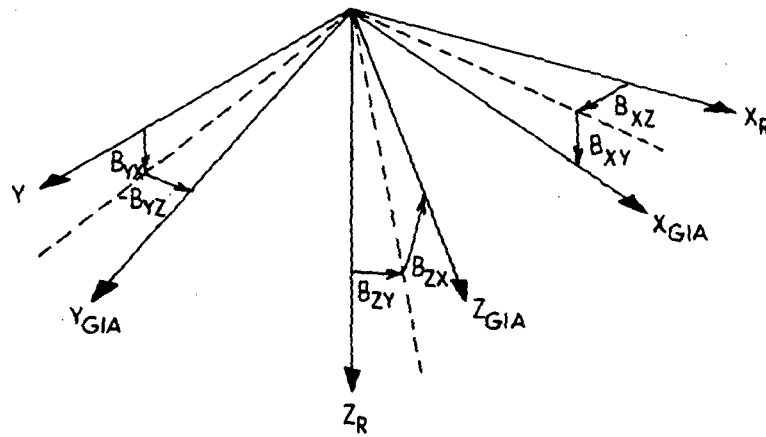


Fig. A-2 Gyroscope to Reference Triad Misalignment

Letting  $A_{ij}$  represent the misalignment of accelerometer  $i$  about  $j_R$ , and  $B_{ij}$  represent the misalignment of gyroscope  $i$  about  $j_R$ , we have:

$$C_R^A = \begin{bmatrix} 1 & 0 & 0 \\ -\sin A_{YZ} & \cos A_{YZ} & 0 \\ \sin A_{ZY} & -\sin A_{ZX} & \cos A_{ZY} \end{bmatrix}$$

or approximately:

$$C_R^A \approx \begin{bmatrix} 1 & 0 & 0 \\ -A_{YZ} & 1 & 0 \\ A_{ZY} & -A_{ZX} & 1 \end{bmatrix}$$

Similarly, the gyro misalignment can be represented for small angles as:

$$C_R^G = \begin{bmatrix} 1 & B_{XZ} & B_{XY} \\ -B_{YZ} & 1 & B_{YX} \\ B_{ZY} & -B_{ZX} & 1 \end{bmatrix}$$

Given these matrices,  $\Delta V$  information quantized in the accelerometer frame may be transposed to either the reference (inertial) frame for navigation or if required to the gyroscope frame for compensation as:

$$\begin{aligned} \bar{V}_I &= C_R^A{}^T \bar{V}_A \\ \bar{V}_G &= C_R^G C_R^A{}^T \bar{V}_A \end{aligned}$$

#### A.2.2 Gimbal Order and Gimbal Triads

Proceeding from the stable member to the vehicle, the gimbal order defined by the KT-70 IMU is shown in Figure 3 as:

- Azimuth (stable member) gimbal (AZ)
- Inner roll gimbal (IR)
- Pitch gimbal (PG)
- Outer roll gimbal (OR)
- Navigation base (vehicle) (NB)

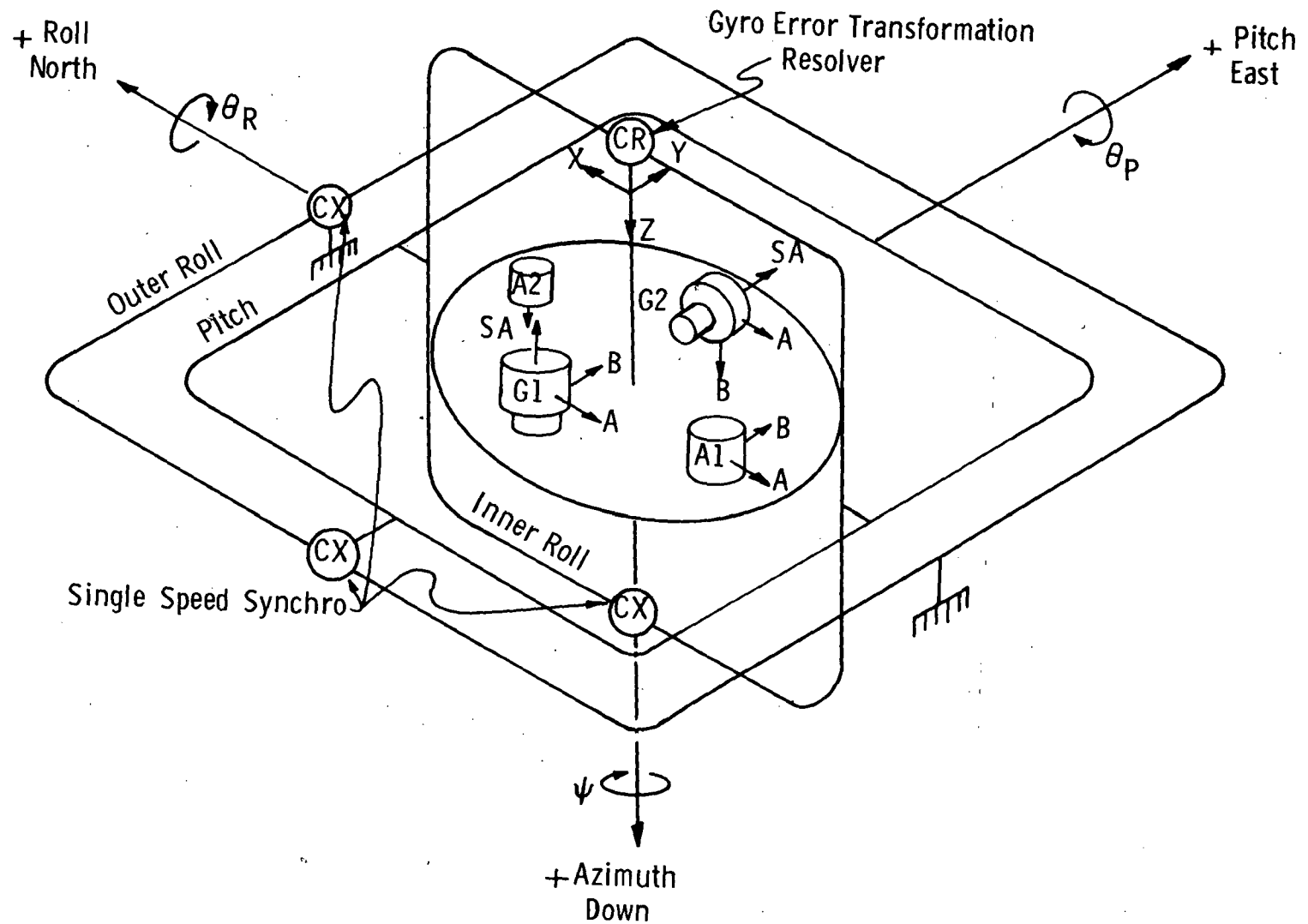


Figure A-3 Inertial Platform Mechanical Schematic

Angles between two adjacent frames are measured by a synchro mounted on the outermore gimbal. Positive angles are defined here about an outward pointing axis for purposes of laboratory testing.

### A.2.3 Gimbal Non-Orthogonalities and Offset Errors

It is desirable to model gimbals to reflect readout errors accurately since the proposed IMU model is used in studies of failure detection based upon attitude indication in multiple IMU systems. The attitude chain is also important in the problem of stable member alignment capability in earth orbit. This section will define gimbal non-orthogonalities and gimbal angle offset errors which appear when determining the relative orientation of the stable member with respect to the vehicle.

Each of the gimbal reference frames contain an angular offset from their reference zero position due to the repeatability of the synchro zero reference. The non-orthogonality of successive gimbal axes are also separately modeled. These two angles are defined in Figure 4. Notice in this figure that  $\epsilon_{Oj}$  is the gimbal offset error and  $\epsilon_{Nj}$  is the gimbal non-orthogonality errors where  $j$  denotes the appropriate gimbal axis. This definition closely re-resembles the gimbal definitions used in the Apollo Command Module IMU.

The synchro offset is modeled as a constant bias term plus an angle dependent sinusoidal term. That is

$$\psi_{ind} = \psi_{mech} - \epsilon_{Oj} + A_{\psi} \sin (n (\psi_{mech} - \psi_{off}))$$

where  $\psi_{ind}$  is the indicated angle,  $\psi_{mech}$  the physical (or mechanical) angle and  $A_{\psi}$  is the magnitude of the  $n$ x dominant synchro error term.  $\psi_{off}$  is the difference between mechanical and electrical zeros.

### A.2.4 Gimbal Angle Readout Errors

Error sources which are modeled as gimbal readout errors include the synchro offset errors previously defined and the additional A/D converter errors due to linearization and quantization effects. For this initial definition the only additional readout error source will be due to quantization. The linearization errors will be sized when actual A/D converter designs are evaluated since A/D electronic designs are not included in the standard interface definition.

### A.2.5 Attitude Transformation

#### A.2.5.1 Attitude Transformation from the Reference to Body Frame

The successive transformations from the reference triad to the body frame are functions of both gimbal angles and gimbal misalignments where gimbal angles are time varying, depending on body rotations and gyro drifts.

In the absence of misalignments, each transformation represents a simple rotation, and may be exactly written in either the quaternion form or as a direction cosine matrix:

1) Reference Triad to Azimuth Frame	$q_R^{AZ}$	or	$C_R^{AZ}$
2) Azimuth to Inner Roll Frame	$q_{AZ}^{IR}$	or	$C_{AZ}^{IR}$
3) Inner Roll to Pitch Frame	$q_{IR}^{PG}$	or	$C_{IR}^{PG}$
4) Pitch to Outer Roll Frame	$q_{PG}^{OR}$	or	$C_{PG}^{OR}$
5) Outer Roll to Nav Base-Vehicle	$q_{OR}^{NB}$	or	$C_{OR}^{NB}$

Of these, number 1 is time independent, while 2, 4 and 5 vary with the gimbal angles  $\psi$ ,  $\theta_P$ ,  $\theta_R$  as defined in Figure 3. The Inner Roll to Pitch transformation is constant except when the gimbals pass near or through the gimbal flip region. In these regions, the inner roll gimbal angle,  $\delta$ , can change widely and rapidly, depending on servo loop design, gimbal angles and body rates. The only general rule is that, near gimbal flip, gimbal motions are significantly larger than the vehicle motions which cause them.

#### A.2.5.2 Attitude Transformations Using Readout Angles

This series of transformations (section A.2.5.1 above) represents actual rotations and is derived using true gimbal angles and misalignments. However, the true gimbal angle is never observable. A corrupted readout angle is available. The superposition of the synchro readout error means the computer will have available for attitude estimation and failure detection only similar transformations except that:

$$\text{for } \psi_{AZ} \text{ substitute } \psi_{AZ} - \epsilon_{OAZ} + A_\psi \sin n(\psi_{AZ} - \psi_{OFF})$$

$$\begin{aligned} \text{for } \theta_P \text{ substitute } \theta_P &= \epsilon_{OPG} + A_{\theta P} \sin n(\theta_{PG} - \theta_{P_{OFF}}) \\ \text{for } \theta_R \text{ substitute } \theta_R &= \epsilon_{OOR} + A_{\theta R} \sin n(\theta_{RG} - \theta_{R_{OFF}}) \end{aligned}$$

### A.3 AN/ASN 90 IMU ERROR MODEL

This section of the system model definition is a discussion of the actual IMU Error Model being used, first, as a basis for digital simulation of a multiple IMU system and, second, as a standard in evaluating failure detection and isolation methods.

#### A.3.1 Mechanical Configuration

Figure 3 shows a mechanical schematic of the four-gimbal inertial platform. Mounted on the inner gimbal are two two-degree-of-freedom gyroflex gyros, a two axis pendulous accelerometer, and a single axis pendulous accelerometer. One gyro is mounted with its spin axis along the vertical and provides pitch and roll stability. The second gyro has its spin axis along the positive pitch axis. One of its sensitive axes is along the vertical, while the other (providing a redundant input) is along the negative roll axis. The two axis accelerometer has its axes in the horizontal planes and the single axis instrument completes the triad.

Mounted along the azimuth axis is a coordinate resolver which provides directional resolution of the gyro error signals sent to the pitch and outer roll gimbal servos. Attitude information is obtained from synchros mounted along the azimuth, pitch, and outer roll axes. The outer roll gimbal is slaved to the inner roll gimbal, but displaced by an angle of  $90^\circ$  about the roll axis. By this means gimbal lock is avoided and an all attitude capability is obtained.

#### A.3.2 Platform Orientation

In normal operation, the AN/ASN-90 IMU's reference triad is oriented

$$\begin{bmatrix} X_R \\ Y_R \\ Z_R \end{bmatrix} = \begin{bmatrix} \text{NORTH} \\ \text{EAST} \\ \text{DOWN} \end{bmatrix}$$

Normal operation is in a local vertical mode. The redundant system feasibility demonstration program will use this IMU in an inertial mode, but will mount the system in the present aircraft orientation. It is to be noted that leveling the two

axis accelerometer with gimbal angles zeroed requires that the roll axes be horizontal.

### A.3.3 Gimbal and Synchro Errors

Kearfott specifications state all instrument input axes shall be within a cone of half angle  $0.3 \text{ mr} (1\sigma)$  of their respective reference axes. The gimbal axis bias uncertainty angle of  $0.6 \text{ mr} (1\sigma)$  and gimbal nonperpendicularity of  $0.6 \text{ mr} (1\sigma)$  are considered typical. The magnitude of the sinusoidal synchro error is estimated to be less than  $0.6 \text{ mr} (1\sigma)$ .

### A.3.4 Inertial Component Error Models

#### A.3.4.1 Gyroscopes

The gyroflex gyroscope is a dry, flexure supported instrument. Sensitive to input about two axes, it has a two axis pickoff. Two orthogonal torquers reposition the gyro wheel to its null position. Separate windings are provided for analog and digital (compensation) torquing. One gyroflex has two "horizontal" input axes, nearly parallel to the IMU reference plane. The other is mounted with a vertical (or azimuth) IA, but has its second axis slaved to null. For this discussion, X and Y shall refer to the input axes of the horizontal gyro, and Z shall refer to the azimuth gyro.

A model for the gyroflex, following that presented by Kearfott, is developed in the following paragraphs.

A constant drift about each axis is assumed. This drift is denoted by

$$D_R = \begin{bmatrix} D_{RX} \\ D_{RY} \\ D_{RZ} \end{bmatrix}$$

and has the units of rate ( $^{\circ}/\text{hr.}$ ). The sign convention assumed is that positive bias drift implies float rotation in the same sense as a negative real input rate. The sign convention for all other drift terms shall agree with this definition.

Mass unbalance error terms have been defined by Kearfott. These correspond to drifts about the IA due to specific force along the gyro axes. Here,



$M_{Sj}$  = Spin axis mass unbalance term ( $^{\circ}/\text{hr}/g$ ),

$M_{Ij}$  = Input axis mass unbalance term ( $^{\circ}/\text{hr}/g$ ),

$M_{Oj}$  = Cross axis mass unbalance term ( $^{\circ}/\text{hr}/g$ ),

where  $j=X, Y, Z$ . Mass unbalance drifts are given by

$$W_U = \begin{bmatrix} W_{UX} \\ W_{UY} \\ W_{UZ} \end{bmatrix} = \begin{bmatrix} -M_{IX} & M_{OX} & -M_{SX} \\ -M_{OY} & M_{IY} & M_{SY} \\ M_{OZ} & M_{SZ} & M_{IZ} \end{bmatrix} \begin{bmatrix} A_{GX} \\ A_{GY} \\ A_{GZ} \end{bmatrix} \quad \text{where } A_G = C_R^G C_R^A A_A$$

Anisoelastic drift is the drift about the IA due to simultaneous linear accelerations along the SA and IA. The drift is given by

$$W_A = \begin{bmatrix} W_{AX} \\ W_{AY} \\ W_{AZ} \end{bmatrix} = \begin{bmatrix} (K_{AX}) (A_{GY}) (A_{GZ}) \\ (K_{AY}) (A_{GY}) (A_{GZ}) \\ (K_{AZ}) (A_{GX}) (A_{GY}) \end{bmatrix}$$

where  $K_{Aj}$ ,  $j=X, Y, Z$ , is given in  $^{\circ}/\text{hr}/g^2$ , and the specific forces are scaled in gs. Scale factor error is given by Kearfott in the form

$$K_{AFj} = K_{Fj} (1 + K_{FEj})$$

where  $j=X, Y, Z$ .  $K_{Fj}$  is the loaded scale factor (sec/pulse) and  $K_{FEj}$  is the scale factor error.  $K_{AFj}$  represents the actual gyro scale factor (sec/pulse).

Random drift of the gyro is modeled as an exponentially correlated (Markovian) Gaussian noise. For each axis,

$$W_{Rj}(t) = e^{-\Delta t / G_j} W_{Rj}(t - \Delta t) + G_j (1 - e^{-2\Delta t / G_j})^{1/2} N_j(t)$$

where,  $j = X, Y, Z$

$W_{Rj}(t)$  = random noise time at  $t$

$W_{Rj}(t-\Delta t)$  = random noise at time  $t-\Delta t$

$\Delta t$  = sampling time

$\tau_{Gj}$  = correlation time of gyro j random noise

$\sigma_{Gj}$  = standard deviation of noise of gyro j

$N_j(t)$  = noise sample from a random Gaussian noise table with  $\sigma = 1$  and mean = 0

In Kearfott's model,  $\tau_{GX} = \tau_{GY} = \tau_{GZ} = 1$  sec and  $\sigma_{GX} = \sigma_{GY} = \sigma_{GZ} = 0.003^\circ/\text{hr}$ . This symmetry may be relaxed to allow differing  $\tau$  and  $\sigma$  values for each axis if  $W_{Ri}$  is found to be a significant term. The three equations ( $W_{RX}$ ,  $W_{RY}$ ,  $W_{RZ}$ ) will be started at different points on the Gaussian table.

An analytical model of transients due to gyro warm up has been derived. It includes exponential terms with characteristic times of  $\tau = 1.3$  and  $\tau = 20$  minutes. These terms are excluded from the proposed model on the assumption that the IMU will be temperature for a period  $\gg 3\tau$  before launch. Also excluded are non-orthogonality of pickoff axes and of torquer axes.

The total drift is given by:

$$W_{OUT} = \begin{bmatrix} W_{OUTX} \\ W_{OUTY} \\ W_{OUTZ} \end{bmatrix} = D_R + W_U + W_A + W_R$$

and the compensation torquing will be decided by

$$W_{CMD} = -W_{OUT} = - \begin{bmatrix} D_R + W_U + W_A \end{bmatrix}$$

The maximum compensation range is  $\pm 50^\circ/\text{hr}$ . Compensation torquing will introduce platform drift due to miscompensation of error terms, random drift and scale factor errors.

#### A.3.4.2 Two-Degree-of-Freedom Accelerometer

A two axis (Kearfott 2414) accelerometer is used for the horizontal axes. This instrument is described as a dry, force-rebalanced, inverted flexure-joint pendulum. Displacements along two mutually perpendicular axes are detected by high gain capacitive pickoffs. Rebalancing is accomplished using two analog DC current permanent magnet torquers. The torquer current is digitized for use by the navigation computer.

Kearfott suggests modeling three error terms: constant bias along each IA, an acceleration independent scale factor error and random noise. Not suggested are scale factor linearity and crosscoupling terms.

Bias is given in units of acceleration,  $B_{Lj}$ ,  $j = X, Y$ . The scale factor error appears as

$$K_{ATj} = K_{Sj} (1 + K_{SEj}), j = X, Y$$

Here  $K_{Sj}$  is the loaded scale factor, and  $K_{SEj}$  is the scale factor error.

The random noise is given by

$$A_{Rj}(t) = e^{-\Delta t / \tau_{Aj}} A_{Rj}(t - \Delta t) + \tau_{Aj} (1 - e^{-\Delta t / \tau_{Aj}})^{1/2} N_j(t)$$

where  $j = x, y$

$A_{Rj}(t)$  = random noise at time  $t$

$A_{Rj}(t - \Delta t)$  = random noise at time  $(t - \Delta T)$

$\Delta t$  = sampling time

$\tau_{Aj}$  = correlation time of accelerometer random noise

$\sigma_{Aj}$  = standard deviation of accelerometer random noise

$N_j(t)$  = Noise sample from a Gaussian noise table with  $\sigma = 1$  and mean = 0

The total sensed specific force then is given by (units are  $\Delta V$  pulses/sec):

$$A_{OUTj} = \frac{(A_{inj} - g_j + B_{Lj} + A_{Rj})}{(K_{Sj})(1 + K_{SEj})}$$

If required, a more detailed model would include scale factor nonlinearity and cross coupling given by:

$$A_{OUTj} = \frac{\left\{ -g_j + B_{Lj} + A_{Rj} + \begin{bmatrix} 1 & A_{CXY} & A_{CXZ} \\ A_{CYX} & 1 & A_{CYZ} \end{bmatrix} \begin{bmatrix} A_{INX} \\ A_{INY} \\ A_{INZ} \end{bmatrix} \right\}}{\left\{ (K_{Sj})(1 + K_{SEj}) \left( 1 + \frac{A_{INj}}{A_{IN \max}} K_{LEj} \right) \right\}}$$

<u>Term</u>	<u>General Platform Model Nomenclature</u>	<u>Nominal Value or Representative Error (1<math>\sigma</math>)</u>
<u>Equivalent Channel Drift</u>		
Horizontal Gyro	$D_{RX}, D_{RY}$	0.01°/hr
Azimuth Gyro	$D_{RZ}$	0.01°/hr
<u>GYPTO/Torquer Scale Factor</u>		
Horizontal Gyro	$K_{FX}, K_{FY}$	0.4 $\widehat{\text{sec}}$ /pulse
Azimuth Gyro	$K_{FZ}$	0.4 $\widehat{\text{sec}}$ /pulse
<u>GYPTO/Torquer Scale Factor</u>		
Horizontal Gyro	$K_{FEX}, K_{FEY}$	300 ppm
Azimuth Gyro	$K_{FEZ}$	300 ppm
<u>Mass Unbalances</u>		
Horizontal Gyro Spin Axis	$M_{SX}, M_{SY}$	0.05°/hr/g
Azimuth Gyro Spin Axis	$M_{SZ}$	0.05°/hr/g
Horizontal Gyro Input Axis	$M_{IX}, M_{IY}$	Negligible
Azimuth Gyro Input Axis	$M_{IZ}$	Negligible
Horizontal Gyro Cross Axis	$M_{OX}, M_{OY}$	TBD
Azimuth Gyro Cross Axis	$M_{OZ}$	TBD
<u>Anisoelasticity</u>		
Horizontal Gyro	$K_{AX}, K_{AY}$	Negligible
Azimuth Gyro	$K_{AZ}$	Negligible
<u>Random Drift</u>		
Horizontal Gyro	$W_{RX}, W_{RY}$	$\tau_{GX} = \tau_{GY} = \tau_{GZ} = 0.003 \text{ deg/hr}$
Azimuth Gyro	$W_{RZ}$	$\tau_{GX} = \tau_{GY} = \tau_{GZ} = 1 \text{ sec}$
		Long Term
		$\tau_{GX} = \tau_{GY} = \tau_{GZ} = 0.005^\circ/\text{hr}$
		$\tau_{GX} = \tau_{GY} = \tau_{GZ} = 1800 \text{ sec}$

<u>Term</u>	<u>General Platform Model Nomenclature</u>	<u>Representative Error (1σ)</u>	
<u>Accelerometer/CAPRI Bias</u>			
Horizontal Accelerometer	B <sub>LX</sub> , B <sub>LY</sub>	0.067 cm/s <sup>2</sup>	
Vertical Accelerometer	B <sub>LZ</sub>	0.100 cm/s <sup>2</sup>	
<u>Accelerometer/CAPRI Scale Factor</u>		<u>Low Gain</u>	<u>High Gain</u>
Horizontal Accelerometer	K <sub>SX</sub> , K <sub>SY</sub>	1.0 cm/s/pulse	0.01 cm/s/pulse
Vertical Accelerometer	K <sub>SZ</sub>	1.0 cm/s/pulse	0.01 cm/s/pulse
<u>Accelerometer/CAPRI Scale Factor Error</u>			
Horizontal Accelerometer	K <sub>SEX</sub> , K <sub>SEY</sub>	267 ppm	
Vertical Accelerometer	K <sub>SEZ</sub>	300 ppm	
<u>Accelerometer/CAPRI Scale Factor Nonlinearity</u>			
Horizontal Accelerometer	K <sub>LEX</sub> , K <sub>LEY</sub>	TBD ppm/g	
Vertical Accelerometer	K <sub>LEZ</sub>	TBD ppm/g	

<u>Term</u>	<u>General Platform Model Nomenclature</u>	<u>Representative Error (1<math>\sigma</math>)</u>
<u>Accelerometer Cross Coupling</u>	$A_{CXY}$	TBD
	$A_{CXZ}$	TBD
	$A_{CYX}$	TBD
	$A_{CYZ}$	TBD
	$A_{CZX}$	TBD
	$A_{CZY}$	TBD
<u>Accelerometer/CAPRI Random Noise</u>		<u>Short Term</u>
Horizontal Accelerometer	$A_{RX}, A_{RY}$	$\tau_{AX} = \tau_{AY} = \tau_{AZ} = 2 \times 10^{-5} g$
Vertical Accelerometer	$A_{RZ}$	Effectively White Noise
<u>Misalignments</u>		
X-Gyro About $Y_R$	$B_{XY}$	$2.9 \times 10^{-4}$ rad
X-Gyro About $Z_R$	$B_{XZ}$	$2.9 \times 10^{-4}$ rad
Y-Gyro About $X_R$	$B_{YX}$	$2.9 \times 10^{-4}$ rad
Y-Gyro About $Z_R$	$B_{YZ}$	$2.9 \times 10^{-4}$ rad
Z-Gyro About $X_R$	$B_{ZX}$	$2.9 \times 10^{-4}$ rad
Z-Gyro About $Y_R$	$B_{ZY}$	$2.9 \times 10^{-4}$ rad
Y-Accelerometer About $X_R$	$A_{YX}$	$2.9 \times 10^{-4}$ rad
Z-Accelerometer About $X_R$	$A_{ZX}$	$2.9 \times 10^{-4}$ rad
Z-Accelerometer About $Y_R$	$A_{ZY}$	$2.9 \times 10^{-4}$ rad

$K_{LE}$  represents scale factor nonlinearity, while  $A_{cij}$  represents cross-coupling of input along  $j$  into the output of accelerometer  $i$ .

#### A.3.4.3 Single-Degree-of-Freedom Accelerometer

A single axis (Kearfott 2404) accelerometer is used on the vertical axis. It is a dry, force rebalanced, inverted flexure-joint pendulum. In general, its description is the same as that of the (2414) two axis accelerometer.

Error terms in the single axis instrument are identical with those of the two axis instrument. Indeed, if  $j$  is understood to be  $j=X, Y, Z$ , and the cross-coupling matrix is rounded out to

$$\begin{bmatrix} 1 & A_{CXY} & A_{CXZ} \\ A_{CYX} & 1 & A_{CYZ} \\ A_{CXZ} & A_{CYZ} & 1 \end{bmatrix}$$

the equations of the previous section will cover the triad of accelerometers.

#### D. Estimates of Instrument Uncertainties

Kearfott has provided estimates of the bulk of instrument error parameters needed for this model. In the table which follows, nominal scale factor values are given. All other terms are one sigma error estimates. "TBD" or "to be determined" means simply that no estimate is given in the published material now available.

#### A-IV Multiple IMU System Model

The single IMU error model has been defined. A model of a multiple IMU system is being constructed using the single IMU model as a building block, and subject to system definition ground rules described in this section.

Feasibility of a multiple IMU inertial system is to be demonstrated in this program. The system is to conform to these general rules.

- 1) The system will contain 4 four-gimbaled IMUs, mounted on a common navigation base. They will have coplanar gimbal axes.

- 2) There will be a central computer which, among its functions, will perform failure detection and isolation.
- 3) The system is to be FO-FO-FS.

Four identical IMU's will be used. For the demonstration program, they shall be off-the-shelf Kearfott AN/ASN-90's. All individual inertial systems are assumed to be commonly mounted on a single navigation base. Consideration will be given to other IMU's and to alternative AN/ASN-90 gimbal arrangements. Further, a study of non-coplanar IMU axes mounted orientations will be made at a later time in this study effort.

#### A-v KT-70 Electrical Interface Definition

The interface to the AN/ASN-90 IMU and its associated electronics carries both power and signal lines. It should be noted that signal voltage levels are specified at the IMU. With the system mated with other than the dedicated AN/ASN-90 computer, an interface unit will have to be designed to mate these signals to the given system interface unit/data bus/computer complements.

#### A. IMU and Electronics Power Requirement

- |                           |                         |
|---------------------------|-------------------------|
| 1. 115V, 400 Hz, 3 $\phi$ | 4 wire, 940 watts (max) |
| 2. 26V, 400 Hz, $\phi$ C  | 6 watts                 |
| 3. 5V, 400 Hz             | 7.5 watts               |
| 4. 28 VDC                 | 10 watts                |

The proposed laboratory test system will employ the A-7 adapter power supply for each IMU.

#### B. IMU Signals to the Computer

##### 1. Discrete Status Signals

Each IMU will have available the following discrete status signals:

IMU Fault Warning	IMU Fail = Logic "1"*
System Ready	IMU Ready = Logic "1"*

\* Converse is true for logic "0".



Here, and in the following pages, logic "1" =  $5 \pm 1$  VDC, logic "0" =  $0 \pm 0.5$  VDC. Noise levels on logic lines must be under 1 volt.

In addition to these discretes, there is a multiposition "mode" switch. Modes mechanized in the AN/ASN-90 system include Ground Align, Inertial, Normal (Local Vertical Navigation), Magnetic Slave and Grid.

## 2. Analog Data Signals

There will be three single speed synchros, mounted on the outer roll, pitch and azimuth gimbal axes, in each IMU. Synchro to digital conversion (S/D) will be performed by a yet to be specified gimbal angle readout. The synchros will have 3 wire outputs and will be characterized by

Null	0.035 V	400 Hz
Gradient at Null	$0.185 \text{ V/}^\circ$	400 Hz
Max. Output	10.5 V	400 Hz

## 3. Digital Data Signals

Digital output to the computer will comprise  $\Delta V$  pulses only. Six dedicated pairs of wires will carry these six signals:  $\pm \Delta V_X$ ,  $\pm \Delta V_Y$  and  $\pm \Delta V_Z$ . Pulse characteristics are given by:

Pulse Rate	0 - 10,000 pps
Pulse Width	$13 \pm 12 \mu\text{s}$
Logic "1"	$5 \pm 1$ VDC
Logic "0"	$0 \pm 0.5$ VDC
Pulse Time Constants	$T_R, T_F \text{ max} = 3 \mu\text{s}$
Currents	3 mA sink at Logic "0" 0.05 mA source at Logic "1"

## C. Computer Output Signals (Commands)

### 1. Discrete Signals to IMU

Pulse shape for all Discretes	IMU 2 mA sink either state $T_R, T_F = 10 \mu\text{s max}$ All signals are single-ended
Computer Fault	Computer fail = Logic "1"*

Autocal in Progress	In Progress = Logic "1"*
Computer Control	Accept Computer Control = Logic "1"*
Accel. SF Change	Change SF = Logic "1"*
AZ Slew ( $90^{\circ}/\text{min}$ )	} Slew Command = Logic "1"*
X Slew ( $30^{\circ}/\text{min}$ )	
Y Slew ( $30^{\circ}/\text{min}$ )	
AZ Slew Sense	Decreasing True Hdg CX = Logic "1"*
X slew Sense	With True Hdg CX at $0^{\circ}$ , Decreasing Roll CX = Logic "1"*
Y Slew Sense	With True Hdg CX at $0^{\circ}$ , Decreasing Pitch CX = Logic "1"*

\* Converse is true for Logic "0".

Note that "X Slew" and "Y Slew" refer to slewing about the X and Y gyro input axes, respectively. No provision is made for slewing about the outer roll or the pitch axis alone.

## 2. Gyro Pulse Torquing Signals

Gyro pulse torquing for drift compensation, earth rate compensation and motion compensation (used for maintaining the local vertical frame) is commanded by the flight computer. Signals needed are:

GYPTO Logic, $W_X$	} {	Pulse Train
GYPTO Logic, $W_Y$		200pps
GYPTO Logic, $W_Z$		Pulse Width = 5000 $\mu s$
		Current Requirements = 3 mA max
GYPTO Clock Pulses	Pulse Rate = 200 pps	
	Pulse Stability = 100 ppm	
	Pulse Width = 1 $\mu s$ at 4 VDC	

## A-VI. Critical Design Feature Definition

Several design features of the AN/ASN-90 IMU have been identified as critical to the demonstration program. That is, normal performance of these system features

may be marginal for a complete demonstration of failure detection for the space shuttle.

A. Gimbal and Gimbal Angle Readout Problems

There is a general problem of gimbal accuracy requirements with respect to inflight alignment and failure detection. Angle readouts are presently limited. To modify the system would require changing the gimbal accuracy specification or developing a new calibration technique. Single speed synchros should be replaced, and additional temperature control provided.

All synchros should be read as close to simultaneously as possible. If individual tracking S/D converters are used (three per IMU or nine in all), then it is possible to read all synchros 50 times/second. If an attempt is made to multiplex synchro outputs and use a single S/D converter, reading all angles will require 900 ms (update/sec). Therefore, nine individual, tracking S/D converters are suggested.

B. IMU Mounting

A mounting orientation of KT-70 in the shuttle vehicle for both pre-launch gyrocompassing and avoidance of gimbal flip during boost requires further careful study.

IMU case isolation pads cause a possible problem for gimbal angle failure detection on a common navigation base.

1. Accelerometer Counters

The two  $\Delta V$  loop is presently unsynchronized with accelerometer counter readings.

All accelerometer counters should be frozen simultaneously and read in a time less than the time required for two pulses from any accelerometer. This assumes that the one bit sensing circuitry is designed for no fault operation. This is different from a single KT-70 interface where accelerometer counters are frozen and read sequentially.

#### D. GYPTO Computer Requirements

The requirement for GYPTO inputs every 5 ms is out of proportion with the number of data transfers needed for velocity and gimbal information. This is in no way a serious problem using a parallel interface, as is envisioned, but would cause congestion on a serial bus such as might be used in a flight vehicle application of multiple systems and redundant computers. It is, therefore, recommended that the binary torquing be handled by circuitry in the interface. This will not limit the ability to compensate for errors. It will simply reduce the computer overhead for handling compensation to actual net torquing.

#### A-VII. Summary

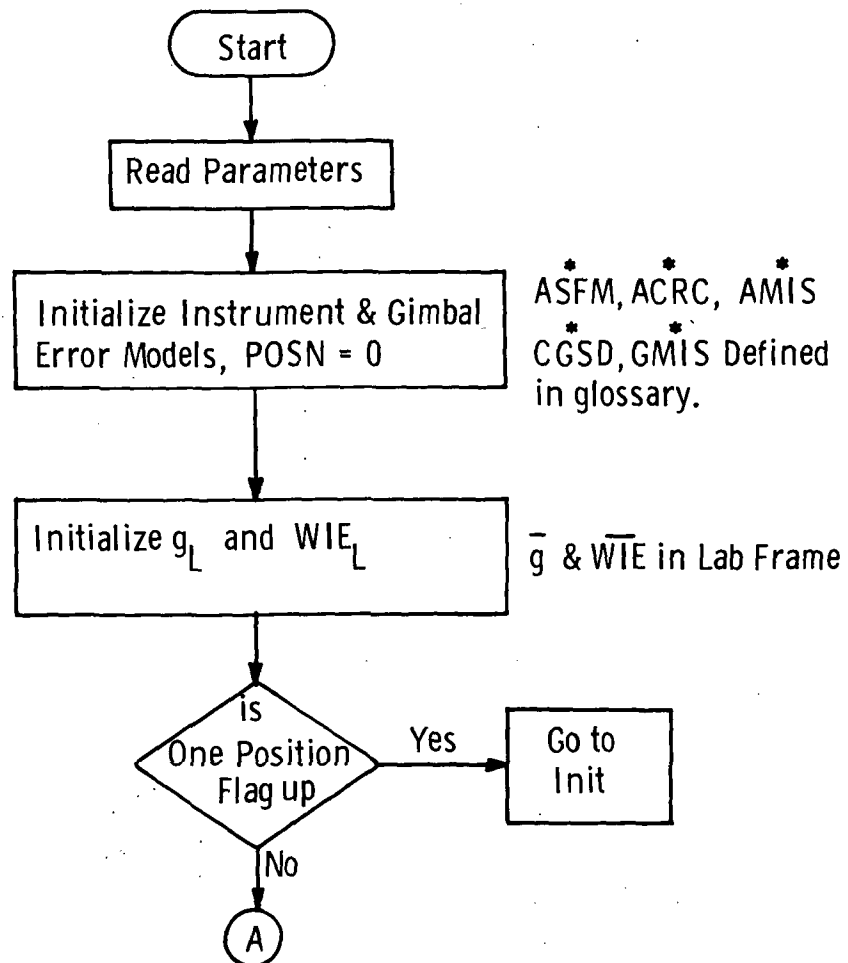
This Appendix is an effort to gather baseline information on the KT-70 IMU in a single source. A model of the IMU and its inertial components is given and complemented by estimated parameter values. The electrical interface at the IMU is described, although no attempt to describe the proposed system mechanization is made.

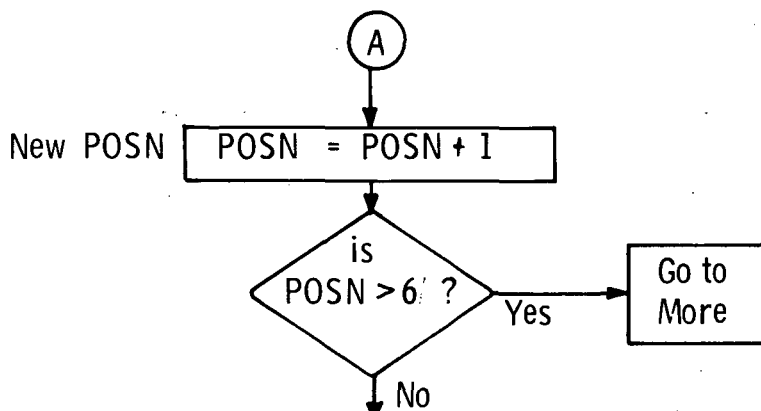
**Page intentionally left blank**

## B. Flow Chart of the Multiple IMU System

### B.1 Introduction

The digital model of the multiple IMU system is explained by an annotated flow chart. This description includes the logic for both the single position tests described in Chapter 6. A glossary follows the flow chart.





INIT

Command Gimbal Angles  
Initialize  $\Delta V$  Count.  
 $t = 0$

$\overline{\text{GANG}}$  is a 12-Vector of  
Gimbal Angles  
 $t$  = Test Time

Modify  $\overline{\text{GANG}}$  by Resolver  
Error Model  
Record Initial GANG

Construct  $C_{JK}^*$  where

$$C_{JK} = \begin{bmatrix} c_1 \\ c_2 \\ c_3 \\ c_4 \end{bmatrix}$$

$C_i = C_{\psi_i} \ C_{\delta_i} \ C_{\phi_i} \ C_{\theta_i}$ , a  $3 \times 3$  matrix

$C_{JK}$  is a  $12 \times 3$  matrix

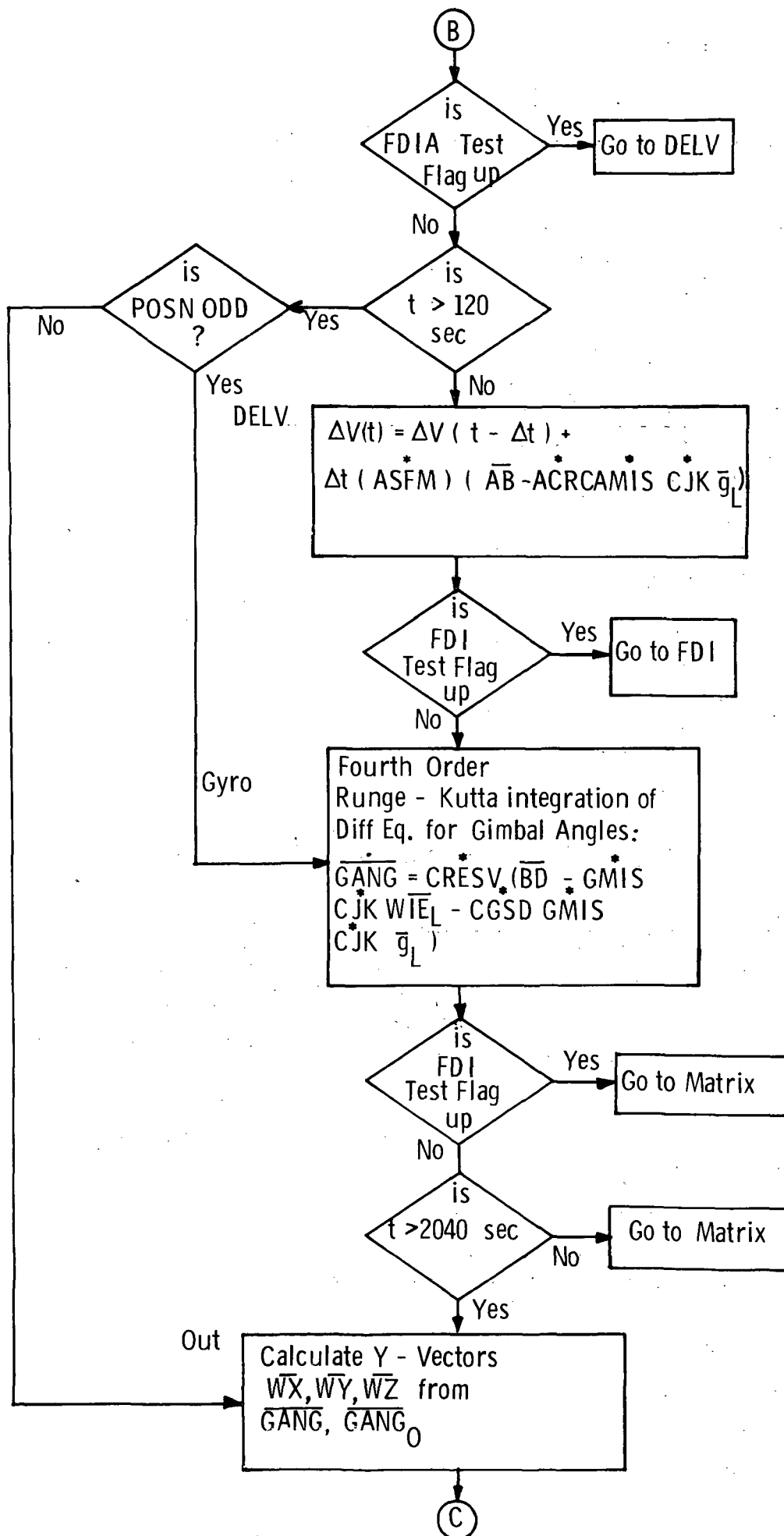
Construct  $C_{RESV}^*$   
where

$$C_{RESV}^* = \begin{bmatrix} R_1 & 0 & 0 & 0 \\ 0 & R_2 & 0 & 0 \\ 0 & 0 & R_3 & 0 \\ 0 & 0 & 0 & R_4 \end{bmatrix}$$

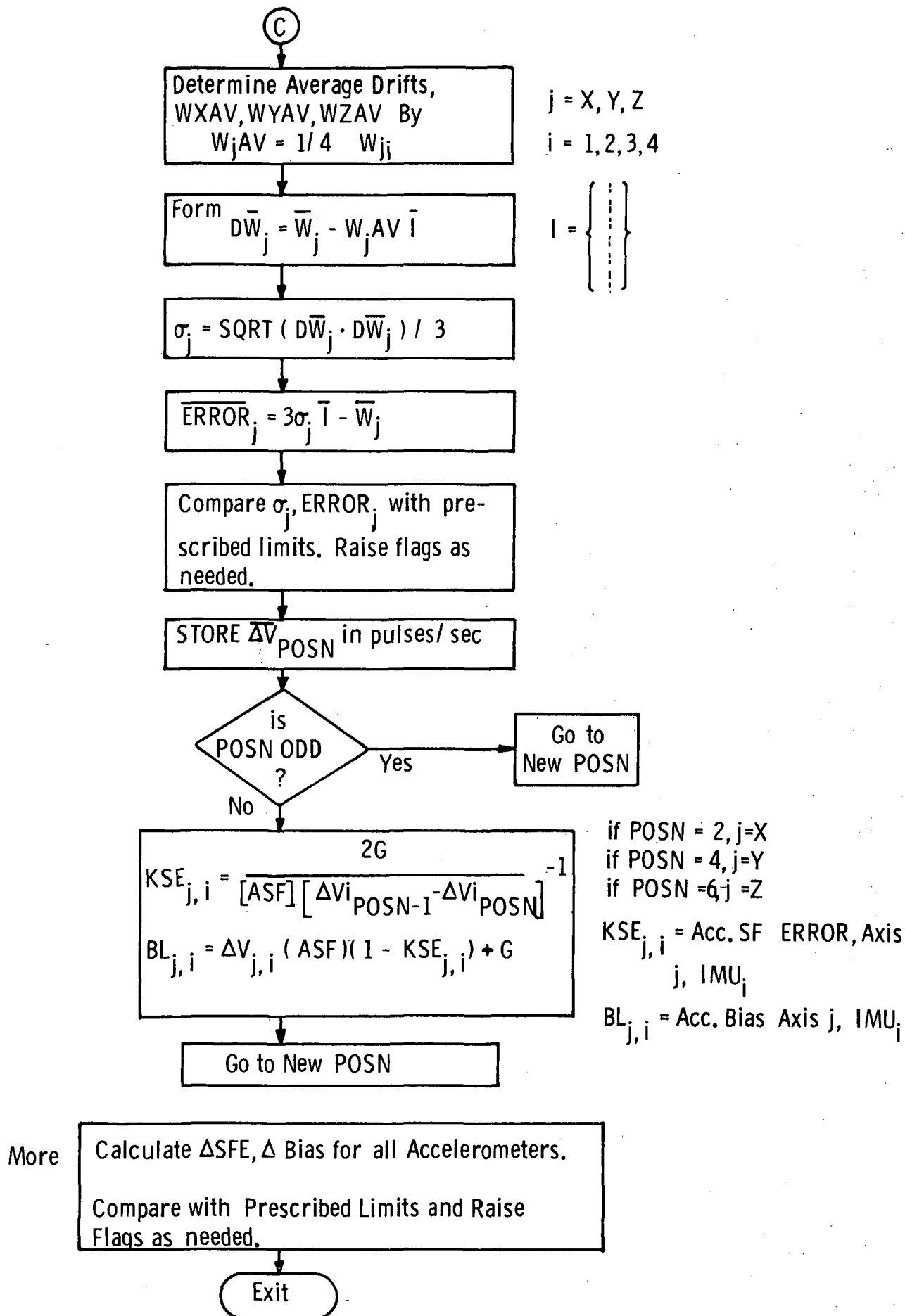
$O$  is a  $3 \times 3$  zero matrix

$$R_i = \begin{bmatrix} \cos \psi_i & \sec \psi_i & -\sin \psi_i & \sec \phi & 0 \\ \sin \psi & & \cos \psi & & 0 \\ 0 & & 0 & & 1 \end{bmatrix}$$

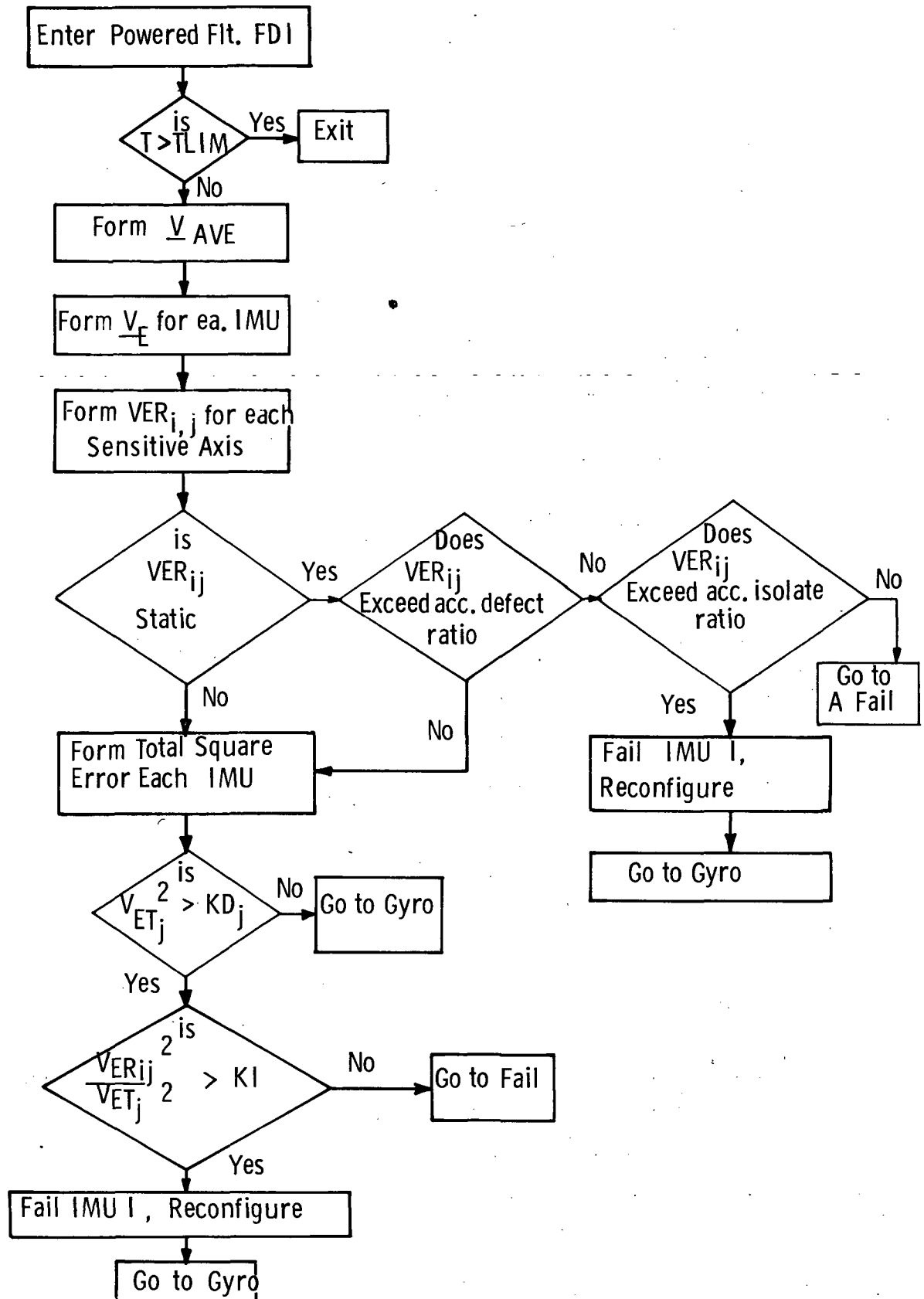
B







FDI



**Page intentionally left blank**

## GLOSSARY

BD A 12-vector of gyro acceleration insensitive drifts.

<sup>\*</sup>  
CGSD A 12 x 12 matrix modeling gyro g sensitive drifts

$$\begin{bmatrix} G_1 & O & O & O \\ O & G_2 & O & O \\ O & O & G_3 & O \\ O & O & O & G_4 \end{bmatrix}$$

where O is a 3 x 3 zero matrix

and  $G_j$  is given by

$$\begin{bmatrix} -M_{ixi} & M_{oxi} & M_{sxi} \\ -M_{oyi} & M_{lyi} & M_{syi} \\ M_{ozi} & M_{szi} & M_{lzi} \end{bmatrix}$$

Here,  $\begin{matrix} M_{li} \\ M_{si} \\ M_{oi} \end{matrix} \left\{ \begin{array}{l} \text{are the g sensitive drift} \\ \text{terms about a given axis} \\ \text{due to linear acceleration} \\ \text{along the } \left\{ \begin{array}{l} \text{input} \\ \text{spin} \\ \text{cross} \end{array} \right\} \text{ axis.} \end{array} \right.$

<sup>\*</sup>  
 $G_{mis}$  A 12 x 12 matrix modeling gyro sensitive axis misalignments about the platform reference axes.

$$\begin{bmatrix} G_1 & & & O \\ & G_2 & & \\ & & G_3 & \\ O & & & G_4 \end{bmatrix}$$

<sup>\*</sup>  
 $A_{mis}$  A similar matrix modeling accelerometer misalignments.

AB A 12-vector of accelerometer biases.

\*  
ACRC

A 12 x 12 matrix representing accelerometer measurement and cross coupling errors.

$$\begin{bmatrix} A_1 & 0 & 0 & 0 \\ 0 & A_2 & 0 & 0 \\ 0 & 0 & A_3 & 0 \\ 0 & 0 & 0 & A_4 \end{bmatrix}$$

where  $A_j = \begin{bmatrix} 1 & A_{cxy} & A_{cxz} \\ A_{cyx} & 1 & A_{cyz} \\ A_{czx} & A_{czy} & 1 \end{bmatrix}$

\*  
ASFM

A 12 x 12 diagonal matrix consisting of factors of the form

$$\frac{1}{K_s (1 + K_{SEij})}$$

where  $K_{SEij}$  is the SF error of the ij accelerometer axis,

i = x, y, z, j = 1, 2, 3, 4

## DISTRIBUTION LIST

### Internal:

R. Ragan	E. Jones	
D. Hoag	W. Woolsey	
N. Sears	G. Ogletree	
R. Battin	R. McKern	(80)
L. Larson	R. Trueblood	
A. Boyce	M. Hamilton	
J. Harper	S. Copps	
G. Silver (MSC)	J. Kernan	
T. Lawton (MSC)	J. Higgens	
E. Olsson (MSC)	B. Kriegsmann	
R. Cooper	G. Levine	
D. Dove	E. Muller	
G. Edmonds	T. Chien	
J. Feldman	T. Shuck	
P. Felleman	D. Brown	
J. Gilmore	J. St Amand	
S. Helfant	R. White	
R. Hutchinson	E. Salamin	
G. Bukow	J. Deckert	
R. Booth	J. Potter	
R. Blaha	D. Fraser	
K. Vincent	M. Johnston	
H. Musoff	R. Millard	
J. Oehrle	R. Stengel	
A. Laats	W. Tanner	
M. Landey	G. Stubbs	
J. Fish	H. McQuat	
D. Swanson	Apollo Library	(2)
A. Hopkins	MIT Doc. Center	(10)

External:

NASA/MSFC

National Aeronautics and Space Administration  
George C. Marshall Space Flight Center  
Huntsville, Alabama 35812

(30)

Attn: M. Brooks, S & E-ASTR-SG  
H. Brown, S & E-ASTR-SGA  
G. Doane, S & E-ASTR-SGA  
B. Doran, S & E-ASTR-SGA  
B. Gaines R-ASTR-GCC  
B. Moore S & E-ASTR-DIR  
F. Wojtalik, S & E-ASTR-S

Codes: A & TS-PR-RS (1)  
A & TS-PR-M (1)  
A & TS-MS-IL (1)  
A & TS-MS-IP (2)  
A & TS-MS-IP (2)  
S & E-ASTR-GD (2)  
S & E-ASTR-ZI (12)  
S & E-ASTR-S (2)

NASA/MSC

National Aeronautics and Space Administration  
Manned Spacecraft Center  
APOLLO Document Control Group (BM86)  
Houston, Texas 77058

(18)

Attn: T. Lins, EG2  
K. Cox, EG2  
W. Swingle, EG5  
M. Jones, EG5  
T. Barry, EG5  
J. Hanaway, EG7  
W. Bradford, EA2  
H. Tindall, FA  
R. Chilton, EG  
R. Nobles, FM7  
D. Cheatham, EG  
S. Mann, FM7  
P. Pixley, FM4  
R. Savely, FM4  
A. Weatherstroem, EG5  
S. Kamin, FM7  
B. Cochrell, FM4  
R. Eckelkamp, FM4

NASA/HDQ

National Aeronautics and Space Administration  
600 Independence Ave., SW  
Washington 25, D. C. 20546

(2)

Attn: R. Murad, MHE  
R. Livingston, MHE